

Université du Québec
Institut National de la Recherche Scientifique
Centre Eau Terre Environnement

**Characterization of extreme precipitation at multiple spatio-temporal scales in
historical and future climate**

By
Silvia Innocenti

for the degree of *Philosophiæ Doctor*, Ph.D.
in Sciences de l'eau
2018-2019

External examiner Juliette Blanchet
Institut des Géosciences de l'Environnement

External examiner Anne Frigon
Ouranos

External examiner Ramon De Elia
Servicio Meteorologico Nacional de Argentina

Internal examiner André St-Hilaire
Institut National de la Recherche Scientifique

Director Alain Mailhot
Institut National de la Recherche Scientifique

Co-Director Alex J. Cannon
Environment and Climate Change Canada

Remerciements

Tout en imaginant que ces premiers mots sonneront étranges pour plusieurs d'entre vous, je suis sûre qu'en arrivant à la fin de ces deux pages, les raisons pour lesquelles je peux dire avoir autant apprécié cette longue et difficile entreprise seront claires. D'avoir eu la possibilité de rencontrer et côtoyer toutes les personnes qui ont été derrière cette thèse est sans doute l'un de plus beaux cadeaux que le hasard et le destin m'ont faits dans cette petite vie.

Alain, tout d'abord, a ouvert la porte sur ce monde merveilleux qui est le climat. Il n'a sûrement pas été simple de diriger mes premiers pas incertains et émotifs dans ce nouvel univers, mais il a toujours réussi à guider et améliorer mon travail et ma personnalité de chercheuse avec une patience et une rigueur scientifique incomparables. Il a été un directeur de recherche très présent et qui a fait en sorte que cette thèse ait l'appui de collaborateurs externes formidables.

Je tiens aussi à exprimer ma profonde gratitude à **Anne** qui m'a accueilli à **OURANOS**, sans quoi ce projet n'aurait pas pu voir le jour. Anne, tu t'es toujours rendue disponible et attentive à mes questionnements, en essayant de valoriser mes travaux et mes efforts avec un intérêt sincère et bénéfique pour mes analyses. I would also like to thank **Alex** for his contribution and useful advises. His outstanding pedagogic approach in discussions and the time he spent for this thesis have been a precious help.

Merci à l'équipe de recherche, en particulier à **Guillaume et Samuel** pour leur assistance technique, leur bonne humeur et leur écoute pendant des présentations qui donnaient mal à la tête. Avec **Pradeebane**, en revanche, on a moins eu la possibilité d'échanger au travail mais sa compagnie en dehors du bureau est toujours bien agréable. **Gérémy** ensuite, merci d'avoir illuminé mes premiers regards sur le monde de l'hydrologie. Tu as toujours été prêt pour des discussions passionnantes et pour des pauses café fort importants pour faire avancer la science. Je garderai toujours un souvenir reconnaissant de mes jours de géographe passés dans ton bureau et j'espère être capable, un jour, d'aider un nouvel arrivé comme tu l'as fait avec moi (en fait, même une toute petite partie de ça serait déjà énorme!).

Un remerciement d'exception doit aller à **Dikra**, celle qui de plus près à vu (subi) les difficultés et les bonheurs quotidiens de cette thèse. Beaucoup plus qu'un support scientifique et une amie extraordinaire. J'ai l'impression d'avoir partagé quelque chose d'unique avec toi, Dikra, de difficile à décrire, mais tu sais bien de quoi je parle. J'ai grandi, grâce à toi, sur un chemin que nous avons marché de plusieurs manières ensemble et qui t'a emmené à occuper une place spéciale dans mon cœur. **François (le sien)** aussi, sans trop s'en apercevoir, a souvent donné un support et des conseils pragmatiques qui ont littéralement changé la direction de mes recherches.

Plein de remerciements différentes doivent aller à mes collègues et amis de l'INRS. **Carlotta**, grazie anche alla tua generosità senza limiti. In tua compagnia, pure la tua pasta scondita del martedì sera diventa un momento speciale. **Pierre**, et **YoH**, qui sera content de savoir que je n'ai épargné

aucune larme pour écrire ce texte, et **Vero**, qui a été là dans plein de moments fort délicats de cette thèse et qui a accompagné la plupart de mes transferts à Montréal. Je ne saurais jamais pourquoi vous avez toujours autant cru dans mes capacités, mais vous avez ponctuellement rehaussé mon estime de moi aux moments où j'en avais besoin. **Lau**, c'est surtout en fin de thèse qu'on a appris à se connaître, en posant, j'espère, des bases pour une amitié de longue vie. Je remercie les circonstances qui ont permis ce rapprochement. **Etienne**, au contraire, a été un pilastre des premières années mais important comme tout jusqu'à cette petite fin.

Une pensée spéciale doit ensuite aller "aux externes". **Jenny et Gab**, avec qui j'ai tourné plein de pages et partagé des moments de bonheur indescriptible. Je vous aime. **Ana**, femme incroyable qui sera toujours un modèle pour moi, en recherche comme dans la vie de tous les jours. La distance qui nous sépare à l'instant ne nous empêchera pas d'accomplir nos projets et de peaufiner nos compétences de sorcières. **Boris**, sais-tu comment tes câlins sont productifs pour la science? Mais **les swing ba***s** aussi, pour avoir favorisé mon intégration au Québec en m'instruisant sur la musique la plus *québécoise* que ce pays a à offrir, et surtout **Luc**, toujours prêt à allumer le gyrophare pour courir en ville si j'en avais besoin. **Filippo** qui s'est fait embarquer dans cette *frette* aventure et **Adam** qui dans le fond me tient toujours, même si je ne lui demande pas. Et finalement le comité de soutien à distance: **Teo e Cate, Vittoria**, le magnifique 4 di scienze statistiche (**Carol, Silvia, Lorena e Saretta**), **Paola e Annalisa, Leone, Paola di Paolo, Gianni e Marcella** e ovviamente la specialissima **Eleonora**. Se in questi anni ho tenuto botta tanto è dovuto ai vostri messaggi trans-oceanici.

Mes proches-à-distance, dont mon père, ma bellissima soeur **Laura** et mes frères méritent un paragraphe tout à eux pour les remercier de toujours croire en moi. Ho certato di contare tutte ma-proprio-tutte le goccioline che trovavo perché **Paolo** possa esser un giorno fiero di me.

Il ne reste qu'un grand merci pour **mon François**. Son appui inconditionnel et ses indénombrables encouragements représentent juste une petite partie de sa contribution à ce projet. Il a su maîtriser tant les moments où toute attention allait à mes gouttelettes, tant ceux où il fallait me sortir -de force- de mes chiffres d'ordinateur, en acceptant un mode de vie ... de doctorant. Merci aussi à sa famille qui rend ma vie à côté de cette personne exceptionnelle encore plus agréable.

Résumé

Les précipitations constituent l'élément moteur des extrêmes hydrologiques et interviennent sur une vaste gamme d'échelles spatiales et temporelles. Leur suivi à ces différentes échelles est essentiel pour de nombreuses applications, telles que le dimensionnement d'ouvrages hydrauliques, la gestion des ressources, et l'évaluation des risques pour les écosystèmes naturels ainsi que pour les populations et les infrastructures urbaines.

Suite à l'augmentation globale de la température prévue pour les décennies à venir, un nombre croissant d'événements extrêmes de précipitation est aussi attendu. Pourtant, la caractérisation de cette augmentation et la description des extrêmes aux différentes échelles d'intérêt hydrologique demeurent difficiles. En particulier, les biais et les incertitudes des séries simulées par les modèles de climat demeurent élevés quand on considère les extrêmes à de fines échelles spatiales et temporelles. Par conséquent, la possibilité de prévoir la fréquence d'occurrence et l'intensité des extrêmes à partir des séries simulées nécessite d'être évaluée en profondeur.

De façon plus générale, la couverture spatiale et la résolution des données disponibles, qu'elles aient été enregistrées à des stations météorologiques ou qu'elles soient issues des modèles climatiques, ne correspondent souvent pas à celles nécessaires pour les applications. Par exemple, les séries observées aux stations sont généralement courtes (au mieux quelques décennies au Canada) et fournissent des informations limitées sur la structure spatiale des précipitations. Cette étude s'intéresse donc à l'estimation des extrêmes de précipitation et de leur variabilité sur plusieurs échelles spatio-temporelles à partir de plusieurs ensembles de données. Pour ce faire, nous cherchons à établir des relations simples reliant les extrêmes estimés à différentes durées et sur différentes échelles spatiales.

De nombreuses études ont démontré que les propriétés physiques des fractales peuvent être utilisées pour décrire la variabilité spatiale et temporelle des précipitations et des extrêmes. Notamment, il a été démontré d'un côté que les modèles multifractals (*multiscaling*) sont appropriés pour représenter les changements d'échelle pour l'ensemble de la distribution des précipitations (c'est-à-dire pas seulement les extrêmes). D'un autre côté, de nombreuses études confirment la validité de modèles monofractals (*simple scaling*) pour les queues de la distribution (c'est-à-dire les extrêmes). Néanmoins, l'utilisation de ces modèles de lois d'échelle a été généralement restreinte à des régions spécifiques ou à des petites bases de données. Une analyse plus fine des facteurs géoclimatiques définissant les lois d'échelle est donc nécessaire pour des régions plus étendues et des données plus variées en termes de résolution spatiale et temporelle. Également, les effets possibles des changements climatiques sur la structure spatio-temporelle des précipitations et sur les lois d'échelle doivent être évalués.

Cette étude visait donc trois objectifs spécifiques. Dans un premier temps, des modèles de *simple scaling* ont été utilisés pour décrire la structure temporelle des précipitations extrêmes en Amérique

du Nord (Canada et États-Unis) à l'échelle journalière et sous-journalière. La validité des modèles des lois d'échelle a été confirmée en utilisant un grand nombre de séries (environ 2700 stations météorologiques) et la variabilité spatiale des paramètres des modèles de lois d'échelle a été explorée. Les analyses fournissent des informations importantes sur l'influence des caractéristiques locales ainsi que des structures climatiques régionales sur le changement d'échelle des précipitations extrêmes.

Dans un second temps, les lois d'échelle des précipitations extrêmes ont été évaluées pour différents jeux de données sur grille et comparées aux chroniques des stations. Deux jeux de données observés ont été considérés (p. ex. données satellites et données interpolées provenant de plusieurs sources). De même, des séries simulées par deux Modèles régionaux du climat (MRC) ont été utilisées: une simulation provenant du modèle WRF à haute résolution (4 km) et celles provenant d'un grand ensemble simulé à l'aide du Modèle régional canadien du climat de 5^{ème} génération (CRCM5, à la résolution de 0,11°). L'analyse a mis en évidence l'influence des caractéristiques de base de données sur l'estimation des modèles des lois d'échelle (p. ex. la résolution temporelle ou spatiale des données), et des techniques de transformation des séries utilisées, comme les méthodes de correction de biais. Une expression analytique simple a aussi été proposée pour décrire la variation des distributions des précipitations extrêmes sur plusieurs échelles spatiales et temporelles.

Troisièmement, des séries de précipitations simulées pour le siècle futur ont été analysées dans le but de décrire la réponse des lois d'échelles aux changements climatiques sur différents horizons de temps. Pour cela, les chroniques de précipitation de 50 membres du grand ensemble CRCM5 ont été regroupées sur des courtes périodes (p. ex. 3 ans) et analysées à plusieurs échelles spatio-temporelles. Cela a permis d'évaluer les quantiles des événements les plus extrêmes sur des périodes courtes et d'estimer les lois d'échelle en utilisant une large base statistique. Les résultats décrivent la façon dont les distributions des extrêmes de précipitation vont évoluer dans le futur et soulignent des changements importants des lois d'échelle. L'analyse illustre également l'impact de la variabilité naturelle du climat sur l'estimation des lois d'échelle et d'autres caractéristiques des précipitations extrêmes.

Mots-clés: Précipitations extrêmes; Echelle spatio-temporelle, Loi d'échelle; Changements climatiques.

Abstract

Characterizing extreme precipitation at different spatial and temporal scales is crucial in order to evaluate and predict the impacts of natural hazards on infrastructures and regional ecosystems. Being governed by climate and weather processes acting at different scales, extreme precipitation is highly variable in space and time. However, historical observational datasets (e.g., station records) provide limited information on the spatio-temporal structure of extreme precipitation. Also, the spatial coverage and the resolution of available data, whether observed at meteorological stations or simulated by weather and climate models, often mismatch the resolution needed in hydrological applications.

One interesting paradigm for the multi-scale analysis of extreme precipitation is the scaling model framework, based on the concept of statistical scale invariance and the fractal properties of precipitation probability distributions. By means of these models, the statistical distributions of the extremes estimated at specific spatial and temporal scales are related to the distributions at other scales. Several studies have provided physical evidence of the fractal and multifractal properties of precipitation. On the one hand, it has been shown that multifractal models are more appropriate for representing the scaling features of the whole precipitation distribution (i.e., not only the extremes). On the other hand, many studies confirmed the validity of simple scaling for the tails of precipitation distribution. However, the use of scaling models has been mainly restricted to specific regions and small observational datasets. A deeper analysis of the effect of geo-climatic factors on the estimated scaling models is thus needed for large regions and various datasets having different temporal and spatial resolutions.

The present study aims at deepening the knowledge of the scale-invariant properties of extreme precipitation and has three specific objectives. First, simple scaling models were used to describe the temporal structure of observed daily and sub-daily extreme precipitation across North America. The validity of the temporal scaling models was confirmed over various duration ranges using a large number of station series (approx. 2700 meteorological stations). The regional variability of the estimated temporal scaling parameters across the domain was then investigated. The analysis provides important guidance on the influence of both local geographical characteristics and regional climatic features on extreme precipitation scaling.

Second, the spatio-temporal scaling properties of daily and sub-daily extreme precipitation were analyzed for various gridded datasets and compared to scaling properties of station series. Two observational gridded datasets were considered: the bias-corrected satellite CMORPH and the Multi-Source Weighted-Ensemble Precipitation (MSWEP) v2 datasets. Also, two simulated datasets from Regional Climate Models (RCMs) were used: a convection-permitting high-resolution WRF model (4 km resolution) and a large ensemble from the Canadian RCM v5 (CRCM5, 0.11° resolution). The analysis illustrated the influence on temporal scaling exponent estimation of basic dataset char-

acteristics, such as their spatial and temporal resolutions, and series processing techniques, such as bias correction methods. Also, a simple analytical expression was suggested for describing the variation of extreme precipitation quantiles across a wide range of spatio-temporal scales.

Third, the evolution of simulated extreme precipitation under climate change was analyzed to assess how the spatio-temporal scaling of the extremes responds to climate warming over different time horizons. To this end, precipitation series from 50 CRCM5 members were pooled for various spatio-temporal scales. This allows to assess high return period quantiles over short periods of few years and estimate their extreme scaling properties using a large statistical basis. The results underline the critical increase in AM precipitation quantiles, especially important for the shortest durations and longest return periods. Accordingly, an intensification of the spatio-temporal scaling regimes of projected extremes was detected for most of the model grid boxes, as well as some important changes in the characteristics of the annual and daily cycles of precipitation AM.

Keywords: Extreme precipitation; Spatio-temporal scale; Scaling; Climate change.

Contents

Remerciements

Résumé

Abstract

Contents **iii**

| | |
|----------------------------|-----|
| List of Figures | vii |
| List of Tables | ix |
| List of Acronyms | xi |

Synthèse **xiii**

| | |
|---|------|
| Problématique | xiii |
| Analyse multi-échelle des précipitations extrêmes | xv |
| Les modèles des lois d'échelle | xvii |
| Objectifs, méthodologie et synthèse des résultats | xix |
| Plan de la thèse | xxi |

Introduction **1**

I Literature review, objectives, and methods **5**

1 Extreme precipitation: preliminary considerations **7**

| | |
|---|----|
| 1.1 Complex spatio-temporal structure of precipitation extremes | 11 |
| 1.2 Biases and uncertainty in recorded precipitation series | 12 |
| 1.3 Use of climate models to estimate extreme precipitation | 14 |

2 Climate Change (CC) impacts on mean and extreme precipitation **19**

| | |
|--|----|
| 2.1 Observed changes in historical climate | 20 |
| 2.2 Projecting CC | 22 |
| 2.3 Uncertainty in projected changes | 25 |

| | | |
|-----------|--|------------|
| 3 | Statistical modeling of precipitation extremes | 27 |
| 3.1 | Extreme Value Theory (EVT) for precipitation | 27 |
| 3.2 | Intensity-Duration-Frequency (IDF) curves | 32 |
| 3.3 | Areal Reduction Factors (ARFs) and Intensity-Duration-Area-Frequency (IDAF) curves | 34 |
| 4 | Scaling models for extreme precipitation | 39 |
| 4.1 | Scale invariance and self-similarity of precipitation | 39 |
| 4.2 | Simple Scaling (SS) models | 41 |
| 4.3 | Scale invariance in space and time | 44 |
| 4.4 | Multiscaling | 47 |
| 5 | Thesis overview | 49 |
| 5.1 | Research questions | 49 |
| 5.2 | Specific project objectives | 50 |
| 5.3 | Data and Study region | 52 |
| 5.4 | Annual Maxima (AM) extraction | 59 |
| II | Articles | 63 |
| 1 | Simple Scaling of extreme precipitation in North America | 65 |
| | Résumé en français | 66 |
| 1.1 | Introduction | 67 |
| 1.2 | Simple Scaling models for precipitation intensity | 69 |
| 1.3 | Data and study region | 72 |
| 1.4 | SS estimation through Moment Scaling Analysis (MSA) | 74 |
| 1.5 | Regional analysis | 84 |
| 1.6 | Simple Scaling GEV estimation | 87 |
| 1.7 | Discussion and conclusion | 92 |
| 2 | Observed and simulated precipitation over North East North-America: how do sub-daily extremes scale in space and time? | 99 |
| | Résumé en français | 100 |
| 2.1 | Introduction | 101 |
| 2.2 | Data and study area | 103 |
| 2.3 | Extraction of Annual Maxima series at various spatiotemporal scales | 107 |
| 2.4 | Statistical characterization of AM series | 108 |
| 2.5 | Evaluating dataset performances | 111 |
| 2.6 | Gridded dataset and station AM statistics at native resolution | 112 |
| 2.7 | Spatio-temporal scaling of AM rainfall | 115 |
| 2.8 | AM statistics for the CRCM5-LE | 118 |
| 2.9 | Summary and conclusion | 121 |
| 3 | Extreme precipitation under climate change: probability distributions, season- ality, and spatio-temporal scaling of sub-daily annual maxima. | 129 |

| | |
|--|------------|
| Résumé en français | 130 |
| 3.1 Introduction | 131 |
| 3.2 Data | 133 |
| 3.3 Methods | 134 |
| 3.4 Results | 140 |
| 3.5 Discussion and Conclusion | 152 |
| | |
| III Conclusion | 159 |
| | |
| 6 Discussion and conclusion | 161 |
| 6.1 Synthesis and discussion of results | 161 |
| 6.2 Original contributions | 167 |
| 6.3 Limitations and perspective on future works | 168 |
| | |
| Bibliography | 171 |
| | |
| IV Appendix | 185 |
| | |
| A GEV parameter estimation | 187 |
| A.1 Maximum Likelihood (ML) estimation | 187 |
| A.2 Probability Weighted Moment (PWM) estimation | 189 |
| | |
| S1 Supplementary Material of Article 1 | 191 |
| | |
| S2 Supplementary Material of Article 2 | 213 |
| | |
| S3 Supplementary Material of Article 3 | 231 |

List of Figures

Chapter 1

| | | |
|-----|---|----|
| 1.1 | Extreme precipitation definition | 10 |
| 1.2 | Characteristic spatial and temporal scales of various weather and climatic processes influencing precipitation extremes | 11 |
| 1.3 | Exemple of CGM and RCM grids and domains | 15 |
| 1.4 | Characteristic spatial resolution of GCMs and RCMs | 16 |

Chapter 3

| | | |
|-----|--|----|
| 3.1 | GEV probability distribution function: examples for several parameter values | 30 |
| 3.2 | GEV return level plots: examples | 31 |
| 3.3 | IDF curves for the PET Airport gage station, Montreal, QC | 33 |
| 3.4 | ARF as a function of the area and return period | 36 |
| 3.5 | ARF as a function of the area and duration | 37 |

Chapter 4

| | | |
|-----|---|----|
| 4.1 | Moment Scaling Analysis (MSA) | 42 |
| 4.2 | Scaling moment function - Multiscaling | 47 |
| 4.3 | Simple Scaling versus Multiscaling pdf scale change | 48 |

Chapter 5

| | | |
|-----|--|----|
| 5.1 | Stations and temporal resolution of recorded series | 53 |
| 5.2 | Spatial domains of gridded datasets: CRCM5, WRF, CMORPH, and MSWEP | 56 |

List of Tables

- 5.1 Station datasets for point-scale SS analysis 55
- 5.2 Stations and gridded datasets used for extracting extremes at various spatial scales . 59
- 5.3 Spatial scales considered for each gridded dataset. 60

List of Acronyms

| | |
|-----|-----------------------------|
| CC | Climate Change |
| CPM | Convection-Permitting Model |
| GCM | Global Climate Model |
| RCM | Regional Climate Model |

Datasets

| | |
|----------|---|
| 15PD | 15-Min Precipitation Data |
| CMORPH | Climate Prediction Center Morphing technique v1.0 CRT |
| CRCM5 | Canadian Regional Climate Model generation 5 |
| CRCM5-LE | CRCM5 Large Ensemble |
| DMPD | Daily Maxima Precipitation Data |
| HCPD | Hourly Canadian Precipitation Data |
| HPD | Hourly Precipitation Data |
| MSWEP | Multi-Source Weighted-Ensemble Precipitation v2 |
| WRF | Weather Research and Forecasting Model v3.4.1 |

Methods

| | |
|------|---|
| AM | Annual Maxima |
| AMS | Annual Maxima Series |
| ARF | Areal Reduction Factor |
| BM | Block Maxima |
| DDF | Depth-Duration-Frequency (curve) |
| EVT | Extreme Value Theory |
| GEV | Generalized Extreme Value (distribution) |
| IDAF | Intensity-Duration-Area-Frequency (curve) |
| IDF | Intensity-Duration-Frequency (curve) |
| ML | Maximum Likelihood |
| MS | Multiscaling (model) |
| MSA | Moment Scaling Analysis |

| | |
|-----|---------------------------------|
| POT | Peak-Over-Threshold |
| PWM | Probability Weighted Moments |
| SS | Simple Scaling (model) |
| STS | Spatio-Temporal Scaling (model) |

Synthèse

La compréhension de la structure des précipitations extrêmes est devenue une problématique critique en météorologie et climatologie puisque l'évaluation des risques environnementaux dépend de la prévision des aléas naturels. Les précipitations extrêmes sont associées à des événements potentiellement dangereux tels que les inondations ou les sécheresses, mais sont aussi impliquées dans la gestion des ressources (par exemple ressources en eau douce, agriculture, territoires forestiers), les plans d'aménagement à long terme, et la sécurité publique (Seneviratne et al. [2012](#); Field et al. [2014](#)). La caractérisation des événements de précipitations extrêmes est cruciale pour la conception des infrastructures (Mailhot et Duchesne [2010](#)) et dans l'évaluation et la prévision de l'impact des aléas naturels sur les écosystèmes et les sociétés humaines.

Problématique

Plusieurs méthodes existent pour mesurer et enregistrer les précipitations, notamment les pluviomètres aux stations météorologiques, les radars météorologiques et les mesures satellites (Tapiador et al. [2017](#)). Cependant, suite à la faible densité et couverture spatiale et temporelle des observations, il est difficile de caractériser la structure spatio-temporelle complexe des précipitations (Cooley et al. [2007](#); Kidd et al. [2016](#); Trenberth et al. [2017](#)). De plus, en ayant à disposition des séries courtes, il est impossible de tenir compte des tendances à long terme ou des cycles qui peuvent affecter les précipitations et il n'est pas possible de constituer un échantillon de taille adéquate pour l'analyse des précipitations extrêmes qui, par définition, sont rares (Kunkel [2013](#)).

Par exemple, seules quelques décennies de données sont disponibles au Canada (Mekis et Vincent [2011](#)), ce qui rend impossible une fine caractérisation des tendances temporelles des précipitations. De même, le réseau de stations pluviométriques en Amérique du Nord n'est pas assez dense pour

capter systématiquement les événements intenses de courte durée (p. ex., quelques heures) qui sont généralement produits par des systèmes météorologiques très localisés (par exemple dans les régions montagneuses de l'ouest des États-Unis; Kunkel 2013).

De nombreux efforts ont été consacrés à la mise au point de bases de données complémentaires, incluant des simulations de modèles dynamiques météorologiques et climatiques (p. ex. Mearns et al. 2007; Scinocca et al. 2016), des jeux de données interpolées sur grille (p. ex. Haylock et al. 2008), et des séries de réanalyses produites par l'assimilation de données observées dans les modèles numériques (p. ex. Dee et al. 2011; Rienecker et al. 2011). Bien qu'elles soient constituées par des séries couvrant de vastes territoires faiblement couverts par des stations météorologiques, les bases de données complémentaires présentent d'autres désavantages en termes de résolution temporelle ou spatiale ou au niveau des périodes de temps couvertes (Arritt et Rummukainen 2010; Flato et al. 2013). Par exemple, les Modèles climatiques globaux (MCG) et les Modèles régionaux du climat (MRC) présentent encore des résolutions trop grossières (typiquement de 200 km à 10 km environ) pour reproduire de manière satisfaisante les systèmes météorologiques qui génèrent le plus souvent les précipitations extrêmes (Rummukainen 2016; Kendon et al. 2017). De même, les réanalyses qui utilisent des données satellites ou radars couvrent généralement seulement les décennies les plus récentes et présentent souvent les mêmes limitations que les MRC pour la simulation des extrêmes de précipitation de courte durée.

Ces limitations deviennent d'autant plus contraignantes quand l'intérêt porte sur l'évolution temporelle des extrêmes climatiques. Comme le climat évolue sous l'effet de différents facteurs de forçages (naturels et anthropiques), il est probable que plusieurs caractéristiques des précipitations évoluent aussi. Certains de ces changements ont déjà été observés, notamment l'intensification et l'accélération du cycle hydrologique en réponse à l'augmentation globale de température. Suivant l'expression "*intensification hydro-climatique*" introduite par Giorgi et al. (2011), cela signifie qu'une augmentation de la sévérité des fortes précipitations est attendue de pair avec une diminution du nombre total de ces événements.

Cependant, en plus des difficultés qu'on rencontre dans la collecte des données, l'analyse de l'évolution temporelle des caractéristiques des précipitations extrêmes est complexifiée par le fait que différentes sources de variabilité spatiale et temporelle agissent sur les chroniques de précipitations (Hawkins et Sutton 2009; Deser et al. 2012a). En particulier, les fluctuations temporelles des

séries des précipitations dues à la *variabilité naturelle du climat* rendent difficile l'estimation des changements à long terme des statistiques des précipitations extrêmes. Cette variabilité naturelle est en fait associée à la nature chaotique du système climatique et peut amplifier significativement l'importance des erreurs d'échantillonnage, en particulier aux échelles spatiales fines et pour les événements les plus extrêmes intervenant sur des durées courtes (Hawkins 2011; Deser et al. 2012a). Dans le but de produire des estimations des changements intervenus en climat passé et des projections fiables de l'évolution future des précipitations extrêmes, la différenciation des impacts des différentes sources de variabilité à des échelles spatio-temporelles variées est d'autant plus importante. Notamment, la distinction doit être faite entre les changements des précipitations extrêmes dus aux forçages anthropiques et ceux connectés à la variabilité naturelle du climat. De plus, la compréhension de la manière dont ces changements affectent les caractéristiques des précipitations aux différentes échelles spatiales et temporelles est importante pour appréhender la nature des modifications du climat et ses possibles impacts sur les écosystèmes régionaux et locaux.

Analyse multi-échelle des précipitations extrêmes

Le besoin d'analyses multi-échelles des précipitations extrêmes a largement été reconnu dans le passé (Rodriguez-Iturbe et al. 1984; Blöschl et Sivapalan 1995; Hartmann et al. 2013; Westra et al. 2014), et des efforts particuliers ont été consacrés au développement de relations pouvant lier les caractéristiques statistiques des précipitations à différentes durées et différentes résolutions spatiales.

L'approche conventionnelle pour décrire les transitions d'échelle entre plusieurs durées consiste à construire des courbes d'Intensité-Durée-Fréquence (IDF) (Bernard 1932; Sivapalan et Blöschl 1998; Koutsoyiannis et al. 1998; Veneziano et Yoon 2013) ou, de manière équivalente, des courbes Hauteur-Durée-Fréquence (en anglais *Depth-Duration-Frequency*, DDF). Ces courbes sont couramment utilisées dans la conception des ouvrages hydrauliques et dans l'analyse des risques liés aux extrêmes puisqu'elles décrivent les relations entre la fréquence d'occurrence d'évènements de précipitations ayant une intensité (hauteur) donnée, $x_{d,T}$, et leurs durées d (p. ex. CSA 2012). Dans cette représentation, la fréquence d'occurrence des évènements de précipitations est généralement exprimée en termes de *période de retour* T (Rootzén et Katz 2013), définie comme l'inverse de la probabilité de dépassement annuelle de la valeur $x_{d,T}$, qui est donc appelée *niveau de retour*. Un exemple de courbe IDF est présenté en Fig. F1.

Les courbes IDF et DDF sont typiquement définies en estimant séparément les distributions de probabilité de X_d sur différentes durées (voir Koutsoyiannis et al. 1998 et Papalexiou and Koutsoyiannis 2013a sur les discussions des distributions de probabilité généralement utilisées). Les paramètres ou les quantiles de ces distributions théoriques sont ensuite reliés de manière empirique les uns aux autres pour décrire les variations des propriétés des précipitations extrêmes sur l'ensemble des durées considérées. Malgré sa simplicité, cette procédure présente de nombreux désavantages. En particulier, elle ne garantit pas la cohérence statistique des distributions des précipitations puisque celles-ci sont estimées indépendamment sur les durées considérées. De plus, cette méthode ne permet pas d'extrapoler les IDF à des échelles de temps non observées ou à des sites non jaugés. Les incertitudes sur les quantiles estimés sont aussi importantes puisque les distributions des précipitations et les paramètres des courbes IDF sont estimés séparément.

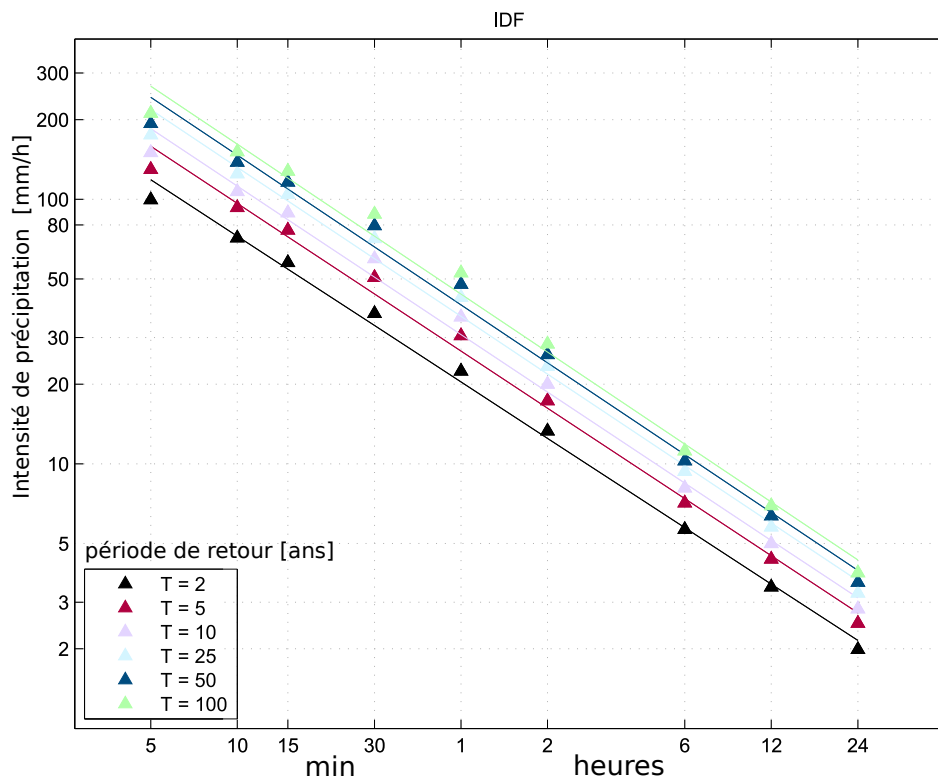


Figure F1: Exemple de courbe IDF estimée à partir des précipitations observées à la station météorologique de l'aéroport Pierre-Elott-Trudeau (Montréal, Québec) pour la période 1943 – 1993. Adaptée de *Fichiers IDF, Ensembles de données climatiques en génie, ECRC*. http://climate.weather.gc.ca/prods_servs/engineering_f.html

Basée sur une approche similaire, la définition de coefficients d'abattement spatial (en anglais *Areal-Reduction-Factors*, ARF) est un outil standard permettant de relier statistiquement les intensités de précipitations ponctuelles (c'est-à-dire des extrêmes estimés à des stations météorologiques) et les intensités de précipitation sur une surface (Svensson et Jones 2010). Le coefficient d'abattement spatial pour une période de retour T est défini comme le ratio entre le niveau de retour de précipitations estimée sur une surface A et pour une durée d et l'intensité ponctuelle (à la station) correspondante pour les mêmes T , A et d .

Dans la pratique, les coefficients d'abattement spatial sont souvent estimés de manière empirique en moyennant les estimations des niveaux de retour des précipitations extrêmes ponctuelles disponibles sur une surface A couvrant le territoire visé (Musy et Laglaine 2005). De nombreuses approches analytiques ont été aussi proposées (Svensson et Jones 2010). Cependant, ces approches ne modélisent pas explicitement la dépendance des coefficients d'abattement spatial à la durée de la précipitation, alors que ceux-ci devraient augmenter avec d (Veneziano et Langousis 2005; Ceresetti 2011). L'autocorrélation spatiale qui définit la structure des précipitations dépend en fait largement de d puisque les événements de plus haute intensité sont généralement associés à des systèmes météorologiques ayant une étendue spatiale réduite et une durée de vie courte. Les méthodes permettant d'estimer simultanément les paramètres des distributions de probabilité des extrêmes de précipitations et ceux décrivant la variation des coefficients d'abattement spatial avec A et d devraient donc être préférées.

Les modèles des lois d'échelle

Des modèles des lois d'échelle (modèles de *scaling*, en anglais) (Lovejoy et Mandelbrot 1985; Gupta et Waymire 1990; Veneziano et al. 2007) basés sur le concept de l'invariance d'échelle (Dubrulle et al. 1997) ont été proposés pour relier les distributions de probabilité des précipitations à différentes échelles spatiales et temporelles. Selon l'invariance d'échelle, les caractéristiques statistiques (par exemple les moments ou les quantiles des distributions) des intensités des précipitations observées à deux différentes échelles ℓ et $\lambda\ell$ peuvent être reliées entre elles par une loi de puissance de la forme:

$$f(X_{\lambda\ell}) = \lambda^H f(X_\ell), \quad (\text{F1})$$

où $f()$ est une fonction de X dont la forme ne varie pas quand on change l'échelle d'observation de la variable X d'un facteur multiplicatif λ^H et où H est un scalaire ($H \in \mathbb{R}$).

Dans le cas le plus simple, un facteur multiplicatif constant suffit à représenter correctement le changement d'échelle. Les modèles statistiques correspondants sont connus sous le nom de modèles *Simple Scaling* (SS) (Gupta et Waymire 1990). Ces modèles sont attrayants vu le petit nombre de paramètres impliqués. Un seul exposant de changement d'échelle, H , est en fait utilisé pour caractériser les relations entre les distributions de probabilité des précipitations extrêmes à toutes les échelles pour lesquelles le principe de l'invariance d'échelle est valable.

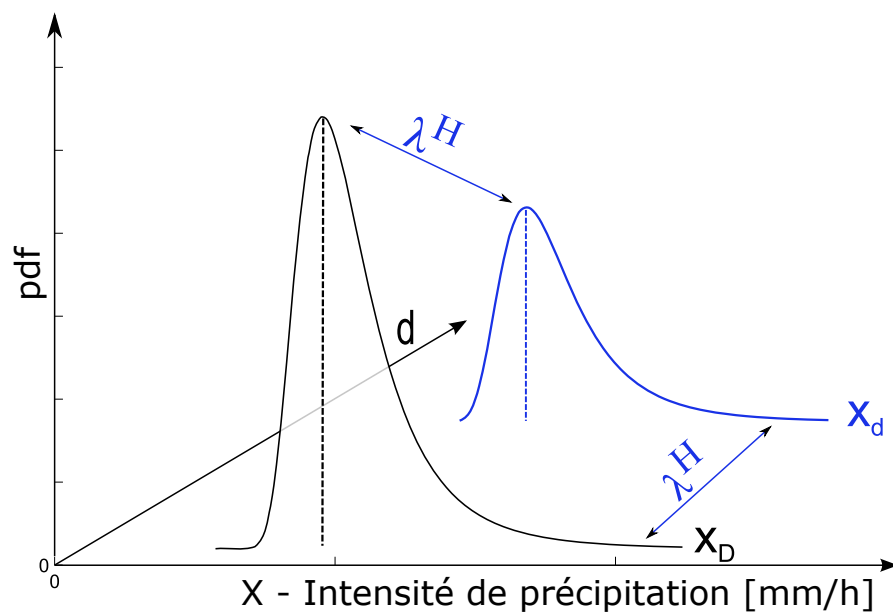


Figure F2: Modèle de Simple Scaling (SS) temporel: les distributions de probabilité des intensités de précipitations observées à différentes durées d et D sont reliées entre elles par le facteur multiplicatif $\lambda^H = (d/D)^H$.

Par conséquent, une estimation efficace des caractéristiques des précipitations extrêmes est possible, même pour des échelles partiellement non-observées. Par exemple, on pourrait inférer les quantiles de précipitations extrêmes de durée $d = 1\text{h}$ à partir des séries des précipitations observées à l'échelle journalière.

À partir de relations du même type que l'Éq. (F1), des formulations parcimonieuses des courbes IDF et des coefficients d'abatement spatial sont aussi possibles (Menabde et al. 1999; Burlando et Rosso

1996; De Michele et al. 2001; Veneziano et Furcolo 2002; Panthou et al. 2014). Ces courbes et coefficients peuvent donc être estimés analytiquement tout en tenant compte des propriétés statistiques de X aux différentes durées d et surfaces spatiales A .

Tout aussi important, l'impact des changements climatiques sur la structure spatio-temporelle des précipitations extrêmes peut être évalué et décrit synthétiquement en caractérisant l'évolution temporelle des paramètres des lois d'échelle.

Plusieurs études ont confirmé la validité des modèles de lois d'échelle temporelles (*Simple Scaling* temporel) pour les distributions des extrêmes de précipitations (Gupta et Waymire 1990; Burlando et Rosso 1996; De Michele et al. 2001; Boukhelifa et al. 2018). Néanmoins, l'application de ces modèles a été généralement restreinte à de petites bases de données et des régions géographiques peu étendues. Une analyse plus fine des facteurs géoclimatiques définissant et influençant les lois d'échelle et une évaluation extensive de leur validité sur plusieurs intervalles d'échelles spatiales et temporelles est donc nécessaire avant d'analyser leur évolution en climat futur.

Objectifs, méthodologie et synthèse des résultats

La présente étude a pour but d'approfondir les connaissances sur la structure spatiale et temporelle des précipitations extrêmes dans le cadre de la théorie de l'invariance d'échelle. En particulier, on cherche à définir des relations analytiques reliant les distributions de probabilité des extrêmes de précipitations à différentes échelles spatio-temporelles pour produire une caractérisation détaillée de la variabilité des champs des précipitations. Pour ce faire, les modèles des lois d'échelle existant dans la littérature seront initialement considérés. La représentation synthétique des caractéristiques des précipitations que de tels modèles fournissent sera utilisée pour comparer la description des précipitations fournie par divers ensembles de données, différentes régions spatiales et pour différentes périodes pour évaluer comment les précipitations extrêmes journalières et sous-journalières répondent au réchauffement climatique.

Le premier objectif de la présente étude était donc de valider l'usage des modèles des lois d'échelle pour la description des propriétés statistiques des Maxima Annuels (MA) de précipitation sur une grande partie de l'Amérique du Nord (Canada et États-Unis) en utilisant un grand nombre de séries

des précipitations mesurées aux stations météorologiques.

La validité statistique des modèles de SS temporel a été confirmée pour une vaste gamme de durées entre 15 min et 7 jours. La possibilité de construire des courbes IDF basées sur l'hypothèse d'invariance d'échelle a été évaluée, en considérant les performances des modèles de SS dans l'approximation des quantiles extrêmes des distributions de probabilité des MA. Finalement, l'analyse de la variabilité spatiale des paramètres de SS temporel à travers le domaine a montré l'influence des caractéristiques géographiques et climatiques locales sur les estimations des lois d'échelle, en soulignant l'importance de les considérer pour l'estimation des paramètres des courbes IDF.

Le second objectif était d'investiguer comment les estimations des lois d'échelle varient quand on change les jeux de données utilisés pour l'extraction des MA de précipitations. Ceci avait pour but de décrire l'influence des caractéristiques des données (par exemple leur résolution temporelle ou la résolution de mesure) sur la représentation de la structure spatio-temporelle des précipitations extrêmes que l'on peut en tirer.

La validité de l'invariance d'échelle des précipitations extrêmes a été ainsi vérifiée pour plusieurs ensembles de données sur grille, tant observés que simulés. Les jeux de données suivants ont été considérés pour l'extraction des séries de précipitations:

- les données satellites CMORPH produites par correction de biais (Xie et Xiong 2011);
- l'ensemble MSWEP, obtenu par l'interpolation de séries provenant de différentes sources (données satellites, séries aux stations et données de réanalyses) (Beck et al. 2017a);
- une simulation provenant du modèle WRF à haute résolution (4 km) (Liu et al. 2017; Prein et al. 2017a);
- les séries issues d'un grand ensemble simulé par le Modèle Régional Canadien du Climat de 5^{ème} génération (MRCC5) (Martynov et al. 2013; Separovic et al. 2013; Leduc et al. 2019).

En comparant les estimations des modèles de SS pour ces ensembles de données sur grille, l'analyse a montré l'influence que les caractéristiques de base des jeux de données (p.ex. leur résolution spatiale ou temporelle) ainsi que les techniques de traitement des séries (p. ex. les méthodes de correction de biais) ont sur l'estimation des lois d'échelle pour des durées entre 1 h et 3 jours.

Les modèles de SS temporel estimés pour différentes échelles d'agrégation spatiale ont été ensuite comparés. Les résultats suggèrent qu'une simple expression analytique décrit la variation des paramètres de SS temporel à différentes échelles spatiales. Ceci permet de définir un modèle des lois d'échelle spatio-temporelle (*Spatio-Temporal Scaling*, STS) reliant les quantiles des distributions de probabilité des MA de précipitations sur une vaste gamme d'échelles spatio-temporelles. En utilisant cette nouvelle relation analytique, il serait en théorie possible d'estimer les courbes IDF et les coefficients d'abattement spatial (ARF) même à des endroits non jaugés, c'est-à-dire les endroits où aucune station météorologique n'est disponible pour enregistrer les séries de précipitations.

Finalement, le troisième objectif était d'évaluer l'évolution temporelle des propriétés des précipitations extrêmes sous l'effet des changements climatiques en se basant sur des séries projetées par MRCC5 sur la période 1950-2100. Afin de déterminer l'impact des diverses sources d'incertitude et de variabilité sur les estimations de précipitations extrêmes, les modèles de STS ont été estimés pour des échantillons de MA provenant des 50 membres du grand ensemble du MRCC5 et combinés sur de courtes périodes de temps (par exemple des périodes de 3 ou 7 ans).

Les résultats décrivent comment les distributions des précipitations extrêmes vont évoluer dans les décennies à venir, en mettant en évidence l'intensification critique des quantiles des distributions des MA pour tout le domaine spatial à l'étude. Environ 99% des points de grille du MRCC5 présentent en fait des tendances temporelles significatives des quantiles de MA pour des durées de 24h ou moins. En ce qui concerne les lois d'échelle, ces résultats se traduisent par une modification significative des paramètres des modèles STS projetés pour les décennies à venir. Aussi, les analyses sur les séries du grand ensemble du MRCC5 illustrent l'influence de changements climatiques sur les caractéristiques des cycles annuels et journaliers d'occurrence des MA de précipitations.

Plan de la thèse

Le manuscrit est structuré tel que suit. La Partie I décrit les aspects de la caractérisation des précipitations extrêmes qui posent défis, les solutions proposées dans la littérature ainsi que les objectifs du projet. Après une discussion générale à propos des problèmes liés à la définition et la modélisation des précipitations extrêmes (chapitre 1), le chapitre 2 présente les principaux problèmes liés à l'évaluation des impacts des changements climatiques sur les précipitations extrêmes quotidiennes et sous-quotidiennes. Le cadre statistique de l'analyse des précipitations extrêmes et la formulation

théorique des modèles des lois d'échelle sont présentés dans les chapitres 3 et 4. Finalement, la méthodologie, les jeux de données disponibles et les objectifs détaillés du projet sont décrits dans le chapitre 5.

La Partie II rassemble les trois articles scientifiques qui ont été produits dans le cadre de cette thèse et qui adressent les trois objectifs principaux de l'étude:

- L'article 1: "*Simple Scaling of extreme precipitation in North America*". Innocenti, S., Mailhot, A., et Frigon, A. Publié sur en Novembre 2017, Hydrol. Earth Syst. Sci., 21, 5823-5846, <https://doi.org/10.5194/hess-21-5823-2017>, 2017.
- L'article 2: "*Observed and simulated precipitation over North East North-America: how do sub-daily extremes scale in space and time?*". Innocenti, S., Mailhot, A., et Frigon, A., Cannon, A.J., Leduc, M. En révision.
- L'article 3: "*Extreme precipitation under climate change: probability distributions, seasonality, and spatio-temporal scaling of sub-daily annual maxima*". Innocenti, S., Mailhot, A., et Frigon, A., Cannon, A.J., Leduc, M. Prêt à soumettre.

Finalement, la Partie III présente une synthèse et une discussion des résultats. Les principales conclusions de l'étude sont aussi discutées, ainsi que les perspectives sur des possibles développements futurs de l'étude.

Introduction

Understanding the behavior of extreme precipitation has become a critical issue in weather and climate research as environmental risk assessment depends heavily on our ability to predict natural hazards. Being often associated with potentially critical events such as floods and droughts, heavy precipitation also has strong implications in monitoring resources (e.g. freshwater and agricultural resources or forests), in long-term planning, and for public safety [Seneviratne et al. 2012; Field et al. 2014]. Characterizing extreme precipitation events is thus crucial for infrastructure design and evaluating and predicting the impacts of natural hazards on ecosystems and human societies.

Several monitoring techniques exist for recording precipitation, including gauge-stations, ground-based weather radars, and satellite measurements [Kidd et al. 2016; Tapiador et al. 2017]. However, the sparsity of the measurement networks makes it difficult to capture the complex spatial structure and the intermittent temporal patterns of precipitation [Cooley et al. 2007; Trenberth et al. 2017]. Additionally, the usually short records do not allow an accurate investigation of trends and cycles. Finally, the errors and uncertainties associated with both direct (stations) and indirect (e.g., radar and satellite) measurements further hinder detecting the complex structure of precipitation systems [AghaKouchak et al. 2012; Beck et al. 2017b].

Several efforts have been also devoted to the development of complementary datasets, including dynamical weather and climate model simulations [e.g., Mearns et al. 2007; Scinocca et al. 2016], interpolated gridded datasets [e.g., Haylock et al. 2008], and reanalysis products [e.g., Dee et al. 2011; Rienecker et al. 2011]. Although providing precipitation series with complete spatial coverage over regions sparsely covered by existing observational networks, each of these datasets comes with drawbacks in terms of either its temporal or spatial resolution or the covered time period [Arritt and Rummukainen 2010; Flato et al. 2013]. For instance, Global Climate Models (GCMs) and

Regional Climate Models (RCMs) still have too coarse spatial resolutions (typically from about 200 km to 10 km) to adequately reproduce small weather systems, which are likely to generate short duration precipitation extremes [Rummukainen 2016; Kendon et al. 2017]. Similarly, reanalyses which use satellite and radar among other data sources, usually cover only the most recent decades. Finally, biases and uncertainties related to data interpolation techniques [Hofstra et al. 2008], and inhomogeneity of the underlying observed series should be taken into consideration when considering gridded datasets [Gervais et al. 2014b; Beck et al. 2017b].

These constraints become further onerous when we are interested in the climatic evolution of the extremes. As the climate system evolves under the stimulus of different forcing factors (e.g., external forcing from volcanic atmospheric aerosols, or human induced changes in greenhouse gases), it is likely that many characteristics of precipitation will change as well. Some of these changes have already been observed. The main evidence is the higher *hydro-climatic intensity* in response to the global increase of temperature and atmospheric water holding capacity. Following the terminology introduced by Giorgi et al. (2011), this means that the severity of heavy precipitation is expected to increase while the total number of precipitation events is expected to decrease. However, the assessment of the temporal evolution of extreme precipitation characteristics is further complicated by the presence of several sources of spatial and temporal variability in precipitation series [Hawkins and Sutton 2009; Deser et al. 2012a]. In particular, the *natural climate variability* associated with the chaotic nature of the climate system may hide the climate change signal for precipitation extreme statistics and amplify sampling errors, especially at small spatial scales, short durations, and for the most extreme events [Hawkins 2011; Deser et al. 2012a].

In order to produce reliable assessments of observed and projected changes, it is important to better characterize how these changes affect precipitation at various scales in order to fully understand the nature of climate modifications and their possible impacts on regional and local ecosystems.

One interesting paradigm for conducting a multi-scale analysis of extreme precipitation is the *scaling model* framework [Schertzer and Lovejoy 1987; Menabde et al. 1999], based on the concept of *scale-invariance* [Dubrulle et al. 1997]. Physical evidence of the scale-invariant properties of precipitation has been provided by several studies [e.g., Gupta and Waymire 1990; Burlando and Rosso 1996; De Michele et al. 2001; Boukhelifa et al. 2018]. Scaling models define relationships between the statistical characteristics (e.g., moments or quantiles) of precipitation extremes estimated at different spatial and temporal scales. Accordingly, the statistical spatio-temporal structure of pre-

precipitation extremes may be in principle approximated for non-observed spatio-temporal scales. The impact of climate changes may also be evaluated at various scales through the evolution of extreme scaling properties in time.

Research questions and project objectives

The present study aims to deepen the knowledge on the spatial and temporal structure of precipitation extremes within the framework of the scale invariance theory. In particular, the relationships occurring between the probability distributions of extremes at different spatio-temporal scales were investigated. Scaling models were also used for comparing precipitation features from various datasets and to evaluate how daily and sub-daily precipitation extremes respond to climate warming over different time-horizons.

Several data sources were thus considered: i) observed series at stations (gauge measurements provided by the Environment and Climate Change Canada, ECCC, and the *Ministère du Développement Durable, de l'Environnement et de la Lutte contre les Changements Climatiques*, MDDELCC, networks for Canada and from NOAA precipitation datasets for United states); ii) the CMORPH bias-corrected satellite dataset [Xie and Xiong 2011], iii) the Multi-Source Weighted-Ensemble Precipitation (MSWEP) v2 [Beck et al. 2017a], iv) a series simulated by the convection-permitting Weather Research and Forecasting model (WRF) [Liu et al. 2017; Prein et al. 2017a], and v) a 50-member ensemble recently produced by the 5th generation of the Canadian Regional Climate Model (CRCM5) [Martyanov et al. 2013; Separovic et al. 2013; Leduc et al. 2019].

The first specific objective of the present study was to validate the use of scaling models for describing the spatial-temporal structure of daily and sub-daily extreme precipitation over most of North-America using observational datasets. To this end, the validity of temporal Simple Scaling (SS) was evaluated and confirmed over a broad range of temporal scales considering Annual Maxima (AM) precipitation from 1 h to 3 days and using a large number of station series (≈ 2700 meteorological stations). The accuracy of SS estimation for approximating empirical AM quantiles was evaluated. The spatial variability of the estimated temporal scaling parameters across the domain was then investigated, providing important guidance on the influence of both local geographical characteristics and regional climatic features on extreme precipitation scaling.

The second specific objective was to investigate the influence of dataset characteristics (e.g., their temporal and spatial resolution) on the scale-invariant properties of daily and sub-daily precipitation extremes. The validity of temporal SS was thus verified for observational gridded datasets and simulated series. The analysis illustrated the influence on scaling estimation of basic datasets characteristics, such as their temporal or measurement resolutions, and series processing techniques, such as bias correction methods. Finally, the temporal SS estimates for various spatial scales were considered for gridded datasets. Results suggest that a synthetic analytical expression can be used for describing the scaling of AM precipitation quantiles across a wide range of spatio-temporal scales.

The third objective was to assess the temporal evolution of scaling models under climate change based on the CRCM5 Large-Ensemble (CRCM5-LE) simulated series. Series from various members of the CRCM5-LE members were pooled and AM scaling models were compared across different time-horizons and spatial regions. To better characterize changes in the meteorological systems generating AM, the temporal evolution of AM annual and daily cycles were also investigated. The results describe how extreme precipitation distributions evolve in future decades and underline the critical intensification of their spatio-temporal scaling regimes. The analysis also illustrates the influence of sampling errors and uncertainty related to the natural climate variability on the spatio-temporal scaling of extreme precipitation at local and regional scales. Finally, important modifications in annual and daily cycles of AM were also observed.

Thesis structure

The manuscript is structured as follows. Part I discusses the specific challenges related to extreme precipitation analysis, reports some approaches proposed in the literature, and describes the thesis objectives and methods. Part II gathers the scientific articles produced, each of them addressing one specific thesis objective. Finally, Part III summarizes the results, underlines the original contributions, and presents the limitations of the study and perspective on future works.

Part I

Literature review, objectives, and methods

Chapter 1

Extreme precipitation: preliminary considerations

This chapter introduces the basic concepts related to extreme precipitation analysis, focusing on challenging aspects of data collection and dynamical simulation of precipitation extremes.

What are precipitation extremes ?

Heavy precipitation monitoring at global and local scales is critical for environmental risk assessment, resource management (e.g., water supply and quality issues), and infrastructure design [East-erling et al. 2000b; Mailhot and Duchesne 2010; Seneviratne et al. 2012]. Severe weather episodes are a natural component of climatological systems and their effects highly depend on the exposure and vulnerability of the systems they impact on. As a result, it may be inadequate to define extreme weather events only in terms of their absolute magnitude or severity [Stephenson et al. 2008; McPhillips et al. 2018], and many definitions of extreme have been proposed in the climate science literature.

In the absence of an absolute characterization of what is "normal" and what is "extreme", meteorological and hydro-climatological extremes can only be identified in relation to their peculiarity of being uncommon [IPCC 2013]:

"An extreme weather event is an event that is rare at a particular place and time of year",

as opposed to "typical" states of the climate system in that particular place for the period considered. When the observed extreme weather conditions last for a relatively long period of time, such a season, the event may be considered as a climatological extreme, according to the mentioned definition of the IPCC (2013) Glossary. Detailed discussion about meteorological and climate extreme identification can be found in Seneviratne et al. (2012) and Westra et al. (2014), while general analyses of the problem of extreme characterization in natural and social sciences are presented in Albeverio et al. (2006) and McPhillips et al. (2018).

In the present study we will refer to "extreme precipitation" as any weather episode that produces the maximum value of precipitation depth or intensity in a given time frame (e.g., a year), regardless of other characteristics (e.g., either solid and liquid precipitation is considered) and of the type of event involving precipitation (thunderstorm, snowstorm, hurricane, cyclone, etc.). Expressions such as "extreme precipitation", "heavy precipitation", or "severe precipitation" will be thus considered as synonyms even if potentially different in essence.

Specifically, a precipitation event can be defined as any continuous manifestation of meteorological water falling in solid or liquid state on a given area at a given rate [Musy and Laglaine 2005]. The duration of this event may vary from few minutes to several hours, while its spatial extent can range from less than one to thousand square kilometers. However, precipitation can only be measured with respect to a fixed accumulation period and area. Since it is difficult to effectively assess the spatial extent of each particular event from available observations (e.g., meteorological stations), this characteristic has often been neglected in the analysis of extreme precipitation [e.g., Touma et al. 2018].

Precipitation events can be identified by considering the successions of contiguous time steps with precipitation greater than a specified minimum precipitation depth, and separated by a dry period of a minimal fixed length [Minimum Interevent Time, MIT; Dunkerley 2008]. However, following another approach, precipitation events are generally identified through the precipitation totals accumulated over a time interval (e.g., one hour) and a spatial window of fixed length [e.g., Karl and Knight 1998; Easterling et al. 2000a].

Accordingly, the following point-measures of precipitation are typically defined at a particular point in space for a selected duration, d :

Precipitation Depth [mm]: total precipitation amount collected over a time interval of length d , i.e.

$$Z_d(t) = \int_{t-d}^t Z(u)du, \quad (1.1)$$

where $Z(t)$ represents the precipitating water measured at a point in space, for instance at a gauge station, at time t .

Precipitation Intensity [mm/h]: average precipitation rate over d , i.e. $Y_d(t) = d^{-1}Z_d(t)$.

Spatially aggregated measures may be subsequently considered to characterize the spatial distribution of precipitation by simply considering the depth,

$$Z_{d,A}(t) = \frac{1}{A} \int_A Z_d(t, x)dx, \quad (1.2)$$

and the intensity, $Y_{d,A}(t) = d^{-1}Z_{d,A}(t)$, where \mathbf{x} is the vector of the spatial coordinates of an arbitrary point inside the area A over which precipitation is recorded or estimated.

The frequency of occurrence of precipitation extremes over a specific period can then be assessed from available precipitation records by considering the $Z_{d,A}(t)$ values that display some specified characteristics (e.g., depth or intensity values above a given threshold) for a fixed spatial scale A and duration d . For instance, considering the $Z_{d,A}(t)$ series as a realization of a random variable, precipitation extremes can be identified as the events with low frequency in historical observations, e.g. lower than 10% according to the IPCC (2013) report. In other words, extremes are defined as $Z_{d,A}(t)$ accumulations that have low probability of occurrence.

Figure 1.1 illustrates these concepts on a theoretical probability distribution used for the precipitation depth: extremes are identified as events in the tail of the distribution (violet part) defined, for example, as the interval of precipitation values above a given percentile.

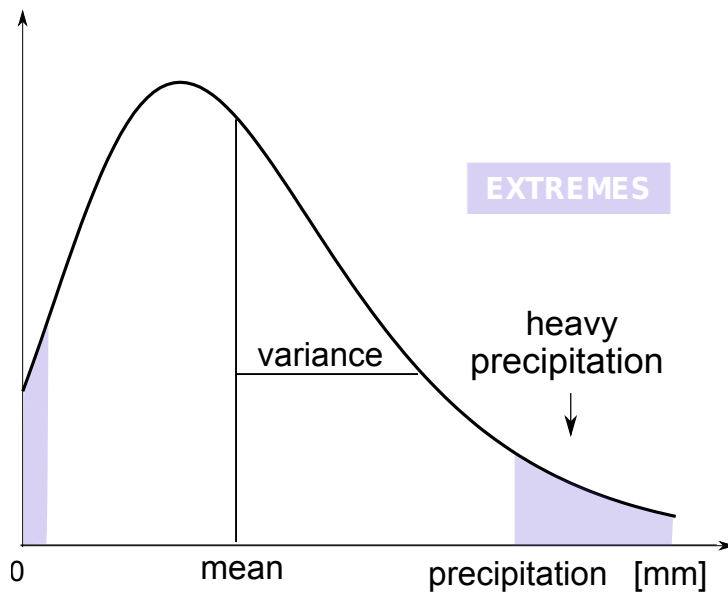


Figure 1.1: Extreme precipitation definition as the events with low probability of occurrence, i.e. associated to the tail of the precipitation distribution.

Once extreme events have been defined, three major issues must be considered:

- The complex spatio-temporal structure of severe precipitation events imposes a concurrent analysis of the spatial and temporal features of the extremes. Equally important, several sources of bias and uncertainties affect precipitation estimates and need to be accounted for when dealing with the extreme characterization.
- The chaotic nature of the climate system implies that extremes are subject to important variations over a wide range of spatial and temporal scales. The variability of precipitation extremes over these scales therefore needs to be considered.
- The rarity of the extremes, implicit in their definition, necessarily reduces the number of recorded extremes. Hence, adapted statistical techniques must be considered to efficiently extract the information from small observation samples and evaluate the impact of sampling errors on extreme characteristic estimates.

1.1 Complex spatio-temporal structure of precipitation extremes

Precipitation generation involves the combination of various atmospheric processes occurring at different spatial and temporal scales. For instance, large-scale mechanisms, such as front formation or convection, cause air to move and rise, cool down, and moisture to condense [Hand et al. 2004]. At the same time, specific micro-scale conditions must be met for vapor condensation and for droplets to coalesce into bigger drops and to produce precipitation [Trenberth et al. 2003; Hand et al. 2004].

Precipitation extremes further require specific favorable atmospheric conditions. For example, a strong powerful upward motion allowing air to rise quickly is usually needed to cause intense short-duration precipitation, while a continuous and abundant supply of moisture is needed for heavy precipitation events to take place over daily and longer durations [Trenberth et al. 2003; Kunkel 2013].

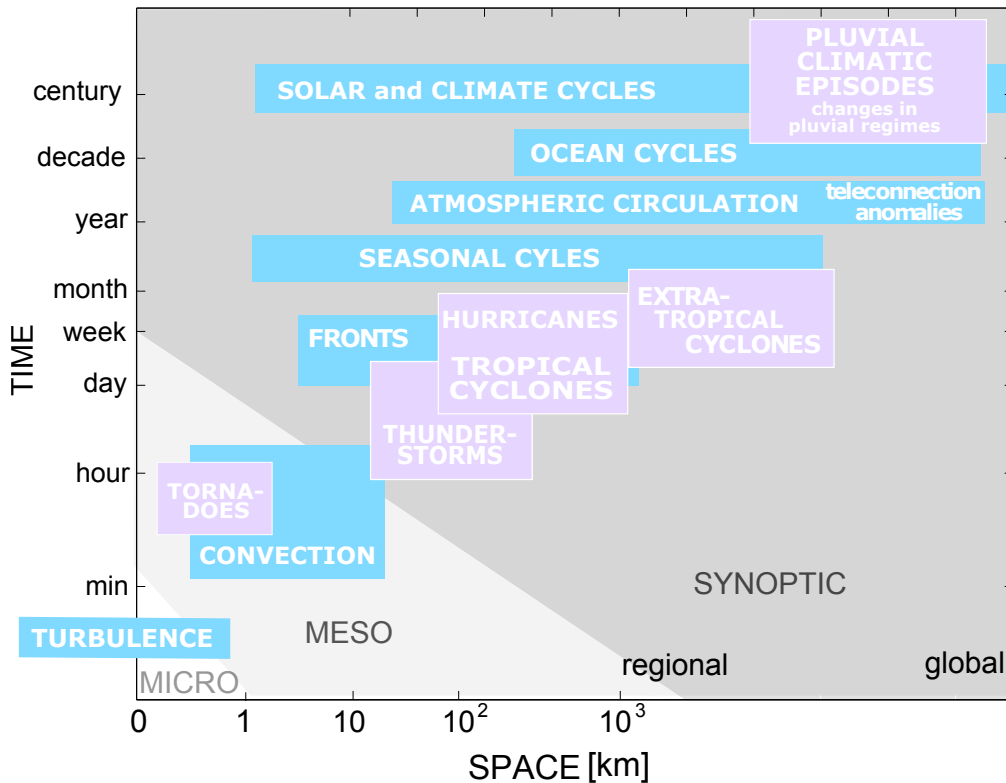


Figure 1.2: Characteristic spatial and temporal scales of various weather and climatic phenomena (violet) and related major sources of variability and atmospheric processes involved in precipitation generation (light blue). Adapted from Blöschl and Sivapalan (1995) and Westra et al. (2014).

Figure 1.2 depicts the characteristic temporal and spatial scales of the main weather and climatic processes involved in the generation of precipitation, illustrating the main spatial and temporal variability components influencing extreme characteristics.

The complex interactions between atmospheric and climate system components involved in precipitation genesis prevent a sharp distinction between the various sources of variability in precipitation series [Westra et al. 2014]. The chaotic and non-linear nature of the climate system further complicate these multi-scale interactions as small perturbations of the system at small spatio-temporal scales may rapidly result in drastic changes of system conditions at large scales.

However, the multi-scale nature of precipitation and the effects of the various variability sources on extremes are difficult to assess, primarily because of deficiencies in available observational and simulated precipitation datasets which limit our ability to adequately sample extremes across a wide range of spatio-temporal scales [Beck et al. 2017a; Herold et al. 2017].

1.2 Biases and uncertainty in recorded precipitation series

The evaluation of the possible biases and uncertainties present in recorded series is an essential preliminary step to any statistical analysis of extreme precipitation. Measurement errors in records and sampling errors due to short series and sparse networks are the major sources of biases and uncertainties which must be accounted for [Herold et al. 2017].

Several studies have demonstrated the presence of both systematic (i.e. constantly present) and random (i.e. variable in magnitude and timing) errors in precipitation series measured at ground-gauge stations, or estimated by radar and satellites.

The wind under-catchment effect has been recognized as a major cause of systematic gauge errors [e.g., Groisman and Legates 1994; Devine and Mekis 2008; Sevruk et al. 2009], mainly due to the deflection of rainfall and snow particles from measurement bucket [Metcalf et al. 1997]. Other important biases may also be produced under specific meteorological conditions which may cause evaporation loss, wetting loss¹ and trace precipitation (i.e., amounts that are below the instrument resolution) [Sevruk et al. 2009; Mekis and Vincent 2011].

¹Water that adheres to the walls of the pluviometer and is not measured in precipitation volume.

Significant uncertainties in gauge station estimates may also result from one-off events (e.g., damage of instruments) or changes in measurement technology and station locations, causing temporal inhomogeneities and discontinuities in records [Groisman and Legates 1994; Kunkel 2013]. More generally, precipitation measurements depend on station exposure and local environment (e.g., local topography) which affect both the quality and the spatial representativeness of gauge records [Tapiador et al. 2017; WMO 2008]. The aggregate effect of all these biases is an underestimation of precipitation, which can be larger than 10% of the observed rainfall depth, and than 100% for solid precipitation [Sevruk et al. 2009; Kochendorfer et al. 2017]. Reviews and examples of bias correction methods can be found in Adam and Lettenmaier (2003), Kochendorfer et al. (2017), and in the WMO (2008) report.

For remote sensing techniques (radar and satellites), the main sources of systematic errors are related to the empirical or theoretical relationship used to transform electromagnetic radiation measurements into precipitation amounts [Wright et al. 2017; Teegavarapu 2012]. Other factors such as topography and specific weather conditions (e.g., particular air humidity and temperature conditions) can seriously impact the measured electromagnetic signal [Berne and Krajewski 2013; Xie et al. 2017]. Despite these weaknesses, remote sensing techniques are superior to gauge products in spatial coverage and have relatively high temporal resolution. A pedagogical discussion about the working principles and uses of radars and satellites systems for precipitation measurement can be found in Teegavarapu (2012) and references therein.

1.2.1 Sampling issues

Sampling errors arise due to the fact that measurements are limited in space and time and do not record all occurring precipitation events. For instance, the average spatial density of major gauge networks in the United States has been estimated to be approximately one every 30-35km [Kunkel 2013]. Lower station densities, however, characterize the sparsely populated regions, such as the western intermountain United States and northern Canada. This strongly limits the possibility of recording many intense precipitation events.

The impacts of measurement density and coverage is dependent on the spatial heterogeneity and temporal intermittency of the specific type of extreme [Kunkel 2013]. For instance, short-duration

convective events are more rarely sampled by sparse networks as they are highly localized in space. Conversely, smaller uncertainties are expected for the estimation of long-duration event characteristics as they generally display higher spatial homogeneity [Gervais et al. 2014b].

1.2.2 Uncertainties related to interpolation techniques

Different spatial interpolation techniques are used to assess precipitation characteristics at non-sampled locations and to evaluate their spatial distribution. Uncertainties on resulting gridded datasets depend on the used interpolation method and can be especially important for extremes, because of the smoothing process involved in the transformation of sparse measures in gridded values [Tustison et al. 2001; Gervais et al. 2014b]. Also, the inhomogeneity of the underlying observed records may strongly affect the inference of precipitation characteristics from gridded datasets [Hofstra et al. 2009; Trenberth et al. 2017], as well as the topographic characteristics of the region under study [Daly et al. 2008]. Extremes, in particular, are altered by the interpolation in an incommensurable way with respect to the center of the precipitation distribution [Hofstra et al. 2009]. Accordingly, the interpolation of at-site precipitation series should be avoided when interested in sub-daily extremes, owing to the inherent high variability of precipitation at fine temporal and spatial scales [Kidd et al. 2016].

1.3 Use of climate models to estimate extreme precipitation

Datasets produced by meteorological and climatological models represent an interesting option to access data about extreme precipitation as they provide simulated precipitation series with complete spatial coverage over large regions [Arritt and Rummukainen 2010; Flato et al. 2013; Rummukainen 2016]. Models currently used in climate analysis are Global Climate Models (GCMs) and their regional version, Regional Climate Models (RCMs).

1.3.1 Global Climate Models (GCMs)

GCMs can generate Earth scale simulations over long time horizons [from decades to several centuries; e.g., Taylor et al. 2011]. Consisting of a discrete representations of the climate system [IPCC

2013], GCMs numerically reproduce the dynamics of the climate system and the complex interactions between the atmosphere, oceans, land surface (including vegetation) and cryosphere, and give access to precipitation series and future projections spanning the globe over a regular grid. However, due to their high complexity GCMs are computationally expensive and simulations are typically run at spatial resolutions that are too coarse [typically coarser than 100 km for state-of-the-art GCMs; Rummukainen 2016] to simulate small scale atmospheric processes which are relevant for most of precipitation extremes [Mearns et al. 2018]. In particular, GCMs rely on parameterized representations of processes which occur on scales too small to be directly resolved by the dynamical equations [e.g., convection and clouds and cloud processes occurring on smaller spatial scales than the model grid box; see, for instance, Fig. 1.2].

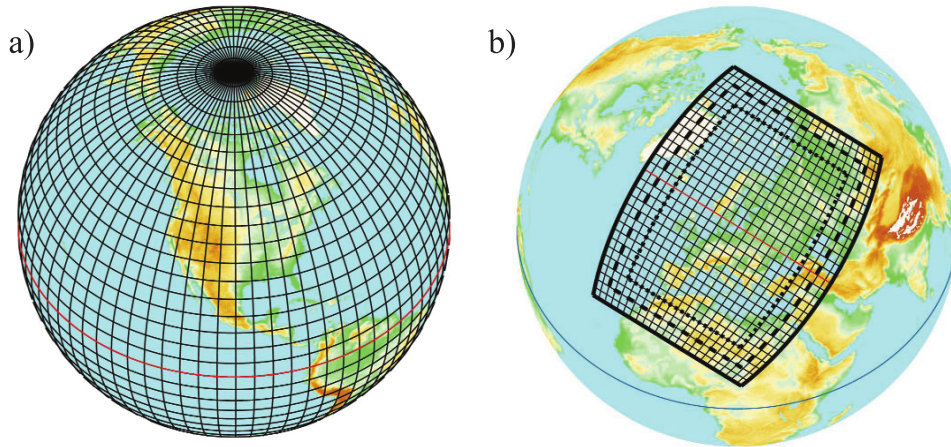


Figure 1.3: Examples of dynamical model grids and domains: a) global uniform grid typical of GCMs b) uniform grid over a limited-area domain typical of RCMs. For clarity, grid resolutions are coarser than state-of-the-art CGMs and RCMs. Adapted from Fig. 1 in Zadra et al. (2008).

1.3.2 Regional Climate Models (RCMs)

RCMs use representations of climate processes comparable to those of GCMs to numerically simulate the patterns of the climate system on smaller geographical areas [Mearns et al. 2018]. RCMs are forced by lateral and ocean conditions for large scale variables (e.g., winds, air temperature, and humidity) specified either from a GCM or reanalysis² and develop their own meteorology in

²Reanalyses are simulated datasets obtained by assimilating observed series from a variety of sources (e.g., ground meteorological stations, ships, and satellites) in Numerical Weather Prediction (NWP) models in order to simulate short term predictions. NWP forecasts are then updated in light of the new assimilated observations [e.g., Uppala et al. 2005; Dee et al. 2011; Parker 2016].

the interior of their domain in response to the large scale boundary conditions [e.g., Scinocca et al. 2016]. Running at higher spatio-temporal resolution than GCMs (e.g., from 12 to 50 km in space), state-of-the-art RCMs allow a more realistic representation of topography, land use, and their corresponding forcings (e.g., land-sea contrasts, sea surface temperature, and sea-ice coverage). An example of the topography details reproducible at the typical horizontal spatial resolutions of GCMs and RCMs are showed in Fig. 1.4. Moreover, RCMs are sometimes based on more sophisticated subgrid-scale parameterizations than GCMs, can rely on parameterization regional tuning, and allow for a better simulation of small scale atmospheric processes and coupled feedbacks which are relevant for precipitation and precipitation extremes [Rummukainen 2016].

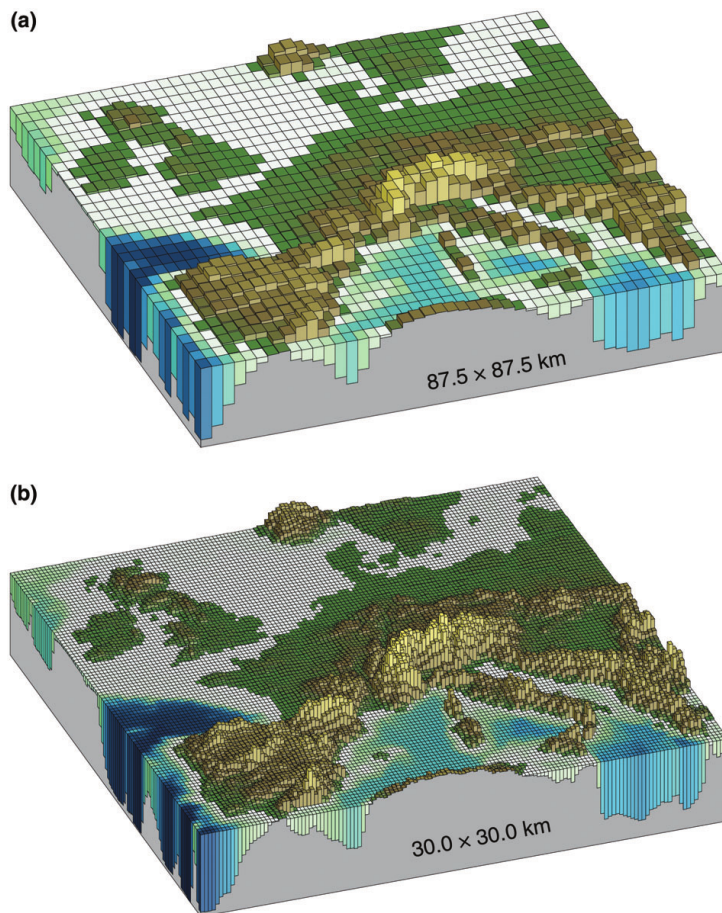


Figure 1.4: European topography at the horizontal spatial resolution of a) a very high-resolution GCM (87.5×87.5 km) and b) a typical state-of-the-art RCM (30×30 km). From Rummukainen (2016) [Fig. 2].

By means of comparative studies with observed data, RCMs have been shown to adequately reproduce the statistical properties of precipitation totals at annual and monthly time scale [Gutowski et al. 2010; Flato et al. 2013], though important inaccuracies have often emerged while comparing the distribution of simulated precipitation extremes to those estimated from records [e.g., Min et al. 2011; Gervais et al. 2014a]. More recently, some improvements in RCM structure, parameterization schemes, and spatial resolution have led to significant advances in RCM ability to simulate crucial features of precipitation such as the annual cycle and the statistics of daily rainfall extremes [e.g., Ban et al. 2014; Sunyer et al. 2016; Lucas-Picher et al. 2017].

However, RCMs may still display large biases for sub-daily extremes (e.g., diurnal cycle and hourly extremes), especially for regions and seasons where small spatio-temporal scale processes are the main driver of extreme events [Cavicchia et al. 2016; Kendon et al. 2017 and references therein]. This has been ascribed to two specific model limitations. First, the model spatial resolution is still too coarse to represent highly localized precipitation systems which are more often associated with extreme precipitation [Toreti et al. 2013; Gervais et al. 2014a; Hartmann 2015]. Second, the representation of physical processes involved in the generation of short-duration intense precipitation [i.e., the sub-grid parametrization; Hartmann 2015] is still inadequate [e.g., Westra et al. 2014; Liu et al. 2017]. This often results in too-frequently simulated light precipitation [the so-called *drizzling problem*; Dai 2006; Trenberth et al. 2017] and underestimated intensity and frequency of short duration heavy precipitation, as it also happens for GCMs [Gutowski et al. 2007; Stephens et al. 2010; Woodhams et al. 2018].

Promising approaches for improving the simulation of short duration extremes rely on the use of Convection-Permitting Models (CPMs) [e.g., Ban et al. 2015; Prein et al. 2015; Dai et al. 2017]. Running simulations at grid resolutions of a few kilometers, CPMs more completely resolve physical equations of deep convection with a limited use of parametrization schemes [Prein et al. 2017b; Rasmussen et al. 2017]. This is expected to improve extreme precipitation simulation, especially in regions of strong spatial heterogeneities (mountains and urban areas) and where deep convection dominates [Prein et al. 2016; Kendon et al. 2017].

However, the high computational and storage costs of CPM simulations limit the possibility of exploring many crucial aspects such as their sensitivity to spatial domain size or to nesting and driving strategies, which remain largely unexplored [Prein et al. 2015; Prein et al. 2017a]. More-

over, relatively few continuous CPM runs have been produced to date and they generally cover short time periods (e.g., 10 years or less) and small spatial domains [Brisson et al. 2015; Prein et al. 2016; Mantegna et al. 2017]. For these reasons, investigating the characteristics of rare precipitation extremes remains difficult and it is challenging to robustly assess CPM biases and uncertainties [Kendon et al. 2017; Gadian et al. 2017].

Chapter 2

Climate Change (CC) impacts on mean and extreme precipitation

The climate is changing owing to anthropogenic forcings linked to land use, population growth, and alteration of the chemical composition of the atmosphere that have the effect of increasing the mean temperature at the global scale [AghaKouchak et al. 2012; Melillo et al. 2014].

Global warming results in increasing evaporation and moisture-holding capacity of the atmosphere, as the saturation water vapor pressure increases by approximately 7 % per degree of temperature rise according to the Clausius-Clapeyron relationship. A warmer atmosphere having a larger water vapor content, an increase in precipitation is also expected, especially in the form of severe and heavy intensity events, as more atmospheric moisture is drawn into storms [Trenberth 2011; Fischer and Knutti 2016]. In particular, extreme precipitation could be expected to scale according to the Clausius-Clapeyron relationship based on the consideration that in intense storms a constant and considerable fraction of water vapor is converted into rain. However, different scaling rates of precipitation extremes on temperature have been empirically estimated and may depend on various factors, including the geographical region and the precipitation spatial scale and duration considered [e.g., Westra et al. 2014; Drobinski et al. 2016; Lenderink et al. 2017 and references therein]. Moreover, enhanced by changes in the atmospheric circulation, the acceleration of the hydrological cycle in a warmer climate [Giorgi et al. 2011] is likely to have important impacts on other characteristics of precipitation extremes, such as their frequency and/or spatio-temporal structure depending on

the regions and seasons [e.g., Lenderink et al. 2017; Skeeter et al. 2018; Pendergrass 2018].

In climate science, Climate Change (CC) is defined as the ensemble of modifications of the statistical characteristics of the climatological variables that persist for an extended period, typically decades or longer [IPCC 2013]. According to this definition, a strong body of evidence that the frequency and intensity of heavy precipitation are changing has been constructed based on the combined use of climate models and historical records [e.g., Hartmann et al. 2013]. Nevertheless, the detection and characterization of changes in the spatio-temporal structure represent a big challenge [Zhang and Zwiers 2013; Dittus et al. 2015], especially for short-duration intense extremes owing to their high spatio-temporal variability [Westra et al. 2014; Barbero et al. 2017; Kendon et al. 2017].

2.1 Observed changes in historical climate

Following Ch. 2 of the IPCC report [Hartmann et al. 2013], historical CC mainly resulted in a global redistribution of precipitation over land areas without significant impacts on the total volume of precipitation at a global scale. Conversely, changes in mean and total annual or seasonal precipitation have been recorded in different regions, with increases at mid- and high- latitudes of the Northern Hemisphere and decreases in tropical and subtropical areas.

Some authors also showed how changes in total precipitation are often driven by changes in the contribution from the most extreme events. For instance, Karl and Knight (1998) have shown that the increasing trend in daily precipitation over the United States during the 20th century is mainly due to increasing heavy precipitation (e.g., daily precipitation above the 90th percentile of the daily precipitation distribution) compared to moderate precipitation (e.g., between the 50th and the 55th percentile). The frequency of days with precipitation also increased [Karl and Knight 1998].

Generally, there is a broad consensus on the increase in the frequency and/or the intensification of daily and multi-daily precipitation extremes for the last decades at global and regional scales [e.g., Alexander et al. 2006; Fischer and Knutti 2016; Kendon et al. 2018 and references therein]. However, the amplitude of the observed changes greatly varies at local scales [e.g., Donat et al. 2013].

2.1.1 Observed changes over the United States and Canada

Significant increases in total precipitation have been reported during the 20th century in several regions of the United States (US) and Canada [Karl and Knight 1998; Zhang et al. 2000; Easterling 2017].

The analysis of historical data over the US highlighted changes in the frequency and/or intensity of extreme events at daily and coarser temporal scales [e.g., Karl and Knight 1998; Trenberth et al. 2003; Kunkel et al. 2013; Mallakpour and Villarini 2017 and references therein], especially in mountainous regions, the Midwest, and the Northeast [Hoerling et al. 2016; Huang et al. 2017]. Less significant trends are reported for west coastal regions [e.g., Karl and Knight 1998; Kunkel et al. 2013; Easterling 2017].

Using gridded daily precipitation records from 1948 to 2012, Mallakpour and Villarini (2017) found limited evidence for changes in the magnitude and seasonality of heavy precipitation over the US. However, they highlighted that the frequency of extreme precipitation events increased over large areas of the contiguous US, with strong effects of large-scale circulation modes. Considering various precipitation indexes, Easterling (2017) underlined that both the intensity and frequency of daily and longer precipitation extremes increased in most parts of the US since 1901 and with important regional differences in trends. Skeeter et al. (2018) provided further evidence for the increased frequency and magnitude of intense precipitation events for the southeastern US using station records and related these results to changes in the frequency of specific surface weather conditions.

Concerning Canada, some studies [e.g., Zhang et al. 2001; Vincent and Mekis 2006] did not find evidence for consistent and spatially coherent trends for extreme indices¹ during the 20th century, while attesting trends in daily intensity [e.g., a decrease of about 5% of mean daily intensity over the period 1950-2003 in Vincent and Mekis 2006] and in the total annual or seasonal precipitation, especially in southern regions [Akinremi et al. 1999; Stone et al. 2000; Zhang et al. 2000; Wazneh et al. 2017]. Akinremi et al. (1999) also showed that the observed increase in the number of days with precipitation (wet days) for Canadian prairies was mainly due to an increase in the number of days with light (≤ 5 mm) precipitation during the period 1921-1995. Conversely, for the second

¹For instance, Vincent and Mekis (2006) defined the following four indices for the analysis of extremes: the number of days with precipitation greater than 10 mm; the annual maximum precipitation total for 5 consecutive days; the number of days with precipitation \geq than the 95th percentile of the non-zero daily precipitation amount distribution over the considered period; and the annual maximum number of consecutive days without precipitation.

half of the 20th century, Stone et al. (2000) observed an increase of total seasonal precipitation due to increasing intermediate (≥ 2 mm) and heavy (station-specific threshold) daily events in southern Canada. Trends connected with increasingly frequent daily heavy events were detected for northern Canada during winter [Easterling et al. 2000a], while Mailhot and Talbot (2011) found a statistically significant intensification of hourly and sub-hourly extremes only for a few stations in southern Quebec.

More recently, some studies highlighted important non-stationarity in daily and sub-daily extremes at regional scale using regional trend analysis [Shephard et al. 2014; Sarhadi and Soulis 2017]. However, at-site analyses of homogenized daily precipitation series showed that extreme daily rainfall, snowfall, and precipitation trends were statistically significant only for a few Canadian stations [Vincent et al. 2018]. Assessing trends for sub-daily precipitation is, in fact, difficult, as available recorded sub-daily series are usually short (e.g., typically shorter than 30 years) and network density is much lower than for daily stations [Shephard et al. 2014; Barbero et al. 2017], especially in northern regions. Some authors also underlined the difficulty of assessing precipitation trends in Canada due to the evolving measurement practice [Metcalf et al. 1997; Akinremi et al. 1999; Stone et al. 2000; Vincent and Mekis 2006].

2.2 Projecting CC

GCMs and RCMs are the primary tools available to project the impact of changes in the external and internal forcings on the climate system. Forcing scenarios depend on several factors, such as the evolution of world demography, energy, land uses, and economic and technological development, ultimately determining the future greenhouse gas (GHG) and aerosols concentrations in the atmosphere [Myhre et al. 2013]. Different sets of forcing scenarios have been produced, including those from the IPCC Special Report on Emission Scenarios (SRESs) [Nakicenovic and Swart 2000] and the more recent Representative Concentration Pathways (RCPs) [Van Vuuren et al. 2011; Myhre et al. 2013].

SRES are 40 different scenarios describing plausible socio-economic evolutions along with their corresponding levels of GHG emissions without assuming specific climate policy interventions. They are organized in four families (A1, A2, B1, and B2 scenario families), each containing qualitative

"storylines" similar in terms of the future demographic and economic growth and repartition across the world, and similar for the future technological evolution they assumed [Nakicenovic and Swart 2000].

The RCPs represent the projected radiative forcing (i.e. the incoming-outgoing energy balance in the atmosphere primarily caused by changes in the atmospheric composition) associated with specific greenhouse gas, aerosols, land-use emissions. RCPs are intended to serve directly as input for climate and atmospheric chemistry models [Van Vuuren et al. 2011]. Each RCP covers the period 1850-2100 (with some extensions up to 2300) and can correspond to a wide range of possible socio-economic and development scenarios. RCPs take their name from the values of total radiative forcing reached in the year 2100 (RCP2.6, RCP4.5, RCP6, and RCP8.5 indicating values of +2.6, +4.5, +6.0, and +8.5 Watts per square meter [W/m^2], respectively).

Starting from a specific set of initial conditions, any individual dynamical model simulation represents one of the possible trajectories that the climate system might follow in response to the prescribed external forcing scenario [Flato et al. 2013].

2.2.1 Projected changes for United States and Canada

Numerous studies agreed on the expectation of changes in total precipitation and daily or longer extremes at global scale resulting from increasing GHG concentration in the atmosphere [e.g., Collins et al. 2013; Fischer and Knutti 2016; Kharin et al. 2018]. In particular, the contrast between wet and dry regions and among seasons will likely exacerbate in future years [e.g., Giorgi et al. 2011]. An increasing frequency of extreme events linked with the positive trend of temperatures is expected as well [e.g., Toreti et al. 2013; Kharin et al. 2013; Collins et al. 2013].

In agreement with these changes at the global scale, RCMs project modifications in annual and seasonal precipitation over many regions of North America [Plummer et al. 2006; Wehner 2013; Mearns et al. 2018 and references therein]. Wehner (2013), for instance documented changes in future mean seasonal precipitation rates and in average seasonal maximum daily precipitation through a comparison between the 2038-2070 period projections (A2 SRES scenario) and the simulations for the 1968-1999 period in the context of the North American Regional Climate Change Assessment Program (NARCCAP) multi-model numerical experiment [Mearns et al. 2009]. The author found

an increase of these variables at high latitudes (largest in northern regions during winter) and a decrease at low latitudes (strongest in southern regions during summer). The magnitudes of the changes in average seasonal maximum daily precipitation are smaller than those for mean precipitation [Wehner 2013].

The analysis of Chen et al. (2005) also suggested a potential increase in the frequency and intensity of heavy daily precipitation events ($\geq 32 \text{ mm/d}$) over the US, as a warming climate favors the increase of convective precipitation.

Mladjic et al. (2011) underlined the increase in the projected intensity of daily and multi-daily precipitation depth maxima between April and September over Canada for the 2041-2070 period, with relatively larger increases in northern regions. Analyzing simulations provided by the NARCCAP for the same emission scenario (SRES A2), Mailhot et al. (2012) showed that the intensity of annual maxima precipitation of several durations is also expected to increase. In accordance with these findings, Jalbert et al. (2015) underlined the expected increase of North-American daily extremes for all seasons, especially in northern Canada during summer.

Increases in hourly precipitation extremes were found by Prein et al. (2016) for the US when analyzing a 13-year 4-km CPM simulations with a *pseudo-global-warming* approach [Rasmussen et al. 2017 and references therein]. Considering GCM simulation under RCP4.5 and RCP8.5 over the US, Fix et al. (2018) found increases in annual maximum daily precipitation over the US, with larger changes being associated with larger temperature changes.

Finally, important modifications in the frequency, intensity, and increases in the heterogeneity of the spatial characteristics of weather systems producing precipitation extremes have been found in Canada and US by Guinard et al. (2015) and Prein et al. (2017b) using RCM projections.

More generally, possible modifications of the spatio-temporal structure of extreme rainfall are expected, based on projected changes in extreme characteristics such as duration, seasonality, daily timing, and spatial extents [Touma et al. 2018]. The assessment of the specific mechanisms driving these changes remains a fertile field still largely unexplored [Wasko et al. 2016; Dwyer and O’Gorman 2017].

2.3 Uncertainty in projected changes

The identification and quantification of uncertainty in climate model simulations are particularly critical when assessing and interpreting their results. Projections provide in fact a range of possible future climate evolutions under the assumption that climate and weather processes are correctly represented in dynamical models and assuming the validity of forcing scenarios. Evaluating the uncertainties associated with these assumptions is crucial for correctly assessing CC impacts and for the development of adequate adaptation strategies [Zhang and Zwiers 2013].

Uncertainty in climate projections are typically classified as [Tebaldi and Knutti 2007; Flato et al. 2013; Knutti 2018]:

- *scenario uncertainty*, related to the unknown external forcing on the climate system for future years;
- *model uncertainty*, associated with model structure, resolution, and parametrization [Tebaldi and Knutti 2007; Kendon et al. 2017]; and
- *intrinsic uncertainty*, linked with the natural variability of the climate system [Hawkins 2011; Deser et al. 2012b].

Natural variability represents the climate *internal variability* which occurs solely with the internal interactions of the climate system components [e.g., Deser et al. 2012b; Hingray and Saïd 2014]. These fluctuations may transiently hide or amplify long-term trends due to CC [Vecchi and Soden 2007; Hawkins 2011]. While CCs are generally considered to affect the climate system systematically and structurally, internal variability generates near-term fluctuations and randomness of the observed signal, resulting in substantial unpredictability [Hawkins 2011].

Some climatic experiments focused on the characterization of these three sources of uncertainty by the use of multi-model and/or multi-member ensemble simulations [Deser et al. 2012b; Flato et al. 2013]. These experiments consist of the use of multiple climate trajectories simulated by several models over a common period, considering various initial conditions and/or several forcing scenarios for running the simulations [Tebaldi and Knutti 2007; Sanderson et al. 2018]. In particular, the generation of ensembles of simulations using various forcing scenarios has been widely considered

for analyzing the sensitivity of the climate responses to different forcing sources [used, for instance, for the detection and attribution of the human contribution to the projected climate changes; e.g., Stott et al. 2010]. In the same vein, sets of simulations from various GCMs and/or RCMs have been generated to evaluate how structurally different models² respond to the same external forcing [IPCC 2013]. Pooling information from various simulations, multi-model ensembles may allow for a more robust assessment of the climate signal and provide a measure of the model uncertainty, quantified as the spread of the model responses [Galmarini et al. 2018]. Finally, initial-condition ensembles from a single climate model and forcing scenario have been used to discriminate CCs from natural variability for global and regional climate extremes, through the comparison of the estimated long-term changes in climate statistics and their spread across the independently initiated simulations [e.g., Thompson et al. 2015; Fyfe et al. 2017; Martel et al. 2018].

Using these approaches, various authors highlighted that natural variability is expected to be the major source of uncertainty for precipitation, especially for the most extreme events and short time horizons, while uncertainties on emission scenarios dominate for 30-year and longer projections and for most of the other climate variables [e.g., Hawkins and Sutton 2009; Hingray and Saïd 2014].

However, giving a comprehensive picture of the uncertainty in climate projections remains a difficult task due to a number of reasons. In particular, the representativeness of simulated ensembles with regard to the mentioned sources of uncertainties has been questioned since different models cannot be expected to be independent from each other, and various practical constraints determine the composition and size of multi-model / multi-member ensembles [e.g., computational limitations Tebaldi and Knutti 2007; Abramowitz et al. 2019]. Considering the inter-model dependencies and possible common biases, the uncertainty range spanned by the ensemble spread is likely to be underestimated, while a clear assessment of model dependence effects on projection results is not straightforward in practice [Ylhaisi 2014; Abramowitz et al. 2019 and references therein]. Accordingly, some difficulties also emerge for the definition of how to statistically combine information from global- and regional-scale simulations run at different spatio-temporal resolutions and the interpretation of ensemble results in different applications [Knutti et al. 2010; Galmarini et al. 2018].

²Ensembles of simulations from a single model that use different tuning of parameters can also be considered to explore parameter uncertainties [perturbed physics ensembles; e.g., Tebaldi and Knutti 2007].

Chapter 3

Statistical modeling of precipitation extremes

In order to represent the likelihood of a precipitation event to occur, both in terms of precipitation depth [mm] and intensity [mm/h], one usually refers to the quantiles of the precipitation distribution [e.g., Cunnane 1978]. However, as previously noted, the estimation of quantiles is usually carried out on the basis of time series covering a short period, even for the more extreme quantiles. For this reason, techniques for extrapolating the information about non-observed extreme events from the available samples must be defined [Coles 2001]. The statistical methods belonging to the Extreme Value Theory (EVT) perform these estimations based on the properties of order statistics of precipitation samples.

This chapter introduces the basic concepts of the EVT and describes their application to extreme precipitation analysis. Statistical methods commonly used for the characterization of the spatial distribution of precipitation extremes are also briefly reviewed.

3.1 Extreme Value Theory (EVT) for precipitation

First formulations of the EVT were set by Fisher and Tippett (1928), Von Mises (1936), and Gnedenko (1943). The discipline was then systematically formalized by Gumbel (1958), which

also promoted its use for modeling physical processes such as hydrology extremes. Gumbel (1958) further introduced the distribution which bears the same name, and which is still fairly used in hydrological applications.

The first step in the application of the EVT is the definition of some practical strategies to select events belonging to the tail of the distribution from the available time series of precipitation. Two main approaches are used: the Block Maxima (BM) and the Partial Duration Series (PDS) approach, also known as Peak-Over-Threshold (POT) method.

Block Maxima (BM) approach: it consists in splitting the available time series in sub-samples of the same size; the maximum value of each sample is then selected as a realization of an extreme event. The most common BM application in hydrology uses 1-year blocks, which enables a clear phenomenological interpretation of the maximum of each block. In this case, the series of selected extremes are called Annual Maxima Series (AMS).

Peak-Over-Threshold (POT) approach: this method relies on extracting all the time series values exceeding a certain threshold in order to construct the sample of extremes. As a result, extreme samples constructed by this approach correspond to the N largest time series values.

When dealing with precipitation, the BM approach is often preferred since it overcomes problems linked with seasonal components and clustered values in precipitation series that are particularly important at certain spatio-temporal scales (e.g., for daily and sub-daily precipitation) [Coles et al. 1999; Katz et al. 2002]. The independence assumption for sample observations is more easily applicable. Also, the selection of a threshold value for implementing the POT approach is not straightforward, to some extent arbitrary, and more difficult to handle in a non-stationary context. For these reasons, only the BM approach will be considered in this thesis.

It has to be noted, however, that the use of AMS series may entail to neglect some extreme events in the case that several heavy precipitation events have occurred during the same year. By the same token, the maximum value in a given year may be very small compared to other large events occurring during other years. In these cases, the use of POT methods may provide better information about extremes from the available series.

3.1.1 BM approach to the EVT

BM series are represented by the probability distribution family known as *Generalized Extreme Value* (GEV) distribution. This distribution originates from the following asymptotic result: the maximum $X_M = \max\{Z_1, Z_2, \dots, Z_M\}$ of a sequence of continuous i.i.d. random variables Z_1, Z_2, \dots, Z_M converges to a known distribution as $M \rightarrow \infty$, after proper renormalization and without any particular assumption regarding the exact distribution of Z [Fisher-Tippett theorem, 1928].

The distribution of the Annual Maxima (AM) of precipitation is thus known and corresponds to one of the distributions of the GEV family, as long as the block length (i.e., M for each year) can be assumed to be long enough for respecting the Fisher-Tippett asymptotic condition. If we represent the AM series with (x_1, x_2, \dots, x_n) , the GEV cumulative distribution function (cdf) of the random variable X can be written as [Coles 2001]:

$$F(x) = \begin{cases} \exp \left\{ - \left[1 + \xi \left(\frac{x-\mu}{\sigma} \right) \right]^{-1/\xi} \right\} & \text{if } \xi \neq 0 \\ \exp \left\{ - \exp \left\{ - \left(\frac{x-\mu}{\sigma} \right) \right\} \right\} & \text{if } \xi = 0 \end{cases} \quad (3.1)$$

where the support of the distribution is $-\infty < x \leq \mu + \sigma/\xi$ if $\xi < 0$, $1/\mu + \sigma\xi \leq x < +\infty$ if $\xi > 0$, and $-\infty < x < +\infty$ if $\xi = 0$. Parameters $\mu \in \mathbb{R}$, $\sigma > 0$ et ξ respectively represent the position, scale, and shape¹ parameters of the distribution.

The shape parameter plays here a critical role because it describes the characteristics of the distribution tails. It thus controls the frequency and the magnitude of the extreme events generated by $F(x)$. For $\xi = 0$ the distribution has a light-tailed shape and corresponds to the Gumbel distribution (GEV-type I). Conversely, the Weibull distribution (GEV-type III), corresponding to the case $\xi < 0$, shows an upper bounded tail, meaning that no value exceeding the upper bound can be observed. Finally, when $\xi > 0$, the distribution is known as the Fréchet distribution (GEV-type II) and presents an upper unbounded tail. In this last case we say that the distribution is heavy-tailed meaning that more frequent and "more extreme extremes" may be generated by $F(x)$ [Papalexiou et al. 2013]. To appreciate the difference between these three cases, Fig. 3.1 presents some examples of GEV probability density functions (pdf) corresponding to different parameter values.

¹Note that in hydrology the parametrization $k = -\xi$ is also common.

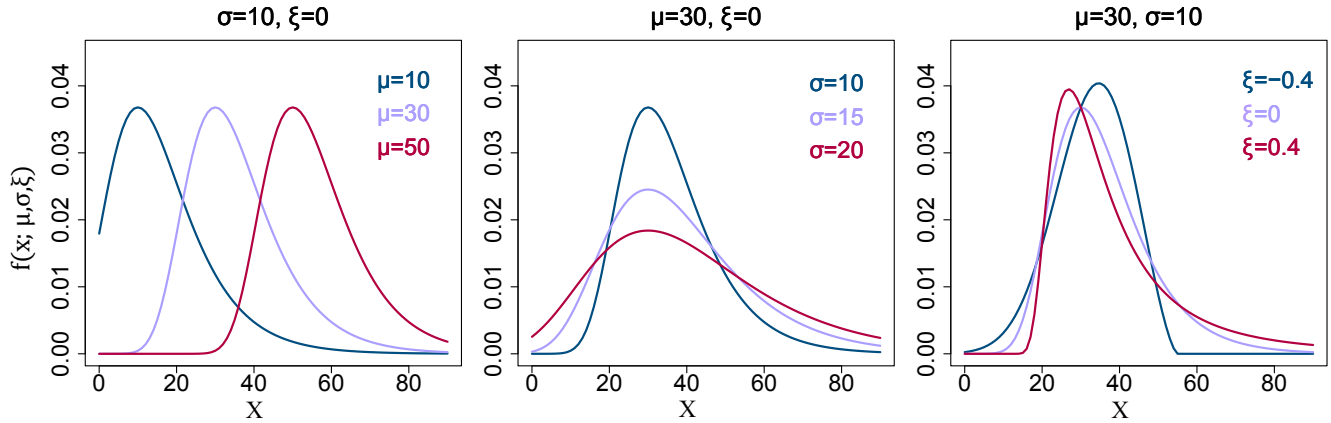


Figure 3.1: Examples of GEV pdf $f(x; \mu, \sigma, \xi)$ corresponding to different parameters values [adapted from Blanchet and Lehning 2010].

Precipitation extremes are often characterized in terms of their **return period** which can be defined as the average time interval expected between two events with intensity larger or equal to x_T [e.g., Gumbel 1941; Cooley 2013]. If X represent the AM precipitation measured a particular location for a given duration (e.g., one hour or one day), the return period T [years] can be expressed as:

$$T = [1 - F(x_T)]^{-1} = [1 - P(X \leq x_T)]^{-1}, \quad (3.2)$$

where $1 - F(x_T)$ corresponds to the probability of occurrence of an event larger than x_T over a year. The chosen intensity x_T is referred as **return level** and simply corresponds to the p^{th} quantile of the X distribution when $p = (1 - 1/T)$ [Rootzén and Katz 2013]. The present definition of return period and return level relies on the implicit assumption of the stationarity of precipitation distribution over the observational time period. For discussions about return period definitions in non-stationary contexts see Cooley (2013), Rootzén and Katz (2013), and Naveau et al. (2018).

For the GEV distribution, the solution of the equation $F(x) = p$ gives:

$$x_T = F^{-1}(p; \xi, \mu, \sigma) = \begin{cases} \mu + (\sigma/\xi) \{[-\ln(p)]^{-\xi} - 1\} & \text{if } \xi \neq 0; \\ \mu + \sigma \{-\ln[-\ln(p)]\} & \text{if } \xi = 0. \end{cases} \quad (3.3)$$

Figure 3.2 shows some examples of return levels against $-\ln(p)$ on a logarithmic scale (return level plot), for different $F(x)$ parameter values. It is worth to appreciate the difference between the three curves in the right panel [Fig. 3.2, 3rd col]. While, as expected, the intensity of return levels

increases with the return period for each of the three GEV types, the relative increase of x_T with $T \rightarrow \infty$ for the Fréchet distribution is clearly larger than for the Weibull and Gumbel distributions.

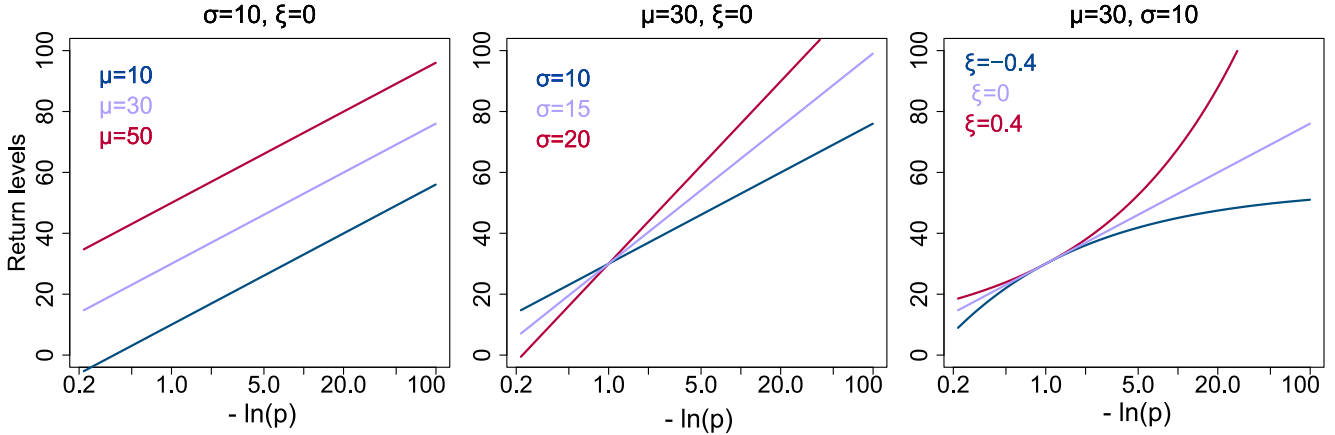


Figure 3.2: Return level plots corresponding to different parameter values [adapted from Blanchet and Lehning 2010].

An accurate estimation of the GEV parameter values, and in particular of the shape parameter, is thus critical to evaluate the characteristics of more (rare) extremes (i.e., for small values of p). This estimation is usually achieved by the use of the Maximum-Likelihood (ML) or the Probability Weighted Moments (PWMs) methods [Greenwood et al. 1979; Hosking et al. 1985]. Detailed descriptions of both ML and PWM estimation procedures are provided in Appendix A.

Although the PWM method is sometimes preferred for its good performances on small samples [Hosking et al. 1985], the ML estimation is often promoted because of its optimal asymptotical properties [Katz et al. 2002]. Moreover the ML method easily handles reparametrizations and the inclusion of covariates in GEV models [Katz 2013]. This could be useful, for instance, for modeling spatial and temporal trend in the AM distribution [see, for instance, Appendix A, and Blanchet and Lehning 2010; Kharin et al. 2018]

3.1.2 Estimated GEV for AM precipitation: literature review

Due to its importance in terms of more extreme AM quantiles, many studies focused on the accuracy of shape GEV distribution estimation [e.g., Koutsoyiannis 2004a; Koutsoyiannis 2004b; Papalexiou and Koutsoyiannis 2013b]. Those that investigated daily precipitation extremes are reviewed in Ragulina and Reitan (2017) and Ye et al. (2018).

Based on theoretical and empirical analyses, Koutsoyiannis (2004a) and (2004b) highlighted that daily rainfall AMS are better described by GEV distributions with positive shape parameter, while the common assumption of $\xi = 0$ (Gumbel hypothesis) may severely underestimate the risk associated with extreme events. Extending these analyses, Papalexiou and Koutsoyiannis (2013b) showed that different regions are characterized by different precipitation regimes, hence the geographical location may affect the shape parameter estimation [see also Ragulina and Reitan 2017; Blanchet et al. 2009]. Even more importantly, high uncertainty affects the GEV shape at local scales. Therefore, its estimation critically depends on the length of the series under consideration [Koutsoyiannis 2004a]. For series of 40 to 163 years, ξ is likely to range in a narrow value interval [approximately between 0 and 0.23; Papalexiou and Koutsoyiannis 2013b].

Methods such as the Regional Frequency Analysis (RFA) [Hosking and Wallis 1997] have been proposed for better estimating GEV parameters when only short series are available at single spatial locations. RFA combines several AMS from various locations (e.g., from several meteorological stations). If a geographical region can be considered homogeneous, the estimation of ξ is then performed on the pooled sample of AMS.

3.2 Intensity-Duration-Frequency (IDF) curves

Intensity-Duration-Frequency (IDF) curves are used to synthetically represent information about extreme precipitation. These curves describe the relationships between rainfall intensity $X(T, d)$ and duration for given values of the return period (e.g., T equal to 2, 5, and 10 years) [CSA 2012]. An example of IDF curve is given in Fig. 3.3.

Many mathematical expressions have been proposed to estimate IDF. Typical IDF relationships found in early literature [e.g., Bernard 1932; Chow et al. 1988] can be represented by the following general expression [Koutsoyiannis et al. 1998]:

$$X(T, d) = \frac{f(T)}{g(d)} \quad (3.4)$$

where $X(T, d)$ represent the precipitation intensity quantile parametrized in terms of the duration d and return period T and the functions $f(T)$ and $g(d)$ are assumed to be two explicit functions of T and d , or two constant values.

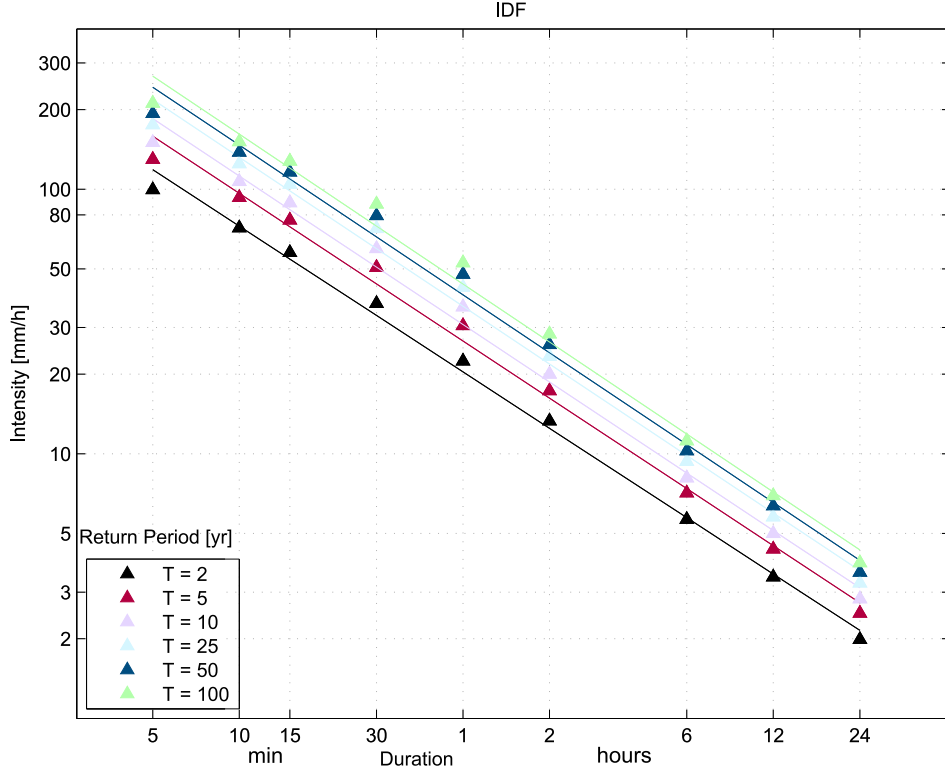


Figure 3.3: IDF curves for the Pierre-Elliott-Trudeau Airport gage station (Montreal, Quebec) for the period 1943 – 1993. Adapted from *Short Duration IDF Data, Engineering Climate Dataset, ECCO*, <https://www.canada.ca/en/sr/srb.html?q=Intensity-Duration-Frequency&wb-srch-sub=#wb-land>.

In particular, $g(d)$ is often defined as [Koutsoyiannis et al. 1998]:

$$g(d) = (d + \theta)^\eta, \quad (3.5)$$

where θ and η are non-negative coefficients to be estimated, and $0 < \eta < 1$. The wide use of this expression is due to the fact that, intuitively, $X(T, d)$ must be a monotonically decreasing function of duration, regardless of the specific distribution adopted for the precipitation intensity. In fact, for a fixed occurrence frequency, the intensity of a short-duration precipitation event is expected to be larger than for long-duration ones. Expressions similar to Eq.(3.4) have been also proposed based on more rigorous procedures. For instance, Koutsoyiannis (2006) justifies the same expression based on considerations about maximum entropy properties of rainfall processes.

A power or logarithmic form may be chosen for $f(T)$ [e.g., Chow et al. 1988]. More often, however, $f(T)$ is set constant, i.e. $f(T) = \omega$ [CSA 2012]. The parameters θ , η , and ω are then estimated by numerical optimization. Figures 3.3 shows IDF curves corresponding to various return periods.

In this case, a Gumbel distribution was used for modeling the AM intensity of the observed series at each duration. η and ω have been estimated by linear regression, while θ has been fixed to 0 [http://climate.weather.gc.ca/prods_servs/engineering_e.html].

More conveniently, $f(T)$ can be also derived from the analytic expression of the return levels provided by the parametric expression of $F(x)$. This technique has been strongly recommended by Koutsoyiannis et al. (1998) in order to ensure IDF theoretical consistency with the statistical behavior of precipitation intensity. Accordingly, a practical IDF relationship for the GEV distribution is [Koutsoyiannis et al. 1998; Eq. (13) and (22)]:

$$X(T, d) = \frac{x_T}{(d + \theta)^\eta} = \frac{\mu + (\sigma/\xi) \left\{ [-\ln(p)]^{-\xi} - 1 \right\}}{(d + \theta)^\eta}, \quad (3.6)$$

where the GEV quantile x_T is expressed in terms of the GEV-type I and -type II cdf² for the reference duration chosen, for simplicity, as equal to $1h$. In this case, the GEV parameters, θ and η can be estimated at the same time by fitting Eq.(3.6) to the empirical quantiles of X at duration d [Koutsoyiannis et al. 1998]. This estimation, however, does not consider the statistical properties of the GEV parameters and does not insure the optimal properties of ML and PMW estimators.

Note that Eq.(3.4) and (3.6) assume that IDF curves are *separable*, in the sense that the duration and the return period affect the intensity in an independent multiplicative way. However, some authors [e.g., Bendjoudi et al. 1997; Veneziano and Furcolo 2002] noted that this is not a suitable property for IDFs because precipitation intensity is more sensitive to T for small d than that for longer durations. A different formulation of the IDF curves which allows to account for this property will be thus presented in Ch. 4.

3.3 Areal Reduction Factors (ARFs) and Intensity-Duration-Area-Frequency (IDAF) curves

Areal rainfall models describe the distribution of precipitation aggregated over a selected area. Generally, this is accomplished by explicitly modeling the spatial correlation structure of the pre-

²The Gumbel expression of the IDF can be obtained by simply considering $\xi \rightarrow 0$ in Eq.(3.6).

precipitation field. Many models have been constructed to describe areal measures of precipitation in space and time [Coles and Tawn 1996]. Various authors also showed how the EVT paradigm can be applied to areal measures [e.g., Coles and Tawn 1996; Allen and DeGaetano 2005; Overeem et al. 2009].

However, modeling the transition between point precipitation intensities and the aggregated measures over a surface is not straightforward. This is a critical issue, since gauge stations are still considered the most reliable source of observations in precipitation analysis [Ceresetti 2011; Tapiador et al. 2017]. The computation of Areal Reduction Factors (ARFs) is the standard tool used to this end [Svensson and Jones 2010 and references therein].

ARFs are generally defined as the ratio between the areal (maxima) intensity corresponding to a specified return period T and a specific duration d , and the point (maxima) intensity corresponding to the same T and d , i.e.:

$$ARF(T, A, d) = \frac{X(T, A, d)}{X(T, d)}, \quad (3.7)$$

where $X(T, A, d)$ represent the Intensity-Duration-Area-Frequency (IDAF) curve, which defines the intensity of AM rainfall for a given area, duration, and return period. Note that $X(T, d) = X(T, 0, d)$ and that we usually consider the area A as centered to the location where the IDF is defined (e.g., gauge station). For alternative definitions and a detailed discussion on ARFs, see Svensson and Jones (2010).

In practice IDAF are typically estimated empirically, by averaging the numerator of Eq.(3.7) over various areas A covering the target domain. These areas are selected through a sliding spatial moving-window (fixed-area ARFs) or by defining concentric windows around given precipitation events (storm-centered ARFs) [Musy and Laglaine 2005]. However, storm-centered ARFs do not have a clear return period interpretation [Veneziano and Langousis 2005] and some concerns have been expressed about their construction, which may involve the use of areal- and point- maxima generated by different weather systems [Omolayo 1993; Ceresetti 2011].

First attempts to analytically derivate of ARFs and IDAF curves accounting for extreme precipitation properties have been made by Lebel and Laborde (1988) and Sivapalan and Blöschl (1998),

while precedent studies were based on inconsistent assumptions regarding the spatial correlation structure of the extremes [e.g., Rodriguez-Iturbe and Mejía 1974]. Examples of the ARFs estimated for Austria [Sivapalan and Blöschl 1998] and United Kingdom [NERC 1975] are shown in Fig. 3.4 and 3.5.

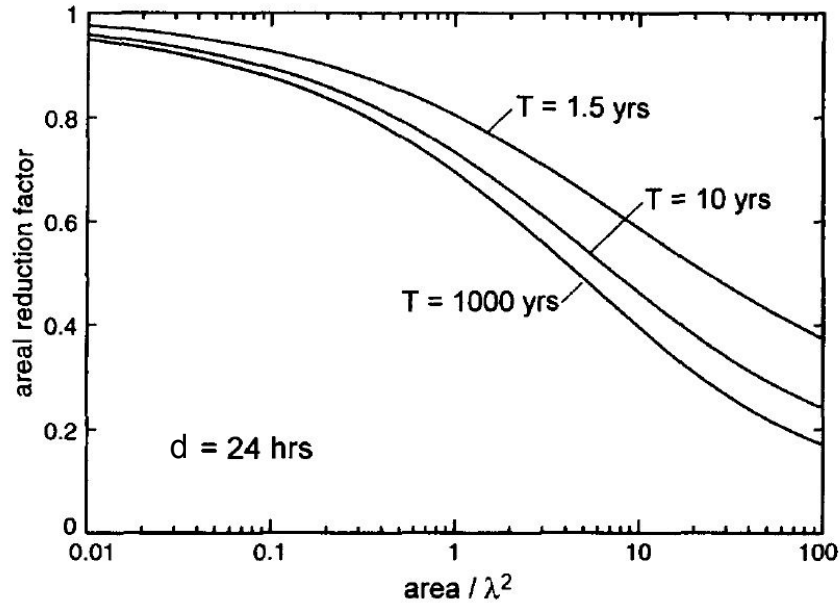


Figure 3.4: ARFs for the rainfall intensity in Austria, as a function of the catchment area considered A/λ^2 and return period T . λ represents the spatial correlation length involved in the definition of the exponential isotropic correlogram for X . Adapted from Sivapalan and Blöschl (1998)

From Fig. 3.4, it is evident that the ARF is a decreasing function of both the area A and return period T . Nonetheless, for long T the ARF dependence on return period is less obvious [Veneziano and Langousis 2005]. For $A \rightarrow 0$ ARF tends to 1, the areal precipitation approaching the gauge-point value.

First analytical approaches, such as the one used by Sivapalan and Blöschl (1998), did not explicitly model the ARF dependence on precipitation duration, while the ARF is expected to increase with increasing d [Veneziano and Langousis 2005; Mineo et al. 2018], as shown by Fig. 3.5. In fact, the spatial correlation structure of precipitation largely depends on the duration because higher intensity events are generally associated with meteorological systems having small spatial extent and "shorter lifetime".

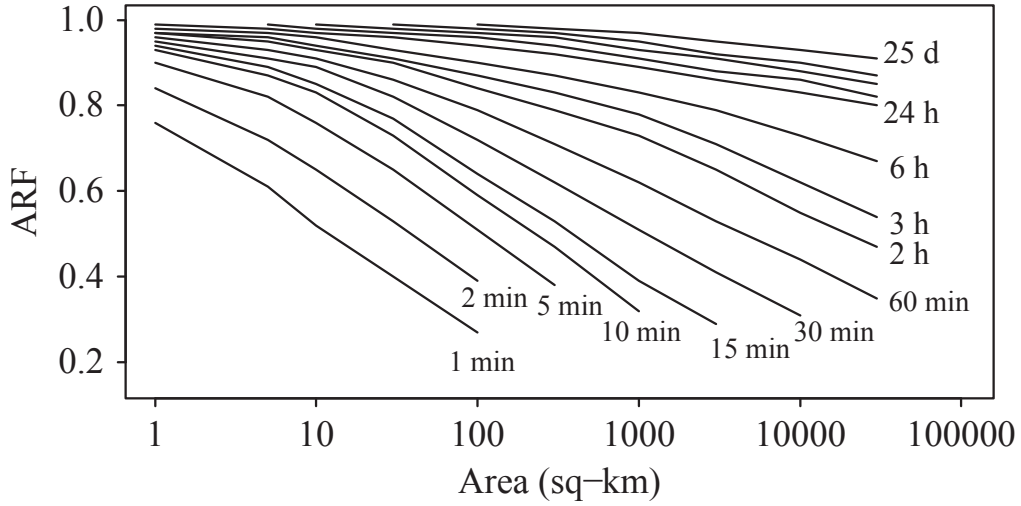


Figure 3.5: ARFs for the United Kingdom derived from the tabulated values in the *Flood studies report* [NERC 1975]. Figure presented in Svensson and Jones (2010).

An explicit formulation of the IDAF curves within the framework of the EVT has been proposed by Overeem et al. (2010) by using d and A as covariates for the GEV-parameters³:

$$X(T, A, d) = \frac{\mu(A, d) + \sigma(A, d) \left\{ [-\ln(p)]^{-\xi(A, d)} - 1 \right\}}{\xi(A, d)}, \quad (3.8)$$

where $\mu(A, d)$, $\sigma(A, d)$, and $\xi(A, d)$ are linear combinations of the duration and the area of the measured AM.

³More precisely, Overeem et al. (2010) studied and modeled Depth-Duration-Area-Frequency (DDAF) curves which actually consider the rainfall depth as a function of duration and area. However, the same results are easily extended to IDAF.

Chapter 4

Scaling models for extreme precipitation

This chapter describes how scaling models can be used to provide a fine characterization of precipitation variability across various spatio-temporal scales. First, Simple Scaling (SS) laws are defined for modeling the statistical structure of extreme precipitation at different time scales (durations). The construction of IDF curves in this scale-invariant context is presented. Then, SS models are extended to consider the Spatio-Temporal Scaling (STS) of precipitation for the construction of IDAF curves. Finally, Multiscaling (MS) laws are briefly introduced.

4.1 Scale invariance and self-similarity of precipitation

In mathematics, scale invariance refers to the invariant shape of a function $f(x)$ under rescaling the variable x by a multiplicative factor λ :

$$f(\lambda x) = \lambda^H f(x) \tag{4.1}$$

for some choice of exponent $H \in \mathbb{R}$. In geometry, scale invariance is related to the concept of *self-similarity*¹, which indicates that one or some features of an object do not change if its dimension

¹More precisely, self-similarity usually indicates the combination of scale invariance with statistical isotropy [Tessier et al. 1993]. In the literature, it is however common to find different terminologies to describe the concept of scale

or the observational scale are changed [Dubrulle et al. 1997]. As a consequence, no reference scale characterizes the object, and no preferred observational point of view better outlines object features. Such objects are currently referred as fractals and they are typically the result of highly non-linear processes involved in chaotic systems [Mandelbrot 1977].

First arguments about scale invariance of precipitation mainly originated from the observation of characteristic patterns in the spatial organization of mesoscale weather systems [e.g., Austin and Houze 1972; Houze 1981]. These patterns define a hierarchical structure of precipitation in which low-intensity synoptic-scale systems contain higher-intensity mesoscale areas which are formed, in turn, by small-scale clusters of higher-intensity convective cells.

Lovejoy (1982) and Lovejoy and Schertzer (1985) were among the first to link precipitation scale-invariance to other self-similar processes occurring in the atmosphere [e.g., hydrodynamic turbulence, Kolmogorov 1941]. They also related the self-similar properties of precipitation to the highly erratic nature of the climate. Then, various studies provide empirical evidences of this property [e.g., Gupta and Waymire 1990; Burlando and Rosso 1996; Menabde et al. 1999; Yu et al. 2004; Bara et al. 2009; Ceresetti et al. 2010; Veneziano and Yoon 2013; Panthou et al. 2014].

Self-similarity implies that the statistical characteristics (e.g., moments) of precipitation intensity (or depth) observed at several scales are related to each other by a power law similar to the one defined in Eq. (4.1). The corresponding mathematical models are known as *scaling models*.

Two types of scaling models are usually considered: *Simple Scaling (SS)* and *Multiscaling (MS)* models. In SS models, a constant multiplicative factor is used to describe the relationships among the precipitation distributions at different spatial or temporal scales. In MS models, conversely, several parameters are used to describe the scale change in terms of moments or quantiles of the precipitation distribution.

invariance [Dubrulle et al. 1997], and also some ambiguous uses of the same notion to refer to different types of self-similarity [Gupta and Waymire 1990]. For excellent definitions and discussions of these concepts see Dubrulle et al. (1997) and Mandelbrot (1977).

4.2 Simple Scaling (SS) models

When equality in Eq.(4.1) holds for the statistical properties of a random variable X , it defines a statistical *scaling model*. Denoting by X_ℓ and X_L the variable (e.g., the precipitation intensity) considered at two different scales ℓ and $L = \lambda\ell$ (e.g., two different durations), the *scaling model* implies that [Gupta and Waymire 1990; Menabde et al. 1999]:

$$X_L \stackrel{dist}{=} \lambda^H X_\ell, \quad (4.2)$$

where $H \in \mathbb{R}$ is called *scaling exponent*. Expression Eq. (1.2) means that the same probability distribution applies for the precipitation intensity at scales l and L , up to a magnification or contraction equal to $\lambda^H = (L/\ell)^H$, i.e.:

$$F_{X_L}(x) = P(X_L \leq x) = P(\lambda^H X_\ell \leq x) = P(X_\ell \leq \lambda^{-H} x) = F_{X_\ell}(\lambda^{-H} x). \quad (4.3)$$

Eq. (1.2) defines the so-called Simple Scaling (SS) model. It implies that the X distribution shape remains unchanged when the variable is rescaled.

An interesting consequence of the SS assumption is that, if X_L and X_ℓ have finite moments of order q , their moments respect the following relationship [Gupta and Waymire 1990]:

$$E[X_L^q] = \lambda^{Hq} E[X_\ell^q]. \quad (4.4)$$

This last relationship is usually referred to as *wide sense* simple scaling property, because it is less general than Eq. (1.2) [i.e. the *strict sense* scaling valid for the whole distribution; Gupta and Waymire 1990].

4.2.1 Moment Scaling Analysis (MSA)

Based on the definition of wide sense SS, scale invariance results in a simple translation of the log-moments between scales:

$$\ln E[X_L^q] = Hq \ln \lambda + \ln E[X_\ell^q]. \quad (4.5)$$

By checking the log-log linearity of the X moments versus the λ , the SS model can be thus validated and estimated [Gupta and Waymire 1990]. This moment-based estimation of the scaling law consists in

- i) estimating the slopes of the log-log relationships between the empirical q -moments of $X_{\ell_1}, X_{\ell_2}, \dots$, and X_{ℓ_L} and the corresponding scales $\ell_1 < \ell_2 < \dots < \ell_L$; and
- ii) verifying that the estimated slopes vary linearly with the order of moment q .

If the scaling exponent H estimated for the first moment equals the exponents (slopes) for the other moments, the precipitation intensity X is considered to be scale invariant under SS in the range of durations ℓ_1 to ℓ_L .

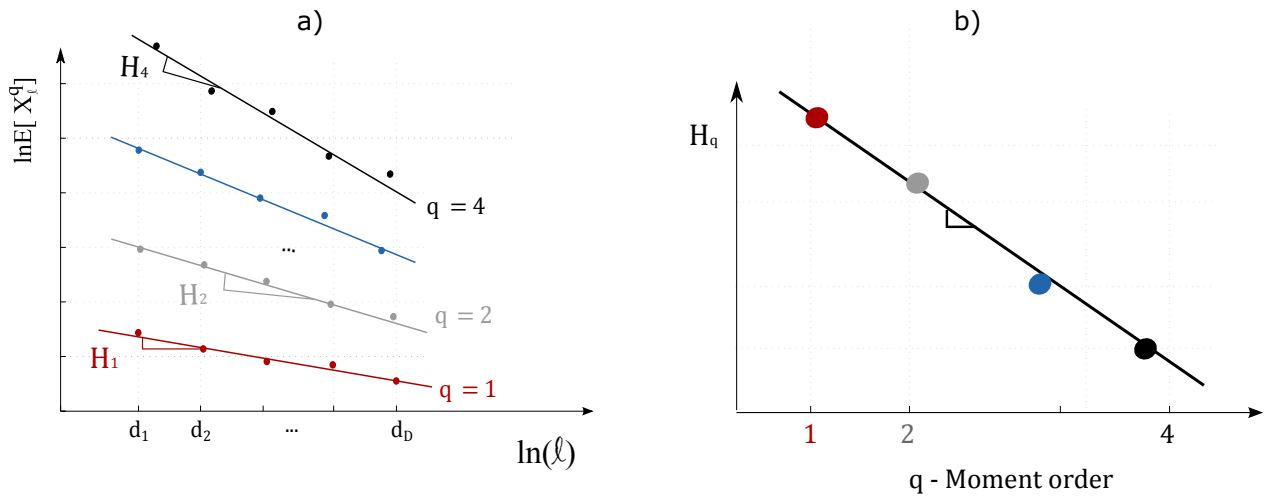


Figure 4.1: MSA: (a) the linear relationships between moments $E[X_\ell^q]$ and scale ℓ is estimated in a double-logarithmic plane for various q ; (b) the linearity of the slopes as a function of q is checked. Adapted from Innocenti et al. (2017).

More refined methods have also been proposed for detecting and estimating scale invariance, such as dimensional analysis [Lovejoy and Schertzer 1985; Tessier et al. 1993; Dubrulle et al. 1997], spectral analysis and wavelet estimation [Olsson et al. 1999; Ceresetti 2011], and empirical pdf power law detection [Hubert and Bendjoudi 1996; Ceresetti et al. 2010]. However, the MSA is by far the simplest and most intuitive tool to check the scaling hypothesis and has been widely applied [Menabde et al. 1999; Burlando and Rosso 1996; Borga et al. 2005; Nhat et al. 2007; Panthou et al. 2014].

4.2.2 SS in time

The SS framework has been used to model the relationships between the precipitation intensity distributions at several durations $d_1 < d_2 < \dots < d_D$, ranging from a few minutes up to several days. The values for the scaling exponents H depend on the climatological and geographical characteristics of the study region and typically range between -0.8 and -0.5 for precipitation intensity [e.g., Menabde et al. 1999; Ceresetti 2011; Panthou et al. 2014; Casas-Castillo et al. 2018; Sane et al. 2018]. Note, however that the parametrization $H' = -H$ has also been used in the literature and has been considered for Paper 1. Also it could be easily shown that the following relationship links the SS exponents for precipitation depth and intensity: $H_{depth} = H_{intensity} + 1$.

An interesting result emerging from some of these studies concerns the difference between H values estimated for different duration ranges. In particular, some authors noticed a sharp difference between the scaling regime of short-duration intensity (e.g., for durations shorter than a few hours) and the scaling regime for longer duration intervals [e.g., Borga et al. 2005; Ceresetti 2011]. This finding has been interpreted as a manifestation of the transition from weather dynamics dominated by synoptic systems to a highly variable convective regime [Ceresetti et al. 2010]. This hypothesis has also been supported by two main results. First, the transition between the two scaling regimes occurs at different breakpoint-durations depending on the geographical region and on its climatology. Second, the H value seems to depend on the topographic characteristics of the geographical region considered [Borga et al. 2005; Ceresetti et al. 2010].

For short-durations ranges (e.g., less than one hour) some authors also reported that the scaling exponent is generally homogeneous in space, which suggests that local convective precipitation has similar properties independently of the region considered [e.g., Alila 2000; Borga et al. 2005 and references therein]. Opposite results have been observed for the scaling regimes characterizing long duration precipitation [e.g., Borga et al. 2005].

4.2.3 SS-GEV model and SS-IDF curves

For the GEV distribution it is straightforward to verify that, if $X \stackrel{dist}{=} GEV(\mu, \sigma, \xi)$ then $\lambda X \stackrel{dist}{=} GEV(\lambda\mu, \lambda\sigma, \xi)$ for any $\lambda \in \mathbb{R}$. This means that the GEV family, respects scale invariance for any constant multiplicative transformation of X .

Many authors proposed IDF and IDAF models for extreme precipitation series based on this scale invariant formulation of the GEV distribution [e.g., Bara et al. 2009; Panthou et al. 2014; Blanchet et al. 2016]. Under SS, in fact, GEV distribution parameters can be expressed as:

$$\mu_d = d^H \mu_*, \quad \sigma_d = d^H \sigma_*, \quad \text{and} \quad \xi_d = \xi_*, \quad (4.6)$$

where μ_* , σ_* , and ξ_* represent the parameters of the reference X_{d_*} chosen, for simplicity, such that $d_* = 1\text{h}$. Hence, the GEV return level formula [Eq. (3.3)] can also be rewritten as [Mélèse et al. 2018]:

$$X(T, d) = d^H \mu_* + \frac{d^H \sigma_*}{\xi} \left\{ [-\ln(p)]^{-\xi_*} - 1 \right\} = \frac{\mu_* + (\sigma_*/\xi_*) \left\{ [-\ln(p)]^{-\xi_*} - 1 \right\}}{d^{-H}} \quad (4.7)$$

Note the similarity of this expression with the one proposed by Koutsoyiannis et al. (1998) [Eq.(3.6)]. However, Eq.(4.7) state that $\eta = -H$ and $\theta = 0$ on scaling arguments and naturally suggests the use of an estimation of H , μ_* , σ_* , and ξ_* more consistent with the statistical behavior of X . In fact, a Least Square estimation of the four parameters which make use of empirical cdf estimates (e.g., Gringorten or Cunanne plotting positions) is used by Koutsoyiannis et al. (1998). Conversely, the scaling formulation provides for the use of more suitable estimators for H (e.g., MSA) and for the GEV parameters [e.g., the ML method, Blanchet et al. 2016, or PWM²]

Accordingly, all available AMS for the range of durations $d_1 < d_2 < \dots < d_D$ that satisfies the SS hypothesis can be merged in one sample. Then, the GEV parameters corresponding to the reference $d_* = 1$ can be estimated on the pooled sample of series, reducing the uncertainty for the shape parameter.

4.3 Scale invariance in space and time: dynamic scaling

Spatial scaling has mainly been studied using the *dynamical scaling* approach proposed by Lovejoy and Schertzer (1985) and Venugopal et al. (1999). Within a dynamic scaling approach the scale-invariance hypothesis is formulated in both space and time using a relationship of the follow-

²Some authors also use alternative equivalent expressions of the scaling Gumbel or GEV IDF. For instance, Ceresetti (2011) and Borga et al. (2005), used the common formulation of the return level based on frequency factors, as introduced by Chow (1951), that better outline how the PWM can be used for estimating SS-GEV parameters.

ing type [Venugopal et al. 1999; De Michele et al. 2001]:

$$\frac{a}{A} = f\left(\frac{D}{d}\right), \quad (4.8)$$

where (D,d) and (a,A) respectively represent two couples of temporal and spatial scales. By a simple mathematical argument, Venugopal et al. (1999) demonstrated that the only transformation $f(\cdot)$ which allows Eq.(4.8) is a power law, i.e.:

$$f\left(\frac{D}{d}\right) = \left(\frac{D}{d}\right)^z = \lambda^z \quad (4.9)$$

Hence the spatial variability of precipitation intensity over a particular time interval can be simply expressed in terms of its temporal variability over a particular area [Venugopal et al. 1999; Ceresetti 2011]. Introducing then a SS hypothesis we have:

$$X_{D,A} \stackrel{dist}{=} \lambda^H X_{d,\lambda^z a}, \quad (4.10)$$

which states that the dependence of precipitation on spatial and temporal scales can be reduced to a one-dimensional problem involving only the temporal scale ratio λ and the scaling exponent H of point precipitation in time (time scaling). In Eq. (4.10), the spatial scaling is assessed through the *dynamical scaling exponent* z which links space and time scales [Eq. (4.8)-(4.9)]: $(a/A) = \lambda^z$.

Several studies applied Eq.(4.10) to precipitation series over time scales ranging from a few minutes to several hours [e.g., from 20min to 6h in the application of De Michele et al. 2002, and up to 24h in Panthou et al. 2014; station series and interpolation on a regular grid were used in these cases] and from 1 to some hundreds of Km^2 . However, the number of applications presented in literature remains low and scaling exponents are considered difficult to estimate [Castro et al. 2004].

4.3.1 Scaling models for ARFs and IDAF curves

Within the dynamical scaling framework the same scaling exponent can be used to link the statistical distribution of precipitation at different temporal scales (scaling in time) and to extend the estimated scaling IDF to IDAF curves [Panthou et al. 2014]. Based on dimensional considerations, De Michele

et al. (2001) demonstrated that the ARF of dynamical scaling AMS can be expressed as:

$$ARF(A, d) = \left[1 + \omega \left(\frac{A^\alpha}{d^\beta} \right) \right]^{\frac{H}{\beta}}, \quad (4.11)$$

where $\alpha > 0$ and $\beta > 0$ are two constants linked to the dynamical scaling exponent through $\alpha \times \beta = z$. α, β express the variation of the ARFs with d and A , while ω is a normalization factor.

By means of this ARF expression an IDAF relationship for the annual maxima series $X_{A,d}$ modeled with a GEV distribution is given by:

$$X(T, A, d) = \frac{\mu(A, d) + \sigma(A, d) \left\{ [-\ln(p)]^{-\xi(A,d)} - 1 \right\}}{\xi(A, d)}, \quad (4.12)$$

where [Panthou et al. 2014],

$$\mu(A, d) = ARF(A, d) \lambda^H \mu_*, \quad \sigma(A, d) = ARF(A, d) \lambda^H \sigma_*, \quad \text{and} \quad \xi(A, d) = \xi_* \quad (4.13)$$

Note the similarity of the IDAF in Eq.(4.12) and the formulation presented by Overeem et al. (2010) [Eq.(3.8)]. However, while Overeem et al. (2010) suggested polynomial approximations of GEV parameters on A and d based on empirical estimates, Eq.(4.12) is based on the dynamical scaling hypothesis and statistical scale invariance.

As a concluding remark, it has to be mentioned that the absence of the T index for the ARF in Eq.(4.11)-(4.12) means that this quantity is independent of the return period, while this dependence is introduced in the IDAF only through the use of the GEV quantile. As previously noted, some theoretical considerations [e.g., Veneziano and Langousis 2005] and empirical evidence [e.g., Bacchi and Ranzi 1996; De Michele et al. 2001] suggest that ARFs should decrease with increasing T . A possibility to solve this theoretical inconsistency is offered by the multiscaling framework briefly introduced in next section.

4.4 Multiscaling

While SS processes result from many additive random components of variability [Tessier et al. 1993; Dubrulle et al. 1997], the large fluctuations of the climate system governing precipitation are likely to produce a "cascade of random multiplicative effects" [Gupta and Waymire 1990]. These multiplicative processes can also be described by a power law connecting the statistical distributions of X among different scales. However, a single multiplicative factor, such as λ^H in SS, is no longer adequate to model this relationship. Accordingly, many authors argued that distribution moments and quantiles of different orders may need a different (i.e. order-specific) scaling exponent [e.g., Gupta and Waymire 1990; Burlando and Rosso 1996; Ceresetti 2011].

A broader definition of scale invariance of precipitation has thus been given, by considering the following wide sense Multiscaling (MS) model [Gupta and Waymire 1990]:

$$E[X_L^q] = \lambda^{K(q)} E[X_\ell^q], \quad (4.14)$$

where the *moment scaling function* $K(q)$ is a non-linear function of the moment order q [Fig. 4.2]. This means that moments of different orders scale differently between the ℓ and the L scale.

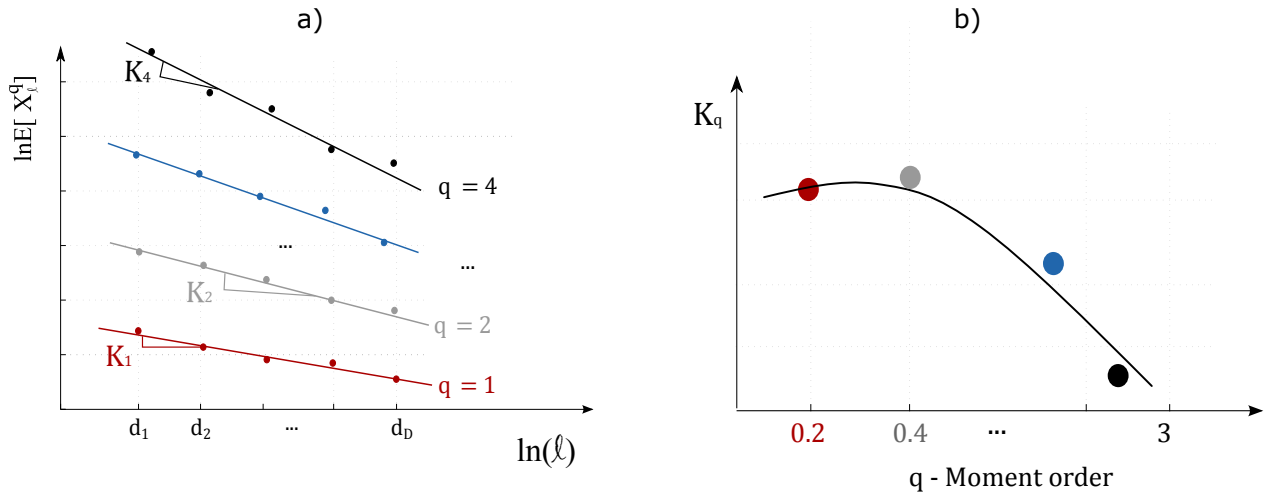


Figure 4.2: Scaling moment function in a MS model.

A change of scale therefore implies a modification of the shape of the X distribution and not only its magnification or contraction. In order to appreciate this difference Fig. 4.3 graphically represents pdf scale change under SS and MS.

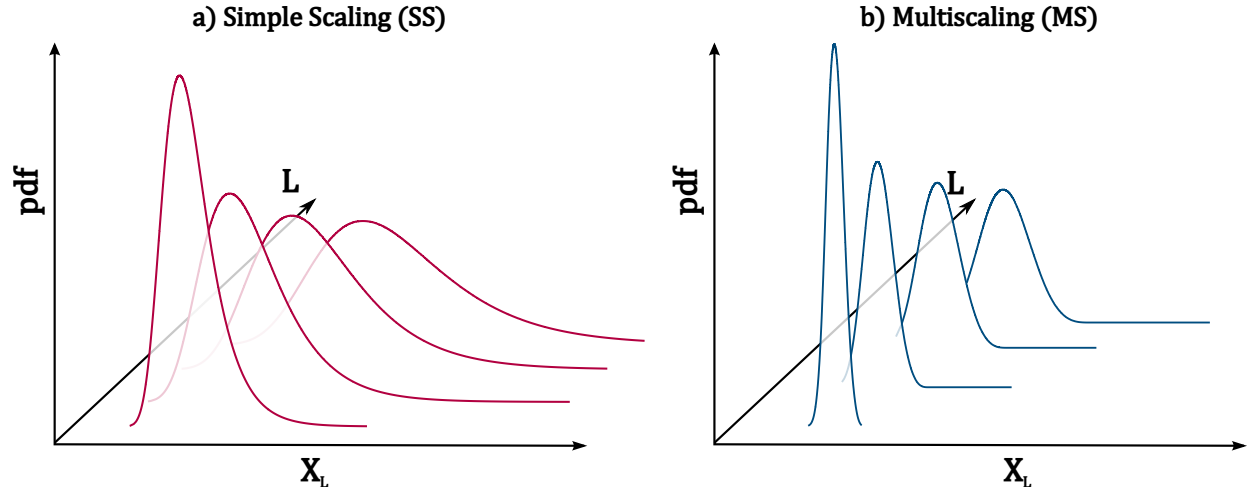


Figure 4.3: Probability distribution scaling: a) SS and b) MS. Adapted from Ceresetti (2011).

Some authors [e.g., Gupta and Waymire 1990; Burlando and Rosso 1996] derived the explicit expression of $k(q)$ for some particular distribution functions and stochastic processes, based on the mathematical properties of $k(q)$ [Gupta and Waymire 1990]. Formulations of IDF and IDAF curves in a MS context have also been developed, among others, by Veneziano and Furcolo (2002), De Michele et al. (2001), and Veneziano et al. (2007) and (2013).

However, some limitations to the use of the MS models in extreme precipitation analysis still exist. In particular, due to the difficulty to deal with EVT distributions in an MS framework³ and because of the larger number of parameters that MS involves, the estimation of IDF and IDAF curve has been often limited to SS models. Moreover, while MS has been demonstrated to be more appropriate for modeling scale invariance of the overall precipitation distribution (i.e., not only the extremes), abundant studies confirmed the validity of SS for precipitation distribution tails [Ceresetti et al. 2010; Panthou et al. 2014; Sane et al. 2018].

³For instance, the GEV naturally respects the mono-fractal SS property, as it has been showed in Sec. 4.2.3.

Chapter 5

Thesis overview

The previous chapters showed the importance of a multi-scale analysis of extreme precipitation. No single statistical modeling technique seems to comprehensively embody all the crucial aspects of the precipitation distribution and spatio-temporal structure. However, several issues can be addressed and modeled at the same time using scaling models.

5.1 Research questions

Taking advantage of the physical basis of the scale invariance property of precipitation, and integrating the central elements of the EVT, scaling models allow an efficient description of the extreme precipitation variability across scales. Data from different scales can be pooled under the hypothesis of scale invariance, reducing sampling errors and uncertainties in the inference of extreme precipitation distribution.

Moreover, the scaling framework allows for a statistically consistent and parsimonious definition of IDF and IDAF curves, while in engineering practice their estimation is mainly empirical and may involve some arbitrary assumptions. Even more interesting, within the range of spatial and/or temporal scales for which the scale-invariance holds, the statistical characteristics of extreme precipitation may also be approximated for scales with no available record. For instance, assuming that the SS is valid for sub-daily to daily precipitation, sub-daily extreme characteristics can be in principle inferred from longer-duration series (e.g., daily precipitation data) which are more widely

available than short-duration records. The approach could thus provide a more comprehensive representation of precipitation extremes for spatio-temporal scales which are more difficult to sample and over regions that are sparsely covered by meteorological network.

However, the use of scaling models has been mainly restricted to specific regions and small observational datasets. An extensive analysis of the effects of local climate and geographic characteristics on the estimated scaling relationships, as well as the evaluation of their validity across a wide range of spatio-temporal scales, is thus needed.

Moreover, the number of applications of spatio-temporal scaling models remains small, as available observations (e.g. station records) limits the investigation of extreme precipitation across various spatial scales. In the literature, STS investigations were often based on interpolated gridded datasets obtained from station series [e.g., De Michele et al. 2002; Ceresetti et al. 2010; Panthou et al. 2014]. This entailed the use of correction, interpolation, and averaging techniques in order to construct gridded precipitation series that may ultimately impair the spatio-temporal structure of extreme precipitation. The impacts of such preliminary processing, as well as some other basic characteristics of precipitation datasets (e.g., their spatial or temporal resolution), on estimated scale invariance properties might be substantial but, to our knowledge, no exhaustive study has focused on the subject.

Finally, as stressed in Ch. 2, many authors highlighted that important modifications of the spatio-temporal structure of extreme precipitation are expected under CC, with direct implications regarding IDFs and ARFs [e.g., Li et al. 2015; Cannon and Innocenti 2018]. Scaling models can be thus considered for providing a comprehensive assessment of projected extreme precipitation changes across scales. However, only a few studies exploited the scale invariance framework to efficiently evaluate these changes [e.g., Casas-Castillo et al. 2018] and, to our knowledge, they were mainly restricted to temporal SS applications.

5.2 Project objectives

The overall objective of the thesis was to conduct a comprehensive analysis of the spatio-temporal structure of extreme precipitation based on scaling models in historical and future climate.

Temporal SS models were first defined and the scale-invariance properties of heavy precipitation with respect to duration were assessed using a large dataset of meteorological station series. This aimed at evaluating the possibility of drawing information on both observed and non-observed temporal scales through the SS framework. To this end, the following specific objectives were considered:

- 1.1 Find the specific formulations of SS suitable for different duration intervals and determine the SS IDF expressions that adequately represent the statistical distributions of at-site precipitation intensity for each station of the study domain (see Sec. 5.3).
- 1.2 Evaluate biases arising from temporal SS approximations for extreme precipitation quantiles. The variability of temporal scaling estimates across various spatial scales was also investigated for observational gridded datasets (e.g., satellite data).
- 1.3 Assess the spatial distribution of scaling parameters over a large spatial domain and examine if the geo-climatic characteristics of the study region have an impact on the scale-invariance properties of extreme precipitation.
- 1.4 Evaluate the influence on temporal SS estimators of dataset characteristics, such as their spatio-temporal or measurement resolutions. The range of validity, the magnitude, and the spatial variability of the estimated scaling laws were also compared among datasets, in order to assess the impacts of data processing techniques (e.g., series interpolation).

The second objective was to evaluate CC impacts on precipitation extremes based on scaling models evolution in next decades.

The validity of the scale-invariance property for simulated series covering past periods was verified in order to evaluate the ability of climate models to reproduce the spatio-temporal structure of extreme precipitation and their probability distributions. Hence, the specific objectives of the second part of the project were:

- 2.1 Evaluate the effectiveness of RCMs in reproducing the scale-invariance relationships previously identified on observational datasets. The differences between the simulated and observed datasets were analyzed in terms of the estimated SS parameter values.

2.3 To identify specific biases and uncertainties for simulated extreme characteristics, the annual and daily cycles of extreme precipitation occurrences were also compared between simulated and observational datasets.

2.3 Analyze the temporal evolution of scaling laws in future climate using projected precipitation series. The impacts of the climate variability and CC on precipitation scaling properties were studied through the analysis of precipitation projections for various periods of different lengths. Using samples of various sizes allowed to assess the uncertainty of the estimations at local spatial scales.

5.3 Data and Study region

Five datasets with different characteristics were considered in the project:

- series from ≈ 3000 meteorological stations covering the continental US and Canada;
- a 50-member ensemble and two ERA-Interim driven simulations from the Canadian RCM generation 5 (CRCM5) [Leduc et al. 2019];
- one high-resolution CPM simulation from the Weather Research and Forecasting (WRF) model [Liu et al. 2017; Prein et al. 2017a];
- the CMORPH bias-corrected satellite dataset [Xie and Xiong 2011]; and
- the Multi-Source Weighted-Ensemble Precipitation (MSWEP) v2 dataset [Beck et al. 2017a].

Meteorological stations were used to assess SS properties of point-scale precipitation AM over most of North America [Fig. 5.1a] for durations between 15 min and 7 days. Then, both stations and gridded datasets were considered to evaluate the variability of SS estimates across various spatial scales over the northeastern part of North America [CRCM5 North-American domain; Fig. 5.1-5.2]. Finally, CRCM5 simulations for future decades were considered to evaluate the temporal evolution of scaling model estimates.

The main characteristics of the available datasets and series used in the three steps of the analysis are summarized in Tables 5.1 and 5.2.

5.3.1 Meteorological station series

Four gage-station datasets were considered for the extraction of point-scale AMS: the Hourly Precipitation Data (HPD) and 15-Min Precipitation Data (15PD) datasets made available by the National Oceanic and Atmospheric Administration (NOAA) agency¹ for the United States, and the Daily Maxima (DM) and Hourly (H) series provided by Environment and Climate Change Canada (ECCC) and the *Ministère du Développement Durable, de l'Environnement, de la Lutte contre les Changements Climatiques du Québec* (MDDELCC) for Canada. For consistency of notation, datasets for Canada are referred to as Daily Maxima Precipitation Data (DMPD) and Hourly Canadian Precipitation Data (HCPD).

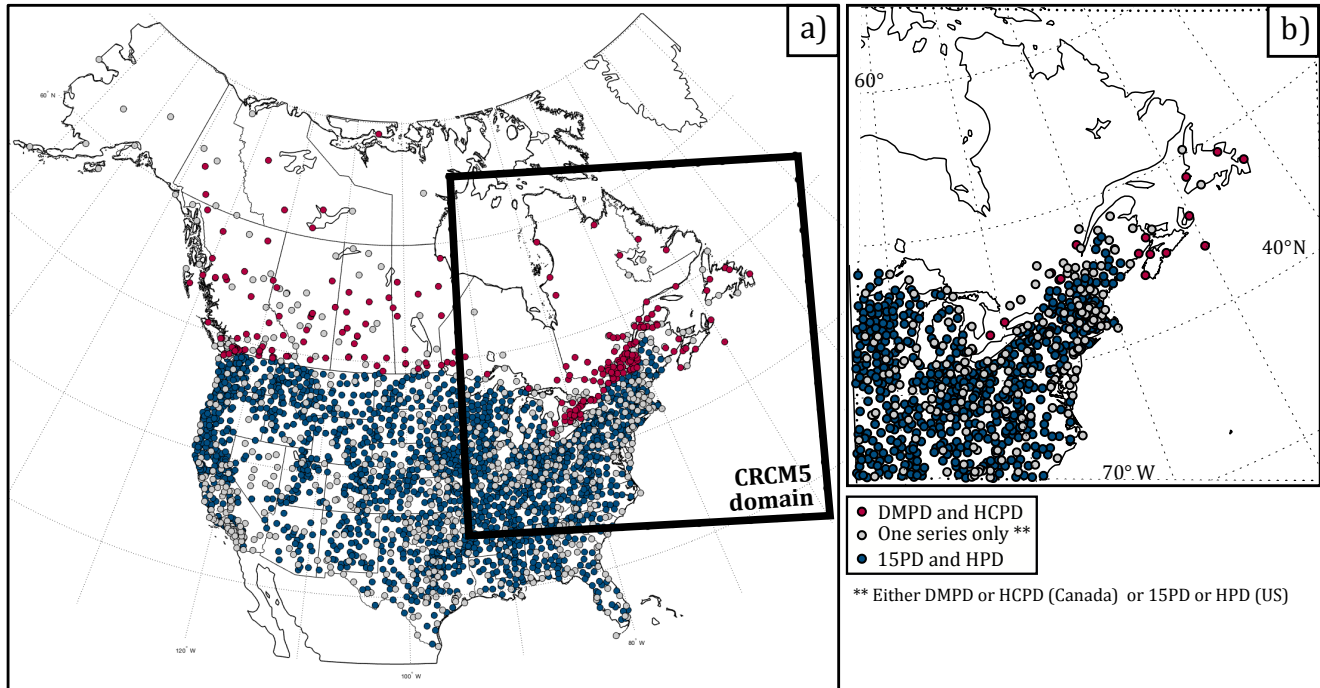


Figure 5.1: Stations and temporal resolution of recorded series selected for the analysis of: a) temporal SS properties of point-scale AMS; b) temporal SS comparison between station and gridded dataset AMS.

DMPD, Canada: DMPD series were available from 370 stations generally equipped with tipping bucket gauges and recording daily maxima depth for durations of 5, 10, 15, and 30 minutes and 1, 2, 6, and 12 hours. Each day is defined as the fixed 24-hour window starting at 8:00 AM.

¹Data and documentation are available at <http://gis.ncdc.noaa.gov/geoportal/catalog/search/resource/details.jsp?id=gov.noaa.ncdc%3AC00313> and <http://gis.ncdc.noaa.gov/geoportal/catalog/search/resource/details.jsp?id=gov.noaa.ncdc%3AC00505>, respectively for HPD and 15PD.

The period covered by DMPD series goes from 1937 to 2010, but many records are shorter than 15 years. Moreover, for most stations, the annual recording period does not cover winter months, and available series generally include precipitation measured from May to October.

HCPD, Canada: A total of 655 hourly precipitation series were available from 1953 to 2012. HCPD stations record precipitation with weight-type or tipping bucket gauges [Mailhot and Talbot 2011; CSA 2012] and are often located next to DMPD stations. Similarly to DMPD series, winter month precipitation is generally not recorded.

HPD and 15PD, US: Hourly and 15-min precipitation accumulations are measured by two different gauges (tipping bucket and weighing gauge) located at National Weather Service, Federal Aviation Administration, and cooperative observer stations in the United States. The total number of stations included in the datasets is 5500 [NCDC 2003], but a far smaller number was available for the present study. The recording period ranges approximately from 1948 to 2011, while the record length varies considerably by state and region. The earliest records date back to 1900 for a few stations and 1970s for the most recent stations [NCDC 2003], especially for 15-min series.

5.3.1.1 Station selection and quality control

The selection of stations aimed at providing the most comprehensive coverage of the study region with the longest series. This procedure takes into consideration missing data² through the following criteria:

- at least 85% of the observations must be valid for each year, otherwise, the year is considered as missing;
- each station must have at least 15 valid years.

These criteria ensure not to reject too many years/stations while maintaining a minimal number of observations for computing the annual maximum of each year.

²Lists of identified and possible errors in available recorded series are provided in Metcalfe et al. (1997), Mailhot and Talbot (2011), Mekis and Vincent (2011), and CSA (2012) for Canada station measurements, and in NCDC (2003) for US series.

Because the recording period for the DMPD and HPD datasets does not generally include winter months, point-scale SS assessment (see Article 1) considered series covering:

- the period from June to September for the stations located north of the 49th Parallel (122 days/year are used);
- the period from May to October for stations located south of the 49th Parallel (184 days/year are used);

Selected stations were mainly located in the United States and southern and most densely populated parts of Canada, as shown by Fig. 5.1a. For the comparison between stations and gridded datasets [see Table 5.2 and Article 2], only stations with valid records over the entire year (i.e., also during winter months) were considered, resulting in fewer series concentrated in the southern part of the CRCM5 domain [Fig. 5.1b].

Table 5.1: List of available meteorological station series selected for point-scale SS analysis.

| Dataset | Region | N. of stations | Period* | Temporal resolution |
|-------------------------------|--------|----------------|-----------|---------------------|
| Daily Max. Prec. Data (DMPD) | Canada | 230 | 1964-2007 | 1, 2, 6, 12 h |
| Hourly Can. Prec. Data (HCPD) | Canada | 379 | 1967-2003 | 1 h |
| Hourly Prec. Data (HPD) | USA | 2278 | 1948-2013 | 1 h |
| 15-Min Prec. Data (15PD) | USA | 1083 | 1971-2013 | 15 min |

* Main operational network period corresponding to the 0.25th percentile of starting recording years and the 0.75th percentile of ending recording years of available stations.

5.3.2 CRCM5 series

As a part of the *Climate change and hydrological Extremes (ClimEx)* project ³, a large ensemble of 50 simulations has been produced using the 5th generation Canadian RCM [CRCM5 v3.3.3.1; Martynov et al. 2013; Separovic et al. 2013] for two spatial domains: one covering the northeastern part of North America [Fig. 5.2] and one covering most of Europe [Fig. 2 in Leduc et al. 2019].

³www.climex-project.org

This 50-member CRCM5 Large Ensemble (CRCM5-LE) was simulated for the 1950-2100 period by dynamically downscaling the previously existing CanESM2 [Salzen et al. 2013; Arora et al. 2011] Large Ensemble (CanESM2-LE) [Sigmond and Fyfe 2016; Fyfe et al. 2017] to a 0.11° resolution grid ($\approx 12\text{km}$) [Leduc et al. 2019]. The 50 independent CanESM2-LE runs were generated by applying random perturbations in initial simulation conditions [Fyfe et al. 2017] and considering observed emissions up to year 2005 and the RCP8.5 thereafter [Sigmond and Fyfe 2016; Meinshausen et al. 2011].

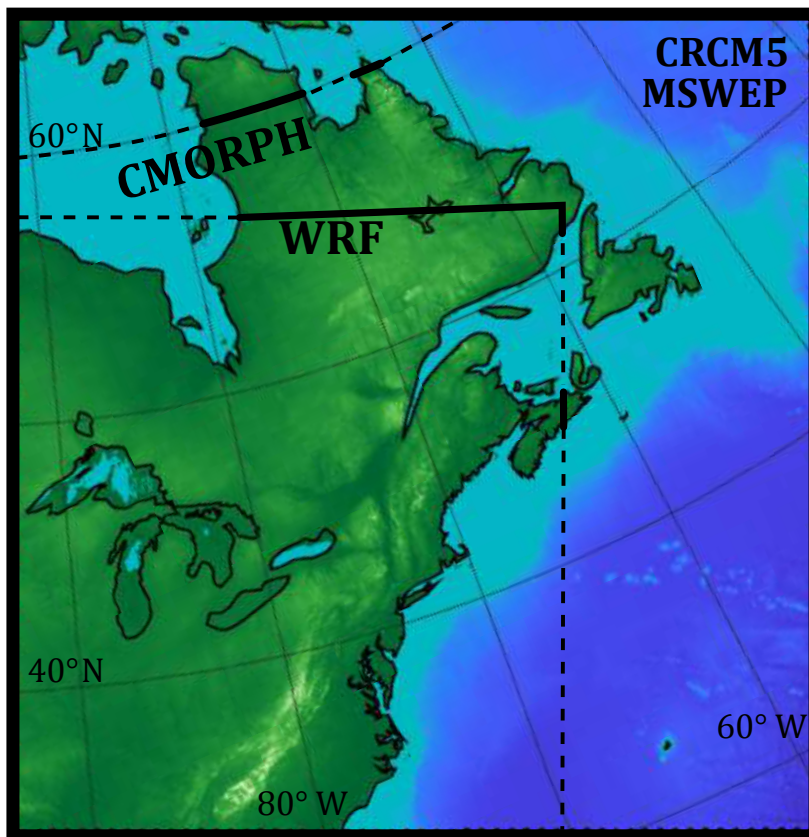


Figure 5.2: Spatial domains of gridded datasets: CRCM5 domain with topography and relevant boundaries of the WRF and CMORPH domains; MSWEP grid covers the entire CRCM5 domain.

After the removal of a 50-grid point buffer, simulated CRCM5-LE hourly precipitation series were available over the 1954-2099 period for 280×280 grid points [domain in Fig.5.2].

For the same domain, two additional CRCM5 simulations driven by the European Centre for Medium Range Weather Forecast (ECMRWF) ERA-Interim reanalysis [Dee et al. 2011] were produced at the same spatial resolution for the 1979-2013 period [Leduc et al. 2019]. For one of these

two simulations, hereby referred to as ERA-CRCM5-SN, large-scale spectral nudging was applied [Riette and Caya 2002; Separovic et al. 2012], as opposed to the other reanalysis-driven simulation, hereafter referred to as ERA-CRCM5. Since ERA-CRCM5-SN and ERA-CRCM5 presented almost indistinguishable estimates [see, for instance Fig. S1-S5 in the Supplementary Material of Article 2], only ERA-CRCM5 results are presented.

The ClimEx set-up for the simulation of the CRCM5-LE and ERA-Interim driven simulations is exhaustively described in Leduc et al. (2019), while CRCM5 dynamics and sub-grid model parametrization are described in Martynov et al. (2013) and Separovic et al. (2013).

5.3.3 WRF simulation

The WRF model, designed by the National Center for Atmospheric Research (NCAR) [Skamarock et al. 2008], has been frequently used to produce high-resolution simulations over short time periods and relatively limited domains in North America [e.g., Mahoney et al. 2012 and 2013; Liu et al. 2011; Rasmussen et al. 2011; and 2014].

Longer WRF simulations were recently run on larger domains to construct synthetic regional climatologies of severe storms and orographic precipitation [Liu et al. 2017; Hoogewind et al. 2017]. In particular, Liu et al. (2017) configured WRF into a RCM covering much of North America [see also Prein et al. 2017a]. A 13-year WRF v3.4.1 simulation was performed by dynamically downscaling the ERA-Interim reanalysis at the 4km resolution from October 2000 to September 2013 [Liu et al. 2017]. Details about WRF model and simulation set-up are provided in Prein et al. (2017a) and Liu et al. (2017).

WRF precipitation series were extracted for land grid boxes included in the CRCM5 domain [Fig. 5.2] for the 2001-2013 period.

5.3.4 CMORPH series

The *CMORPH v1.0 CRT* bias corrected dataset constitutes a homogeneous integration of the Climate Prediction Center (CPC) morphing technique (CMORPH) series at nearly global scale (60°N and 60°S) [Xie et al. 2017].

Original satellite analyses⁴ consist in high resolution precipitation estimates at a $8km - 30min$ resolution obtained after the combination of observations from multiple low-orbit microwave satellites ($\approx 12km \times 15km$ resolution) [Joyce et al. 2004; Xie and Xiong 2011]. Xie et al. (2017) applied a bias correction to the purely satellite-based analyses. Bias correction coefficients were computed against CPC daily gauge analysis [Xie et al. 2010] for land grid boxes. In particular, land grid box bias correction considered the climatological distribution pdf matching between the CPC gauge analysis and CMORPH analyses at the 0.25° resolution and daily scale plus an adjustment at coarser spatio-temporal resolution to account for the year-to-year variability [Xie et al. 2017].

CMORPH v1.0 CRT (hereinafter CMORPH) precipitation series were extracted for the entire record period (1998-2016) for all land grid boxes included in the CRCM5 domain [Fig. 5.2].

5.3.5 MSWEP series

The global Multi-Source Weighted-Ensemble Precipitation (MSWEP) v2 [Beck et al. 2017a and 2017b; <http://www.gloh2o.org/>] has been constructed through a multi-stage merging procedure of various datasets: the CPC Unified v1.0 and real time [Xie et al. 2007; Chen et al. 2008] and the GPCP Full Data Reanalysis and First Guess v7 [Schneider et al. 2014] gauge-based datasets, the quasi-global CMORPH v1.0, GSMaP-MVK v5-v6 [Ushio et al. 2009], and the TMPA 3B42RT v7 [Huffman et al. 2007] satellite analyses, and the Era-Interim and JRA-55 [Kobayashi et al. 2015] reanalyses. A detailed description and preliminary evaluation of MSWEP can be found in Beck et al. (2017a) and [2017b].

MSWEP precipitation series were available at the 3h temporal resolution on a 0.1° grid covering the entire CRCM5 domain for the 1979-2016 period.

Despite its relatively coarse temporal resolution, this dataset can provide valuable information about precipitation extremes occurring in northern regions of the study domain where no sub-daily precipitation records are available. For the same reason, however, MSWEP performances in northern areas should be evaluated due the usually poor quality of satellite data in cold regions and the sparse station network in the north of the domain.

⁴http://www.cpc.ncep.noaa.gov/products/janowiak/cmorph_description.html

Table 5.2: Stations and gridded datasets used for extracting AM at various spatial scales.

| Dataset | Description | Period | Spatio-temporal resolution | Reference |
|-------------------------|-----------------------------------|-----------------------|----------------------------|---------------------------------|
| Meteorological stations | HCPD and DMPD series | 1940 - 2013 | 1h and Daily Maxima* | ECCC MDELCC |
| | 15PD and HPD series | | 15min and 1h | NOAA |
| CRCM5-LE [50 members] | CanESN2-LE driven members | 1954 - 2099 | 0.11° - 1h, (≈12km) | Leduc et al., 2019 |
| ERA-CRCM5 | ERA-Interim driven simulation | 1981 - 2013 | | |
| WRF | ERA-Interim driven simulation | Oct. 2000 - Sep. 2013 | 4km - 1h | Liu et al. (2017) |
| CMORPH [v1.0 CRT] | Bias-corrected satellite analyses | 1998 - 2016 | 8km - 30min | Xie et al. (2017) |
| MSWEP [v2] | Multi-source gridded dataset | 1979 - 2016 | 0.1° - 3h, (≈ 11km) | Beck et al. (2017a) and [2017b] |

* Daily maxima depth over a 24h window beginning at 08:00 (LT) for durations 1, 2, 6, and 12h

5.4 Annual Maxima (AM) extraction

Annual Maxima (AM) were used to characterize precipitation extremes at each spatial location, namely a station or land grid box, for various durations $d = d_0, d_1, \dots, d_D$, and various spatial scales⁵, $a = a_0, a_1, \dots, a_A$. For each dataset, a_0 corresponds to its native grid resolution ($a_0 = 0$ for stations) and d_0 to its native temporal resolution.

A moving window was applied to depth precipitation series to estimate aggregated series at each duration d , excepted that for DMPD station series. For gridded datasets, a fixed window in space was also used to aggregate grid box series at various spatial scales a [see Table 5.3 for the lists of spatial scales considered for each dataset]. In particular, grid box series at d_0 were spatially aggregated for each time step over coarser resolution grids, defined starting at the south-west cor-

⁵Note that the spatial scale is here identified with a for consistency with previous chapters, while the notation r was used in Article 2 and 3 for consistency with datasets resolution notation (e.g., r_0 for dataset native resolution).

ner of native dataset grids and moving toward the opposite (north-east) corner. Native grid boxes associated with water bodies were removed and grid boxes at spatial scales $a > a_0$ were discarded if including less than 75% native land grid boxes. This spatial aggregation procedure was defined to most realistically mimic the possible changes in the spatial resolution of gridded datasets [Eggert et al. 2015].

Finally, for each location, duration, and spatial scale, AM were extracted for each valid year. For stations with both DMPD and HCPD series, or 15PD and HPD series, the maximum value of the two available AM was retained as the annual AM.

Table 5.3: Spatial scales considered for each gridded dataset.

| | a_0 | No. of scales | a |
|-----------------------|-----------------|---------------|--|
| ERA-CRCM5 CRCM5-LE | ≈ 12 km | 6 | 12, 24, \dots , 72 km |
| WRF | 4 km | 12 | 4, 8, \dots , 24 km and 32, 40, \dots , 72 km |
| CMORPH | 8 km | 9 | 8, 16, \dots , 72 km |
| MSWEP | ≈ 11 km | 6 | 11, 22, \dots , 66 km |

Part II

Articles

Article 1

Simple Scaling of extreme precipitation in North America

S. Innocenti¹, A. Mailhot¹, and A. Frigon²

1. Centre Eau-Terre-Environnement, INRS, Québec, Canada;

2. Consortium Ouranos, Montréal, Canada.

Published 24 Nov 2017, Hydrology and Earth System Sciences:

Innocenti, S., Mailhot, A., and Frigon, A.: Simple scaling of extreme precipitation in North America, Hydrol. Earth Syst. Sci., 21, 5823-5846, <https://doi.org/10.5194/hess-21-5823-2017>, 2017.

Résumé

Les précipitations extrêmes sont caractérisées par une forte variabilité spatiale et temporelle. Il est donc important de caractériser les distributions de l'intensité des précipitations à plusieurs échelles spatiales et temporelles. Il s'agit d'un enjeu fondamental autant pour la prévision des risques liés aux aléas naturels que pour la conception des infrastructures et la gestion des ressources. Dans ces domaines, les courbes Intensité-Durée-Fréquence (IDF) sont des outils standards pour décrire les relations entre les intensités, fréquences et la durée des pluies extrêmes. Les modèles des lois d'échelle basés sur l'hypothèse d'invariance d'échelle (*Simple Scaling*, SS) peuvent aussi être utilisés pour décrire les relations entre les distributions de probabilité des extrêmes de précipitations sur plusieurs durées et représentent un outil puissant pour améliorer les estimations des courbes IDF.

Dans cette étude, les modèles SS ont été appliqués sur environ 2700 stations en Amérique du Nord. Des séries des Maxima Annuels (MA) de précipitations extraites sur plusieurs intervalles de durée (de 15 minutes à 7 jours) ont été considérées. L'étendue de la validité, l'ordre de grandeur et la variabilité spatiale des exposants qui définissent les lois d'échelle ont été examinés.

Les résultats enrichissent les connaissances concernant l'influence autant des caractéristiques géographiques locales (telles que la topographie) que celle des propriétés climatiques régionales sur les lois d'échelle des précipitations extrêmes. Les distributions généralisées des valeurs extrêmes (GEV) basées sur les modèles SS ont aussi été analysées. Les résultats montrent une amélioration des estimations des paramètres de la GEV, particulièrement pour le paramètre de forme, lorsque les données sont regroupées sous l'hypothèse d'invariance d'échelle.

Abstract

Extreme precipitation is highly variable in space and time. It is therefore important to characterize precipitation intensity distributions at several temporal and spatial scales. This is a key issue in infrastructure design and risk analysis, for which Intensity-Duration-Frequency (IDF) curves are the standard tools used for describing the relationships among extreme rainfall intensities, their frequencies, and their durations. Simple Scaling (SS) models, characterizing the relationships among extreme probability distributions at several durations, represent a powerful means for improving IDF estimates. This study tested SS models for approximately 2700 stations in North America. Annual Maxima Series (AMS) over various duration intervals from 15 min to 7 days were considered. The range of validity, magnitude, and spatial variability of the estimated scaling exponents were investigated. Results provide additional guidance for the influence of both local geographical characteristics, such as topography, and regional climatic features on precipitation scaling. Generalized Extreme Value (GEV) distributions based on SS models were also examined. Results demonstrate an improvement of GEV parameter estimates, especially for the shape parameter, when data from different durations were pooled under the SS hypothesis.

1.1 Introduction

Extreme precipitation is highly variable in space and time as various physical processes are involved in its generation. Characterizing this spatial and temporal variability is crucial for infrastructure design and to evaluate and predict the impacts of natural hazards on ecosystems and communities. Available precipitation records are however sparse and cover short time periods, making a complete and adequate statistical characterization of extreme precipitation difficult. The resolution of available data, whether observed at meteorological stations or simulated by weather and climate models, often mismatches the resolution needed for applications [e.g., Blöschl and Sivapalan 1995; Maraun et al. 2010; Willems et al. 2012], thus adding to the difficulty of achieving complete and adequate statistical characterizations of extreme precipitation.

The need for multi-scale analysis of precipita-

tion has been widely recognized in the past [Rodriguez-Iturbe et al. 1984; Blöschl and Sivapalan 1995; Hartmann et al. 2013; Westra et al. 2014 among others] and much effort has been put into the development of relationships among extreme precipitation characteristics at different scales. The conventional approach for characterizing scale transitions in time involves the construction of Intensity-Duration-Frequency (IDF) or the equivalent Depth-Duration-Frequency (DDF) curves [Bernard 1932; Burlando and Rosso 1996; Sivapalan and Blöschl 1998; Koutsoyiannis et al. 1998; Asquith and Famiglietti 2000; Overeem et al. 2008; Veneziano and Yoon 2013]. These curves are a standard tool for hydraulic design and risk analysis as they describe the relationships between the frequency of occurrence of extreme rainfall intensities (depth) X_d and various durations d [e.g., CSA 2012]. Analysis is usually conducted by separately estimating the statistical distributions of X_d at the different durations [see Koutsoyiannis

et al. 1998; Papalexiou et al. 2013 for discussions about commonly used probability distributions]. The parameters or the quantiles of these theoretical distributions are then empirically compared to describe the variations of extreme rainfall properties across temporal scales.

Despite its simplicity, this procedure presents several drawbacks. In particular, it does not guarantee the statistical consistency of precipitation distributions, independently estimated at the different durations, and it limits IDF extrapolation at non-observed scales or ungauged sites. Uncertainties of estimated quantiles are also presumably larger because precipitation distribution and IDF curve parameters are fitted separately.

Scaling models [Lovejoy and Mandelbrot 1985; Gupta and Waymire 1990; Veneziano et al. 2007] based on the concept of scale invariance [Dubrulle et al. 1997], have been proposed to link rainfall features at different temporal and spatial scales. Scale invariance states that the statistical characteristics (e.g., moments or quantiles) of precipitation intensity observed at two different scales d and λd can be related to each other by a power law of the form:

$$f(X_{\lambda d}) = \lambda^{-H} f(X_d) \quad (1.1)$$

where $f(\cdot)$ is a function of X with invariant shape when rescaling the variable X by a multiplicative factor λ and for some values of the exponent $H \in \mathbb{R}$. In the simplest case, a constant multiplicative factor adequately describes the scale change. The corresponding mathematical models are known as *Simple Scaling* (SS) models [Gupta and Waymire 1990]. SS models are attractive because of the small number of parameters involved, as opposed to *Multiscaling* (MS) models which involve more than one

multiplicative factor in Eq. (1.1) [e.g., Lovejoy and Schertzer 1985; Gupta and Waymire 1990; Burlando and Rosso 1996; Veneziano and Furcolo 2002; Veneziano and Langousis 2010; Langousis et al. 2013]. A single *scaling exponent* H is used to characterize the extreme rainfall distribution at all scales over which the scale invariance property holds. As a consequence, a consistent and efficient estimation of extreme precipitation characteristics is possible, even at non-sampled temporal scales, and a parsimonious formulation of IDF curves based on analytical results is available [e.g., Menabde et al. 1999; Burlando and Rosso 1996; De Michele et al. 2001; Ceresetti 2011].

Theoretical and physical evidence of the scaling properties of precipitation intensity over a wide range of durations has been provided by several studies. MS has been demonstrated to be appropriate for modeling the temporal scaling features of the precipitation process (i.e., not only the extreme distribution) and for the extremes in event-based representations of rainfall (stochastic rainfall modeling) [e.g., Veneziano and Furcolo 2002; Veneziano and Iacobellis 2002; Langousis et al. 2013 and references therein]. These multifractal features of precipitation last within a finite range of temporal scales (approximately between 1 hour and 1 week) and concern the temporal dependence structure of the process. They have been connected to the large fluctuations of the atmospheric and climate system governing precipitation which are likely to produce a "cascade of random multiplicative effects" [Gupta and Waymire 1990].

At the same time, many studies confirmed the validity of SS for approximating the precipitation distribution tails in IDF estimation [for examples of durations ranging from 5 min to 24 h see Menabde et al. 1999; Veneziano and Furcolo 2002;

Yu et al. 2004; Nhat et al. 2007; Bara et al. 2009; Ceresetti et al. 2010; Panthou et al. 2014]. This type of scaling is substantially different from the temporal scaling since it only refers to the power law shape of the marginal distribution of extreme rainfall. Application of the SS models to precipitation records showed that the scaling exponent estimates may depend on the considered range of durations [e.g., Borga et al. 2005; Nhat et al. 2007] and the climatological and geographical features of the study regions [e.g., Menabde et al. 1999; Bara et al. 2009; Borga et al. 2005; Ceresetti et al. 2010; Blanchet et al. 2016]. However, the application of the SS framework has been mainly restricted to specific regions and small observational datasets. A deeper analysis of the effects of geoclimatic factors on the SS approximation validity and on estimated scaling exponent is thus needed.

The present study aims to deepen the knowledge of the scale-invariant properties of extreme rainfall intensity by analyzing SS model estimates across North America using a large number of station series. The specific objectives of this study are: a) assess the ability of SS models to reproduce extreme precipitation distribution; b) explore the variability of scaling exponent estimates over a broad set of temporal durations and identify possible effects of the dominant climate and pluviometric regimes on SS; c) evaluate the possible advantages of the introduction of the SS hypothesis in parametric models of extreme precipitation.

Note that, although modifications in precipitation distributions are expected as a result of climate changes [e.g., Trenberth et al. 2003; Hartmann et al. 2013; Westra et al. 2014], the proposed approach implicitly relies on the assumption of stationarity for extreme rainfall. This choice has

been motivated by both the limited evidence for changes in rainfall intensities for North America extremes during last decades, and the difficulties of assessing distribution changes from short recorded series, especially for sub-daily extremes [Barbero et al. 2017 and references therein].

The article is structured as follows. In Sect. 1.2 the statistical basis of scaling models is presented, while data and their preliminary treatments are described in Sect. 1.3. Sect. 1.4 presents the distribution-free estimation of SS models and their validation using available series. Section 1.5 focuses on to the spatial variability of SS exponents and discusses the scaling exponent variation from a regional perspective. Finally, the SS estimation based on the Generalized Extreme Value (GEV) assumption is discussed in Sect. 1.6, followed by a discussion and conclusions [Sect. 7]. Table S1 of the supplementary material lists in alphabetic order the recurrent acronyms used in text.

1.2 Simple Scaling models for precipitation intensity

When the equality in Eq. (1.1) holds for the cumulative distribution function (cdf) of the precipitation intensity X sampled at two different durations d and λd , the Simple Scaling (SS) can be expressed as [Gupta and Waymire 1990; Menabde et al. 1999]:

$$X_d \stackrel{dist}{=} \lambda^H X_{\lambda d}, \quad (1.2)$$

where $H \in \mathbb{R}$ and $\stackrel{dist}{=}$ means that the same probability distribution applies for X_d and $X_{\lambda d}$, up to a dilatation or contraction of size λ^H . An important consequence of the SS assumption is that X_d

and $\lambda^H X_{\lambda d}$ have the same distribution. Hence, if X_d and $X_{\lambda d}$ have finite moments of order q , $E[X_d^q]$ and $E[X_{\lambda d}^q]$, these moments are thus linked by the following relationship [Gupta and Waymire 1990; Menabde et al. 1999]:

$$E[X_d^q] = \lambda^{Hq} E[X_{\lambda d}^q]. \quad (1.3)$$

This last relationship is usually referred to as the *wide sense* simple scaling property [Gupta and Waymire 1990] and signifies that simple scaling results in a simple translation of the log-moments between scales:

$$\ln \{E[X_d^q]\} = \ln \{E[X_{\lambda d}^q]\} + Hq \ln \lambda \quad (1.4)$$

Moreover, without loss of generality, λ can always be expressed as the scale ratio $\lambda = d/d^*$ defined for a reference duration d^* chosen, for simplicity, as $d^* = 1$. Therefore, the SS model can be estimated and validated over a set of durations $d_1 < d_2 < \dots < d_D$ by simply checking the linearity in a log-log plot of the X moments versus the observed durations d_j , $j = 1, 2, \dots, D$ [see, for instance, Gupta and Waymire (1990); Burlando and Rosso (1996); Fig. 1 of Nhat et al. (2007); and Fig. 2 (a) of Panthou et al. (2014)]. If H estimated for the first moment equals the exponents (slopes) for the other moments, the precipitation intensity X can be considered scale invariant under SS in the interval of durations d_1 to d_D .

More sophisticated methods have also been proposed for detecting and estimating scale invariance [for instance, dimensional analysis, Lovejoy and Schertzer (1985); Tessier et al. (1993); Bendjoudi et al. (1997); Dubrulle et al. (1997); spectral analysis and wavelet estimation Ols-son et al. (1999); Venugopal et al. (2006) Cere-

setti (2011); and empirical probability distribution function (pdf) power law detection Hubert and Bendjoudi (1996); Sivakumar (2000); Ceresetti et al. (2010)]. However, estimation through the moment scaling analysis is by far the simplest and most intuitive tool to check the SS hypothesis for a large dataset. For this reason, the presented analyses are based on this method.

According to the literature, the values of the scaling exponents H generally range between 0.4 and 0.8 for precipitation intensity considered at daily and shorter time scales [e.g., Burlando and Rosso 1996; Menabde et al. 1999; Veneziano and Furcolo 2002; Bara et al. 2009] (note that for the rainfall depth the scaling exponent $H_{depth} = 1 - H$ applies). Values from 0.3 to 0.9 have also been reported for some specific cases [e.g., Yu et al. 2004; Panthou et al. 2014 for scaling intervals defined within 1 h and 24 h].

Higher H values have been generally observed for shorter-duration intervals, and regions dominated by convective precipitation [e.g., Borga et al. 2005; Nhat et al. 2007; Ceresetti et al. 2010; Panthou et al. 2014 and references therein]. Nonetheless, some studies performing spatio-temporal scaling analysis reached a different conclusion. For instance, Eggert et al. 2015, analyzing extreme precipitation events from radar data for durations between 5 min and 6 h and spatial scales between 1 km and 50 km, indirectly showed that stratiform precipitation intensity generally displays higher temporal scaling exponents than convective intensity. For short-duration intervals (typically less than one hour), previous studies have also reported more spatially homogeneous H estimates than for long-duration intervals [e.g., Alila 2000; Borga et al. 2005 and references therein]. This suggests that processes involved in the generation

of local precipitation are comparable across different regions.

More generally, higher H values are associated with larger variations in moment values as the scale is changed (i.e. a stronger scaling), while H close to zero means that the X_d distributions for different durations d more closely match each other.

1.2.1 Simple Scaling GEV models

Annual Maximum Series (AMS) are widely used to select rainfall extremes from available precipitation series. Various theoretical arguments and experimental evidences support their use for extreme precipitation inference [e.g., Coles et al. 1999; Katz et al. 2002; Koutsoyiannis 2004a; Papalexiou et al. 2013].

Based on the asymptotic results of the Extreme Value Theory [Coles 2001], the AMS distribution of a random variable X is well described by the Generalized Extreme Value (GEV) distribution family. If we represent the AMS by (x_1, x_2, \dots, x_n) , the GEV cdf can be written as [Coles 2001]:

$$F(x) = \exp \left\{ - \left[1 + \xi \left(\frac{x - \mu}{\sigma} \right) \right]^{-1/\xi} \right\} \quad (1.5)$$

where $\xi \neq 0$, $-\infty < x \leq \mu + \sigma/\xi$ if $\xi < 0$ (bounded tail), and $1/\mu + \sigma\xi \leq x < +\infty$ if $\xi > 0$ (heavy tail). If $\xi = 0$ (light-tailed shape, Gumbel distribution), Eq. (1.5) reduces to:

$$F(x) = \exp \left\{ - \exp - \left\{ \frac{x - \mu}{\sigma} \right\} \right\} \quad (1.6)$$

where $-\infty < x < +\infty$. In Eq. (1.5) and (1.6), the parameters $\mu \in \mathbb{R}$, $\sigma > 0$ and ξ respectively represent the location, scale, and shape parameters of the distribution. The shape parameter describes

the characteristics of the distribution tails. Thus, high order quantile estimation is particularly affected by the value of ξ .

In applications, the GEV distribution is frequently constrained by the assumption that $\xi = 0$ (i.e., to the Gumbel distribution), due to the difficulty of estimating significant values of the shape parameter when the recorded series are short [e.g., Borga et al. 2005; Overeem et al. 2008; CSA 2012]. However, based on theoretical and empirical evidence, many authors have shown that this assumption is too restrictive for extreme precipitation, and may lead to important underestimations of the extreme quantiles [e.g., Koutsoyiannis 2004a; Koutsoyiannis 2004b; Overeem et al. 2008; Papalexiou et al. 2013; Papalexiou and Koutsoyiannis 2013]. Instead, approaches aimed at increasing the sample size may be used to improve the estimation of the GEV distribution shape parameter [for instance, the Regional Frequency Analysis (RFA), Hosking and Wallis 1997]. Among these approaches, SS models constitute an appealing way to pool data from different samples (durations) and reduce uncertainties in GEV parameters.

For the GEV distribution it is straightforward to verify that, if $X \stackrel{dist}{=} GEV(\mu, \sigma, \xi)$ then $\lambda X \stackrel{dist}{=} GEV(\lambda\mu, \lambda\sigma, \xi)$ for any $\lambda \in \mathbb{R}$. This means that the GEV family described by Eq. (1.5) and (1.6) satisfies Eq. (1.1) and thus complies with statistical scale invariance for any constant multiplicative transformation of X . Hence, when the scale invariance is further assumed for the change of observational scale from duration d to λd [as in Eq. 1.2], the wide sense SS definition [Eq. (1.3)] gives:

$$\mu_d = d^H \mu_*, \sigma_d = d^H \sigma_*, \text{ and } \xi_d = \xi_* \quad (1.7)$$

where μ_* , σ_* , and ξ_* represent the GEV parameters for a reference duration d^* chosen, for simplicity, as $d^* = 1$, so that $\lambda = d$.

1.2.2 SS GEV estimation

Taking advantage of the scale invariant formulation of the GEV distribution, many authors have proposed simple scaling IDF and DDF models for extreme precipitation series [e.g, Yu et al. 2004; Borga et al. 2005; Bougadis and Adamowski 2006; Bara et al. 2009; Ceresetti 2011]. In these cases, the scaling exponent and the GEV parameters are generally estimated in two separate steps: first, the H value is empirically determined through a log-log linear regression, as described above; then, GEV parameters μ_* , σ_* , and ξ_* for the reference duration d^* are estimated on the pooled sample of all available durations. In this case, classical estimation procedures, such as GEV Maximum-Likelihood (ML) [Coles 2001] or Probability Weighted Moment (PWM) [Greenwood et al. 1979; Hosking et al. 1985], can be used.

In a few other cases, a Generalized Additive Model ML (GAM-ML) framework [Coles 2001; Katz 2013] has also been used to obtain the joint estimate of H , μ_* , σ_* , and ξ_* through the introduction of the duration as model covariate [e.g, Blanchet et al. 2016].

1.3 Data and study region

Four station datasets were used for the construction of intensity Annual Maxima Series (AMS) at different durations: the Daily Max-

ima Precipitation Data (DMPD) and the Hourly Canadian Precipitation Data (HCPD) datasets provided by Environment and Climate Change Canada [ECCC n.b.] and the MDDELCC (n.b.) [in french *Ministère du Développement Durable, de l'Environnement et de la Lutte contre les Changements Climatiques*] for Canada, and the Hourly Precipitation Data (HPD) and 15-Min Precipitation Data (15PD) datasets made available by the National Oceanic and Atmospheric Administration [NOAA n.d.] agency [<http://www.ncdc.noaa.gov/data-access/land-based-station-data>] for United States. The total number of stations was approximately 3400, with roughly 2200 locations having both DMPD and HCPD series, or both HPD and 15PD series. The majority of stations are located in the United States and in the southern and most densely populated areas of Canada. In northern regions the station network is sparse and the record length does not generally exceed 15 or 20 years. Moreover, for most of DMPD and HCPD stations, the annual recording period does not cover the winter season and available series generally include precipitation measured from May to October. For this reason, the *year* from which the annual maxima was sampled was limited to the recording season going from June to September for northern stations [stations located north of the 52nd Parallel] and from May to October¹ for the southern stations. As a result, 122 days a year were used for northern stations and 184 days a year for remaining stations.

Data were collected through a variety of instruments [e.g., standard, tipping-bucket, and Fischer-Porter rain gauges] and precipitation values were processed and quality-controlled using both automated and manual methods [CSA 2012

¹The published version of the paper contain the following mistake: "June to September".

Table 1.1: List of available datasets and their main characteristics.

| Dataset | Region | N. of stations | Operational period ^b | Temporal resolution | Prevalent ^c resolution [mm] |
|---|--------|----------------|---------------------------------|---------------------|--|
| Daily Maxima Prec. Data ^a (DMPC) | Canada | 370 | 1964-2007 | 1, 2, 6, 12 h | 0.1 (82.25%) |
| Hourly Canadian Prec. Data (HCPD) | Canada | 665 | 1967-2003 | 1 h | 0.1 (70%) |
| Hourly Prec. Data (HPD) | USA | 2531 | 1948-2013 | 1 h | 0.254 (82.5%) |
| 15-Min Prec. Data (15PD) | USA | 2029 | 1971-2013 | 15 min | 2.54 (80.42%) |

^a Daily maxima depth series over a 24-hour window beginning at 8:00 AM.

^b Main station network operational period corresponding to 25th percentile of the first recording year and the 75th percentile of the last recording year of the stations.

^c Prevalent instrument resolution, estimated by the lowest non-zero value for each series, and corresponding percentage of stations with this resolution.

Table 1.2: Final datasets used in scaling analysis and corresponding AMS characteristics.

| Scaling dataset | Durations | N. of Stations | Mean series length [yr] | Max series length [yr] |
|-----------------|-----------------------|----------------|-------------------------|------------------------|
| SD ^a | 15min, 30min, ..., 6h | 1083 | 20 | 36 |
| ID | 1h, 2h, ..., 24h | 2719 | 37.4 | 66 |
| LD | 6h, 12h, ..., 168h | 2719 | 37.4 | 66 |

^a Only 15PD series.

HPD and 15PD online documentation]. Most often, observations were recorded by tipping-bucket gauges with tip resolution from 0.1 mm to 2.54 mm [CSA 2012; Devine and Mekis 2008]. 15 min series usually present the coarser instrument resolution, with a minimum non-zero value of 2.54 mm, observed for about 80.5% of 15PD stations. The effects of such a coarse instrument resolution on simple scaling estimates could be important leading to empirical X_d cdfs becoming step-wise functions with a low number of steps. Some preliminary analyses aiming at evaluating these effects on SS estimates are presented in the supplementary material [see S2 and S3]. However, the 15PD dataset is important considering the associated network density and its fine temporal resolution, and thus it has been retained for our study. The main characteristics of the available datasets are summarized in Table 1.1.

The scaling AMS datasets were constructed ac-

ording to the following steps:

(i) Three duration sets were defined: a) 15 min to 6 h with a 15-min step; b) 1 h to 24 h with a 1-h step; c) 6 h to 168 h (7 days) with a 6-h step. These duration sets are hereinafter referred to as Short-Duration (SD), Intermediate-Duration (ID), and Long-Duration (LD) datasets, respectively [see Figure 1.1 (a)].

(ii) Meteorological stations that were included in each final dataset were selected according to the following criteria: 1) precipitation series must have at least 85% of valid observations for each May to October (or June to September) period, otherwise the corresponding year was considered as missing; 2) each station must have at least 15 valid years; 3) for each station, it was possible to compute AMS for all durations considered in the scaling dataset (e.g., HCPD and HPD stations were not included in the SD dataset because only

hourly durations were available). Note that, in order to exclude outliers possibly associated with recording or measurement errors, extremely large observations were discarded and assimilated to missing data. In particular, as in some previous studies [e.g, Papalexiou and Koutsoyiannis 2013; Papalexiou et al. 2013], an iterative procedure was applied prior to step (ii)-1) to discard observations larger than 10 times the second largest value of the series.

(iii) A moving window was applied to 15PD, HCPD, and HPD series to estimate aggregated series at each duration. For DMPD series, a quality check was also implemented in order to guarantee that precipitation intensities recorded each day at different durations were consistent with each other. For instance, each pair of DMPD rainfall intensity [mm] (x_{d_1}, x_{d_2}) observed at durations $d_1 < d_2$ must respect the condition $x_{d_2}/x_{d_1} \geq d_1/d_2$ derived from the definitions of daily maximum rainfall intensity and depth; otherwise all DMPD values recorded that day were discarded and assimilated to missing data.

(iv) For each selected station, annual maxima were extracted for each valid year and duration. For stations having both DMPD and HCPD series, or 15PD and HPD series, for each year, the annual maxima extracted from these two series were compared and the maximum value was retained as the annual maximum for that year.

Major characteristics of each scaling AMS dataset are reported in Table 1.2.

1.4 SS estimation through Moment Scaling Analysis (MSA)

Moment Scaling Analysis (MSA) for the SD, ID, and LD datasets was carried out to empirically validate the use of SS models for modeling AMS empirical distributions. Assessing the validity of the SS hypothesis for various duration intervals also aimed at determining the presence of different scaling regimes for precipitation intensity distributions. In order to identify possible changes in the SS properties of AMS distributions, various *scaling intervals* were defined for the MSA. In particular, all possible subsets with 6, 12, 18 and 24 contiguous durations were considered within each dataset. Figure 1.2 and Figure 1.3 show the 136 scaling intervals thereby defined: 40 scaling intervals for SD and ID, and 56 scaling intervals for LD. For instance, the top left matrix of Fig. 1.2(a) presents the 6-duration scaling intervals 15 min - 1 h 30 min, 30min - 1 h 45 min, ..., 4 h 45 min - 6 h defined for the SD dataset [i.e. the 19 scaling intervals containing six contiguous durations defined with a 15min increment]. More schematically, Fig. 1.1(b) shows an example of the first five 6-duration scaling intervals for the ID dataset [i.e. 1 h - 6 h, 2 h - 7 h, ..., 5 h - 10 h, containing six contiguous durations defined with an increment of 1h]. This procedure was defined in order to evaluate the sensitivity of the SS estimates to changes in the first duration d_1 of the scaling interval and in the interval length [i.e. the number of durations included in the scaling interval].

For each scaling interval (for simplicity, their index has been omitted), the validity of the SS hypothesis was verified according to the following

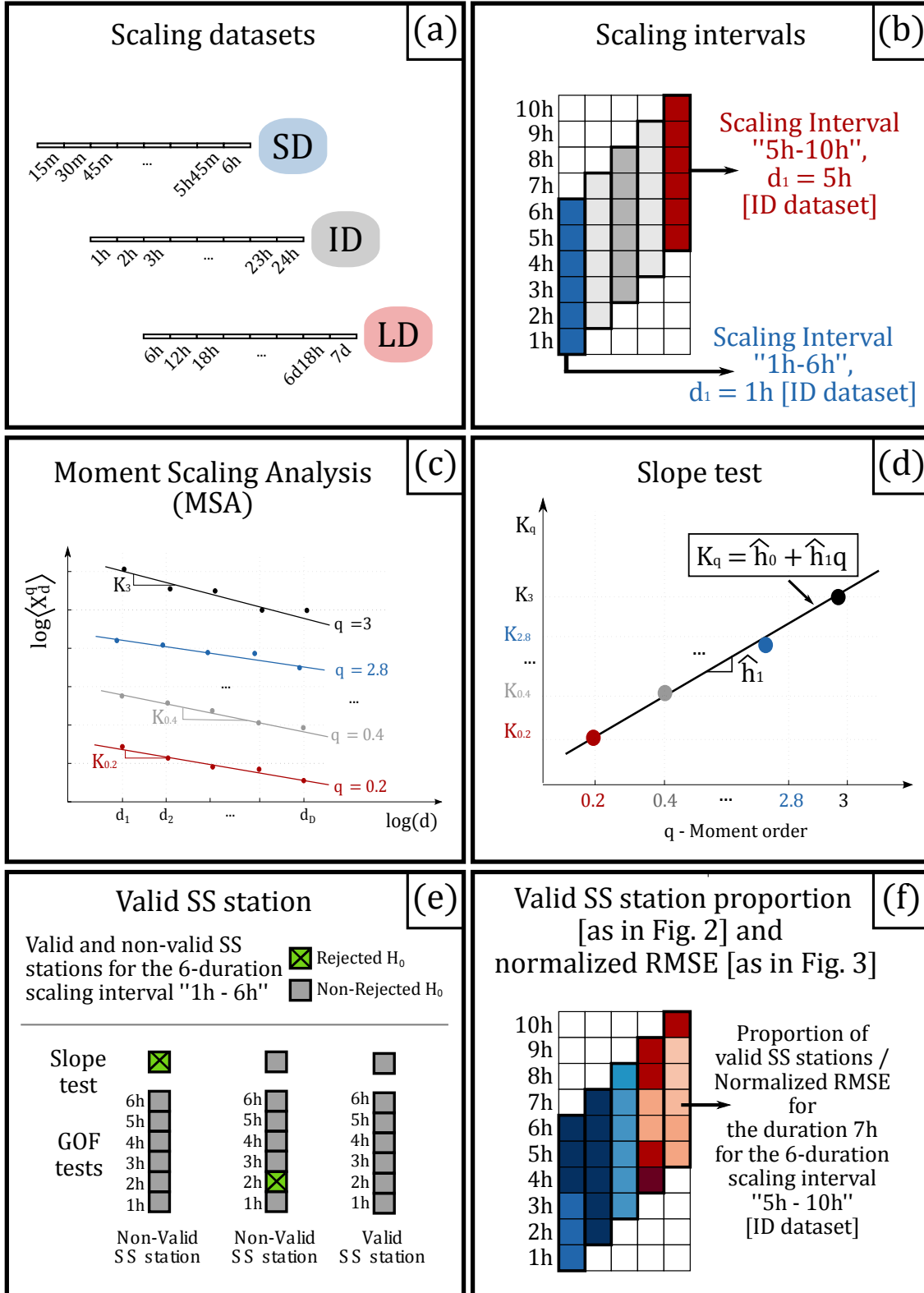


Figure 1.1: Methodology steps: a) Definition of the SD, ID, and LD scaling datasets. b) Identification of durations and scaling intervals within each matrix of Fig. 1.2 and 1.3; c) Moment Scaling Analysis (MSA) regression for the estimation of the slope coefficients K_q ; d) Slope test: regression of K_q on the moment order q and Student's t -test for the null hypothesis $H_0: \hat{h}_1 = K_1$; e) Examples of valid and non-valid SS stations according to the Slope and GOF tests; f) Example of valid SS station proportion values and Normalized RMSE values, \bar{r}_{x_d} , as represented, in Fig. 1.2 and 1.3.

steps:

1. *MSA regression*: for each $q = 0.2, 0.4, \dots, 2.8, 3$, the slopes K_q of the log-log linear relationships between the empirical q -moments $\langle X_d^q \rangle$ of $X_{d_1}, X_{d_2}, \dots, X_{d_D}$ and the corresponding durations d_1, d_2, \dots, d_D in the scaling interval $[d_1, d_D]$ were estimated by Ordinary Least Squares (OLS) [see Fig. 1 (c) for a graphic example]. Order $q \geq 3$ were not considered because of the possible biases affecting empirical high order moment estimates.

2. *Slope test*: to verify the SS assumption that the estimated K_q exponents vary linearly with the moment order q , i.e. $K_q \approx Hq$, an OLS regression between the MSA slopes K_q and q was applied [see Fig. 1.1 (d)]. For the regression line $K_q = \hat{h}_0 + \hat{h}_1 q$, a Student's t-test was then used to test the null hypothesis $\mathbf{H}_0: \hat{h}_1 = K_1$. If \mathbf{H}_0 was not rejected at the significance level $\alpha = 0.05$, the SS assumption was considered appropriate for the scaling interval and the simple scaling exponent $H = K_1$ was retained.

3. *Goodness-of-Fit (GOF) test*: for each duration d , the goodness of fit of the X_d distribution under SS was tested using the Anderson-Darling (AD) and the Kolmogorov-Smirnov (KS) tests. These tests aim at validating the appropriateness of the scale invariance property for approximating the X_d cdf by the distribution of $X_{d,ss} = d^{-H} X_{d^*}$. To this end, each AMS, $\vec{x}_{d_j} = (x_{d_j,1}, x_{d_j,2}, \dots, x_{d_j,i}, \dots, x_{d_j,n})$, recorded at duration d_j was rescaled at the reference duration d^* by inverting Eq. (1.2):

$$\vec{x}_{d_j}^* = \left(d_j^H x_{d_j,1}, d_j^H x_{d_j,2}, \dots, \dots, d_j^H x_{d_j,i}, \dots, \dots, d_j^H x_{d_j,n} \right) \quad (1.8)$$

where n represents the number of observations (years) in \vec{x}_{d_j} . Then, the pooled sample, \vec{x}_{d^*} , of the D rescaled AMS, $\vec{x}_{d_j}^*$, was used to define X_{d^*} under the SS assumption:

$$\vec{x}_{d^*} = \left(\vec{x}_{d_1}^*, \dots, \vec{x}_{d_j}^*, \dots, \vec{x}_{d_D}^* \right) \quad (1.9)$$

Since, in Eq. (1.9), D represents the number of durations d_j in the scaling interval, $n \times D$ rescaled observations were included in \vec{x}_{d^*} .

As in previous applications [e.g., Panthou et al. 2014], the AD and KS tests were then applied at significance level $\alpha = 0.05$ to compare the empirical distributions [Cunnane plotting formula, Cunnane 1973] of the SS sample, $\mathbf{x}_{d,ss} = d^{-H} \vec{x}_{d^*}$, and the non-SS sample, \mathbf{x}_d . In fact, despite the low power of KS and AD tests for small sample tests, they represent the only suitable solution to the problem of comparing empirical cdfs when the data do not follow a normal distribution. Because both AD and KS are affected by the presence of ties in the samples (e.g., repeated values due to rounding or instrument resolution), a permutation test approach [Good 2013] was used to estimate test p-values. According to this approach, data in \mathbf{x}_d and $\mathbf{x}_{d,ss}$ were pooled and randomly reassigned to two samples having same sizes as the SS and non-SS samples. Then, the test statistic distribution under the null hypothesis of equality of the $X_{d,ss}$ and X_d distributions was approximated by computing its value over a large set of random samples. Finally, the test p-value was obtained as the proportion of random samples presenting a test statistic value larger than the value observed for the original sample.

The SS model validity and the mean error resulting from approximating the X_d distribution by the SS model were then evaluated in a cross-validation setting. For this analysis, each du-

ration was iteratively excluded from each scaling interval and the scaling model re-estimated at each station by repeating steps 1 to 3 [MSA regression, Slope test, and GOF tests]. Predictive ability indices, such as the Mean Absolute Error (MAE) and the Root Mean Squared Error (RMSE) between empirical and SS distribution quantiles, were then estimated for highest quantiles for valid SS stations. In particular, to focus on return periods of practical interest for IDF estimation, only quantiles larger than the median were considered (i.e., only return periods greater than 2 years).

For each station s , the normalized RMSE, $\bar{\epsilon}_{x_{d,s}}$, was estimated:

$$\bar{\epsilon}_{x_{d,s}} = \frac{\epsilon_{x_{d,s}}}{\bar{x}_{d,s}} \quad (1.10)$$

where $\epsilon_{x_{d,s}}$ and $\bar{x}_{d,s}$ are, respectively, the RMSE and the mean value of all X_d quantiles of order $p > 0.5$. Then, the average over all stations of the normalized RMSE, $\bar{\bar{\epsilon}}_{x_d}$, was computed for each scaling interval and duration:

$$\bar{\bar{\epsilon}}_{x_d} = \frac{1}{n_s} \sum_{s=1}^{n_s} \bar{\epsilon}_{x_{d,s}} \quad (1.11)$$

where n_s is the number of valid SS stations in the dataset. Note that $\bar{\bar{\epsilon}}_{x_d}$ is a measure of error, meaning that values of $\bar{\bar{\epsilon}}_{x_{d,s}}$ closer to 0 correspond to a better fit than larger values.

1.4.1 Model estimation and validation

Figure 1.2 presents the results of steps 1 to 3 of the methodology for evaluating the SS validity. For all the three scaling datasets, no particular pattern was observed for slope test results, and at most 2% of the stations within each scaling inter-

val displaying a non linear evolution of the scaling exponent with the moment order. For this reason, Fig. 1.2(a)-(c) show, for each scaling interval and duration, the proportion of valid SS stations without differentiating for slope or GOF test results. As showed in the example in Fig.1.1(e), for each scaling interval, valid SS stations were defined as stations having not rejected both the Slope test for the scaling interval and the GOF tests for each duration included in this scaling interval.

As expected, the proportion of valid SS stations decreased when the number of durations within the scaling interval increased and with decreasing d_1 . This is particularly evident for short d in SD and ID datasets. More GOF test rejections were observed for longer scaling intervals [not shown], due to the higher probability of observing large differences between \mathbf{x}_d and $\mathbf{x}_{d,ss}$ quantiles when $\mathbf{x}_{d,ss}$ had larger sample size and included data from more distant durations. However, several factors can impact GOF test results when shorter d_1 are considered. First, GOF tests are particularly sensitive to the presence of very large values in short-duration samples. Second, when considering durations close to the temporal resolution of the recorded series [i.e., 15 min in SD and 1 h in ID and LD], stronger underestimations could affect the measure of precipitation because intense rainfall events are more likely to be split between two consecutive time steps. Finally, preliminary analyses [Fig. S2 and S3 in the supplementary material] showed that the largest GOF test rejections could also be connected to the coarse instrument resolution of 15PD series, which, similar to the temporal resolution effect, induces larger measurement errors in the shortest duration series. Note that comparable resolution issues were previously reported by some authors while estimating fractal and intermittency properties of rain-

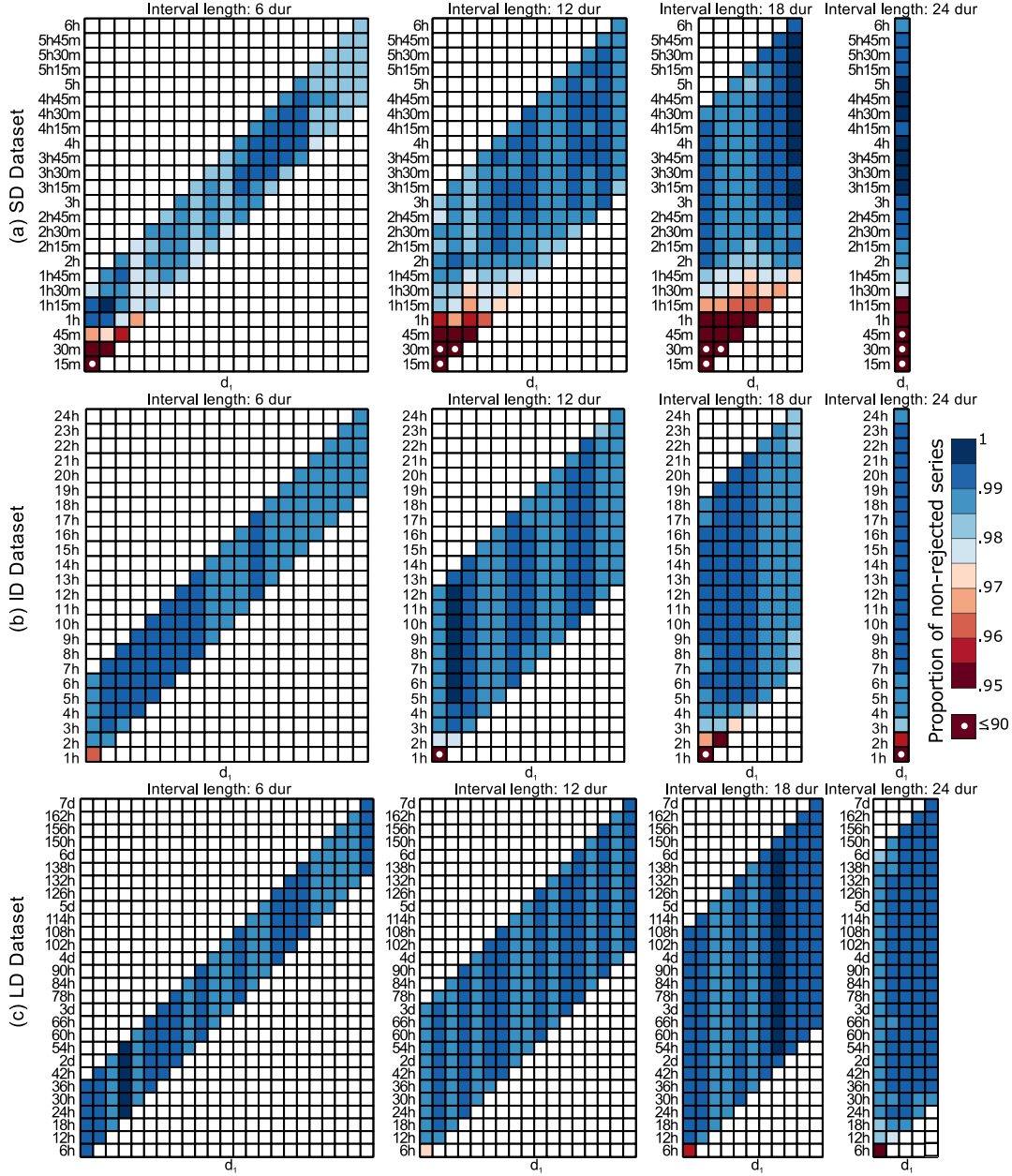


Figure 1.2: Proportion of stations satisfying both the Slope and GOF tests applied at the 0.95 confidence level, for each duration (vertical axis) and scaling interval (horizontal axis) for the SD, ID, and LD datasets [row a), b), and c) respectively]. White circles indicate proportions between 0.25 and 0.90. See Fig. 1 (b) and (f) for the identification of durations and scaling intervals within each matrix.

fall processes [e.g., Veneziano and Iacobellis 2002; Mascaro et al. 2013] and IDF [e.g, Blanchet et al. 2016].

Valid SS station proportions between 0.99 and 1 were always observed for GOF tests in ID and LD datasets, except for some durations shorter

than 3 h (ID dataset) or 6 h (LD dataset). When considering both GOF and Slope test, with the exception of some durations ≤ 1 hour, the proportion of stations satisfying SS was higher than 0.9, and the majority of scaling intervals [65%, 90%, and 98% of the scaling intervals in SD, ID, and

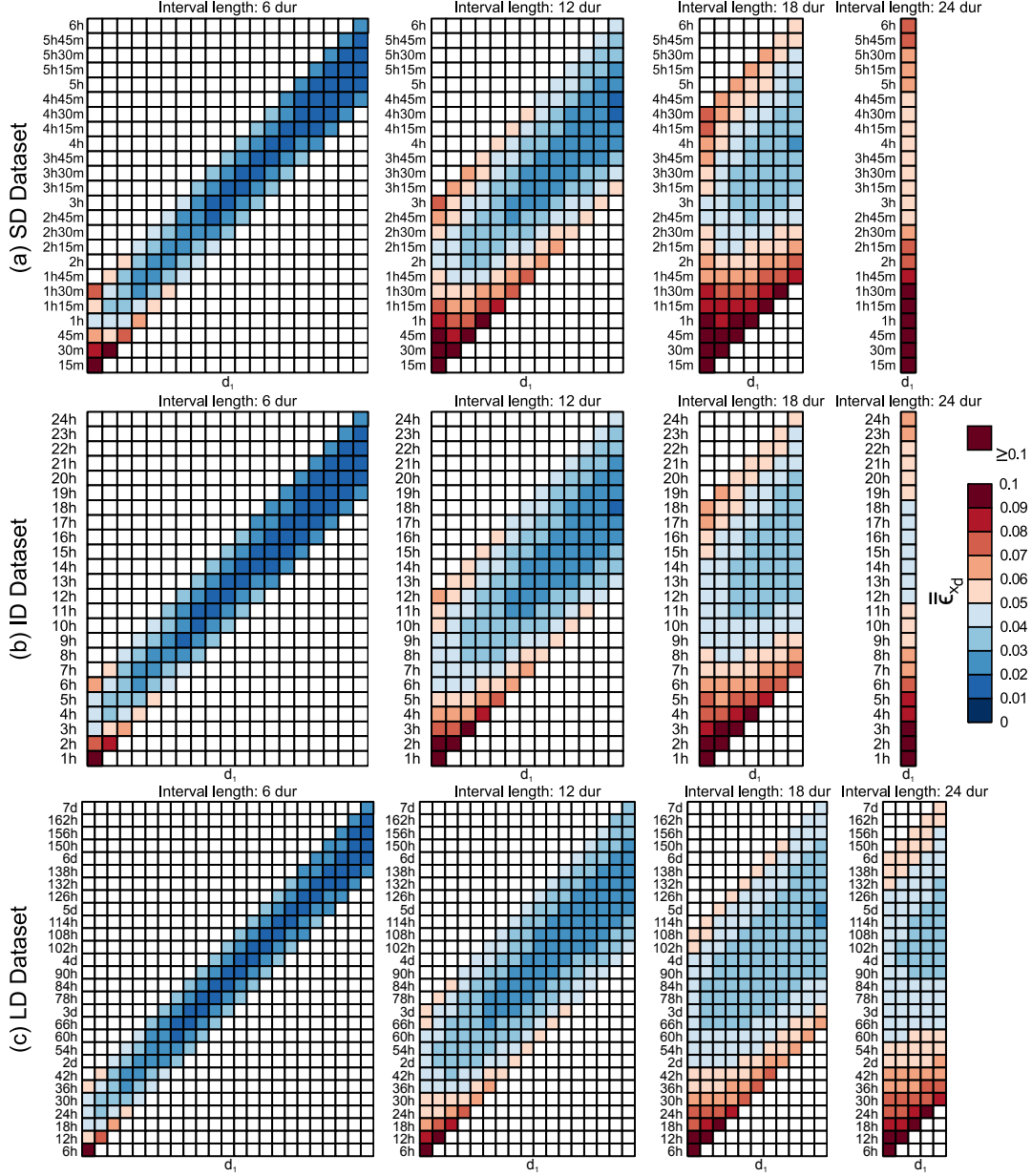


Figure 1.3: Cross-Validation Normalized RMSE averaged over all valid SS stations (\bar{r}_{x_d}) for each duration (vertical axis) and scaling interval (horizontal axis) in the SD, ID, and LD datasets [row a), b), and c) respectively]. White circles indicate values between 0.15 and 0.3. See Fig. 1 (b) and (f) for the identification of durations and scaling intervals within each matrix.

LD, respectively] included at least 95% of valid SS stations. For each scaling interval, only valid SS stations were considered in the rest of the analysis.

These findings were also confirmed by cross-validation experiments. The proportion of valid SS stations resulting from cross-validation Slope

and GOF tests were similar, even if slightly lower, to proportions displayed in Fig. 1.2 [see Fig. S4 of the supplementary material].

Figure 1.3 presents, for each scaling interval and duration, the station average, \bar{r}_{x_d} , of the normalized RMSE. These graphics show that mean relative errors on intensity quantiles did not gener-

ally exceed 5% of the precipitation estimates for 6-duration scaling intervals [Fig. 1.3, first col.]. Greater errors were observed for durations at the border of the scaling intervals. Not surprisingly, this result underlines that, in a cross-validation setting, both the MSA estimation of H and the $X_{d,ss}$ approximation are less sensitive to the exclusion of an inner duration of the scaling interval than to the exclusion of d_1 or d_D . Conversely, the extrapolation under SS of the X_d distribution is generally less accurate for durations at the boundaries or outside the scaling interval used to estimate H . Moreover, as for the valid SS station proportion, the performances of the model deteriorated with decreasing d_1 and with increasing scaling interval length, especially for durations at the border of the scaling intervals. However, for more than 70% of 12-, 18-, and 24-duration scaling intervals, $\bar{\epsilon}_{x_d} \leq 0.1$ for each duration included in the scaling interval. $\bar{\epsilon}_{x_d} \geq 0.25$ were observed for 15 min in 12-duration or longer scaling intervals, pointing out the weaknesses of the model in approximating short duration extremes when the scaling interval included durations ≥ 3 h.

1.4.2 Estimated scaling exponents and their variability

In order to evaluate the sensitivity of SS to the considered scaling interval, the variability of H with d_1 has been analyzed. Then, the spatial distribution of the scaling exponents for each scaling interval was studied to assess the uncertainty in H estimation and the dependence of SS exponents on local geoclimatic characteristics.

Investigating the variability of the scaling exponent with the scaling interval is particularly important since, if SS is assumed to be valid be-

tween some range of durations, one should expect that H remains almost unchanged over the various scaling intervals included in this range. For this reason, the variation $\Delta_{H(j)}$ of the scaling exponents computed for overlapping scaling intervals having the same d_1 but different lengths was analyzed. For each station and d_1 , $\Delta_{H(j)}$ was defined as:

$$\Delta_{H(j)} = H_{(j)} - H_{(6)} \quad (1.12)$$

where $j = 12, 18$, or 24 represents the number of durations considered in the specified scaling interval, $H_{(j)}$ is the corresponding scaling exponent, and $H_{(6)}$ is the scaling exponent estimated for the 6-duration scaling interval having the same d_1 . If SS is appropriate over a range of durations, $\Delta_{H(j)}$ is expected to be small for scaling intervals defined within this range.

Figures 1.4(ii)-(iv) show for all relevant scaling intervals, the median, Interquartile Range (IQR), and quantiles of order 0.1 and 0.9 of the $\Delta_{H(j)}$ distribution over valid SS stations. Adding new durations to the scaling intervals the median $\Delta_{H(j)}$, as well as its IQR, increased for all d_1 . Nonetheless the median scaling exponent variation was generally smaller than 0.05, except for a relatively small proportion of stations. Equally important, $|\Delta_{H(j)}|$ was generally centered on 0 and for all $d_1 \geq 1$ h more than 50% of stations had $|\Delta_{H(12)}| \leq 0.025$ (SD dataset) and $|\Delta_{H(18)}| \leq 0.03$ (ID dataset) [Fig. 1.4 (ii)-(iii)].

For some stations, a dramatic difference could exist in IDF estimations obtained with the different definitions of the scaling interval. For instance, for the 24-duration scaling interval "1h - 24h" (ID dataset), the median $\Delta_{H(24)}$ was equal to 0.047 [Fig. 1.4(iv) b)]. For the interval "15min - 6h" (SD dataset), $\Delta_{H(24)}$ was even larger, with a median scaling exponent variation approximately equal to 0.087 and with 25% of stations having $\Delta_{H(24)} \geq$

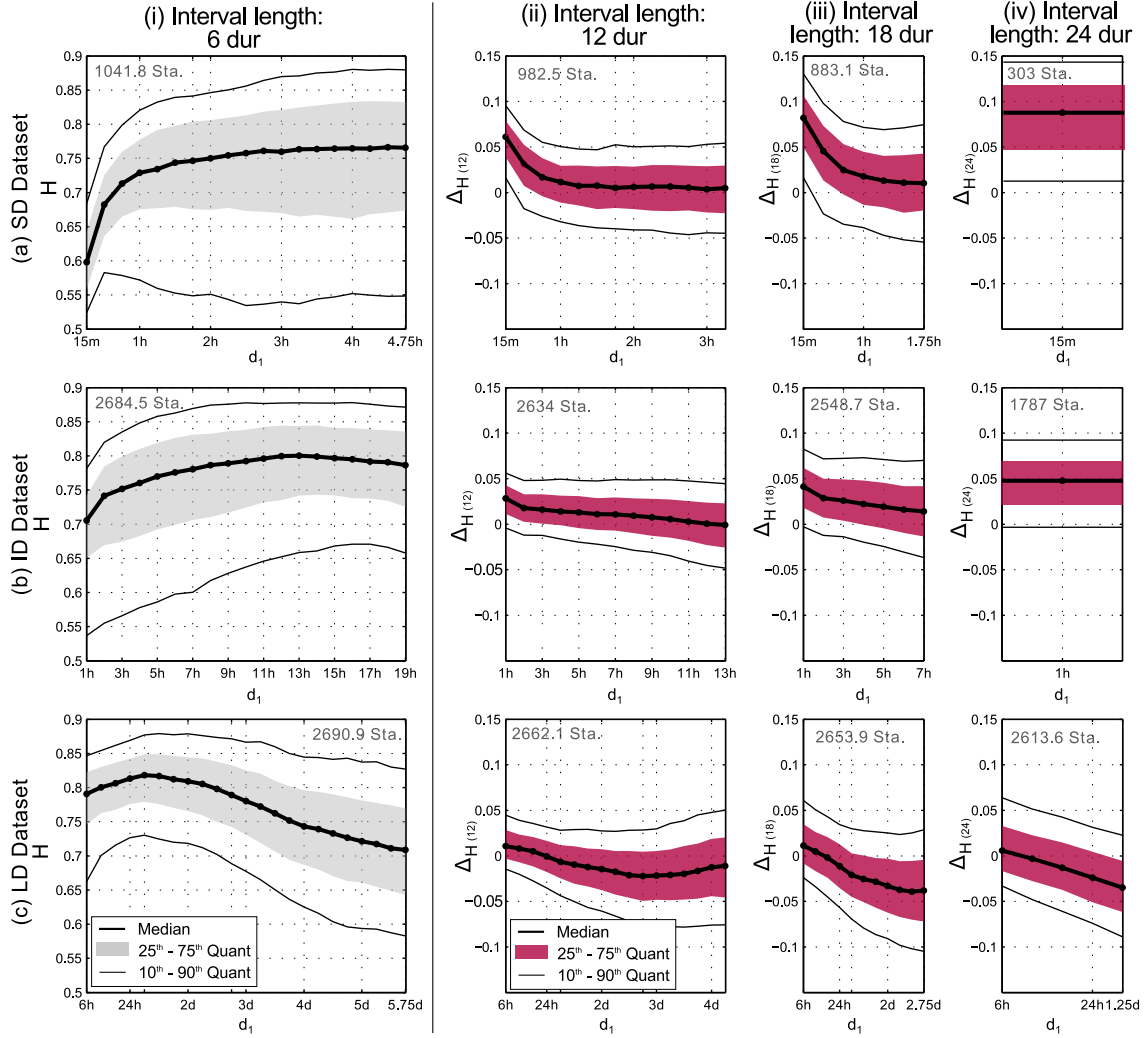


Figure 1.4: Col. (i): Median and relevant quantiles of the scaling exponent distribution over all valid SS stations for each 6-duration scaling interval. Col. (ii)-(iv): Median and relevant quantiles of the distribution of the scaling exponent deviation $\Delta H_{(j)}$ [defined in Eq. (1.12)]. The average number of valid SS stations over the scaling intervals (identified by their first duration, d_1) is indicated at the top of each graph.

0.11 [Fig. 1.4(iv) a)]. Finally, changes in H values were also important when comparing 6- and 12-duration scaling intervals when $d_1 \leq 1$ h (SD and ID datasets) and in LD dataset [Fig. 1.4 (ii)]. The median, Interquantile Range (IQR), and quantiles of order 0.1 and 0.9 of the H distribution across stations, are presented in Fig. 1.4(i) for each 6-duration scaling interval. The smallest median H values were observed for $d_1 \leq 30$ min in Fig. 1.4 (a-i), and for the longest d_1 s in Fig. 1.4 (c-i). Scaling intervals beginning at 15 and 30 min

also displayed the smallest variability across stations. Although fewer stations were available for these intervals (only 15PD stations were used and the number of valid SS stations was smaller), this result is consistent with previous reports in the literature demonstrating that H values are spatially more homogeneous for short durations.

A larger dispersion of H values was observed when d_1 ranged between approximately 1 h and 5 h, in particular in the SD dataset, for which the 10th-90th percentile difference almost covered the en-

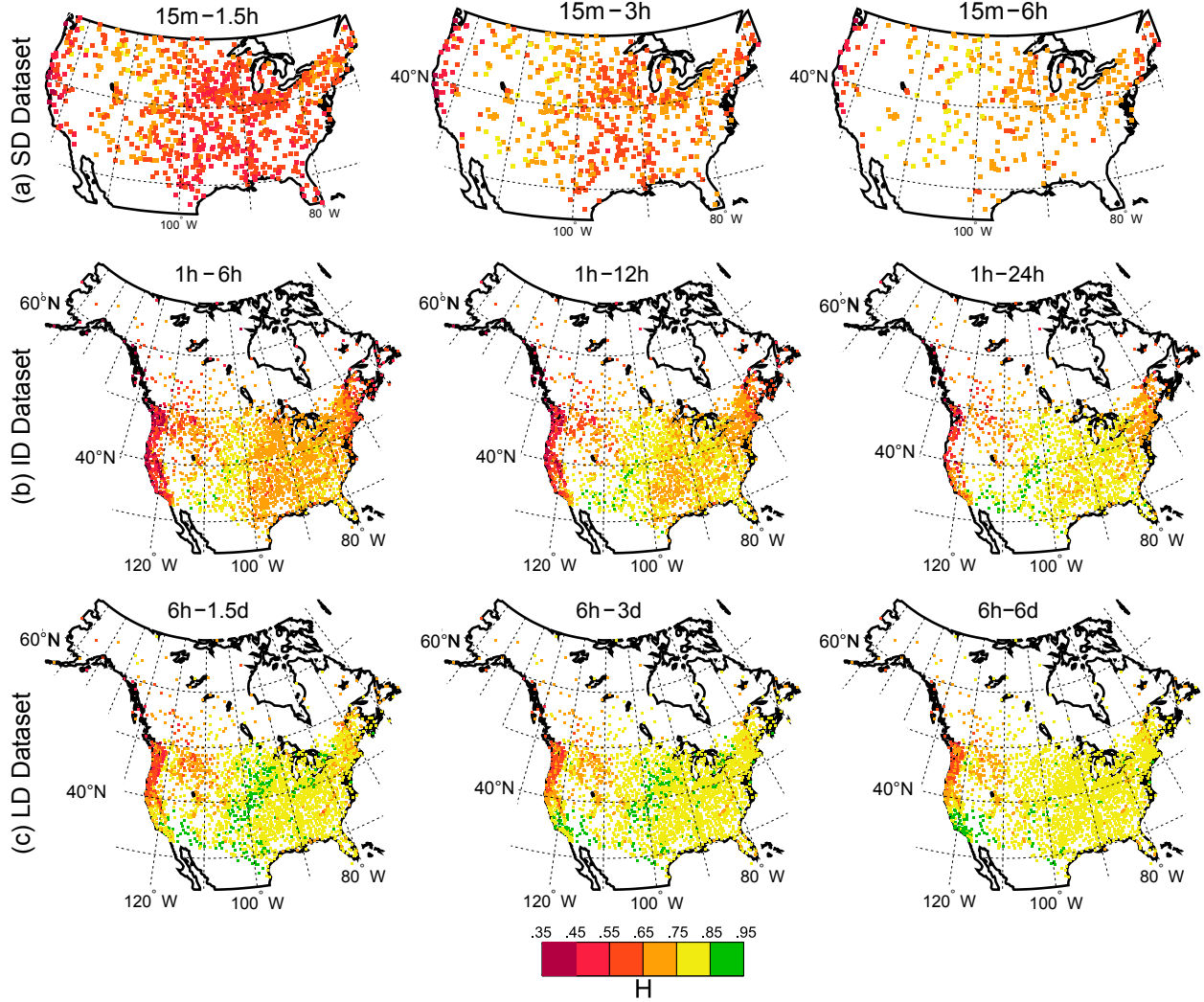


Figure 1.5: Spatial distribution of the scaling exponent for the first (i.e. with minimum d_1) 6-, 12-, and 24-duration scaling intervals (first, second, and third col., respectively) for SD, ID, and LD datasets (first, second, and third row, respectively). These scaling intervals correspond to the first column of matrices in Fig. 1.2 and 1.3.

tire range of observed H values [Fig. 1.4 (i)]. This result could be partially explained by the use of scaling intervals having equally spaced durations. This implies that the mean distance between the logarithms of durations in the scaling interval decreases as d_1 increases. Hence, the OLS estimator of H used in the MSA regression may have larger variance for longer d_1 , especially when scaling intervals include few durations. Larger uncertainty may thus have an impact on the H estimation for the longest d_1 scaling intervals of SD. However,

as showed in next sections, H spatial distribution may also explain the greater variability of the scaling exponent for d_1 greater than a few hours.

Largest median H were observed for d_1 greater than 10 hours [Fig. 1.4 (b-i)] and lower than 2 days [Fig. 1.4 (c-i)], with approximately half of the stations having $H \geq 0.8$. This means that a stronger scaling (i.e., larger H values) is needed to relate extreme precipitation distributions at approximately 12-hours to distributions at daily and longer scales. It may therefore be expected that

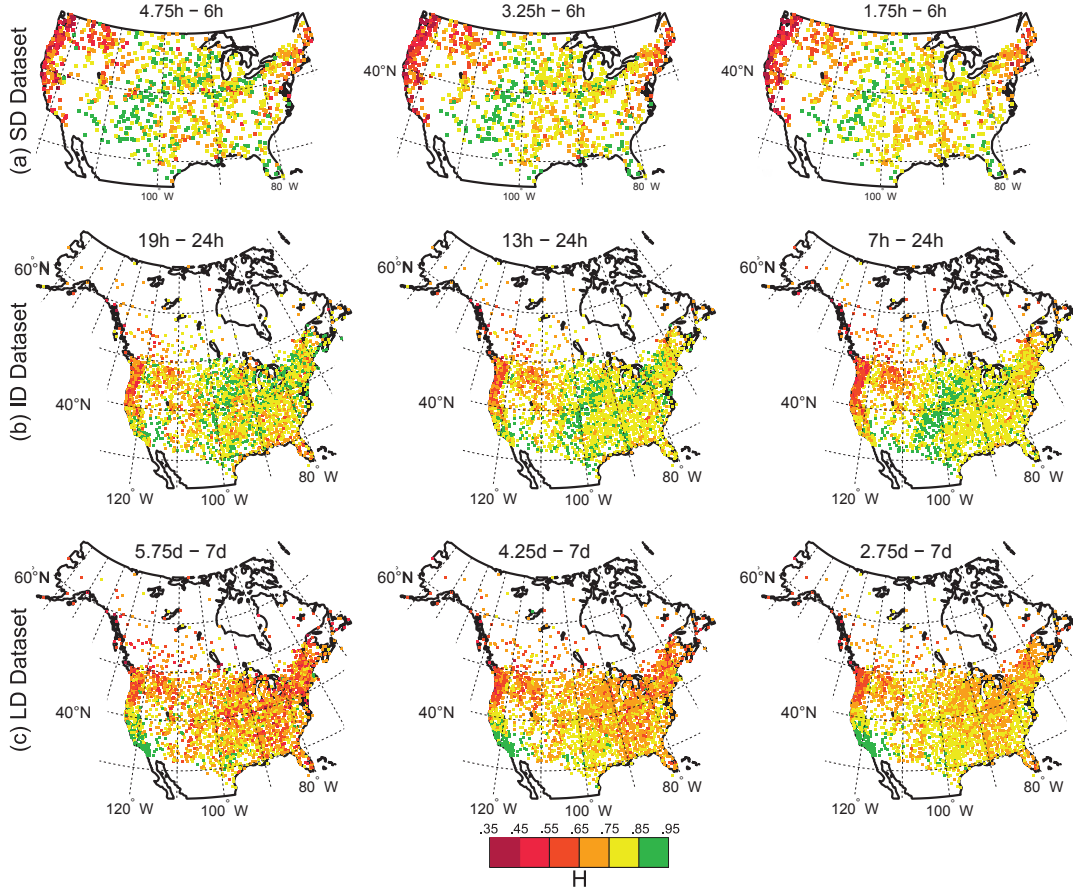


Figure 1.6: Spatial distribution of the scaling exponent for the last (i.e. with maximum d_1) 6-, 12-, and 18-duration scaling intervals (first, second, and third col., respectively) for SD, ID, and LD datasets (first, second, and third row, respectively). These scaling intervals correspond to the last column of matrices in Fig. 1.2 and 1.3.

the stations characterized by H closer to 1 are located in geographical areas where differences in precipitation distributions are important among temporal scales included in these scaling intervals. Examples of the spatial distributions of the scaling exponent are given in Fig. 1.5 and 1.6 for the first and last d_1 for each interval length and dataset, respectively. Since only one 24-duration scaling interval was defined for both the SD and ID datasets, only scaling intervals containing 6, 12, and 24 (Fig. 1.5) or 18 (Fig. 1.6) durations are presented. This avoids the redundancy of showing twice the "15min - 6h" (SD dataset) and "1h - 24h" (ID dataset) scaling intervals.

Generally, the scaling exponent displayed a strong

spatial coherence and varied smoothly in space, although a more scattered distribution of H characterizes maps in Fig. 1.6. In this last figure, the local variability of H may be attributed to the larger estimation uncertainties affecting longer d_1 scaling intervals, as previously mentioned. Meaningful spatial variability and clear spatial patterns emerged for $d_1 \geq 1$ h. In fact, for stations located in the interior and southern areas of the continent, a shift from weaker scaling regimes (smaller H) to higher H values was observed as d_1 increases [e.g., second and third rows of Fig. 1.5]. On the contrary, a smoother evolution of H over the scaling intervals characterized the northern coastal areas, especially in north-western regions, and the Rock-

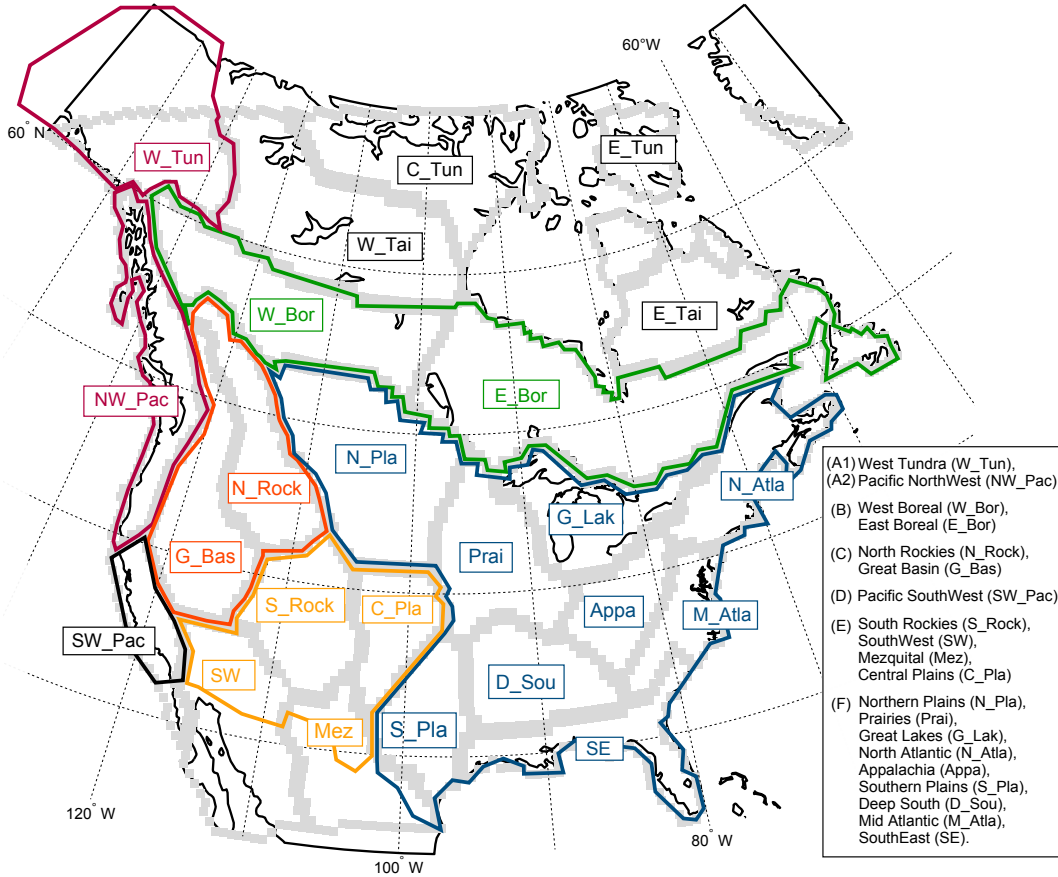


Figure 1.7: Climatic regions of Bukovsky (2012) [grey borders] and regions defined for this analysis [regions A1 to F in the legend; colored borders]. Abbreviations for each region are in parenthesis.

ies, where $H > 0.75$ values were rarely observed even for greater d_1 values.

1.5 Regional analysis

Regional differences in scaling exponents were investigated. Only the results for the 6-duration scaling intervals are presented, similar results having been obtained for longer scaling intervals [see the supplementary material, Fig. S6 and S7 for 12- and 18-duration scaling intervals]. Stations were pooled into six climatic regions based on the classification suggested by Bukovsky (2012) [see Fig. 1.7]. Stations outside the domain covered by the Bukovsky regions were attributed to the

nearest region. Regions with less than 10 stations were not considered (regions without colored borders in Fig. 1.7); regions A1 (W_Tun) and A2 (NW_Pac) were kept separated since only 14 stations were available in region A1 (W_Tun) for ID and LD datasets.

To provide deeper insights about regional features of precipitation associated with specific scaling regimes two variables related to the precipitation events observed within AMS were also analyzed: the mean number of events per year, \bar{N}_{eve} , and the mean wet time per event, \bar{T}_{wet} , contributing to AMS within each scaling interval. For a given year and station, annual maxima associated to different durations of a given scaling interval were considered to belong to the same precipitation

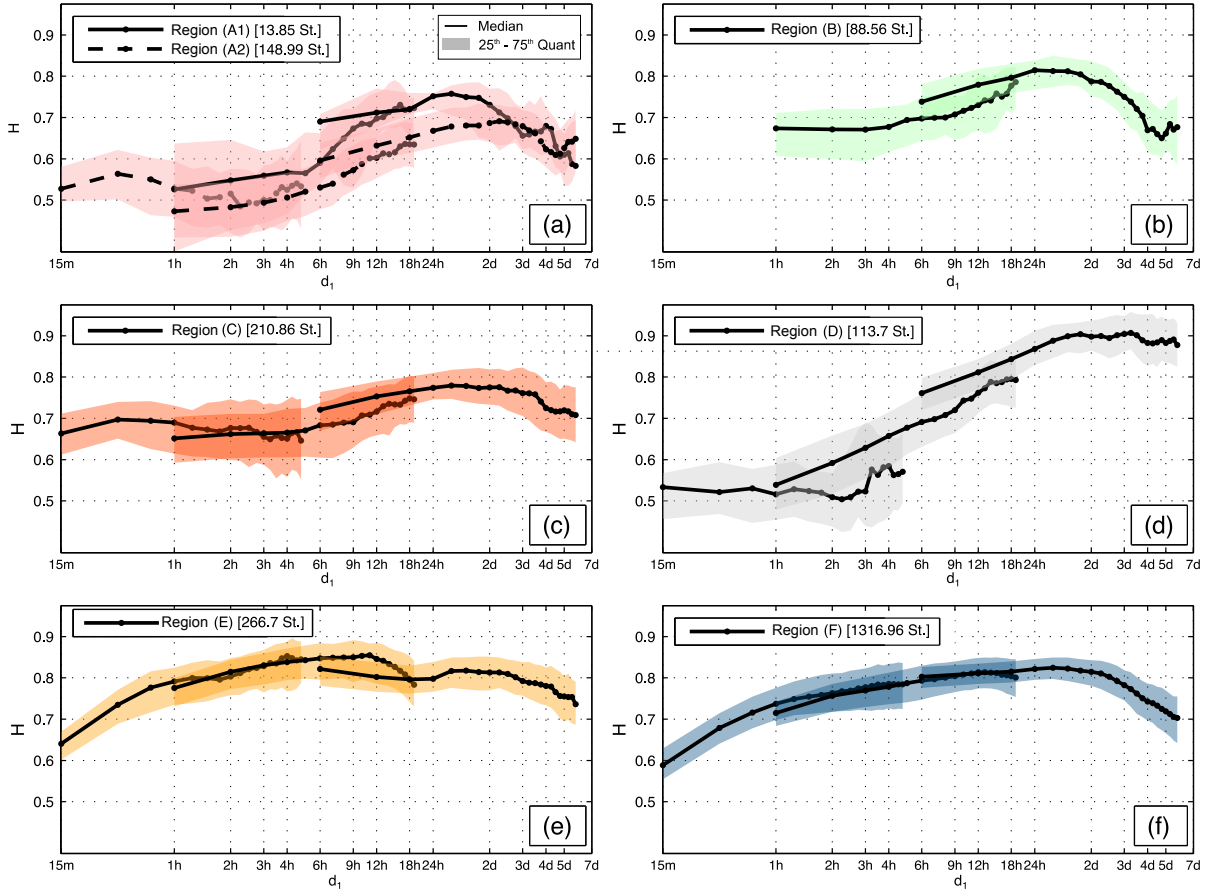


Figure 1.8: Median and Interquartile Range (IQR) of the scaling exponent distribution over valid SS stations within each region of Fig. 1.7 for 6-duration scaling intervals for the SD (left curve), ID (central curve), and LD (right curve) datasets. For each region, the mean number of valid SS stations over the scaling intervals is indicated in brackets in the legend. See Fig. 1.7 for region definition.

event if the time intervals over which they occurred overlapped. The mean wet time per event contributing to AMS, \bar{T}_{wet} , was defined as the mean number of hours with non-zero precipitation within each event. Details on the calculation of \bar{N}_{eve} , \bar{T}_{wet} , and the corresponding results are presented in the supplementary material [Sect. S2 and Fig. S5 and S6].

1.5.1 Regional variation of the scaling exponents.

Figure 1.8 shows the distribution of H within each region. Three types of curves can be identified.

First, curves in Fig. 1.8 (a) to (c) have a characteristic smooth S shape. Conversely, Fig. 1.8 (d) displays a rapid increase of H for scaling intervals defined in ID and LD datasets until $d_1 = 2$ days, preceded and followed by two plateaus: one plateau for the longest d_1 with remarkably high H values, and one for the shortest d_1 with small H values. Finally, an inverse-U-shaped curve can be seen in Fig. 1.8 (e) and (f), with globally high H values already reached at sub-daily durations in dry regions (E).

For $d_1 \leq 24$ h, Fig. 1.8 (a) displays lower values of H than Fig. 1.8 (e)-(f), meaning that smaller variation in AMS moments are observed in A1 and A2 when the scale is changed. This differ-

ence can be partially explained by the weaker impact of convection processes in generating very short duration extremes in rNorth-West coastal regions with respect to southern areas (regions E and F). For northern regions, in fact, the transition between short and long duration precipitation regimes may be smoothed out by cold temperatures which moderate short-duration convective activity, especially for *W_Tun* (region A1). The topography characterizing the northern pacific coast may then explain the smoothing effect for the curve of region *NW_Pac* (A2). In this case, in fact, the precipitation rates at daily and longer scales are enhanced by the orographic effect acting on synoptic weather systems coming from the Pacific Ocean [Wallis et al. 2007].

Similarly, mountainous regions in C [Fig. 1.8 (c)] displayed the smallest variations of H over d_1 , indicating that analogous scaling regimes characterize both short- and long-duration scaling intervals. Again, this may be related to the important orographic effects of precipitation in these regions that are involved in the generation of extremes for both sub-daily and multi-daily time scales.

The mean number of events per year in regions A and C was higher than in regions E-F, in particular for SD scaling intervals, and displayed steeper decreases with increasing d_1 [Fig. S5 (a) and (c) in the supplementary material].

Main differences between regions B and A were the stronger scaling regimes observed in B, which were mainly due to contributions from stations located in the south-eastern part of the *E_Bor* region (not shown). For scaling intervals in the ID dataset, region B was also characterized by the highest mean number of events per year, with most of the stations presenting $\bar{N}_{eve} > 2$ for $d_1 = 1$ h and $d_1 = 2$ h and sharp decreases of \bar{N}_{eve} with increasing d_1 [Fig. S5 (b) in the supplementary

material]. Moreover, a remarkably large range of \bar{N}_{eve} was observed for $1 \text{ h} \leq d_1 \leq 6 \text{ h}$, suggesting that B may be highly heterogeneous.

Two distinct scaling regimes can be observed for *SW_Pac* (region D) at, respectively, $d_1 \leq 3$ h (SD dataset) and $d_1 \geq 2$ days (ID dataset) [region D in Fig. 1.8 (d)]. These plateaus may be interpreted by recalling that $1 - H = H_{depth}$. On the one hand, the low and constant H observed for $d_1 \leq 3$ h indicates that the average precipitation depth increases with duration at the same growth rate for all these intervals. On the other hand, H approximately equal to 0.9 at daily and longer durations demonstrates that the average precipitation depth associated with long-duration annual maxima remained roughly unchanged when the duration increased from 1.5 to 7 days ($\lambda^{H_{depth}} \approx 1$ in Eq. (1.3)). This, along with the fact that the scaling exponent increased almost monotonically for $1 \text{ h} \leq d_1 \leq 24 \text{ h}$ (ID and LD datasets), suggests that extremes at durations shorter than ~ 3 h (SD dataset) drive annual maxima precipitation rates at longer scales, with the rapid and continuous decay in mean intensity caused by the increasing size of the temporal scale of observation.

For *SW_Pac* (region D), the relative absence of long-lasting weather systems able to produce important extremes for long durations, was confirmed by the analysis of \bar{N}_{eve} and \bar{T}_{wet} [see Fig. S5 and S6 of the supplementary material]. In fact, the mean number of events per year was relatively high for short durations (the median \bar{N}_{eve} is equal to 1.82 for $d_1 = 15$ min and to 1.4 for $d_1 = 1$ h), while it rapidly decreased below 1.1 events per year for $d_1 \geq 6$ h (ID dataset) and for $d_1 \geq 18$ h (LD dataset). With the exception of $d_1 = 6$ h (LD dataset), at least 90% of *SW_Pac* stations had $\bar{N}_{eve} \leq 1.25$ for all $d_1 > 3$ h. In other regions,

median \bar{N}_{eve} were never smaller than 1.1 for the SD and ID datasets, except for $d_1 \geq 12$ h in region E.

These results suggests that both the distinctive topography of the west coast and the characteristic large-scale circulation of the south-west areas of the continent are crucial factors determining the transition between the two scaling regimes in region D.

Median H values displayed inverse-U shapes for the remaining regions with very small IQR, despite the high number of valid SS stations: a slow transition from lower to higher H is observed approximately between 1 h and 12 h (region E) or 30 h (region F). The strongest scaling regimes were observed for $1 \text{ h} \leq d_1 \leq 2 \text{ days}$ in arid western regions [Fig. 1.8 (e)], while median H values greater than 0.8 were only observed for approximately $6 \text{ h} \leq d_1 \leq 2 \text{ days}$ in more humid areas [1.8 (f)]. In both region E and F, very short-duration extremes are typically driven by convective processes, while a transition to different precipitation regimes may be expected between 1 h and a few hours. However, H shows a smoother increase in Fig. 7 (f) with respect to Fig. 7(e). This may indicate that in eastern areas [region F] sub-daily duration extremes are more likely associated to embedded convective and stratiform systems, or to mesoscale convective systems, which are less active in western dry areas of region E [Kunkel et al. 2012]. On the contrary, differences between short- and long-duration extreme precipitation intensity seem stronger for south-western dry regions [Fig. 1.8 (e)], where less intense summer extremes are expected compared to eastern areas [see supplementary material, Fig. S1]. In particular, H tended to scatter in a range of higher values for approximately $1 \text{ h} \leq d_1 \leq 12 \text{ h}$ indicating that precipitation intensity moments strongly

decrease as the duration increases.

In summary, these results suggest a regional effect on precipitation scaling of both local geographical characteristics, such as topography or coastal effects, and general circulation patterns. In general, the weakest scaling regimes were observed for short d_1 and along the west coast of the continent and seem to be connected to scaling intervals and climatic areas characterized by homogeneous weather processes. Low H values correspond in fact to small variations in AMS distribution moments. On the contrary, stronger scaling regimes were observed for longer d_1 in the other regions of the study area. This indicates that important changes occur in AMS moments across duration and, thus, in extreme precipitation features. According to these results, it would be important to take into account the climatological information included in the scaling exponent to improve SS and IDF estimation. Even more important, these results give useful guidelines for modeling the spatial distribution of H , which could help for the definition of IDF relationships at non-sampled locations.

1.6 Simple Scaling GEV estimation

Results presented in this section are limited to a descriptive analysis of GEV parameter estimates for 6-duration scaling intervals. Similar results were generally obtained for 12-, 18-, and 24-duration intervals [see supplementary material, Fig. S10 to S16]. An assessment of the potential improvements carried out by Simple Scaling GEV (SS GEV) models with respect to non-SS GEV models is also presented.

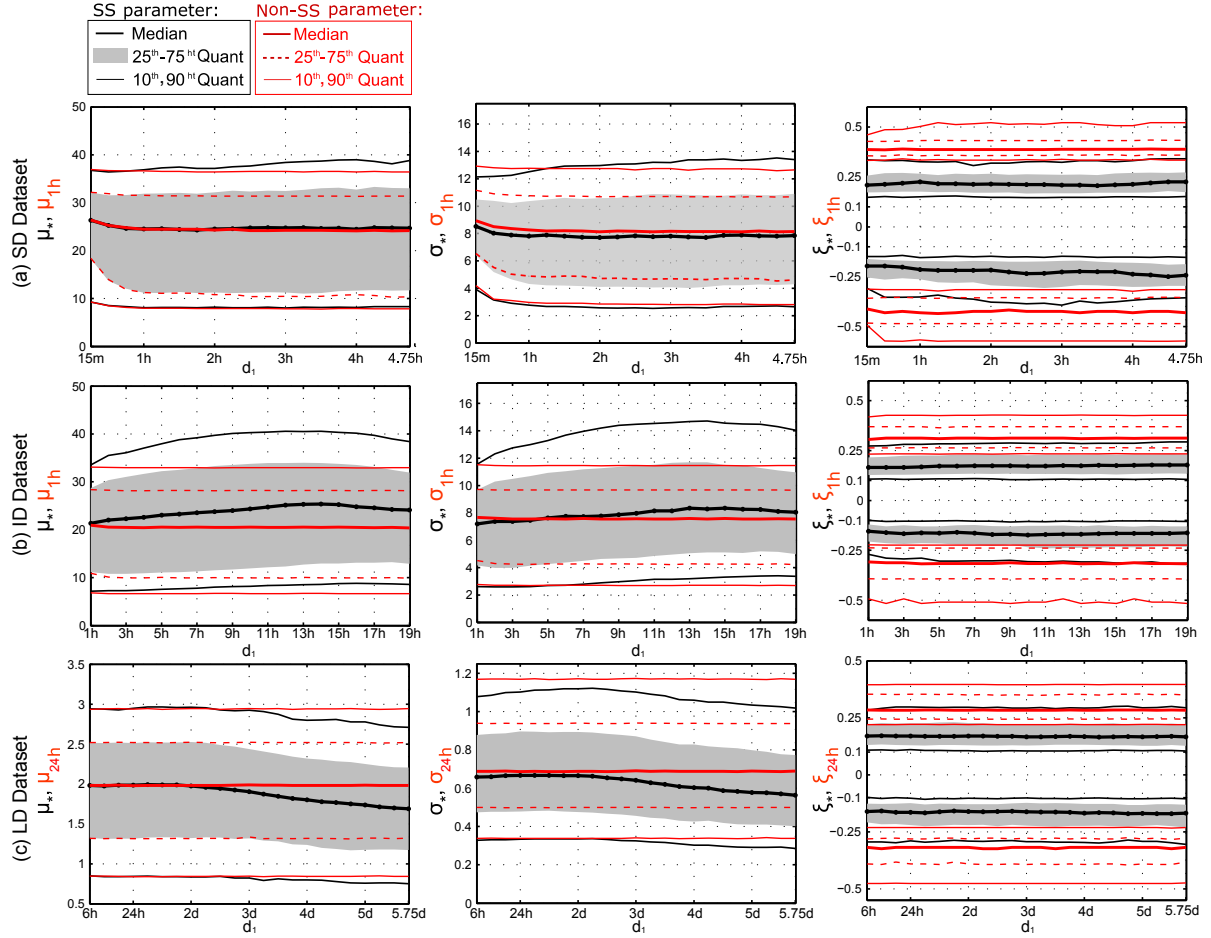


Figure 1.9: Distribution over valid SS stations of SS GEV parameters (gray and black lines) for 6-duration scaling intervals and non-SS GEV parameters (red solid and dashed lines) for reference durations. Location and scale parameters (first and second col., respectively) are scaled at $d_* = 1\text{h}$ (SD and ID datasets) and $d_* = 24\text{h}$ (LD dataset). Distributions for the shape parameter (third col.) are presented for $\xi > 0$ and $\xi < 0$, excluding cases where $\xi = 0$ (Gumbel distribution).

In our study, the Probability Weighted Moment (PWM) procedure was applied to estimate SS-GEV parameters μ_* , σ_* , and ξ_* [Eq. (1.7)] from \mathbf{x}_{d^*} [Eq. (1.9)]. For each duration d , PWM were also used to estimate non-SS parameters μ_d , σ_d , and ξ_d from each of the non-SS samples \mathbf{x}_d . Preliminary comparisons of various estimation methods [PWM, classical ML estimators, and GAM-ML; see Sect. 1.2.2], showed that PWM slightly outperformed the other methods.

Quantiles estimated from the SS and the non-SS GEV were compared with empirical quantiles. Global performance measures, such as RMSE,

were computed to evaluate the overall fit of the estimated GEV to the empirical X_d distributions. In particular, mean errors between SS and non-SS quantile estimates and empirical quantiles were compared using the relative total RMSE ratio, $R_{\overline{rmse}}$, defined as:

$$R_{\overline{rmse}} = \frac{[\overline{R}_{ss} - \overline{R}_{non-ss}]}{\overline{R}_{non-ss}} \quad (1.13)$$

where

$$\overline{R}_{mod} = \sum_{d=d_1}^D \frac{\epsilon_{d,mod}}{\bar{x}_d} \quad (1.14)$$

represents the normalized mean square difference between model and empirical quantiles of order $p > 0.5$ for all the durations included in the scaling interval. See Eq. 1.10 for the definition of $\epsilon_{d,mod}$ for each station.

1.6.1 Estimated SS GEV parameters

Figure 1.9 presents the distributions over valid SS stations of the SS GEV parameters rescaled at $d_* = 1$ h [Fig. 1.9 (a) and (b)] and $d_* = 24$ h [Fig. 1.9 (c)].

For the SD dataset, even for scaling intervals which did not include the reference duration d^* , the μ_* and σ_* distributions appeared to be similar to the non-SS μ_d and σ_d distributions [Figure 1.9, first row]. Similarly, for $6 \text{ h} \leq d_1 \leq 2$ days in the LD dataset, the SS location and scale parameter distributions are in relatively close agreement with the corresponding non-SS parameter distributions. Conversely, for the ID dataset, both μ_* and σ_* distributions are more positively skewed than the corresponding non-SS distributions. Finally, for $d_1 \geq 2$ days in the LD dataset, μ_* and σ_* had distributions shifted toward lower values than μ_{24h} and σ_{24h} . Moreover, the relative differences $\Delta_\mu = (\mu_* - \mu_d)/\mu_d$ and $\Delta_\sigma = (\sigma_* - \sigma_d)/\sigma_d$ were estimated for each station, duration, and scaling interval. Two important results came out of this analysis [see Figures S11 and S12 of the supplementary material]. On the one hand, median values of Δ_μ and Δ_σ were generally smaller than $\pm 5\%$ and $\pm 10\%$, respectively. On the other hand, Δ_σ showed large positive values when $\xi_d = 0$ (i.e. Gumbel distributions), while small $\Delta_\sigma < 0$ were estimated when $\xi_d \neq 0$ [not shown for conciseness]. These results are interesting since the estimation of the scale parameter σ of a GEV distribution may be biased when the shape param-

eter is spuriously set to zero ($\xi = 0$). Hence, while non-SS μ_d values can be considered to be accurate estimates of the X_d location parameter, small uncertainties should be expected for the scale parameter only when the ξ_d value is correctly assessed. In addition, μ_* and σ_* displayed a strong spatial coherence. Their spatial distributions were characterized by an obvious North-West to South-East gradient [Fig. 1.10 shows examples for the scaling intervals 15min - 1.5h, 1h - 6h, and 6h - 36h].

Notable differences between SS GEV and non-SS GEV estimates were observed for the shape parameter [Fig. 1.9, third col., and Fig. 1.11]. Firstly, for cases having shape parameters strictly different from zero [third column of Fig. 1.9], ξ_* absolute values were smaller than non-SS ξ_d absolute values. Secondly, the distributions of ξ_* across stations were generally more peaked around their median value than the corresponding non-SS distributions. Finally, for the non SS model the majority of stations had shape parameter ξ_d non-significantly different from zero, while the fraction of SS GEV shape parameters $\xi_* \neq 0$ was always greater than 39% [asymptotic test for PWM GEV estimators applied at level 0.05; Hosking et al. 1985]. In particular, for each duration, non-SS models estimated light-tailed distributions (i.e., $\xi_d = 0$) for more than 85% of the stations, except that for $d = 15$ min and $d = 30$ min [Fig. 1.11, first col.]. Conversely, for all scaling intervals with $d_1 > 15$ min, SS GEV shape parameters were significantly different from zero for 40% to 45% of valid SS stations [Fig. 1.11, second col.]. Moreover, when using scaling intervals of 12 durations or more, the proportion of $\xi_* > 0$ was always important [greater than 35% for all 18- and 24-duration scaling intervals; see the supplementary material, Fig. S10].

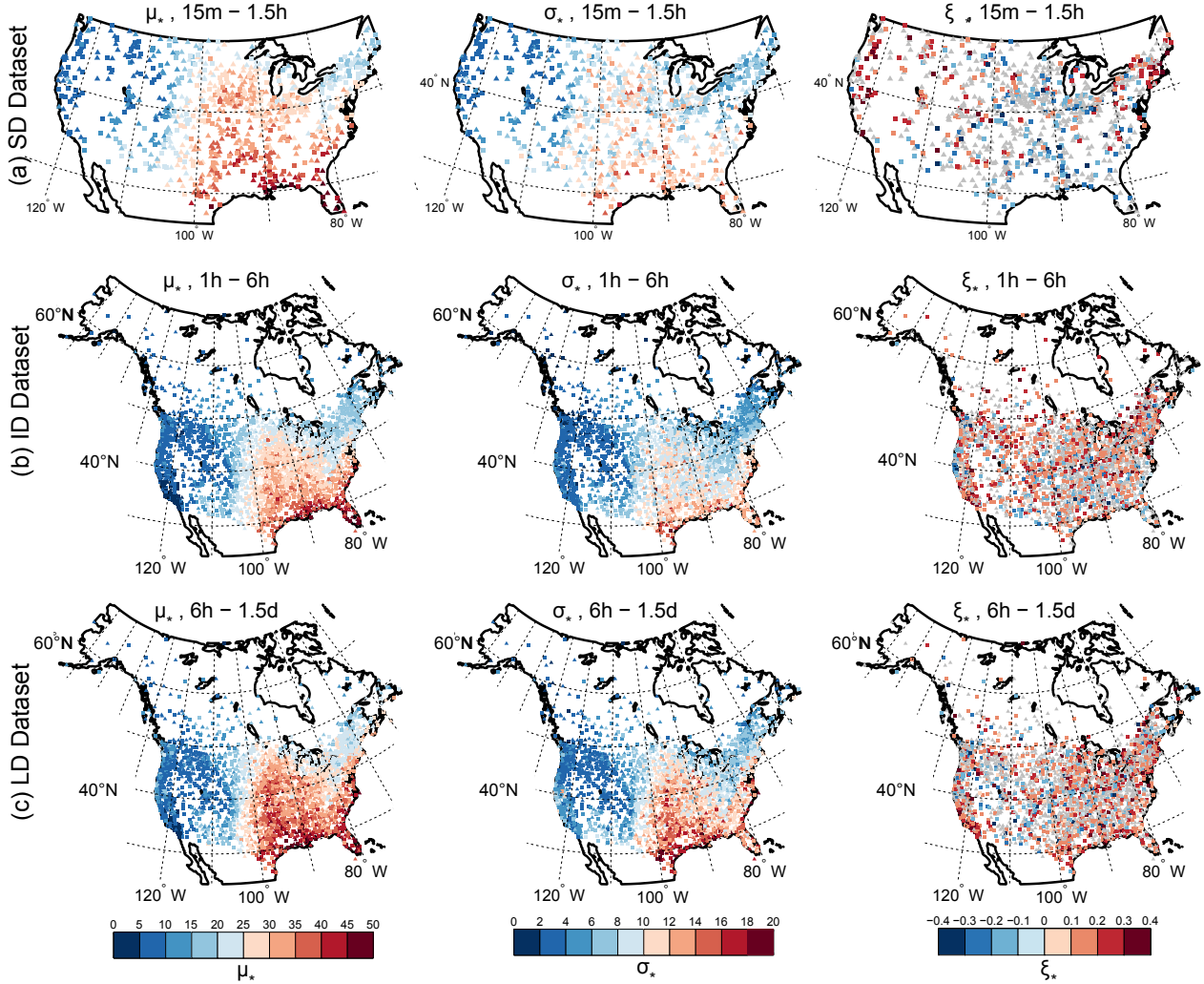


Figure 1.10: Spatial distribution over valid SS stations of SS GEV position (first col.), scale (second col.), and shape (3^{rd} col.; gray symbols indicate Gumbel distributions, $\xi_* = 0$) parameters scaled at $d_* = 1\text{h}$ for the first 6-duration scaling interval (i.e. interval with minimum d_1) of: SD (a), ID (b), and LD (c) datasets.

The previous results suggest that pooling data from several durations may effectively reduce the sampling effects impacting the estimation of ξ , allowing more evidence of non-zero shape parameters, and, in many cases, of heavy tailed ($\xi > 0$) AMS distributions. This conclusion is consistent with previous reports, namely that 100- to 150-year series are necessary to unambiguously assess the heavy-tailed character of precipitation distributions [e.g., Koutsoyiannis 2004b; Ceresetti et al. 2010]. These studies typically reported values of $\xi \approx 0.15$ [e.g., Koutsoyiannis 2004b], which are

close to ξ_* values estimated in the present analysis for cases with $\xi_* > 0$.

However, uncertainties on ξ_* estimates remain important. Support for this comes from the spatial distribution of ξ_* , which was still highly heterogeneous, with local variability dominating at small scales [e.g., Fig. 1.10, third col.].

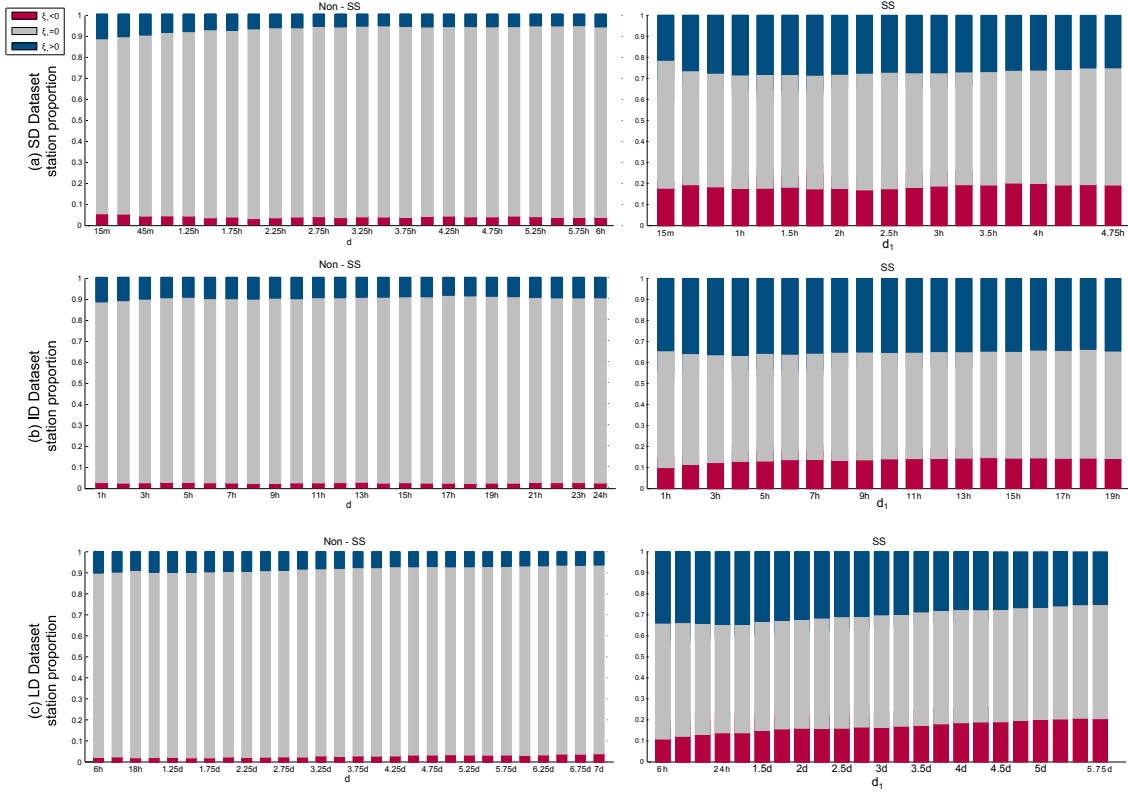


Figure 1.11: Stacked histograms of the fractions of valid SS stations with $\xi < 0$ (in red), $\xi = 0$ (in grey), and $\xi > 0$ (in blue) resulting from the Hosking test applied at the 0.95 confidence level for each duration (non-SS GEV, first col.) and each 6-duration scaling interval (SS GEV, second col.) for: SD (a), ID (b), and LD (c) datasets.

1.6.2 Improvement with respect to Non-SS models

The proportion of series for which the SS model RMSE, $\epsilon_{d,ss}$, was smaller than the non-SS GEV RMSE, $\epsilon_{d,non-ss}$, was analyzed [see the supplementary material, Fig. S11]. For cases with non-zero ξ_* , more than 60% of stations had $\epsilon_{d,ss} < \epsilon_{d,non-ss}$ over most scaling intervals and durations. The 6-duration scaling intervals "15 min - 1 h 30 min" (SD dataset) and "1 h - 6 sih" (ID dataset) showed the largest fractions of stations with increasing errors. On the contrary, increasing errors ($\epsilon_{d,ss} > \epsilon_{d,non-ss}$) were observed for all scaling intervals and durations for most stations (generally more than 70%) having $\xi_* = 0$.

Figure 1.12 presents the $R_{\overline{rmse}}$ distribution over

valid SS stations. When the SS shape parameters were not significantly different from zero [Fig. 1.12, second col.], the relative increases in total RMSE were usually smaller than 0.1 in SD dataset and only scaling intervals with $d_1 < 1$ h had greater $R_{\overline{rmse}}$. For the ID and LD datasets, the medians of the total relative RMSE ratio distributions were smaller than 0.05 for $d_1 \geq 4$ h and $d_1 \geq 24$ h, respectively. Furthermore, more than 90% of stations had $R_{\overline{rmse}} < 0.125$ for $d_1 \geq 6$ h (ID dataset) and $d_1 \geq 30$ h (LD dataset). When $\xi_* \neq 0$, an increase of the mean error in high order quantile estimates was observed for $d_1 = 15$ min (SD dataset) and $d_1 = 1$ h (ID dataset) for at least half of the stations [Fig. 1.12, first col.; note the different scale on the y-axis]. However, for all other d_1 , negative $R_{\overline{rmse}}$ values were observed for

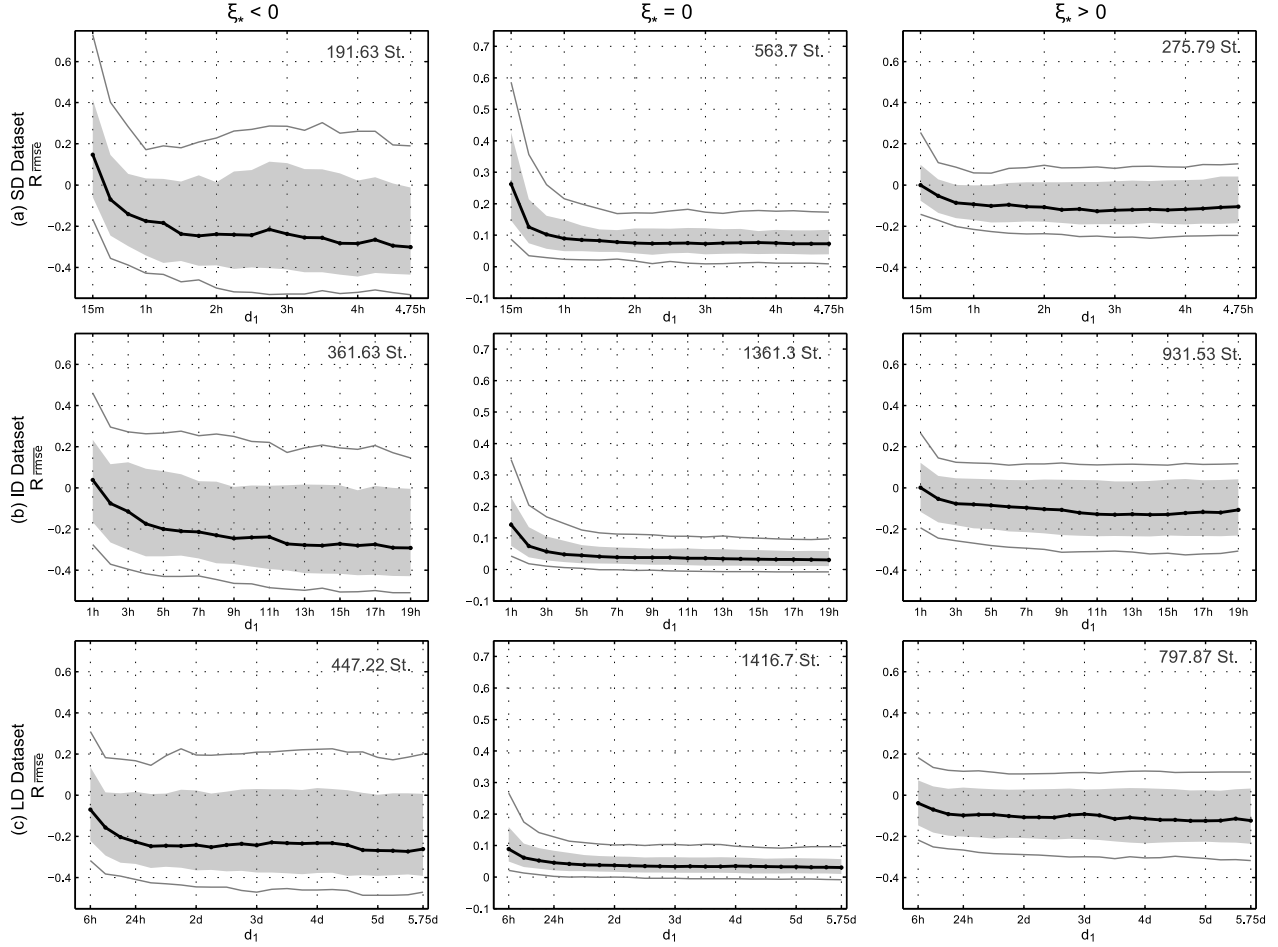


Figure 1.12: Distribution of the relative total RMSE ratio, $R_{\overline{rmse}}$, for $\xi_* < 0$ (first col.), $\xi_* = 0$ (second col.), and $\xi_* > 0$ (third col.) for 6-duration scaling intervals in SD (a), ID (b), and LD (c) datasets. The average number of valid SS station over the scaling intervals is indicated in the right-top corner of each graph.

the majority of stations for all scaling intervals, with a median reduction up to 30% of the mean error. Note that also for 12- and 18-duration scaling intervals the median $R_{\overline{rmse}}$ were generally negative for $d_1 > 1$ h and $\xi_* \neq 0$ [Fig. S14 and S15 of the supplementary material]. Conversely, $R_{\overline{rmse}}$ increased for the majority of stations in all 24-duration scaling intervals having $d_1 < 12$ h [Fig. S17 of the supplementary material]. Note also that no particular spatial pattern characterized the $R_{\overline{rmse}}$ estimates.

1.7 Discussion and conclusion

This study investigated simple scaling properties of extreme precipitation intensity across Canada and the United States. The ability of SS models to reproduce extreme precipitation intensity distributions over a wide range of sub-daily to weekly durations was evaluated. The final objective was to identify duration intervals and geographical areas for which the SS model can be used for an efficient production of IDF curves.

The validity of SS models was empirically confirmed for the majority of the scaling intervals.

In particular, based on the comparison of SS distributions to empirical quantiles, the hypothesis of a scale-invariant shape of the X_d distribution held for all duration intervals spanning from 1 h to 7 days. Less convincing results were obtained for durations shorter than 1 h, especially for the longest scaling intervals (24-duration intervals). One possible explanation is that the coarse instrument resolution of the available 15 min series may strongly impact both the validation tools (for instance, GOF tests) and SS estimates. These results provide important operative indications concerning the inner and outer cut-off durations for AMS scaling and show the importance of a deeper analysis to evaluate the impact of dataset characteristics (e.g., their temporal and measurement resolutions, or the series length) on the scale invariant properties of extreme precipitation.

The majority of the estimated scaling exponents ranged between 0.35 and 0.95, showing a smooth evolution over the scaling intervals and a well-defined spatial structure. Six geographical regions, initially defined according to a climatological classification of North America into 20 regions, displayed different features in terms of scaling exponent values. Specifically, distinct median values of H were observed for the various geographical regions, each characterized by a different precipitation regime. This is consistent with results reported in the literature for some specific regions and smaller observational datasets [e.g, Borga et al. 2005; Nhat et al. 2007; Ceresetti et al. 2010; Panthou et al. 2014 and references therein]. Moreover, while small and smooth changes of H over the scaling intervals were observed in regions containing the majority of stations, one region, *SW_Pac*, displayed two dramatically distinct scaling regimes separated by a steep transition occurring between a few hours

and 24 h. These results limit the applicability of SS models in *SW_Pac*, and were connected to the local features of intense precipitation events by the analysis of the mean number of events per year and the mean wet time of these events.

Weak scaling regimes, characterized by relatively small H values (H close to 0.5), were generally observed for scaling intervals containing very short durations (e.g, less than 2 h) and for regions on the west coast of the continent [regions A1, A2, and D; see Fig. 1.8]. For these scaling intervals and regions, we can expect that extreme precipitation events observed at various durations will have similar statistical characteristics, being governed by homogeneous weather processes.

The interpretation of high H values (e.g., $H > 0.8$), observed between 1 and several days, depending on the region, is more complex. These scaling regimes correspond to mean precipitation depth that varies little with duration. This suggests an important change in precipitation regimes occurring at some durations included in the scaling interval. One interesting example was region *SW_Pac* (region D) for scaling intervals of durations longer than 1 day. In this case, the analysis of the mean number of events per year sampled in AMS suggested that very few long-duration extreme events were produced by large-scale dynamic precipitation systems.

For scaling intervals of durations longer than 4 days, scaling exponents seemed to converge to approximately 0.7 for all regions, except west coast regions (regions A1, A2, and D).

These results suggest that SS represents a reasonable working hypothesis for the development of more accurate IDF curves. This may have important implications for infrastructure design and risk assessment for natural ecosystems, which would benefit from a more accurate estimation

of precipitation return levels. Besides, the spatial distribution of the scaling exponent and its dependency on climatology should be taken into account when defining SS duration intervals for practical estimation of IDF. The accuracy of the SS approximation may in fact depend on the range of considered temporal scales. Equally critical, estimated H values were found to gradually evolve with the considered scaling intervals. In this respect, interesting extensions of the analysis should consider methods for the quantification of the uncertainty in H estimations as well as the possibility of modeling the scaling exponent as a function of both the observational duration and the AMS distribution quantile/moment order, i.e. by the use of a multiscaling (MS) framework for IDFs. Equally important, the events sampled by the AMS also showed different statistical features within different geographical regions and some specific results [e.g., for the *SW_Pac* region] stimulate the interest for an analysis of the scaling property of extreme precipitation by the use of a temporal stochastic scaling approach.

The evaluation of SS model performances under the assumption of GEV distributions for AMS intensity was then performed. Results indicate that the proposed SS GEV models may lead to a more reliable statistical inference of extreme precipitation intensity than that based on the conventional non-SS approach. In particular, a better assessment of the GEV shape parameter seems possible when pooling data from several durations under the scaling hypothesis. The use of the SS approximation may introduce biases in high quantile estimates when AMS distributions move drastically away from perfect scale invariance (short durations and/or longest scaling intervals). Nonetheless, decreases in the SS GEV *RMSE* with respect to non-SS GEV models for d_1 longer than

a few hours and/or scaling intervals shorter than 24 durations indicate that quantile errors in IDF estimates can be generally reduced.

Caution is advised when interpreting these results due to the fact that high order empirical quantiles were used as reference estimates of true X_d quantiles, which could be a misleading assumption especially when available AMS are short. Moreover, two important limitations of the presented SS approach must be stressed. Firstly, a more comprehensive assessment of the scaling exponent uncertainty and of the influence of dataset characteristics on the estimation of AMS simple scaling is recommended for a reliable estimation of Simple Scaling IDF curves. Secondly, the proposed model relies on the implicit hypothesis of stationarity of AMS over the observed period while growing evidence supports the ongoing changes in extreme precipitation intensity, frequency, duration, and spatial patterns as a result of climate change [e.g, Hartmann et al. 2013; Westra et al. 2014; Donat et al. 2016]. In particular, short duration extreme rainfall is expected to respond to global warming with a different sensitivity to temperature than those expected at daily or longer time scales [e.g, Westra et al. 2014; Lenderink and Attema 2015; Wasko and Sharma 2017; Barbero et al. 2017] which implies a change in the temporal scaling properties of precipitation over time.

Hence, considering these limitations and our general results, any future extension of this study should investigate the possibility of introducing spatial information in scaling models as well as the characterization of possible evolution of the scaling exponent in a warmer climate in order to identifying valuable approaches allowing non-stationarity of SS model parameters.

References

- Alila, Y. (2000). “Regional rainfall depth-duration-frequency equations for Canada”. *Water Resources Research* 36.7, 1767–1778. DOI: [10.1029/2000WR900046](https://doi.org/10.1029/2000WR900046).
- Asquith, W. H. and J. S. Famiglietti (2000). “Precipitation areal-reduction factor estimation using an annual-maxima centered approach”. *Journal of Hydrology* 230.1-2, 55–69. DOI: [10.1016/S0022-1694\(00\)00170-0](https://doi.org/10.1016/S0022-1694(00)00170-0).
- Bara, M., S. Kohnová, L. Gaál, J. Szolgay and K. Hlavcová (2009). “Estimation of IDF curves of extreme rainfall by simple scaling in Slovakia”. *Contributions to Geophysics and Geodesy* 39.3, 187–206.
- Barbero, R., H. J. Fowler, G. Lenderink and S. Blenkinsop (2017). “Is the intensification of precipitation extremes with global warming better detected at hourly than daily resolutions?”: *Geophysical Research Letters* 44.2, 2016GL071917. DOI: [10.1002/2016GL071917](https://doi.org/10.1002/2016GL071917).
- Bendjoudi, H., P. Hubert, D. Schertzer and S. Lovejoy (1997). “Interprétation multifractale des courbes intensité-durée-fréquence des précipitations”. *Comptes Rendus de l’Académie des Sciences-Series IIA-Earth and Planetary Science* 325.5, 323–326.
- Bernard, M. M. (1932). “Formulas For Rainfall Intensities of Long Duration”. *Transactions of the American Society of Civil Engineers* 96.1, 592–606.
- Blanchet, J., D. Ceresetti, G. Molinié and J.-D. Creutin (2016). “A regional GEV scale-invariant framework for Intensity-Duration-Frequency analysis”. *Journal of Hydrology* 540, 82–95. DOI: [10.1016/j.jhydrol.2016.06.007](https://doi.org/10.1016/j.jhydrol.2016.06.007).
- Blöschl, G. and M. Sivapalan (1995). “Scale issues in hydrological modelling: A review”. *Hydrological Processes* 9, 251–290. DOI: [10.1002/hyp.3360090305](https://doi.org/10.1002/hyp.3360090305).
- Borga, M., C. Vezzani and G. Dalla Fontana (2005). “Regional rainfall depth-duration-frequency equations for an alpine region”. *Natural Hazards* 36.1-2, 221–235.
- Bougadis, J. and K. Adamowski (2006). “Scaling model of a rainfall intensity-duration-frequency relationship”. *Hydrological Processes* 20.17, 3747–3757. DOI: [10.1002/hyp.6386](https://doi.org/10.1002/hyp.6386).
- Bukovsky, M. S. (2012). “Masks for the Bukovsky regionalization of North America, Regional Integrated Sciences Collective”. *Institute for Mathematics Applied to Geosciences, National Center for Atmospheric Research, Boulder, CO. Downloaded (2015): 05-08*. 06–18.
- Burlando, P. and R. Rosso (1996). “Scaling and multiscaling models of DDF for storm precipitations”. *Journal of Hydrology* 187, 45–64. DOI: [10.1016/S0022-1694\(96\)03086-7](https://doi.org/10.1016/S0022-1694(96)03086-7).
- Ceresetti, D., G. Molinié and J.-D. Creutin (2010). “Scaling properties of heavy rainfall at short duration: A regional analysis”. *Water Resources Research* 46.9. W09531, n/a–n/a. DOI: [10.1029/2009WR008603](https://doi.org/10.1029/2009WR008603).
- Ceresetti, D. (2011). “Structure spatio-temporelle des fortes précipitations: application à la région Cévennes-Vivarais”. PhD thesis. Université de Grenoble.
- Coles, S. G. (2001). *An Introduction to Statistical Modeling of Extreme Values*. London: Springer.
- Coles, S., J. Heffernan and J. Tawn (1999). “Dependence Measures for Extreme Value Analyses”. *Extremes* 2.4, 339–365. DOI: [10.1023/A:1009963131610](https://doi.org/10.1023/A:1009963131610).
- CSA (2012). *Development, interpretation and use of rainfall intensity-duration-frequency (IDF) information: Guideline for Canadian water resources practitioners*. Tech. rep. Canadian Standard Association, Tech. Rep. PLUS 4013, Mississauga, Ontario, 2nd ed. 214.
- Cunnane, C. (1973). “A particular comparison of annual maxima and partial duration series methods of flood frequency prediction”. *Journal of Hydrology* 18.3-4, 257–271. DOI: [10.1016/0022-1694\(73\)90051-6](https://doi.org/10.1016/0022-1694(73)90051-6).
- De Michele, C., N. T. Kottegoda and R. Rosso (2001). “The derivation of areal reduction factor of storm rainfall from its scaling properties”. *Water Resources Research* 37.12, 3247–3252. DOI: [10.1029/2001wr000346](https://doi.org/10.1029/2001wr000346).
- Devine, K. A. and É. Mekis (2008). “Field accuracy of Canadian rain measurements”. *Atmosphere-Ocean* 46.2, 213–227. DOI: [10.3137/ao.460202](https://doi.org/10.3137/ao.460202).
- Donat, M. G., L. V. Alexander, N. Herold and A. J. Dittus (2016). “Temperature and precipitation extremes in century-long gridded observations, reanalyses, and atmospheric model simulations”. *Journal of Geophysical Research: Atmospheres*, 2016JD025480. DOI: [10.1002/2016JD025480](https://doi.org/10.1002/2016JD025480).
- Dubrule, B., F. Graner and D. Sornette (1997). *Scale Invariance and Beyond*. Les Houches Workshop, March 10-14, 1997. Les Ulis, France: EDP Sciences.
- ECCC (n.b.). *Environment Climate Change Canada. Historical Climate Data Canada; editing status 2016-08-09; re3data.org - Registry of Research Data Repositories*. last accessed: 2016-11-09. DOI: [10.17616/R3N012](https://doi.org/10.17616/R3N012).
- Eggert, B., P. Berg, J. O. Haerter, D. Jacob and C. Moseley (2015). “Temporal and spatial scaling impacts on extreme precipitation”. *Atmos. Chem. Phys.* 15.10, 5957–5971. DOI: [10.5194/acp-15-5957-2015](https://doi.org/10.5194/acp-15-5957-2015).
- Good, P. (2013). *Permutation Tests: A Practical Guide to Resampling Methods for Testing Hypotheses*. Springer Science & Business Media.
- Greenwood, J. A., J. M. Landwehr, N. C. Matalas and J. R. Wallis (1979). “Probability weighted moments: definition and relation to parameters of several distributions expressible in inverse form”. *Water Resources Research* 15.5, 1049–1054.
- Gupta, V. K. and E. Waymire (1990). “Multiscaling properties of spatial rainfall and river flow distributions”. *Journal of Geophysical Research: Atmospheres* 95.D3, 1999–2009. DOI: [10.1029/JD095iD03p01999](https://doi.org/10.1029/JD095iD03p01999).
- Hartmann, D. L., A. M. G. Klein Tank, M. Ruscicci, L. V. Alexander, B. Broenniman, Y. Charabi, F. J. Dentener, E. J. Dlugokencky, D. R. Easterling, A. Kaplan, B. J. Soden, P. W. Thorne, M. Wild,

- P. M. Zhai and E. C. Kent (2013). “Observations: Atmosphere and Surface”. *Climate Change 2013: The Physical Science Basis. Contribution of Working Group I to the Fifth Assessment Report of the Intergovernmental Panel on Climate Change*. Ed. by T. F. Stocker, D. Qin, G.-K. Plattner, M. Tignor, S. K. Allen, J. Boschung, A. Nauels, Y. Xia, V. Bex and P. M. Midgley. Cambridge, United Kingdom and New York, NY, USA: Cambridge University Press, 159–254.
- Hosking, J. R. M., J. R. Wallis and E. F. Wood (1985). “Estimation of the generalized extreme-value distribution by the method of probability-weighted moments”. *Technometrics* 27.3, 251–261.
- Hosking, J. R. M. and J. R. Wallis (1997). *Regional Frequency analysis: an approach based on L-moments*. Cambridge University Press.
- Hubert, P. and H. Bendjoudi (1996). “Introduction à l’étude des longues séries pluviométriques”. *XIIème journées hydrologiques de l’Orstom*, 10–11.
- Katz, R. W., M. Parlange and P. Naveau (2002). “Statistics of extremes in hydrology”. *Advances in Water Resources* 25, 1287–1304.
- Katz, R. W. (2013). “Statistical Methods for Nonstationary Extremes”. *Extremes in a Changing Climate*. Ed. by A. AghaKouchak, D. Easterling, K. Hsu, S. Schubert and S. Sorooshian. Water Science and Technology Library 65. Springer Netherlands, 15–37.
- Koutsoyiannis, D. (2004a). “Statistics of extremes and estimation of extreme rainfall: I. Theoretical investigation”. *Hydrological Sciences Journal* 49.4. DOI: [10.1623/hysj.49.4.575.54430](https://doi.org/10.1623/hysj.49.4.575.54430).
- Koutsoyiannis, D. (2004b). “Statistics of extremes and estimation of extreme rainfall: II. Empirical investigation of long rainfall records”. *Hydrological Sciences Journal* 49.4. DOI: [10.1623/hysj.49.4.591.54424](https://doi.org/10.1623/hysj.49.4.591.54424).
- Koutsoyiannis, D., D. Kozonis and A. Manetas (1998). “A mathematical framework for studying rainfall intensity-duration-frequency relationships”. *Journal of Hydrology* 206.1-2, 118–135. DOI: [10.1016/S0022-1694\(98\)00097-3](https://doi.org/10.1016/S0022-1694(98)00097-3).
- Kunkel, K. E., D. R. Easterling, D. A. R. Kristovich, B. Gleason, L. Stoecker and R. Smith (2012). “Meteorological Causes of the Secular Variations in Observed Extreme Precipitation Events for the Conterminous United States”. *Journal of Hydrometeorology* 13.3, 1131–1141. DOI: [10.1175/JHM-D-11-0108.1](https://doi.org/10.1175/JHM-D-11-0108.1).
- Langousis, A., A. A. Carsteanu and R. Deidda (2013). “A simple approximation to multifractal rainfall maxima using a generalized extreme value distribution model”. *Stochastic Environmental Research and Risk Assessment* 27.6, 1525–1531.
- Lenderink, G. and J. Attema (2015). “A simple scaling approach to produce climate scenarios of local precipitation extremes for the Netherlands”. *Environmental Research Letters* 10.8, 085001. DOI: [10.1088/1748-9326/10/8/085001](https://doi.org/10.1088/1748-9326/10/8/085001).
- Lovejoy, S. and B. B. Mandelbrot (1985). “Fractal properties of rain, and a fractal model”. *Tellus A* 37.3, 209–232.
- Lovejoy, S. and D. Schertzer (1985). “Generalized Scale Invariance in the Atmosphere and Fractal Models of Rain”. *Water Resources Research* 21.8, 1233–1250. DOI: [10.1029/WRO21i008p01233](https://doi.org/10.1029/WRO21i008p01233).
- Maraun, D., F. Wetterhall, A. M. Ireson, R. E. Chandler, E. J. Kendon, M. Widmann, S. Brienen, H. W. Rust, T. Sauter, M. Themeßl, et al. (2010). “Precipitation downscaling under climate change: Recent developments to bridge the gap between dynamical models and the end user”. *Reviews of Geophysics* 48.3.
- Mascaro, G., R. Deidda and M. Hellies (2013). “On the nature of rainfall intermittency as revealed by different metrics and sampling approaches”. *Hydrology and Earth System Sciences* 17.1, 355–369. DOI: [10.5194/hess-17-355-2013](https://doi.org/10.5194/hess-17-355-2013).
- MDDELCC (n.b.). Ministère du Développement Durable, de l’Environnement et de la Lutte contre les Changements Climatiques, 2016. Données du Programme de surveillance du climat, Direction générale du suivi de l’état de l’environnement, Québec.
- Menabde, M., A. Seed and G. Pegram (1999). “A simple scaling model for extreme rainfall”. *Water Resources Research* 35.1, 335–339.
- Nhat, L. M., Y. Tachikawa, T. Sayama and K. Takara (2007). “A Simple Scaling Characteristics of Rainfall in Time and Space to Derive Intensity Duration Frequency Relationships”. 51, 73–78. DOI: [10.2208/prohe.51.73](https://doi.org/10.2208/prohe.51.73).
- NOAA (n.d.). 15 min precipitation data (15PD) and hourly precipitation data (HPD), Climate Data Online; editing status 2016-06-17; re3data.org - Registry of Research Data Repositories. last accessed: 2016-11-09. DOI: [10.17616/R32059](https://doi.org/10.17616/R32059).
- Olsson, J., V. P. Singh and K. Jinno (1999). “Effect of spatial averaging on temporal statistical and scaling properties of rainfall”. *Journal of Geophysical Research: Atmospheres* 104.D16, 19117–19126. DOI: [10.1029/1999JD900271](https://doi.org/10.1029/1999JD900271).
- Overeem, A., A. Buishand and I. Holleman (2008). “Rainfall depth-duration-frequency curves and their uncertainties”. *Journal of Hydrology* 348.1-2, 124–134. DOI: [10.1016/j.jhydrol.2007.09.044](https://doi.org/10.1016/j.jhydrol.2007.09.044).
- Panthou, G., T. Vischel, T. Lebel, G. Quantin and G. Molinié (2014). “Characterising the space-time structure of rainfall in the Sahel with a view to estimating IDAF curves”. *Hydrology and Earth System Sciences* 18.12, 5093–5107. DOI: [10.5194/hess-18-5093-2014](https://doi.org/10.5194/hess-18-5093-2014).
- Papalexiou, S. M., D. Koutsoyiannis and C. Makropoulos (2013). “How extreme is extreme? An assessment of daily rainfall distribution tails”. *Hydrology and Earth System Sciences* 17.2, 851–862. DOI: [10.5194/hess-17-851-2013](https://doi.org/10.5194/hess-17-851-2013).
- Papalexiou, S. M. and D. Koutsoyiannis (2013). “Battle of extreme value distributions: A global survey on extreme daily rainfall”. *Water Resources Research* 49.1, 187–201. DOI: [10.1029/2012WR012557](https://doi.org/10.1029/2012WR012557).

- Rodriguez-Iturbe, I., V. K. Gupta and E. Waymire (1984). "Scale considerations in the modeling of temporal rainfall". *Water Resources Research* 20.11, 1611–1619.
- Sivakumar, B. (2000). "Fractal analysis of rainfall observed in two different climatic regions". *Hydrological Sciences Journal* 45.5, 727–738. DOI: [10.1080/02626660009492373](https://doi.org/10.1080/02626660009492373).
- Sivapalan, M. and G. Blöschl (1998). "Transformation of point rainfall to areal rainfall: Intensity-duration-frequency curves". *Journal of Hydrology* 204.1-4, 150–167. DOI: [10.1016/S0022-1694\(97\)00117-0](https://doi.org/10.1016/S0022-1694(97)00117-0).
- Tessier, Y., S. Lovejoy and D. Schertzer (1993). "Universal Multifractals: Theory and observations for rain and clouds". *J. Appl. Meteorol.*, 32, 223-250 32, 223–250.
- Trenberth, K. E., A. Dai, R. M. Rasmussen and D. B. Parsons (2003). "The Changing Character of Precipitation". *Bulletin of the American Meteorological Society* 84.9, 1205–1217. DOI: [10.1175/bams-84-9-1205](https://doi.org/10.1175/bams-84-9-1205).
- Veneziano, D. and P. Furcolo (2002). "Multifractality of rainfall and scaling of intensity-duration-frequency curves". *Water Resources Research* 38.12, 1306. DOI: [10.1029/2001WR000372](https://doi.org/10.1029/2001WR000372).
- Veneziano, D. and V. Iacobellis (2002). "Multiscaling pulse representation of temporal rainfall". *Water Resources Research* 38.8, 13–1. DOI: [10.1029/2001WR000522](https://doi.org/10.1029/2001WR000522).
- Veneziano, D. and A. Langousis (2010). "Scaling and fractals in hydrology". *Advances in data-based approaches for hydrologic modeling and forecasting*. Sivakumar, Bellie and Berndtsson, Ronny. Singapore: World Scientific.
- Veneziano, D., C. Lepore, A. Langousis and P. Furcolo (2007). "Marginal methods of intensity-duration-frequency estimation in scaling and nonscaling rainfall". *Water Resources Research* 43.10, n/a–n/a. DOI: [10.1029/2007wr006040](https://doi.org/10.1029/2007wr006040).
- Veneziano, D. and S. Yoon (2013). "Rainfall extremes, excesses, and intensity-duration-frequency curves: A unified asymptotic framework and new nonasymptotic results based on multifractal measures". *Water Resources Research* 49.7, 4320–4334. DOI: [10.1002/wrcr.20352](https://doi.org/10.1002/wrcr.20352).
- Venugopal, V., S. G. Roux, E. Foufoula-Georgiou and A. Arnéodo (2006). "Scaling behavior of high resolution temporal rainfall: New insights from a wavelet-based cumulant analysis". *Physics Letters A* 348.3, 335–345.
- Wallis, J. R., M. G. Schaefer, B. L. Barker and G. H. Taylor (2007). "Regional precipitation-frequency analysis and spatial mapping for 24-hour and 2-hour durations for Washington State". *Hydrology and Earth System Sciences* 11.1, 415–442. DOI: [10.5194/hess-11-415-2007](https://doi.org/10.5194/hess-11-415-2007).
- Wasko, C. and A. Sharma (2017). "Continuous rainfall generation for a warmer climate using observed temperature sensitivities". *Journal of Hydrology* 544, 575–590. DOI: [10.1016/j.jhydrol.2016.12.002](https://doi.org/10.1016/j.jhydrol.2016.12.002).
- Westra, S., H. J. Fowler, J. P. Evans, L. V. Alexander, P. Berg, F. Johnson, E. J. Kendon, G. Lenderink and N. M. Roberts (2014). "Future changes to the intensity and frequency of short-duration extreme rainfall". *Reviews of Geophysics* 52.3, 2014RG000464. DOI: [10.1002/2014RG000464](https://doi.org/10.1002/2014RG000464).
- Willems, P., K. Arnbjerg-Nielsen, J. Olsson and V. T. V. Nguyen (2012). "Climate change impact assessment on urban rainfall extremes and urban drainage: Methods and shortcomings". *Atmospheric Research*. Rainfall in the urban context: forecasting, risk and climate change 103, 106–118. DOI: [10.1016/j.atmosres.2011.04.003](https://doi.org/10.1016/j.atmosres.2011.04.003).
- Yu, P.-S., T.-C. Yang and C.-S. Lin (2004). "Regional rainfall intensity formulas based on scaling property of rainfall". *Journal of Hydrology* 295.1-4, 108–123. DOI: [10.1016/j.jhydrol.2004.03.003](https://doi.org/10.1016/j.jhydrol.2004.03.003).

Article 2

Observed and simulated precipitation over North East North-America: how do sub-daily extremes scale in space and time?

Silvia Innocenti,¹ Alain Mailhot¹, Anne Frigon²,
Alex J. Cannon³, Martin Leduc²

1. Centre Eau-Terre-Environnement, INRS, Québec, Canada;
2. Consortium Ouranos, Montréal, Canada;
3. Climate Research Division, ECCC, Victoria, Canada.

Under review, *Journal of Climate*.

Résumé

La caractérisation des précipitations extrêmes à de fines échelles spatiales et temporelles représente un défi majeur en sciences hydro-climatiques. En effet, de larges incertitudes affectent l'estimation des précipitations à partir des données disponibles. Comparer la structure spatio-temporelle des précipitations extrêmes estimées à partir de différents jeux de données devient ainsi crucial et constitue une étape essentielle dans l'évaluation des modèles climatiques.

Cette étude vise deux objectifs spécifiques. Premièrement, l'analyse s'intéresse à la comparaison des propriétés statistiques (les distributions de probabilité et les cycles annuels et diurnaux) des précipitations extrêmes extraites à plusieurs échelles spatio-temporelles et à partir de plusieurs jeux de données. Plus précisément, des séries simulées issues du Modèle Régionale Canadien du Climat (MRCC5), le jeu de données du satellite CMORPH v1.0 CRT avec correction du biais, le jeu de donnée Multi Source Weighted-Ensemble Precipitation MSWEP v2 ainsi qu'une simulation de 13 ans du modèle à haute résolution spatial WRF v3.4.1 sont considérés, en plus que des séries provenant de stations météorologiques.

Deuxièmement, l'étude propose et évalue la validité statistique de modèle synthétique pour décrire la structure spatio-temporelle des Maxima Annuels (AM) de précipitations pour des jeux de données sur grille. L'analyse est effectuée pour la période 1980-2013 dans le nord-est de l'Amérique du Nord. Les résultats montrent que la simulation du MRCC5 piloté par la réanalyse ERA-Interim reproduit adéquatement les quantiles des AM pour des courtes durées (p. ex. inférieures à 3h) ainsi que les cycles journaliers et annuels des extrêmes de précipitation. L'analyse illustre aussi certains impacts que les caractéristiques de base des données considérées (p. ex. leurs résolutions spatiales et temporelles) peuvent avoir sur l'estimation des lois d'échelle spatio-temporelles (*Spatio-Temporal Scaling*, STS) des précipitations extrêmes. Les impacts des erreurs d'échantillonnage et de la variabilité locale sur les estimations du STS sont aussi évalués en utilisant les 50 membres d'un grand ensemble climatique simulé par le MRCC5. Les résultats montrent que moyenniser les estimations temporelles des lois d'échelle obtenues sur plusieurs membres du MRCC5 permet de réduire l'incertitude locale et d'estimer de façon robuste les propriétés de changement d'échelle spatio-temporelle des AM.

Abstract

The characterization of extreme precipitation at fine spatial and temporal scales represents a paramount challenge in hydro-climate sciences due to large uncertainties that affect the precipitation estimation from available datasets. Comparing the spatio-temporal structure of precipitation extremes estimated from different datasets is thus crucial and represent an essential step for the evaluation of climate models. This study aims at: i) comparing daily and sub-daily extreme precipitation statistical properties (probability distribution and annual and diurnal cycles) estimated from series simulated by the Canadian RCM version 5 (CRCM5) with the corresponding estimations obtained from meteorological stations and three gridded datasets (the bias-corrected satellite CMORPH v1.0 CRT dataset, the Multi-Source Weighted-Ensemble Precipitation dataset, MSWEP v2, and a 13-year convection-permitting WRF v3.4.1 simulation); and ii) proposing a synthetic model describing the spatio-temporal structure of Annual Maxima (AM) precipitation for gridded datasets. The analysis is conducted for the 1980-2013 period over the north-east part of North America. The results showed that the ERA-Interim driven CRCM5 simulation well reproduced sub-daily extreme quantiles and AM rainfall daily and annual cycles. The analysis also illustrated the influence of basic dataset characteristics (e.g., spatial and temporal resolutions) on the spatio-temporal scaling (STS) of extreme precipitation. The impacts of sampling errors and local variability on the STS estimates was then assessed using the 50 member CRCM5 large ensemble (CRCM5-LE). Results show that averaging temporal scaling estimates from various CRCM5-LE members allows to reduce local uncertainty and robustly estimate AM spatio-temporal scaling properties.

2.1 Introduction

Heavy precipitation may have severe and threatening impacts on human societies and natural ecosystems [e.g., Seneviratne et al. 2012; Goodess 2013]. Moreover, as important changes in the frequency, duration, and spatial distribution of extreme precipitation events are expected at global and regional scales [e.g., Hartmann et al. 2013; Dai et al. 2017; Dwyer and O’Gorman 2017], the need for an accurate characterization of extreme rainfall across various spatial and temporal scales becomes even more important. However, such an objective is still challenging, primarily because of deficiencies in available datasets [Westra et al. 2014; Herold et al. 2017]. Sparse net-

works and short records prevent a comprehensive characterization of the complex spatial structure and the intermittent temporal patterns of extreme precipitation events [Grimaldi et al. 2015; Trenberth et al. 2017]. Equally important, the biases and large uncertainties related to precipitation measurements [e.g., Sikorska and Seibert 2016], data interpolation techniques and representativeness errors [Tustison et al. 2001], as well the inhomogeneity of observed records [e.g., Hofstra et al. 2008], must be considered when using gridded datasets and reanalyses [Tapiador et al. 2017].

In this context, Regional Climate Models (RCMs) represent an interesting option to access climate information about extreme rainfall since they provide precipitation series with complete and physi-

cally coherent spatial and temporal coverage over large regions [Flato et al. 2013]. Increasing RCM spatial resolution and improvements in the representation of key physical processes led to significant advances in RCM ability at simulating key features of precipitation, such as the annual cycle and the statistics of daily extremes [e.g., Prein et al. 2015; Lucas-Picher et al. 2017]. With spatial resolutions typically ranging from 12 to 50 km state-of-the-art RCMs allow for a more realistic representation of surface forcings, such as orography and coastlines, and small scale climate and weather processes [e.g., Rummukainen 2016; Fossler et al. 2017].

However, RCMs may still display important inaccuracies in the simulation of sub-daily rainfall characteristics (e.g., diurnal cycle and hourly extremes) that have been generally ascribed to the inadequate representation of many important processes (e.g. clouds dynamics) at the sub-grid scale [e.g., Westra et al. 2014; Cavicchia et al. 2016; Liu et al. 2017]. Promising approaches for overcoming these inaccuracies rely on the use of Convection-Permitting Models (CPM) [e.g., Ban et al. 2015; Dai et al. 2017]. Running simulations at grid resolutions of a few kilometers, CPMs more completely resolve physical equations of deep convection [Rasmussen et al. 2017] resulting in a more realistic representation of small-scale processes generating sub-daily extremes [e.g., Prein et al. 2016; Kendon et al. 2017]. However, due to their high computational and storage costs, many crucial aspects of CPMs, such as the sensitivity to nesting and driving strategies, or spatial domain size, remain largely unexplored [Prein et al. 2017]. For the same reasons, relatively few continuous CPM runs are currently available and are typically restricted to small spatial domains and short time periods (e.g., 10 years or less) [e.g., Prein et al.

2016; Mantegna et al. 2017]. This prevents a robust assessment of uncertainties through the use of classical multi-model and/or multi-member approaches [Kendon et al. 2017; Gadian et al. 2017].

As part of Climate change and hydrological Extremes (ClimEx) project, a large ensemble of high-resolution (0.11° lat-lon) simulations has been produced for two spatial domains: one covering the north-east part of North America [Fig. 2.1a] and one covering most of Europe [see Leduc et al. 2019, Fig. 2]. This 50-member ensemble has been simulated over the period 1950-2100 through the use of the 5th generation Canadian Regional Climate Model (CRCM5) [Martynov et al. 2013; Separovic et al. 2013] and is hereinafter called CRCM5 Large-Ensemble (CRCM5-LE).

Previous investigations demonstrated the ability of CRCM5 in reproducing annual and seasonal mean precipitation, as well as daily and multi-daily extreme precipitation [e.g., Diaconescu et al. 2016; Whan and Zwiers 2016]. Leduc et al. (2019) validated CRCM5-LE monthly temperature and precipitation by comparing the large ensemble with observational gridded datasets. However, no comprehensive assessment of the spatiotemporal characteristics of CRCM5 extreme precipitation has been provided so far. In particular, evaluating the relative change of simulated extreme properties (e.g., quantiles) with the spatiotemporal scale would be crucial to assess whether the CRCM5 reproduces the statistical structure of observed precipitation [Cortes-Hernandez et al. 2016].

Previous studies showed that observed precipitation extremes are generally scale-invariant, meaning that extreme statistical distributions estimated at different spatiotemporal scales can be related to each other by simple analytical rela-

tionships (e.g., a power law) [e.g., Menabde et al. 1999; De Michele et al. 2001; Veneziano and Langousis 2010]. These relationships are generally referred to as *scaling models* [Veneziano and Langousis 2010]. However, while many studies assessed the validity of scale invariance over a wide range of spatiotemporal scales for observed precipitation series [e.g., Burlando and Rosso 1996; Ceresetti 2011; Panthou et al. 2014; Boukhelifa et al. 2018], investigations of spatiotemporal scaling remain scarce for RCM simulations [Cortes-Hernandez et al. 2016].

The present study aims at: i) assessing and comparing extreme precipitation properties (quantiles, annual and diurnal cycles, and temporal scaling) from CRCM5 simulations with the corresponding estimations obtained from meteorological stations and three gridded datasets: the CMORPH bias-corrected satellite dataset [Xie and Xiong 2011], the Multi-Source Weighted-Ensemble Precipitation (MSWEP) v2 dataset [Beck et al. 2017a], and one series simulated by the convection-permitting Weather Research and Forecasting model (WRF) [Liu et al. 2017; Prein et al. 2017]; and ii) propose a synthetic model that describes the variability of extreme temporal scaling estimates over a wide range of spatial scale. Characterizing quantile changes across spatial and temporal scales, the proposed scaling model concisely describes the spatiotemporal structure of precipitation extremes in gridded datasets.

The paper is structured as follows. Section 2.2 provides information about the datasets used in this study, while Sec. 2.3 describes the procedure used to extract rainfall extremes at various spatiotemporal scales. Sections 2.4 and 2.5 define the statistical indexes used to compare extreme estimates between datasets. Results for the evalua-

tion of gridded datasets against stations are presented in Sections 2.6 and 2.7, and Sec. 2.8 analyses the spatiotemporal scaling for the CRCM5-LE. Finally, Sec. 2.9 summarizes the main conclusions with relevant discussions and perspectives on future work.

2.2 Data and study area

The study area considered corresponds to the North American simulation domain of the CRCM5 model for the ClimEx experiment [Fig. 2.1a]. Basic characteristics of the considered datasets are summarized in Table 2.1.

2.2.1 Meteorological station series

Data from four rain gauge networks operating between 1900 and 2013 over the study domain were pooled for the construction of the point-scale observational dataset: the Daily Maxima Precipitation Dataset (DMPD) and the Hourly Canadian Precipitation Dataset (HCPD) [ECCC; MD-DELCC] for Canada, and the Hourly Precipitation Data (HPD) and 15-min Precipitation Data (15PD) [NOAA] for the United States.

Quality check of available records [see Innocenti et al. 2017 for more details] resulted in the selection of series with at least 15 years of records and less than 15% of missing values each year. A total of 759 stations were therefore selected, 72.2% of them having both 15PD and HPD series (in the US) and 2.24% having both DMPD and HCPD series (in Canada) [blue and red locations in Fig. 2.1b, respectively]. Selected stations are concentrated in the southern part of the study domain [Fig. 2.1b], stations in northern regions having

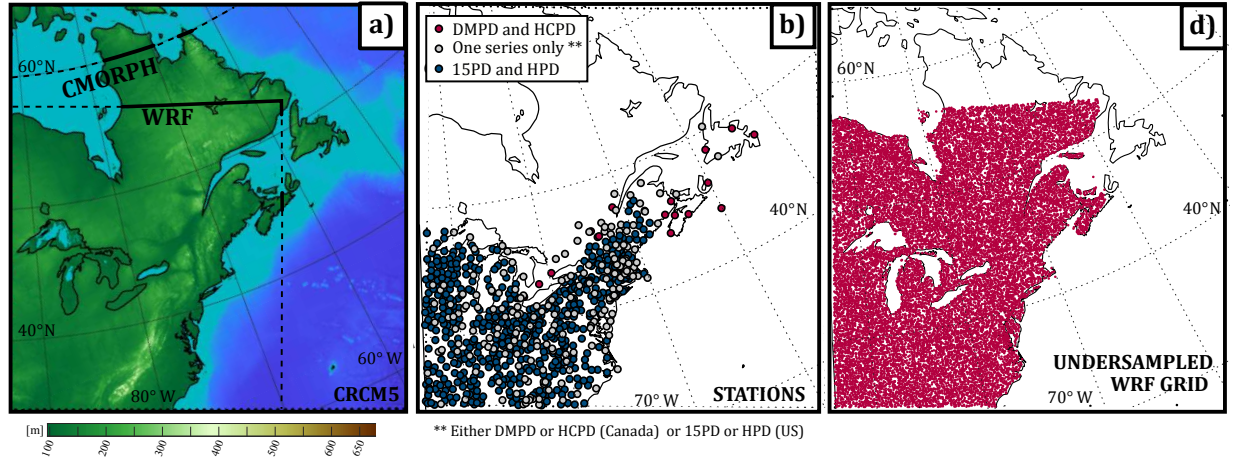


Figure 2.1: Spatial domains of gridded datasets and station networks: a) CRCM5 domain with topography and relevant boundaries of the WRF and CMORPH domains (MSWEP grid covers the entire CRCM5 domain); b) stations and available temporal resolution of recorded series: Daily Maxima and Hourly Canadian Precipitation Dataset (DMPD and HCPD), 15-min and Hourly Precipitation Data (15PD and HPD); c) undersampled WRF grid.

been excluded since their records only cover the summer period (generally May to October).

2.2.2 CRCM5 Large-Ensemble (CRCM5-LE)

Within the ClimEx initiative, 50 CRCM5 v3.3.3.1 runs were produced by downscaling the CanESM2 [von Salzen et al. 2013; Arora et al. 2011] Large Ensemble (CanESM2-LE) [Sigmond and Fyfe 2016; Fyfe et al. 2017] to a 0.11° resolution grid (≈ 12 km) for the period 1950-2100 [Leduc et al. 2019]. The 50 independent and equally likely CanESM2-LE members were generated by applying random perturbations in cloud-overlap parameters [Fyfe et al. 2017]. CanESM2-LE considered observed greenhouse gas, aerosols, and land-use emissions up to the year 2005 and radiative forcing from the RCP8.5 for the 2006-2100 period [Sigmond and Fyfe 2016; Meinshausen et al. 2011]. Hourly precipitation series simulated over the 1954–2099 period were available for 280×280 grid points over northeast North-America [Fig.

2.1a]. The reader is referred to Martynov et al. (2013) and Separovic et al. (2013) for specific details about CRCM5, and to Leduc et al. (2019) for the CRCM5-LE simulation set-up.

An additional CRCM5 simulation was also produced using the European Centre for Medium range Weather Forecast (ECMWF) ERA-Interim reanalysis [Dee et al. 2011] as atmospheric lateral CRCM5 boundaries for the 1979-2013 period [Leduc et al. 2019]. Monthly climatologies of precipitation and temperature from the CRCM5-LE and one ERA-Interim driven simulation (hereafter referred to as ERA-CRCM5) have been validated against observational gridded datasets by Leduc et al. (2019). In the present study, the ERA-CRCM5 simulation was used to evaluate the performance of CRCM5 over the 1981-2013 period.

2.2.3 Convection-permitting WRF simulation

The Weather Research and Forecasting (WRF) model, designed and operated by the National Center for Atmospheric Research (NCAR) [Skamarock et al. 2008], has been recently configured into a regional climate model with a single computational domain of 1360×1016 grid boxes covering much of North America [Liu et al. 2017]. For this experiment, a 13-year WRF (version 3.4.1) simulation was performed by dynamically downscaling the ERA-Interim reanalysis to a 4-km resolution grid from October 2000 to September 2013 [Liu et al. 2017]. Modelling and simulation details are provided in Prein et al. (2017) and Liu et al. (2017).

First evaluations showed good performances of the WRF simulation in capturing the frequency and distribution of seasonal and annual precipitations over most of the contiguous US, as well as in simulating orographic precipitation over complex terrain [Liu et al. 2017; Dai et al. 2017; Prein et al. 2017].

WRF precipitation series were extracted from January 2001 to September 2013 for land grid boxes within the CRCM5 domain after the withdrawal of 50-grid-point buffer due to some border effects observed at northern and eastern boundaries of the WRF domain [e.g., Fig. S1-S2 in the Supplementary material].

2.2.4 CMORPH: bias-corrected satellite dataset

The Climate Prediction Center (CPC) morphing technique (CMORPH) satellite analysis combines

observations from multiple low-orbit microwave satellites ($\approx 12 \text{ km} \times 15 \text{ km}$ resolution) to produce high resolution precipitation estimates at a nearly global scale (60°N and 60°S) [Joyce et al. 2004; Xie and Xiong 2011]. Recently, Xie et al. (2017) reprocessed the CMORPH series throughout the entire record period (January 1998 to December 2016) to get a homogeneous integration of the purely satellite-based estimates, resulting in the *CMORPH v1.0 CRT* bias corrected dataset at a 8km-30min resolution. Bias correction for land grid boxes consisted in a Probability Distribution Function (PDF) matching at 0.25° with the CPC daily gauge analysis [Xie et al. 2010] plus an adjustment at coarser spatiotemporal resolution to account for the year-to-year variability [Xie et al. 2017].

The reprocessed bias-corrected CMORPH, has been validated against other observational products demonstrating the ability of representing sub-daily variability of rainfall during the warm season over land [Xie et al. 2017]. However, the underestimation of the wintertime precipitation linked to satellite deficiencies in detecting snowfall [Xie and Joyce 2014] is a major shortcoming that must be considered when using CMORPH in high-latitude land and/or during the cold seasons [Trenberth et al. 2017].

2.2.5 Gridded MSWEP dataset

The Multi-Source Weighted-Ensemble Precipitation (MSWEP) v2 [Beck et al. 2017b and 2017b] dataset blends observations from two global gauge-based datasets (CPC Unified v1.0 and real time, Xie et al. 2007 and Chen et al. 2008, and GPCC Full Data Reanalysis and First Guess v7, Schneider et al. 2014), three quasi-global satel-

Table 2.1: Precipitation datasets and their basic characteristics.

| Dataset | Description | Period | Spatio-temporal resolution | Reference |
|-------------------------|-----------------------------------|-----------------------|--------------------------------|---------------------------------|
| Meteorological stations | HCPD and DMPD series | 1940 - 2013 | 1h and Daily Maxima* | ECCC MDDELCC |
| | 15PD and HPD series | | 15min and 1h | NOAA** |
| CRCM5-LE [50 members] | CanESN2-LE driven members | 1954 - 2099 | 0.11° - 1h, ($\approx 12km$) | Leduc et al., 2019 |
| ERA-CRCM5 | ERA-Interim driven simulation | 1981 - 2013 | | |
| WRF | ERA-Interim driven simulation | Oct. 2000 - Sep. 2013 | 4km - 1h | Liu et al. (2017) |
| CMORPH [v1.0 CRT] | Bias-corrected satellite analyses | 1998 - 2016 | 8km - 30min | Xie et al. (2017) |
| MSWEP [v2] | Multi-source gridded dataset | 1979 - 2016 | 0.1° - 3h, ($\approx 11km$) | Beck et al. (2017b) and [2017b] |

* Daily maxima depth over a 24h window beginning at 08:00 (LT) for durations 1, 2, 6, and 12h

** <http://www.ncdc.noaa.gov/data-access/land-based-station-data>

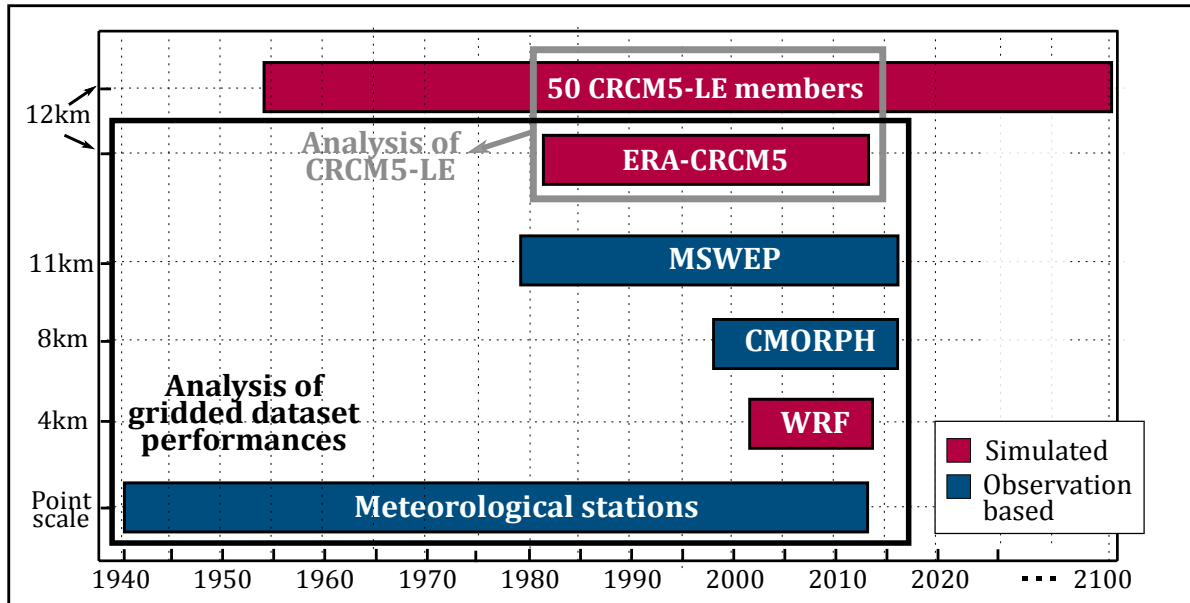


Figure 2.2: Spatial resolution (y-axis) and covered period (x-axis) of datasets; the black rectangle defines the period (1940-2016) and identifies the datasets used for the analysis on gridded dataset performance [see Sec. 2.6], while the gray rectangle defines the period (1980-2015) considered for the analysis of the CRCM5-LE [Sec. 2.8].

lite analyses (CMORPH v1.0, GSMaP-MVK v5-v6, Ushio et al. 2009 and TMPA 3B42RT v7, Huffman et al. 2007), and two reanalyses (ERA-Interim and JRA-55, Kobayashi et al. 2015). Constructed through a multi-stage merging procedure of various datasets at different spatiotemporal resolutions, the MSWEP is a global precipitation dataset spanning the period 1979-2016 on a 0.1° grid with a $3h$ temporal resolution. A detailed description and preliminary evaluation of MSWEP can be found in Beck et al. (2017b) and [2017b].

The MSWEP dataset outperformed other satellite and reanalysis datasets in terms of the 3-day and monthly precipitation patterns and for various precipitation indices [Beck et al. 2017b]. However, considering that the quality of satellite data for northern regions may be questioned in some instances, MSWEP performance for precipitation extremes over our study area must also be evaluated.

2.3 Extraction of Annual Maxima series at various spatiotemporal scales

Let d_0 represent the native temporal resolution and r_0 the nominal spatial resolution of each dataset (consider $r_0 = 0$ for stations). From the series of precipitation depth available at (r_0, d_0) , simulated and observed extremes were assessed through the Annual Maxima (AM) series at various spatiotemporal scales (r, d) . In the remainder of the paper, subscripts for r and d are omitted if referring to a generic spatial and temporal scale.

The aggregated spatial scales $r_k = k \cdot r_0$, with $k = 1, 2, \dots, K$, were used and they are expressed

in km , for simplicity. The coarsest resolution was set to $r_K \approx 72km$, with the number of considered spatial scales ranging from 6 for CRCM5 simulations (with $K_{CRCM5} = 6$) to 12 for WRF (with $K_{WRF} = 18$). The list of spatial scales considered for each dataset appears in Table 2.2.

For each time step, precipitation series were aggregated at scales $r_k > r_0$ with a fixed window in space, i.e. computing the average precipitation depth values for $k \times k$ contiguous grid boxes with no overlap between coarser scale grid boxes. Dataset grids at scales $r_k > r_0$ were defined starting from the south-west corner of the native grid and aggregating the grid boxes toward North-East. This aggregation procedure most realistically mimics the resolution changes for gridded datasets [Eggert et al. 2015]. For each aggregation levels, grid boxes associated to the ocean and water bodies were removed, and spatially aggregated series were discarded if computed over less than 75% native land grid boxes.

A moving window in time was then applied to temporally aggregate precipitation depth series at durations $d = 1, 2, 3, 4, 6, 12, 18, 24, 36, 48, 60$, and $72h$. ($d = 1, 2$, and $4h$ were not considered for MSWEP since $d_0 = 3h$). Finally, the AM series at each spatiotemporal scale (r, d) were extracted.

For the 565 stations having two recorded series [blue and red points in Fig. 2.1b], the maximum of the two AM values was retained for each common year and duration d .

Moreover, to reduce the computational time, the WRF $4km$ -grid was under-sampled with a ratio 1/10 leading to the selection of ≈ 26500 randomly distributed points. All WRF grid boxes containing one or more stations were also retained [see Fig. 2.1c].

The dates and day time of occurrence of the

Table 2.2: Spatial scales considered for each gridded dataset.

| | k | No. of scales | r_k , spatial resolution |
|-----------|--|---------------|--|
| CRCM5-LE* | 1, 2, ..., 6 | 6 | 12, 24, ..., 72km |
| WRF | 1, 2, ..., 6 and 8, 10, 12, ..., 18 | 12 | 4, 8, ..., 24km and 32, 40, ..., 72km |
| CMORPH | 1, 2, ..., 9 | 9 | 8, 16, ..., 72km |
| MSWEP | 1, 2, ..., 6 | 6 | 11, 22, ..., 66km |

* Includes ERA-CRCM5

AM were extracted for each spatiotemporal scale, year, and location (i.e., a station or grid box) considering the AM starting hour (UTC-5).

Since the day time was not available for the DMPD network, such analysis was not performed for stations or years with only DMPD records. Some problems related to the coarse measurement resolution of the tipping-bucket gauges recording 15PD and HPD series were also observed. Since their typical tip resolution (i.e. the minimum recorded non-zero value) is 2.54 *mm* (i.e. 1/10 *in*), only a few distinct rainfall depth values can be recorded at these stations at their native temporal resolution d_0 (15min or 1h) [NOAA *data online documentation*; Innocenti et al. 2017]. This results in numerous ties in recorder series and therefore many occurrences of the same AM values for some specific years, making therefore impossible to uniquely identify the date of AM occurrences for those years. Some preliminary analyses showed that the numbers of ties in AM series are important for 15PD and HPD stations for duration $d \leq 6h$ [see Fig. S9 of the Supplementary material]. To cope with this issue, date and time of all AM ties were also extracted and included in AM occurrence analysis.

2.4 Statistical characterization of AM series

Let $X = (x_1, x_2, \dots, x_n)$ represent the series of AM precipitation depths [*mm*] at the spatiotemporal scale (r, d) for a generic location, namely a station or grid box. AM probability distributions were estimated for each X through the empirical cumulative distribution function (cdf) $\hat{F}(x)$ [Hazen plotting position; Cunnane 1978]. The X quantiles \hat{x}_q were then computed from $\hat{F}(x)$ for all AM series with $n > 1.2q$ observations, where $q = (1 - p)^{-1}$ is the return period [yr] and $p = \hat{F}(x_q) \geq 0.5$ (i.e., $q \geq 2$ yr). Specifically, only return periods $q \leq 10$ yr were considered for the shortest available series (13-yr WRF and 18-yr CMORPH series). For instance, only moderate extremes of return period equal or less than 10 years ($p \leq 0.9$) were computed for WRF series. Similarly, stations with AM series shorter than 1.2 q years were not considered for estimating the q -yr quantiles \hat{x}_q .

2.4.1 Annual and daily cycles

Many different approaches have been proposed in the literature to estimate the annual and daily

precipitation cycles [e.g., Dai et al. 1999; Cortes-Hernandez et al. 2016]. In the present study, the annual cycle has been assessed at each location through the relative monthly frequencies, f_m , of AM occurrences. Each f_m value was estimated by adding the number of hours that each AM belonged to month m . If a given AM overlapped two consecutive months, the total AM duration, d , was split between these two months.

Similarly, the relative hourly frequencies, f_h , $h = 0, 1, 2, \dots, 23$, of AM occurrences were used to evaluate the daily cycles for durations $1 < d < 24h$. Each AM of duration d contributed to the frequencies of exactly d hourly bins of the 24h histogram and was split if overlapping two consecutive days.

2.4.2 Spatial and temporal scaling

The temporal scaling of AM was evaluated considering the changes of AM quantiles with the duration and estimated through the following regressions:

$$\ln(\hat{x}_{r,d}) = \alpha_r + \beta_r \ln(d), \quad (2.1)$$

where $\hat{x}_{r,d}$ represents the q -yr quantile estimated at the spatiotemporal scale (r, d) , and the index r for α_r and β_r indicates that the model was estimated for each spatial scale $r = r_0, r_1, \dots, r_K$. For simplicity, the index q has been omitted from Eq.(2.1) and in the rest of the paper. The Theil-Sen estimator [Sen 1968] was used to estimate regression parameters since more appropriate for small samples [e.g., O-Gorman 2015; Barbero et al. 2017].

The K temporal scaling slopes β_r represent the average relative change of $\hat{x}_{r,d}$ for a relative change in duration, while the intercept α_r represents an

estimate of $\ln(\hat{x}_{r,1h})$. Hence, small β_r correspond to similar AM distributions over different durations, while β_r close to 1 imply larger variations in depth quantiles as the duration is changed. Also, for each quantile order, station β_0 estimates correspond to the slopes of the Depth-Duration-Frequency (DDF) curves [Burlando and Rosso 1996; Koutsoyiannis et al. 1998], and β_r are analogous to the simple scaling exponents $\beta_r^{int} = \beta_r - 1$ that have been widely used for describing the temporal scaling of AM precipitation intensity distributions [e.g., Menabde et al. 1999; Blanchet et al. 2016 for point-scale precipitation; Cannon and Innocenti 2018 for gridded dataset estimates].

Previous studies showed that temporal scaling estimations convey synthetic climatological information about extreme precipitation and geographical and climatological features of the study region [e.g., Ceresetti et al. 2010; Innocenti et al. 2017; Casas-Castillo et al. 2018]. Moreover, some studies highlighted that different weather regimes typically lead to distinctive scaling exponent values for short (e.g., hourly and sub-hourly) and daily and longer durations [e.g., Borga et al. 2005; Eggert et al. 2015]. Preliminary analysis suggested the existence of two scaling regimes for the available datasets [see Fig. S14 in the Supplementary material], although the duration at which the scaling regime changes may depend on the location. Therefore, durations $1h \leq d < 6h$, hereinafter *Short Durations (SD)*, and $6h \leq d \leq 72$, hereinafter *Long Durations (LD)* were analyzed separately. Only LD estimation was considered for MSWEP, since only one duration ($d = 3h$) was available for SD.

Results presented in Sec. 2.7 also suggest that regional averages of β_r values vary linearly with the spatial scale r . To evaluate the validity of this linear approximation at the local scale, the fol-

lowing *Spatio-temporal Scaling (STS)* model was considered at each grid box:

$$\beta_r = h_0 + h_1 r. \quad (2.2)$$

The intercept h_0 represents the temporal scaling slope extrapolated at the station scale (i.e., $r = 0$) from available coarser spatial scales $r = r_0, r_1, \dots, r_K$, while h_1 expresses the average change of β_r associated with a unit spatial scale change (i.e., $1km$). Combining Eq.(2.2) and Eq.(2.1), the q -yr quantile at the spatiotemporal scale (r, d) can be expressed as:

$$\ln(\hat{x}_{r,d}) = \ln(\hat{x}_{r,1h}) + (h_0 + h_1 r) \ln(d). \quad (2.3)$$

Considering that Eq.(2.3) reduces to $\ln(\hat{x}_{0,d}) = \ln(\hat{x}_{0,1h}) + h_0 \ln(d)$ for $r = 0$, a straightforward expression for the spatiotemporal scaling of AM quantiles emerges when writing the difference $\ln(\hat{x}_{r,d}) - \ln(\hat{x}_{0,d})$ as:

$$\ln\left(\frac{\hat{x}_{r,d}}{\hat{x}_{0,d}}\right) = \ln\left(\frac{\hat{x}_{r,1h}}{\hat{x}_{0,1h}}\right) + h_1 r \ln(d) \quad (2.4)$$

The ratios $\left(\frac{\hat{x}_{r,d}}{\hat{x}_{0,d}}\right)$ and $\left(\frac{\hat{x}_{r,1h}}{\hat{x}_{0,1h}}\right)$ between areal and point rainfall quantiles are referred to as Areal Reduction Factors (ARF) [e.g., Sivapalan and Blöschl 1998; Svensson and Jones 2010] for durations d and $1h$. According to Eq.(2.4), h_1 thus represents the variation of quantile ARFs corresponding to changes in the spatiotemporal scale (r, d) with respect to the hourly ARF and may be possibly used to extrapolate the ARF beyond the empirically available range of r and d .

In previous studies, ARF values were found to vary with the geo-climatic characteristics of the region under study [e.g., Omolayo

1993; Asquith and Famiglietti 2000], the season [e.g., Allen and DeGaetano 2005], and in some specific cases with the return period [e.g., Asquith and Famiglietti 2000; Allen and DeGaetano 2005]. These results were attributed to the different spatial correlation structures of precipitation characterized by different weather regimes. For similar reasons, the ARF are expected to increase with duration d [e.g., NERC 1975; Mineo et al. 2018]. Some authors noted that the characteristics of the precipitation datasets (e.g., the density of the recording network or series length) and the methods used for extracting the extremes strongly affect ARF properties and their dependence on d [Kursinski and Zeng 2006; Svensson and Jones 2010]. It is thus crucial to assess the validity of Eq. (2.2)-(2.4) for a wide range of spatiotemporal scales and for various datasets.

The statistical significance of the h_0 and h_1 parameters [Eq.(2.2)] was tested though a linear regression permutation test [Anderson and Robinson 2001]. This test considers the null hypothesis $\mathbf{H}_0 : h_1 = 0$, under which all the $K!$ random pairs of the linear model response, β_r , and the predictor, r , are equally probable. The distribution of the STS model parameters under \mathbf{H}_0 can be thus simulated by repeating the estimation of Eq. (2.2) for a large number of permutations of β_r while r is fixed to the original values r_0, r_1, \dots, r_K . For CRCM5 and MSWEP, all the available $K! = 720$ permutations were used, while for WRF and CMORPH a subset of 1000 random permutations was considered. Since h_1 values were expected to be positive according to some preliminary results [see Sect. 2.7], the one-tailed alternative hypothesis $\mathbf{H}_1 : h_1 > 0$ was used.

2.5 Evaluating dataset performances

Two major issues must be considered when assessing climate model performance: the spatiotemporal resolution mismatch between observed and simulated series [Chen and Dai 2017] and the choice of adequate performance metrics [e.g., Chardon et al. 2016; Herold et al. 2017]. For instance, classical point-to-grid comparison of RCMs against stations makes it difficult to separate the relative contributions of spatial mismatch and structural model error, while averaging the performance metrics over coarse resolution grids may smooth local effects [Tapiador et al. 2017]. Therefore, the use of native grids for both observational and simulated datasets may be justified for local comparison at sub-daily scales [Diaconescu et al. 2016; Lucas-Picher et al. 2017].

The analysis was thus carried out in two steps.

i) Comparison of grid box and station AM characteristics at native resolution: the reanalysis driven CRCM5 simulation was first compared to the other datasets, except CRCM5-LE. Series covering the period 1940-2016 were considered [black rectangle in Fig.2.2a]. Each station was associated to the nearest grid box or discarded if their distance was larger than $\sqrt{2}r$. The selected grid box-station pairs are hereinafter identified by the station coordinates [lat-lon] and referred to as *L1* locations.

ii) AM spatiotemporal scaling for gridded datasets: Spatio-temporal scaling models were estimated and validated at each grid box for all gridded datasets, including CRCM5-LE. To this end, each grid box at native resolution r_0 was associated to the overlapping grid boxes at each

coarser spatial scale r_k . Also, CRCM5-LE estimates over the 1980-2015 period [gray rectangle in Fig. 2.2a] were considered and compared to ERA-CRCM5 over the entire spatial domain.

Gridded dataset performances were first assessed comparing point and areal estimates of AM quantiles using the following relative difference:

$$B_d(\hat{x}) = \frac{\hat{x}_s - \hat{x}_g}{\hat{x}_s} \quad (2.5)$$

where \hat{x}_s and \hat{x}_g represent the q-yr return period quantiles estimated, respectively, at station s and its nearest grid box g for any relevant duration d . For readability, r_0 , q , and d indexes have been omitted for \hat{x}_s and \hat{x}_g and no location index is used for $B_d(\hat{x})$ and all following metrics. $B_d(\hat{x})$ is hereinafter referred to as *quantile relative bias*, although non-zero $B_d(\hat{x})$ values may be attributed to model biases, as well as to *representativeness errors*, namely errors that derive from the temporal and/or spatial resolution mismatch [Tustison et al. 2001].

A permutation test was used to estimate the statistical significance of quantile biases [Good 2013]. The null hypothesis of the permutation test assumed the equality of the station and grid box distributions of X , i.e. $\mathbf{H}_0 : \hat{F}_s(x) = \hat{F}_g(x) \forall x \in \mathbb{R}^+$, which also implies the equality of quantiles for each return period: $\mathbf{H}_0 : \hat{x}_s = \hat{x}_g$. To construct the $B_d(\hat{x})$ distributions under \mathbf{H}_0 , 5000 iterations were used for each station-grid box pair.

Station and gridded dataset annual cycles of AM were compared using the *Perkins Skill Score* (PSS) [Perkins et al. 2007], defined at each loca-

tion as:

$$S_M = \sum_{m=1}^{12} \min\{f_{m,s}, f_{m,g}\} \quad (2.6)$$

with $f_{m,s}$ and $f_{m,g}$ corresponding, respectively, to the relative frequency of AM occurrences at station s and at the corresponding grid box g for month m . Eq.(2.6) therefore measures the common area between the two cycles and $S_M = 1$ corresponds to a perfect match between monthly frequencies $f_{m,s}$ and $f_{m,g}$, while a value of S_M close to 0 means small overlapping between $f_{m,s}$ and $f_{m,g}$ curves.

The PSS was then adapted to measure the overlap between station and gridded dataset daily cycles:

$$S_H = \sum_{h=0}^{23} \min\{f_{h,s}, f_{h,g}\} \quad (2.7)$$

where $f_{h,s}$ and $f_{h,g}$ are the relative hourly frequency of AM occurrences at station s and corresponding grid box g .

2.6 Gridded dataset and station AM statistics at native resolution

The spatial distributions of AM quantiles were consistent across the datasets, with important SW-NE gradients across the study domain [see Fig. S1-S5 in the Supplementary material for some examples]. Local effects were observed for longer durations around the Great Lakes and the northern Atlantic coast for the two RCMs, while clusters of spuriously high AM values were observed in the northern areas for CMORPH.

2.6.1 Relative differences in AM quantiles

Figure 2.3 a-d shows, for each duration (x-axis), the distributions over $L1$ locations of the relative bias, $B_d(\hat{x})$, between station and gridded dataset AM quantiles at their native resolution. For each return period, $B_d(\hat{x})$ distributions generally moved from the positive to negative half-plane when increasing d from $1h$ to longer durations. This means that gridded datasets underestimate station quantiles for the shortest durations, whereas they generally overestimated station rainfall extremes for temporal scales longer than few hours.

ERA-CRCM5 (and WRF) showed good agreement with stations for $d = 1h$ with $|B_{1h}(\hat{x})| \leq 0.05$ for more than 50% (53%) of $L1$ locations for $q = 2yr$ [Fig. 2.3a-b, 1st col.]. As showed by the solid black line in Fig. 2.3a, the ERA-CRCM5 median relative underestimation of station quantiles is between 10% and 20% for $d \geq 3h$ for all return periods. Conversely, beside a large spread across positive and negative values, the median of the WRF $B_d(\hat{x})$ distribution is close to zero for all durations and return periods. Also, while WRF biases were statistically significant for a small fraction of $L1$ locations ($f_{H_1} \leq 0.18$ for all d and q), corresponding fractions are much more important for ERA-CRCM5 ($0.14 \leq f_{H_1} < 0.65$ for $q = 2yr$ and $0.05 < f_{H_1} < 0.38$ for $q \geq 10yr$), with the highest f_{H_1} values at daily and longer durations.

CMORPH and MSWEP biases were important for durations close to their temporal resolution but rapidly decrease as d increases, being approximately centered around zero for long durations and smaller than model biases for $d \geq 12h$ [Fig. 2.3c and d]. Median $B_d(\hat{x})$ curves showed impor-

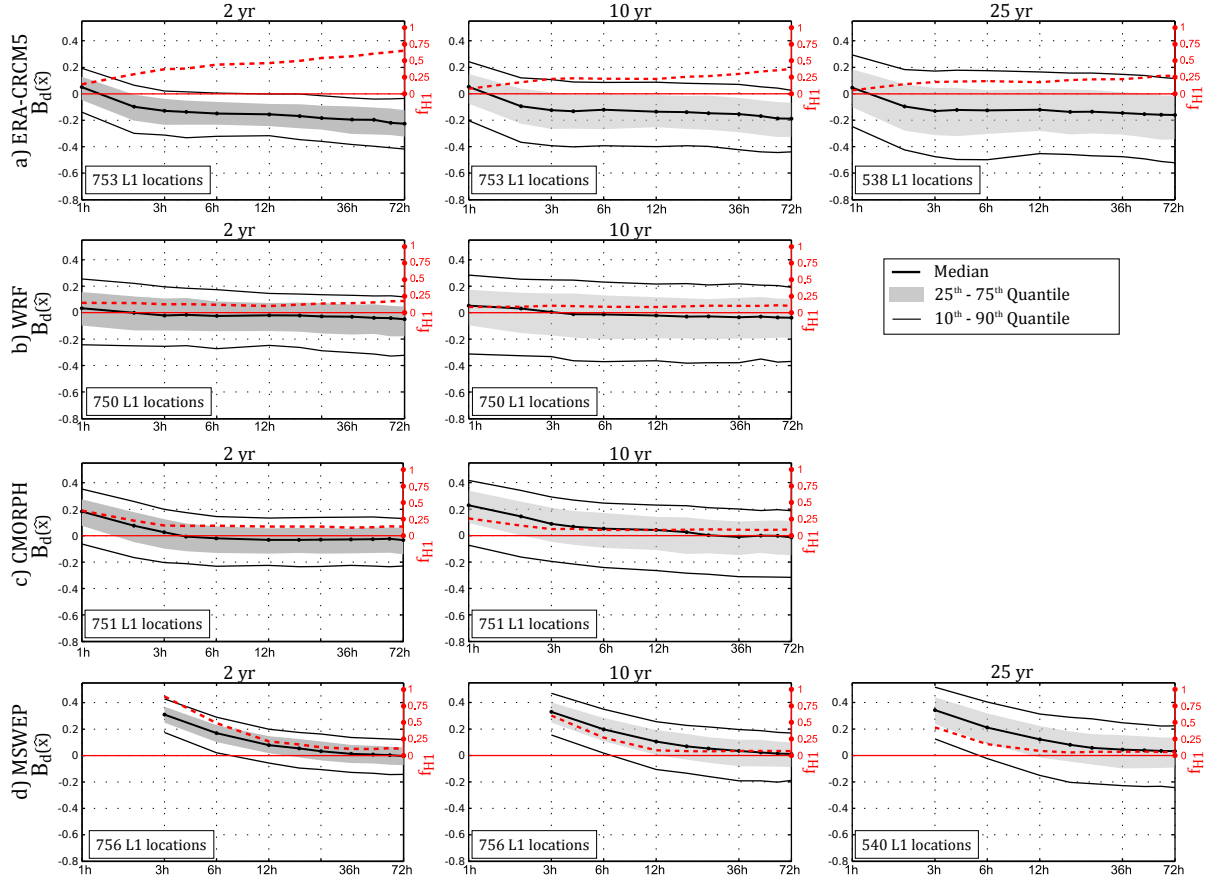


Figure 2.3: Distribution over $L1$ locations of the relative differences, $B_d(\hat{x})$, between station and grid box 2-yr (1st col), 10-yr (2nd col), and 25-yr (3rd col) AM quantiles estimated at the native dataset resolution for: a) ERA-CRCM5; b) WRF; c) CMORPH; and d) MSWEP. The red dashed curves (y-axis on the right) corresponds to the fractions, f_{H_1} , of $L1$ locations with statistically significant bias [i.e. station-grid box pairs rejecting the null hypothesis $H_0 : B_d(\hat{x}) = 0$]. The total number of $L1$ locations available in each case is indicated at the bottom-left corner of each panel.

tant CMORPH underestimations at the hourly scale with $B_d(\hat{x}) \geq 0.2$ for more than 50% of $L1$ locations and both periods.

Compared to the other gridded datasets, MSWEP displayed the highest relative underestimations of AM quantiles for $d \leq 6h$ while at daily and longer durations it presented the smallest bias and the lowest f_{H_1} fractions [Fig. 2.3d].

Fig. 2.4 displays the spatial distributions of $B_d(\hat{x})$ values estimated for the return period $q = 10yr$ and $d = 1, 3,$ and $24h$. Positive significant biases were found in the southern and western areas for the two models for $d \leq 3h$ [Fig. 2.4a-b]. For

ERA-CRCM5, in particular, negative $B_d(\hat{x})$ values are concentrated in eastern and central areas for $d = 1h$ and gradually extended to the rest of the domain as d approaches $24h$ [Fig. 2.4a]. Conversely, beside presenting a small number of locations with significant biases for $d \geq 3h$, WRF and CMORPH displayed a clear regional structure with differences between west ($B_d(\hat{x}) > 0$ values) and north-east areas, where the $B_d(\hat{x})$ are negative and generally significant [Fig. 2.4b-c]. For $d_0 = 3h$, MSWEP biases are positive throughout the entire domain, while at the the daily scale a small number of $L1$ locations displayed the east-west pattern already observed for

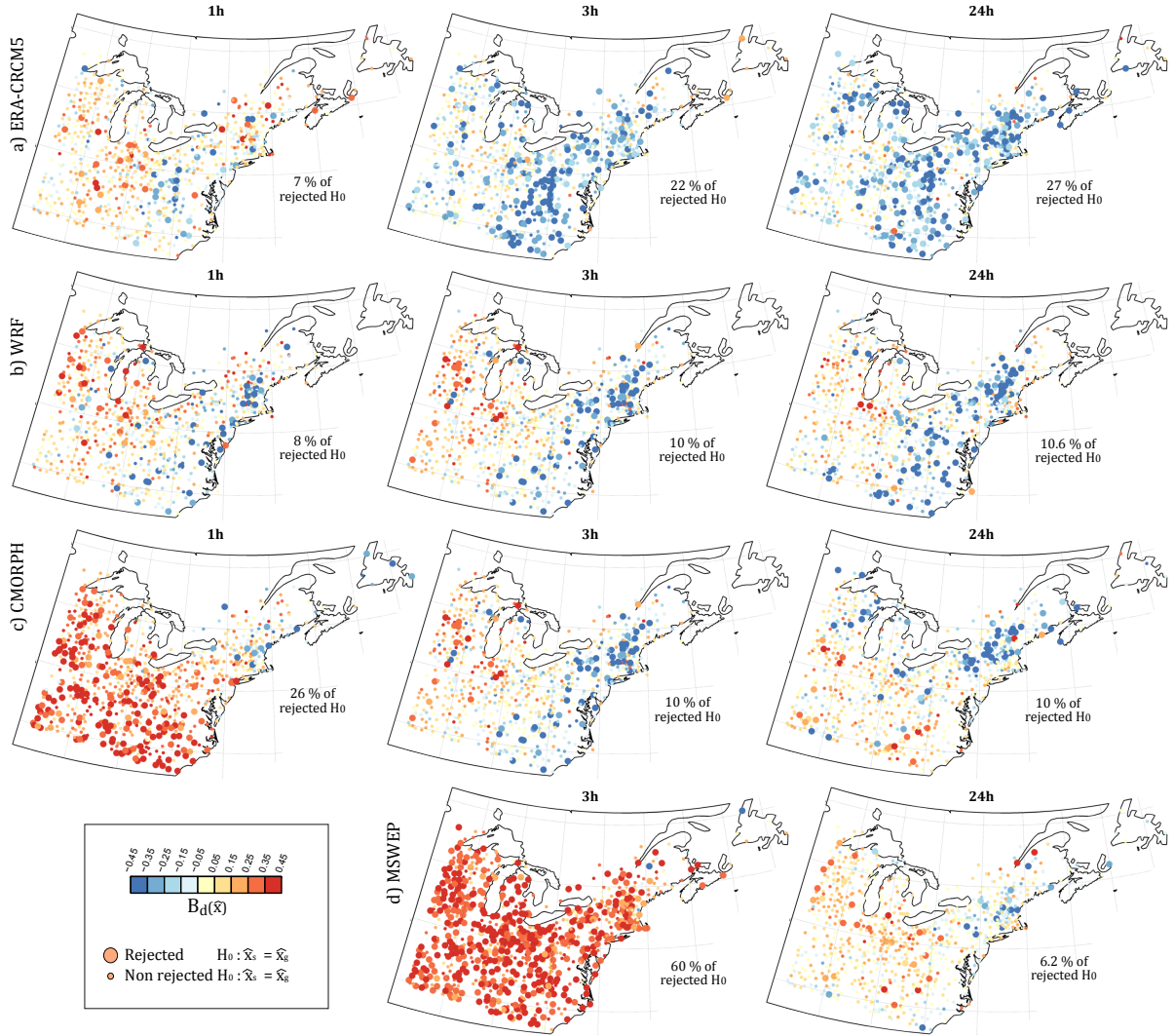


Figure 2.4: Spatial distribution over $L1$ locations of the relative bias, $B_d(\hat{x})$, between station and grid box 10-yr AM quantiles at native dataset resolution for: a) ERA-CRCM5; b) WRF; c) CMORPH; and d) MSWEP. Smaller points represent locations with no statistically significant bias (i.e. station-grid box pairs that did not reject the null hypothesis $H_0 : B_d(\hat{x}) = 0$ at the 0.05 significance level). Percentages of $L1$ locations with significant relative bias are indicated at the bottom right corner of each panel.

the other datasets.

Similar results were found for 2-yr and 25-yr AM quantiles [e.g., Supplementary material, Fig. S6-S7] and coarser spatial scales. Moreover, using aggregated measure of gridded dataset performances over all $L1$ location [e.g., normalized *Root Mean Squared Error*, *RMSE* between station and grid box quantiles; Fig. S8 in Supplementary material], ERA-CRCM5 generally outperformed

the other datasets at d_0 , while the lowest aggregated errors were found for WRF for durations $3h \leq d \leq 6h$ and for MSWEP for $d \geq 12h$.

2.6.2 Annual and daily cycles

Figure 2.5 compares station and gridded dataset annual and daily cycles. Station AM annual cycles were well reproduced by the two RCMs,

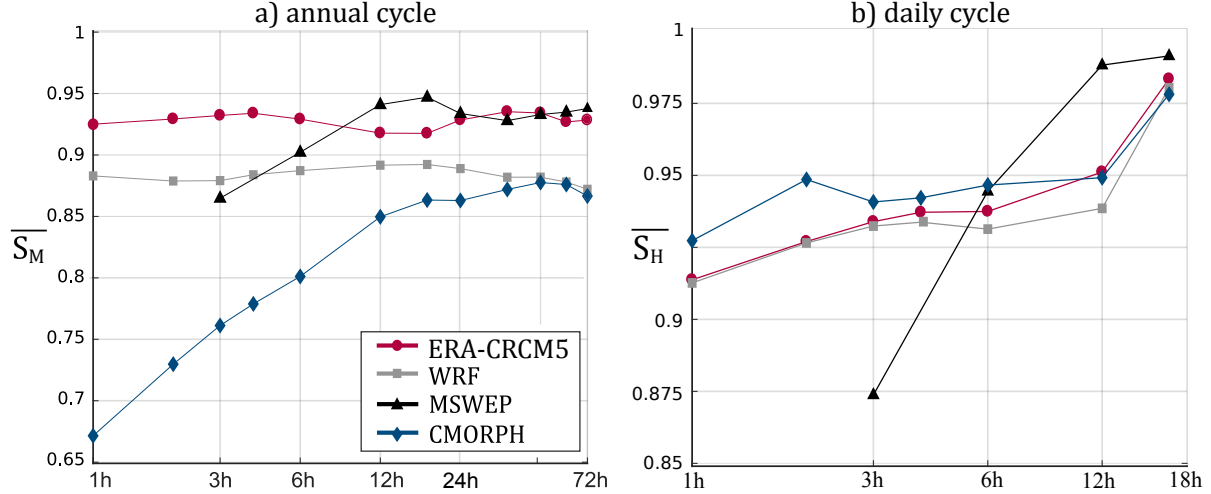


Figure 2.5: PSS between station and gridded dataset for a) annual cycles averaged over $L1$ locations, \overline{S}_M , and b) daily cycles averaged over $L1$ locations, \overline{S}_H .

with ERA-CRCM5 displaying the smallest differences with stations (i.e., highest \overline{S}_M values) for $d \leq 6h$ [Fig. 2.5a]. For longer durations, the two RCMs slightly underestimated winter AM frequencies while WRF anticipated station AM summer peak for short durations [some f_m examples are showed in Fig. S10 of the Supplementary material]. Low \overline{S}_M CMORPH values durations were due to the too high AM frequencies during winter and fall and the consequent underestimation of AM occurrence frequency during summer. This result is consistent with reported CMORPH biases and uncertainties in cold conditions [Trenberth et al. 2017]. MSWEP adequately reproduced station annual cycles, resulting in highest \overline{S}_M for $6h < d \leq 24$ and very good performance at daily and longer durations.

As showed by Fig. 2.5b, the two RCMs well reproduced observed daily cycles, with ERA-CRCM5 and WRF displaying comparable performance for all durations. It has to be noted, however, that hourly AM frequencies presented later peaks compared to stations, namely between 18:00 and 19:00 (17:00 and 18:00) for ERA-CRCM5 (WRF). Conversely, as duration increases, station daily cycles

became generally flatter, and AM more frequently occurred between midnight and 10:00 than in simulated series. ERA-CRCM5 and WRF AM occurrences, instead, clustered around late afternoon and early night values [e.g., Fig. S11a-b in the Supplementary material].

For MSWEP the coarse temporal resolution of this dataset ($d_0 = 3h$) prevented any definite of its daily cycle, which displayed a 2:00 am peak but was globally flat (not shown). While CMORPH slightly outperformed the other datasets for $d \leq 4h$ in terms of \overline{S}_H , it also displayed noisy daily cycle estimates [e.g., Fig. S11d of the Supplementary material].

2.7 Spatio-temporal scaling of AM rainfall

Figure 2.6 presents for each return period and dataset the slopes $\beta_{r,1}$ estimated through Eq. (2.1) for $1h \leq d < 6h$ (SD) and $6h \leq d \leq 72h$ (LD).

As expected, the temporal scaling was weaker for

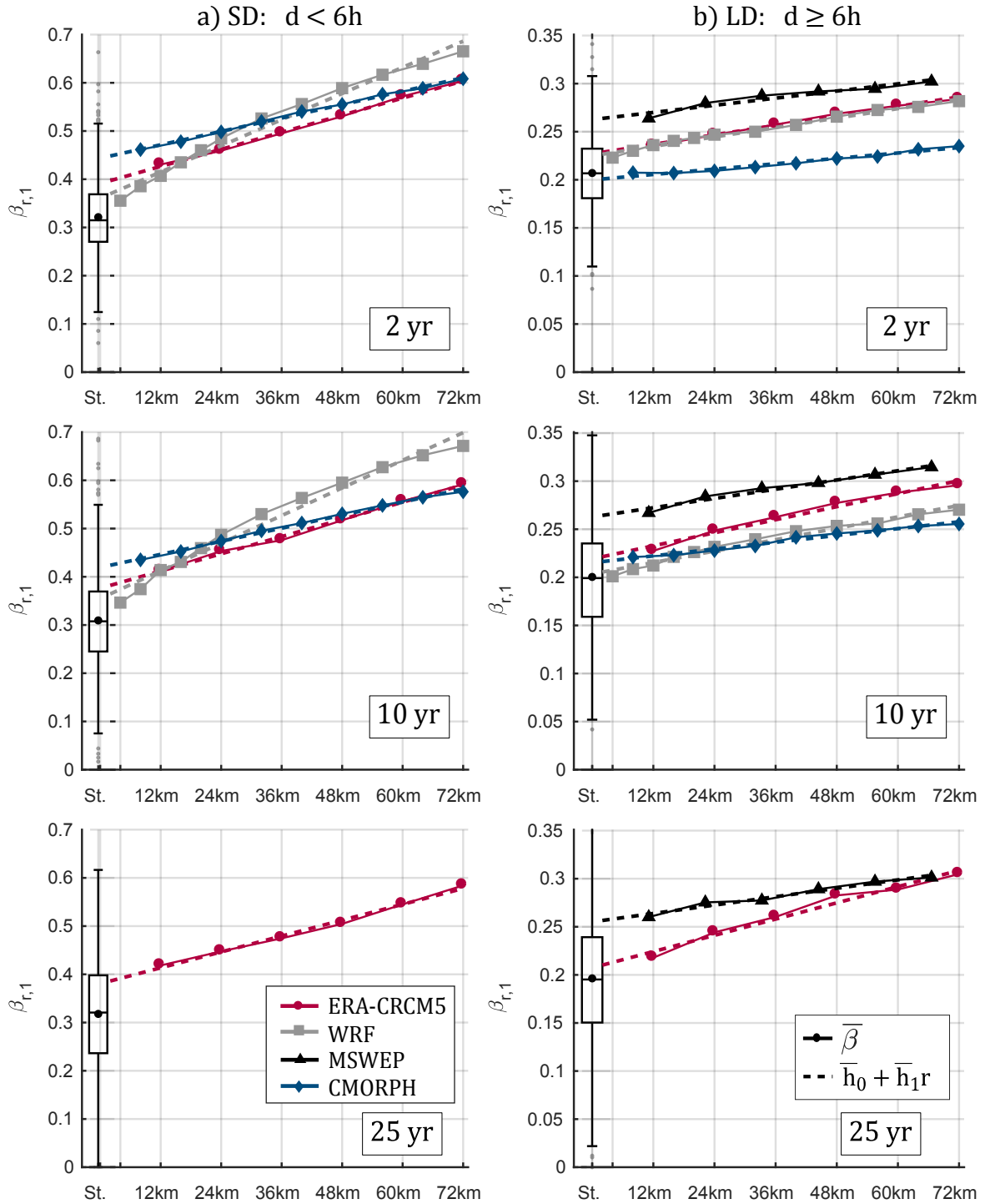


Figure 2.6: Mean temporal scaling slopes over L1-locations, $\bar{\beta}_r$, for 2- (first line), 10- (second line), and 25-yr (third line) AM quantiles as a function of the spatial scale (x-axis) for SD ($1h \leq d < 6h$; left column) and LD ($6h \leq d \leq 72h$; right column). Boxplots show the distribution of β_0 station values. Dotted lines represent the linear fit of $\bar{\beta}_r$ with spatial scales r . For readability reason some whiskers of station box plots are not displayed.

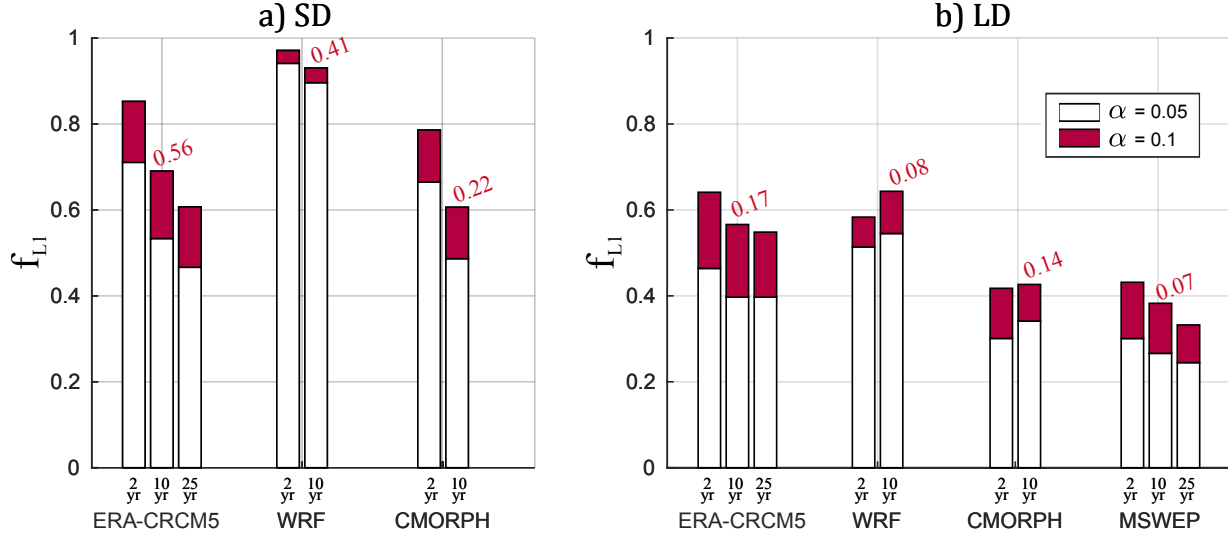


Figure 2.7: Permutation test for Eq.(2.2): fraction, f_{L_1} , of L_1 locations with statistically significant h_1 for each dataset and return period for a) SD and b) LD. Red numbers represent the fraction of L_1 locations with coefficient of determination $R^2 > 0.75$ for Eq.(2.2) estimated for 10-yr return period quantiles.

LD than SD extremes, and more dispersed station β_0 distributions were observed for SD compared to LD. Also, the scaling slope values generally increased with r , and these increases were more important for SD than LD extremes. In particular, gridded datasets showed stronger temporal scaling than stations but the differences between areal and point-scale scaling slopes were more pronounced for SD [Fig. 2.6a]. For LD, $\overline{\beta_{r_0}}$ values were generally within the station interquartile ranges [Fig. 2.6b]. As an exception, MSWEP displayed high LD scaling slopes, with $\overline{\beta_r} > 0.26$ for all r and return periods, possibly due to its coarse temporal resolution. These results are consistent with the smoothing of short duration AM expected as the spatial scale increases. Since SD extremes are more likely associated to localized convective events, changes in AM depth corresponding to duration changes are more pronounced for coarser spatial scales, which results in larger β_r values as r increases. Also, WRF displayed larger $\overline{\beta_r}$ increases with r than ERA-CRCM5 and CMORPH for SD [Fig. 2.6a],

while the differences between WRF and the other datasets are less pronounced for LD [Fig. 2.6b]. These results could be explained by the fine native resolution of WRF, which is expected to have an impact on fine scale SD AM and/or more extreme events.

Interestingly, the increase of the temporal scaling slopes with the spatial scale is nearly linear, as outlined by the good fit of the $\overline{\beta_r} = \overline{h_0} + \overline{h_1}r$ lines [dotted lines in Fig. 2.6] to mean scaling slope values.

To further investigate the linearity of the temporal scaling slopes on r , the β_r estimated at each L_1 location were linearly regressed on the spatial scale according to Eq. (2.2). The validity of this STS relationship was then assessed with a permutation test. Figure 2.7 presents for each dataset the fraction, f_{L_1} , of L_1 locations having significant h_1 for common significance levels (i.e., $\alpha = 0.05$ and $\alpha = 0.1$). Also, as an example of regression fit evaluation, the fractions of L_1 locations with linear coefficient of determination, R^2 ,

higher than 0.75 is reported in Fig. 2.7 (red numbers) for 10-yr quantiles.

For the two RCMs, SD h_1 parameters were significantly different from 0 for most $L1$ locations [Fig. 2.7a]. For instance, $f_{L1} \geq 90$ for WRF at the 0.05 confidence level for all return periods, which could likely be attributed to the fine WRF spatial resolution and to the large number of spatial scales available for estimating Eq. (2.2). However, larger uncertainty is associated with the spatiotemporal LD scaling estimation, resulting in lower f_{L1} values for both ERA-CRCM5 and WRF compared to SD. This is also confirmed by the fact that only a few $L1$ locations revealed $R^2 > 0.75$ for the estimation of Eq.(2.2), suggesting poor linear fit of the spatiotemporal model for LD.

CMORPH and MSWEP showed lower fractions of significant h_1 parameters than RCMs. For LD, in particular, most of $L1$ locations rejected the use of the STS model at typical significance levels, suggesting that little information can be inferred from the use of multiple spatial scales for approximating point-scale DDF curves. A possible explanation is that both CMORPH and MSWEP used post-processing methods that involve the computation of rainfall statistics and the adjustment of the corresponding series at several space and time aggregations [Xie et al. 2017; Beck et al. 2017a]. For instance, CMORPH bias correction was applied in various steps at the $(0.25^\circ, 24h)$ and coarser resolutions through correction coefficients computed on neighboring grid boxes [Xie et al. 2017]. Similarly, the merging of multiple data sources for MSWEP necessarily involved combining data at different spatiotemporal resolutions.

As expected, longer return period quantiles generally had smaller f_{L1} values than 2-yr AM. These differences between return periods are particularly obvious for SD [Fig. 2.7a], since the extreme

estimation is, in this case, more strongly impacted by native resolution and the series length.

2.8 AM statistics for the CRCM5-LE

The proposed STS model was evaluated using the CRCM5-LE, considering ensemble mean temporal scaling slopes. The impact of lateral boundary conditions was also investigated through the comparison of ERA-CRCM5 and CRCM5-LE estimates. The main conclusions of this analysis are summarized in Tab. 2.3.

2.8.1 CRCM5-LE spatiotemporal scaling

The estimation of β_r was first carried out for each member and spatial scale r . The ensemble mean of β_r parameters was then computed for sub-groups of 5, 10, and 50 members and then used to estimate h_0 and h_1 . Sub-groups of 5 (10) members were constructed considering members 1-5, 5-10, ..., 45-50 (1-9, 10-19, ... 41-50).

Figure 2.8 shows the permutation test results for the STS regressions estimated for the first member, all members, and for the first 5- and 10-member sub-groups. The fraction of grid boxes with significant h_1 increased with the number of members, showing that local estimation uncertainty was considerably reduced by averaging β_r over various members before applying Eq. (2.2), especially for SD and high return periods. For instance, STS parameters were significant for less than 50% (40%) of grid boxes for SD (LD) when only the first member was considered for

Table 2.3: Main results of the comparison between between ERA-CRCM5 and CRCM5-LE.

| Statistics | Main results |
|------------------|---|
| Quantiles | Important latitudinal gradient for the relative differences of the estimates: CRCM5-LE quantiles are smaller (larger) than ERA-CRCM5 in the south (north-east). Similar spatial distributions for all d [e.g., Fig. S15 of the Supplementary material] |
| Annual cycle | More AM ERA-CRCM5 occur in summer compared to CRCM5-LE for $d \leq 24h$; for $d > 24h$, CRCM5-LE simulated more AM than ERA-CRCM5 from November to May. Results varies according to the geographical region [e.g., Fig. S16 of the Supplementary material]. |
| Daily cycle | Minor differences. |
| Temporal scaling | Minor differences for SD. CRCM5-LE showed weaker scaling regimes than ERA-CRCM5 for LD. |

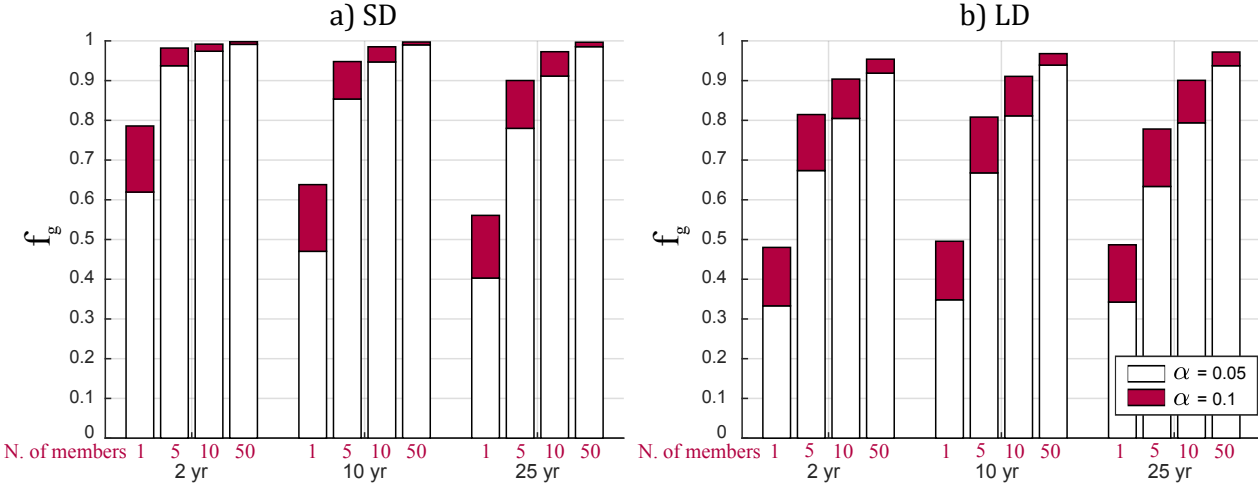


Figure 2.8: Permutation test for Eq.(2.2) for sub-groups of CRCM5-LE members: fraction, f_g , of grid boxes with significant h_1 for each return period for a) SD and b) LD.

$q = 10yr$, while more than 90% of grid boxes had significant h_1 when using 50 members for both SD and LD [Fig. 2.8a-d]. Also, more than 94% (74%) of grid boxes had coefficient of determination $R^2 > 0.9$ for the 50-member estimation of Eq.(2.3) for SD (LD) and all return periods (not shown).

Interesting spatial patterns can be observed for h_0 and h_1 when the 50-member CRCM5 ensemble is considered [Fig. 2.9]. For SD, lower h_0

values were observed for the interior of the domain and east of Great Lakes, while the highest scaling regimes (e.g., $h_0 \geq 0.45$) were observed at the southern and northern borders [Fig. 2.9a]. Similar patterns were found for LD, with strong scaling regimes in south-west and north-east regions [Fig.2.9b]. Very small h_0 values were also estimated in the north-west, between the Great Lakes and the south coast of the Hudson Bay. Similar spatial patterns for stations h_0 values were found by Innocenti et al. (2017) in an extensive

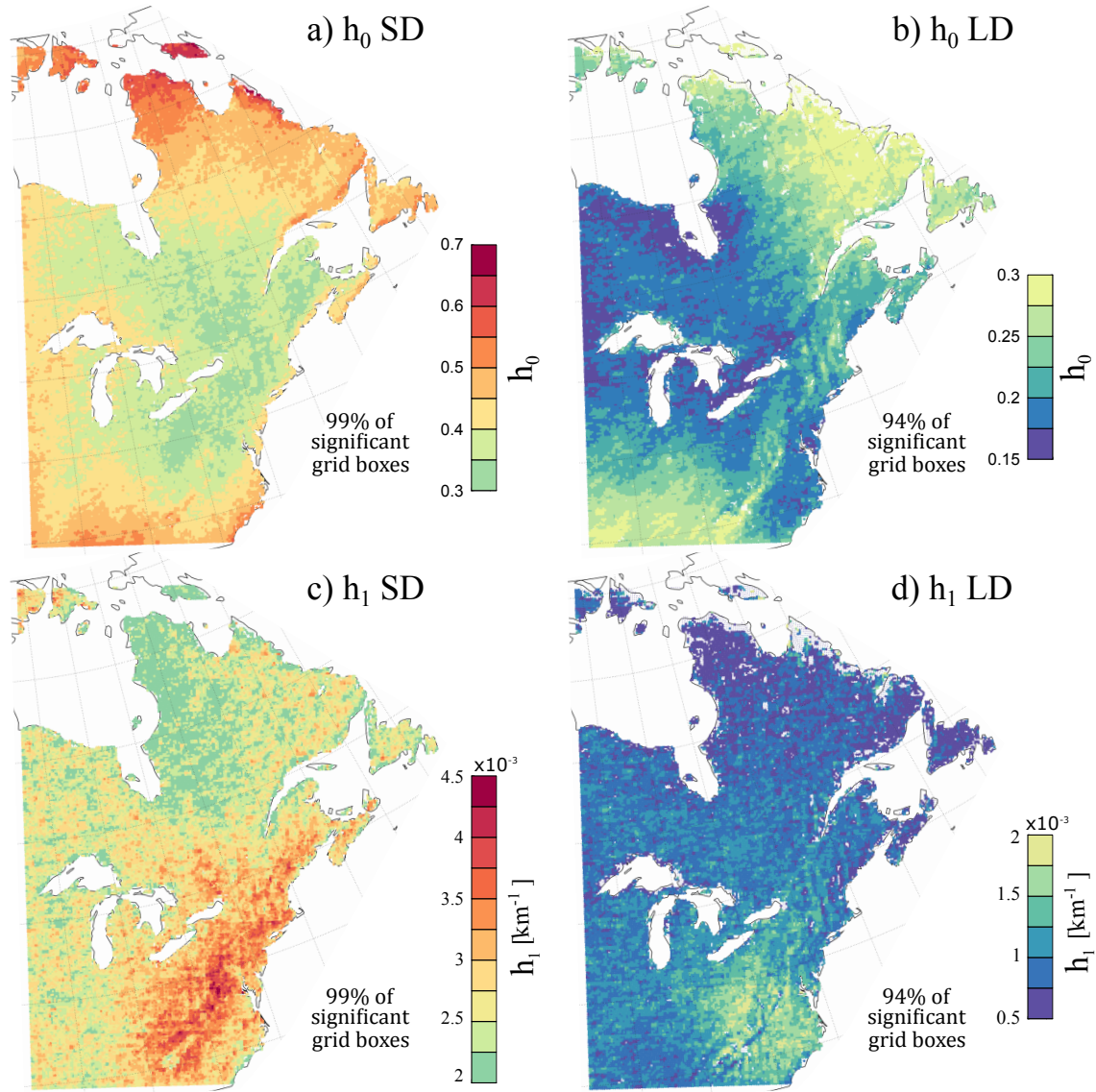


Figure 2.9: Spatial distribution of the spatiotemporal scaling parameters for the 10-yr AM quantiles estimated using the 50 CRCM5-LE members: a) h_0 for SD; b) h_0 for LD; c) h_1 for SD; and d) h_1 for LD. Only grid-boxes with statistically significant spatiotemporal scaling model (0.05 confidence level) are displayed.

study of rainfall intensity scaling exponents over North America.

Important NW to SE gradients were observed for h_1 values, with the highest values found over the Appalachian Mountains, especially for SD [Fig. 2.9c]. This indicates that AM temporal scaling slopes in southern regions are more sensitive to changes in the spatial scale than in northern areas,

or, equivalently, that ARFs vary more strongly with the spatiotemporal scale (r, d) [see Eq.(2.4)]. One possible explanation for these patterns is that the characteristics and the spatial extent of weather systems producing short duration extremes vary with latitude. Conversely, relatively larger spatial extent is expected for weather systems generating LD extremes, as well as weaker changes in weather systems characteristics over

the CRCM5 spatial domain. This would also explain smoother latitudinal gradients and weaker response to topography observed for LD h_1 values.

For h_1 , the differences between western regions and the south-east portion of the domain could also be related to the large-scale circulation patterns which strongly affect the spatiotemporal structure of precipitation extremes in these areas [Touma et al. 2018].

As a final note, although the dependence of h_0 and h_1 on return period should be further investigated, preliminary analysis showed differences between STS parameters for $q = 2yr, 10yr,$ and $25yr$ in some regions. In particular, in areas where both spatiotemporal parameters are small, h_0 and h_1 were found to slightly decrease with increasing return period [see Fig. S17-S18 of the Supplementary material].

2.9 Summary and conclusion

Characterizing the spatiotemporal structure of extreme precipitation is important for many hydrological applications and the development of future projections of extreme precipitation. Before any projection analysis, it is however crucial to evaluate the ability of RCMs to simulate sub-daily and daily precipitation characteristics. Accordingly, the primary objective of the presented analysis was to compare the statistical properties of observed and simulated AM precipitation for various spatial scales and durations ranging from 1 h to 3 days.

Two ERA-Interim driven simulations, one from the CRCM5 (ERA-CRCM5) and one from the convection-permitting WRF model, were evalu-

ated against observational records in terms of extreme precipitation quantiles, their diurnal and seasonal cycles, and considering the spatiotemporal temporal scaling of sub-daily and daily AM. The performances of the bias-corrected satellite CMORPH dataset and the multi-source MSWEP dataset were also considered.

At their native spatial resolution, both ERA-CRCM5 and WRF showed good agreement with stations for short duration AM quantiles and all considered return periods. Few significant biases were observed at stations located in the eastern part of the domain. For daily and longer durations, ERA-CRCM5 significantly overestimated AM quantiles at many stations.

Small differences were observed between station and ERA-CRCM5 annual cycles for all considered durations, while WRF anticipated the summer peak of AM occurrences especially for sub-daily extremes and both RCMs slightly underestimated winter AM frequencies. Interestingly, ERA-CRCM5 and WRF showed comparable performances for the daily cycles, with later afternoon peaks of hourly AM occurrences compared to observations and almost unchanged diurnal cycles for longer d .

A strong underestimation of station AM quantiles was observed for CMORPH and MSWEP for sub-daily extremes, whereas the two observation-based datasets generally showed good performance for durations $d \geq 24h$. In particular, MSWEP showed the smallest biases for daily and longer duration AM and adequately reproduced observed annual cycles for $d \geq 24h$. However, MSWEP coarse temporal resolution (i.e., $d_0 = 3h$) prevents any meaningful assessment of sub-daily AM characteristics.

The presence of some clusters of spuriously high quantiles in northern regions and the overesti-

mation of AM frequencies during fall and winter months corroborates previously identified issues about CMORPH performance in cold regions and during cold seasons [Xie and Joyce 2014; Trenberth et al. 2017].

The spatiotemporal scaling properties of AM quantiles were then analyzed and compared among datasets over $L1$ locations. Three major results were found.

First, temporal scaling regimes were stronger for short durations (SD, $d < 6h$) than longer duration (LD, $d \geq 6h$) AM. Hence, changes in rainfall quantiles across durations are smaller for LD than for SD, which is consistent with the fact that longer duration AM are generated by spatially more homogeneous weather systems.

Second, the temporal scaling slopes increased with the spatial scale. SD, however, showed higher sensitivity to the spatial scale than LD AM. SD extremes are more likely associated with intense localized convective systems and thus more sensitive to changes in the spatial resolution. Accordingly, it is interesting to note that ERA-CRCM5, WRF, and CMORPH displayed similar temporal scaling slope values for SD at spatial scale $r \approx 24km$ but the increase of temporal scaling slopes with r was much larger for WRF, likely because of its finer native spatial resolution.

Third, for both SD and LD the increase of temporal scaling slopes with the spatial scale was found to be approximately linear for all return periods and datasets. Accordingly, two parameters can be used to describe at each location the AM changes with the observational spatiotemporal scale (r, d): the extrapolated temporal scaling slope, h_0 , and the spatiotemporal scaling parameter h_1 .

The use of the STS linear model [Eq.(2.3)] was statistically validated for most locations for SD 2-

yr quantiles, suggesting the possibility of approximating point scale DDF slopes through h_0 values. However, the local estimation of the STS model was highly uncertain for longer return periods and LD extremes. For MSWEP and CMORPH, in particular, few locations adequately fit Eq.(2.3) with significant h_1 values. This suggests that bias corrections and other post-processing methods applied to these datasets likely altered their spatiotemporal scaling properties, while the STS relationship may be further considered to evaluate the consistency of the spatiotemporal statistical structure of AM precipitation estimated from different datasets.

The second objective of this study was to examine whether the empirical linearity of the temporal scaling slopes can be validated at the local scale when sampling errors associated with short series and local variability are reduced. To this end, the temporal scaling estimates from various CRCM5-LE members were averaged to robustly estimate h_0 and h_1 at each CRCM5 grid box.

Increasing the ensemble size improved the estimation of STS parameters and led to increasing fractions of grid boxes with significant h_1 as the sample size (members) increased. Also, improved fit was obtained for Eq.(2.3), validating the use of the STS model for all return periods and both SD and LD extremes. STS parameters also showed clear spatial distributions that may be associated with different precipitation regimes and to large-scale circulation patterns and topographic features, although h_1 displayed higher local variability than h_0 .

The proposed parsimonious STS model may therefore be considered to estimate DDF and ARF at locations where no sub-daily records are available and to downscale AM marginal distributions from large simulated ensembles. More-

over, h_0 and h_1 parameters represent essential AM statistics that synthetically describe the spatiotemporal structure of rainfall extremes.

Future works should explore the following issues. First, the proposed spatiotemporal model should be thoughtfully compared with stations and other methods for approximating local scale AM quantiles (e.g., downscaling distribution methods) and DDF (e.g. station DDF parameters interpolations). Also, it would be essential to extend the study to other model simulations and large ensembles to further examine model-related uncertainty in STS estimation.

Second, although the spatial patterns of considered AM statistic were consistent with station values, the sampling errors due to the low network density may be important for observational datasets. Hence, repeating the analysis for regions with higher network density would allow improving the empirical evidence of the presented STS relationships.

Third, future studies should investigate the seasonality of the STS relationships and analyze shorter duration AM (e.g., $d < 1h$) to investigate the validity of the proposed model at these temporal scales.

Finally, similar investigations using alternative definitions of extreme, such as event-based definitions of heavy rainfall, and projected series under future climate conditions should be carried out. Meteorological explanations for the proposed STS models would help to understand the atmospheric processes involved in the simulation of extreme rainfall and predict their future evolution.

Despite these limitations, this study constitutes a basic work on the spatiotemporal characteristics of simulated extreme precipitation that may provide guidelines for the development of post-treatment tools for RCM series and the future

precipitation projections.

Acknowledgments Silvia Innocenti's scholarship was partly provided by the Consortium OURANOS. Financial support for this project was also provided by the Discovery Grants Program from the Natural Science and Engineering Research Council of Canada. The ClimEx project was financed by the Bavarian State Ministry for the Environment and Consumer Protection. CRCM5 simulations were run by SuperMUC supercomputer at Leibniz Supercomputing Centre (LRZ) of the Bavarian Academy of Sciences and Humanities and funded via the Gauss Centre for Supercomputing (GCS) by the German Federal Ministry of Education and Research and the Bavarian State Ministry of Education, Science and the Arts. The CRCM5 was developed by the ESCER centre of Universite du Quebec á Montreal (UQAM) in collaboration with Environment and Climate Change Canada. The Canadian Centre for Climate Modelling and Analysis (CCCma) executed and made available the CanESM2-LE for the ClimEx project. We acknowledge the Canadian Sea Ice and Snow Evolution Network for proposing the simulations. The authors also thank Jeremy Panthou and Dikra Khedhaouria for useful discussions, and all data providers who kindly give access to their datasets.

Data availability The 15-min Precipitation Data (15PD) and Hourly Precipitation Data (HPD) were downloaded from the NOAA Climate Prediction Center (CPC) [<http://www.ncdc.noaa.gov/data-access/land-based-station-data>]. Houly Canadian Precipitation Data (HCPD) and Maximum Daily

Precipitation Data (DMPD) for Canada were obtained from Environment and Climate Change Canada (ECCC) [data available upon request; Climate.Services@ec.gc.ca] and from the MD-DELCC of Québec [data available upon request; Info-Climat@mddelcc.gouv.qc.ca]. The CRCM5-LE dataset will become publicly available during year 2019 at www.climex-project.org or can be obtained upon request contacting Ouranos. HRCONUS WRF series were provided by the Research Applications Laboratory, National Center for Atmospheric Research (NCAR) from [Rasmussen and Liu 2017]. The CMORPH v1.0 CRT bias corrected dataset is available online at http://ftp.cpc.ncep.noaa.gov/precip/CMORPH_V1.0/CRT/. MSWEP v2 dataset is freely available for download via the www.gloh2o.org website.

References

- Allen, R. J. and A. T. DeGaetano (2005). “Considerations for the use of radar-derived precipitation estimates in determining return intervals for extreme areal precipitation amounts”. *Journal of Hydrology* 315.1-4, 203–219. DOI: [10.1016/j.jhydrol.2005.03.028](https://doi.org/10.1016/j.jhydrol.2005.03.028).
- Anderson, M. J. and J. Robinson (2001). “Permutation tests for linear models”. *Australian & New Zealand Journal of Statistics* 43.1, 75–88.
- Arora, V. K., J. F. Scinocca, G. J. Boer, J. R. Christian, K. L. Denman, G. M. Flato, V. V. Kharin, W. G. Lee and W. J. Merryfield (2011). “Carbon emission limits required to satisfy future representative concentration pathways of greenhouse gases”. *Geophysical Research Letters* 38.5, L05805. DOI: [10.1029/2010GL046270](https://doi.org/10.1029/2010GL046270).
- Asquith, W. H. and J. S. Famiglietti (2000). “Precipitation areal-reduction factor estimation using an annual-maxima centered approach”. *Journal of Hydrology* 230.1-2, 55–69. DOI: [10.1016/S0022-1694\(00\)00170-0](https://doi.org/10.1016/S0022-1694(00)00170-0).
- Ban, N., J. Schmidli and C. Schär (2015). “Heavy precipitation in a changing climate: Does short-term summer precipitation increase faster?”. *Geophysical Research Letters* 42.4, 2014GL062588. DOI: [10.1002/2014GL062588](https://doi.org/10.1002/2014GL062588).
- Barbero, R., H. J. Fowler, G. Lenderink and S. Blenkinsop (2017). “Is the intensification of precipitation extremes with global warming better detected at hourly than daily resolutions?”. *Geophysical Research Letters* 44.2, 2016GL071917. DOI: [10.1002/2016GL071917](https://doi.org/10.1002/2016GL071917).
- Beck, H. E., A. I. J. M. Van Dijk, V. Levizzani, J. Schellekens, D. G. Miralles, B. Martens and A. de Roo (2017a). “MSWEP: 3-hourly 0.25° global gridded precipitation (1979–2015) by merging gauge, satellite, and reanalysis data”. *Hydrol. Earth Syst. Sci.* 21.1, 589–615. DOI: [10.5194/hess-21-589-2017](https://doi.org/10.5194/hess-21-589-2017).
- Beck, H. E., N. Vergopolan, M. Pan, V. Levizzani, A. I. J. M. van Dijk, G. Weedon, L. Brocca, F. Pappenberger, G. J. Huffman and E. F. Wood (2017b). “Global-scale evaluation of 23 precipitation datasets using gauge observations and hydrological modeling”. *Hydrol. Earth Syst. Sci. Discuss.* 2017, 1–23. DOI: [10.5194/hess-2017-508](https://doi.org/10.5194/hess-2017-508).
- Blanchet, J., D. Ceresetti, G. Molinié and J.-D. Creutin (2016). “A regional GEV scale-invariant framework for Intensity-Duration-Frequency analysis”. *Journal of Hydrology* 540, 82–95. DOI: [10.1016/j.jhydrol.2016.06.007](https://doi.org/10.1016/j.jhydrol.2016.06.007).
- Borga, M., C. Vezzani and G. Dalla Fontana (2005). “Regional rainfall depth-duration-frequency equations for an alpine region”. *Natural Hazards* 36.1-2, 221–235.
- Boukhelifa, M., M. Meddi and E. Gaume (2018). “Integrated Bayesian Estimation of Intensity-Duration-Frequency Curves: Consolidation and Extensive Testing of a Method”. *Water Resources Research* 0.0. DOI: [10.1029/2018WR023366](https://doi.org/10.1029/2018WR023366).
- Burlando, P. and R. Rosso (1996). “Scaling and multiscaling models of DDF for storm precipitations”. *Journal of Hydrology* 187, 45–64. DOI: [10.1016/S0022-1694\(96\)03086-7](https://doi.org/10.1016/S0022-1694(96)03086-7).
- Cannon, A. J. and S. Innocenti (2018). “Projected intensification of sub-daily and daily rainfall extremes in convection-permitting climate model simulations over North America: Implications for future Intensity-Duration-Frequency curves”. *Natural Hazards and Earth System Sciences Discussions*, 1–29. DOI: <https://doi.org/10.5194/nhess-2018-290>.
- Casas-Castillo, M. C., A. Llabres-Brustenga, A. Rius, R. Rodriguez-Sola and X. Navarro (2018). “A single scaling parameter as a first approximation to describe the rainfall pattern of a place: application on Catalonia”. *Acta Geophysica*, 1–10. DOI: [10.1007/s11600-018-0122-5](https://doi.org/10.1007/s11600-018-0122-5).
- Cavicchia, L., E. Scocimarro, S. Gualdi, P. Marson, B. Ahrens, S. Berthou, D. Conte, A. Dell’Aquila, P. Drobinski, V. Djurdjevic, C. Dubois, C. Gallardo, L. Li, P. Oddo, A. Sanna and C. Torma (2016). “Mediterranean extreme precipitation: a multi-model assessment”. *Climate Dynamics*, 1–13. DOI: [10.1007/s00382-016-3245-x](https://doi.org/10.1007/s00382-016-3245-x).
- Ceresetti, D., G. Molinié and J.-D. Creutin (2010). “Scaling properties of heavy rainfall at short duration: A regional analysis”. *Water Resources Research* 46.9, W09531, n/a–n/a. DOI: [10.1029/2009WR008603](https://doi.org/10.1029/2009WR008603).

- Ceresetti, D. (2011). “Structure spatio-temporelle des fortes précipitations: application à la région Cévennes-Vivarais”. PhD thesis. Université de Grenoble.
- Chardon, J., A.-C. Favre and B. Hingray (2016). “Effects of Spatial Aggregation on the Accuracy of Statistically Downscaled Precipitation Predictions”. *Journal of Hydrometeorology* 17, 1561–1578. DOI: [10.1175/JHM-D-15-0031.1](https://doi.org/10.1175/JHM-D-15-0031.1).
- Chen, D. and A. Dai (2017). “Dependence of estimated precipitation frequency and intensity on data resolution”. *Climate Dynamics*, 1–23. DOI: [10.1007/s00382-017-3830-7](https://doi.org/10.1007/s00382-017-3830-7).
- Chen, M., W. Shi, P. Xie, V. Silva, V. E. Kousky, R. Wayne Higgins and J. E. Janowiak (2008). “Assessing objective techniques for gauge-based analyses of global daily precipitation”. *Journal of Geophysical Research: Atmospheres* 113.D4.
- Cortes-Hernandez, V. E., F. Zheng, J. Evans, M. Lambert, A. Sharma and S. Westra (2016). “Evaluating regional climate models for simulating sub-daily rainfall extremes”. *Climate Dynamics* 47.5-6, 1613–1628. DOI: [10.1007/s00382-015-2923-4](https://doi.org/10.1007/s00382-015-2923-4).
- Cunnane, C. (1978). “Unbiased plotting positions : A review”. *Journal of Hydrology* 37.3-4, 205–222. DOI: [10.1016/0022-1694\(78\)90017-3](https://doi.org/10.1016/0022-1694(78)90017-3).
- Dai, A., F. Giorgi and K. E. Trenberth (1999). “Observed and model-simulated diurnal cycles of precipitation over the contiguous United States”. *Journal of Geophysical Research: Atmospheres* 104.D6, 6377–6402. DOI: [10.1029/98JD02720](https://doi.org/10.1029/98JD02720).
- Dai, A., R. M. Rasmussen, C. Liu, K. Ikeda and A. F. Prein (2017). “A new mechanism for warm-season precipitation response to global warming based on convection-permitting simulations”. *Climate Dynamics*, 1–26. DOI: [10.1007/s00382-017-3787-6](https://doi.org/10.1007/s00382-017-3787-6).
- De Michele, C., N. T. Kottegoda and R. Rosso (2001). “The derivation of areal reduction factor of storm rainfall from its scaling properties”. *Water Resources Research* 37.12, 3247–3252. DOI: [10.1029/2001wr000346](https://doi.org/10.1029/2001wr000346).
- Dee, D. P., S. M. Uppala, A. J. Simmons, P. Berrisford, P. Poli, S. Kobayashi, U. Andrae, M. A. Balmaseda, G. Balsamo, P. Bauer, P. Bechtold, A. C. M. Beljaars, L. van de Berg, J. Bidlot, N. Bormann, C. Delsol, R. Dragani, M. Fuentes, A. J. Geer, L. Haimberger, S. B. Healy, H. Hersbach, E. V. Hólm, L. Isaksen, P. Kållberg, M. Köhler, M. Matricardi, A. P. McNally, B. M. Monge-Sanz, J.-J. Morcrette, B.-K. Park, C. Peubey, P. de Rosnay, C. Tavolato, J.-N. Thépaut and F. Vitart (2011). “The ERA-Interim reanalysis: configuration and performance of the data assimilation system”. *Quarterly Journal of the Royal Meteorological Society* 137.656, 553–597. DOI: [10.1002/qj.828](https://doi.org/10.1002/qj.828).
- Diaconescu, E. P., P. Gachon, R. Laprise and J. F. Scinocca (2016). “Evaluation of Precipitation Indices over North America from Various Configurations of Regional Climate Models”. *Atmosphere-Ocean* 54.4, 418–439. DOI: [10.1080/07055900.2016.1185005](https://doi.org/10.1080/07055900.2016.1185005).
- Dwyer, J. G. and P. A. O’Gorman (2017). “Changing duration and spatial extent of midlatitude precipitation extremes across different climates”. *Geophys. Res. Lett.* 44.11, 2017GL072855. DOI: [10.1002/2017GL072855](https://doi.org/10.1002/2017GL072855).
- ECCC (n.d.). Environment Climate Change Canada. Hourly Canadian precipitation data (HCPD) and Maximum Daily precipitation data (MDPD), Historical Climate Data Canada; editing status 2016-08-09; re3data.org - Registry of Research Data Repositories. last accessed: 2016-11-09. DOI: [10.17616/R3N012](https://doi.org/10.17616/R3N012).
- Eggert, B., P. Berg, J. O. Haerter, D. Jacob and C. Moseley (2015). “Temporal and spatial scaling impacts on extreme precipitation”. *Atmos. Chem. Phys.* 15.10, 5957–5971. DOI: [10.5194/acp-15-5957-2015](https://doi.org/10.5194/acp-15-5957-2015).
- Flato, G., J. Marotzke, B. Abiodun, P. Braconnot, S. C. Chou, W. Collins, P. Cox, F. Driouech, S. Emori, V. Eyring, et al. (2013). “Evaluation of climate models”. *Climate Change 2013: The Physical Science Basis. Contribution of Working Group I to the Fifth Assessment Report of the Intergovernmental Panel on Climate Change*. Cambridge University Press, 741–866.
- Fosser, G., S. Khodayar and P. Berg (2017). “Climate change in the next 30 years: What can a convection-permitting model tell us that we did not already know?”. *Climate Dynamics* 48.5-6, 1987–2003. DOI: [10.1007/s00382-016-3186-4](https://doi.org/10.1007/s00382-016-3186-4).
- Fyfe, J. C., C. Derksen, L. Mudryk, G. M. Flato, B. D. Santer, N. C. Swart, N. P. Molotch, X. Zhang, H. Wan, V. K. Arora, J. Scinocca and Y. Jiao (2017). “Large near-term projected snowpack loss over the western United States”. *Nature Communications* 8, 14996. DOI: [10.1038/ncomms14996](https://doi.org/10.1038/ncomms14996).
- Gadian, A. M., A. M. Blyth, C. L. Bruyere, R. R. Burton, J. M. Done, J. Groves, G. Holland, S. D. Mobbs, J. Thielen-del Pozo, M. R. Tye and J. L. Warner (2017). “A case study of possible future summer convective precipitation over the UK and Europe from a regional climate projection”. *International Journal of Climatology*.
- Good, P. (2013). *Permutation Tests: A Practical Guide to Resampling Methods for Testing Hypotheses*. Springer Science & Business Media.
- Goodess, C. M. (2013). “How is the frequency, location and severity of extreme events likely to change up to 2060?”. *Environmental Science & Policy*. Global environmental change, extreme environmental events and ‘environmental migration’: exploring the connections 27.Supplement 1, S4–S14. DOI: [10.1016/j.envsci.2012.04.001](https://doi.org/10.1016/j.envsci.2012.04.001).
- Grimaldi, S., A. Petroselli, L. Baldini and E. Gorgucci (2015). “Description and preliminary results of a 100 square meter rain gauge”. *Journal of Hydrology*. DOI: [10.1016/j.jhydrol.2015.09.076](https://doi.org/10.1016/j.jhydrol.2015.09.076).
- Hartmann, D. L., A. M. G. Klein Tank, M. Ruscicci, L. V. Alexander, B. Broenniman, Y. Charabi, F. J. Dentener, E. J. Dlugokencky, D. R. Easterling, A. Kaplan, B. J. Soden, P. W. Thorne, M. Wild, P. M. Zhai and E. C. Kent (2013). “Observations:

- Atmosphere and Surface”. *Climate Change 2013: The Physical Science Basis. Contribution of Working Group I to the Fifth Assessment Report of the Intergovernmental Panel on Climate Change*. Ed. by T. F. Stocker, D. Qin, G.-K. Plattner, M. Tignor, S. K. Allen, J. Boschung, A. Nauels, Y. Xia, V. Bex and P. M. Midgley. Cambridge, United Kingdom and New York, NY, USA: Cambridge University Press, 159–254.
- Herold, N., A. Behrangi and L. V. Alexander (2017). “Large uncertainties in observed daily precipitation extremes over land”. *Journal of Geophysical Research: Atmospheres* 122.2, 2016JD025842. DOI: [10.1002/2016JD025842](https://doi.org/10.1002/2016JD025842).
- Hofstra, N., M. Haylock, M. New, P. Jones and C. Frei (2008). “Comparison of six methods for the interpolation of daily, European climate data”. *Journal of Geophysical Research: Atmospheres* 113.D21, D21110. DOI: [10.1029/2008JD010100](https://doi.org/10.1029/2008JD010100).
- Huffman, G. J., D. T. Bolvin, E. J. Nelkin, D. B. Wolff, R. F. Adler, G. Gu, Y. Hong, K. P. Bowman and E. F. Stocker (2007). “The TRMM Multisatellite Precipitation Analysis (TMPA): Quasi-Global, Multiyear, Combined-Sensor Precipitation Estimates at Fine Scales”. *Journal of Hydrometeorology* 8.1, 38–55. DOI: [10.1175/JHM560.1](https://doi.org/10.1175/JHM560.1).
- Innocenti, S., A. Mailhot and A. Frigon (2017). “Simple scaling of extreme precipitation in North America”. *Hydrol. Earth Syst. Sci.* 21.11, 5823–5846. DOI: [10.5194/hess-21-5823-2017](https://doi.org/10.5194/hess-21-5823-2017).
- Joyce, R. J., J. E. Janowiak, P. A. Arkin and P. Xie (2004). “CMORPH: A Method that Produces Global Precipitation Estimates from Passive Microwave and Infrared Data at High Spatial and Temporal Resolution”. *Journal of Hydrometeorology* 5.3, 487–503. DOI: [10.1175/1525-7541\(2004\)005<0487:CAMTPG>2.0.CO;2](https://doi.org/10.1175/1525-7541(2004)005<0487:CAMTPG>2.0.CO;2).
- Kendon, E. J., N. Ban, N. M. Roberts, H. J. Fowler, M. J. Roberts, S. C. Chan, J. P. Evans, G. Fossler and J. M. Wilkinson (2017). “Do Convection-Permitting Regional Climate Models Improve Projections of Future Precipitation Change?”. *Bulletin of the American Meteorological Society* 98.1, 79–93. DOI: [10.1175/BAMS-D-15-0004.1](https://doi.org/10.1175/BAMS-D-15-0004.1).
- Kobayashi, S., Y. Ota, Y. Harada, A. Ebata, M. Moriya, H. Onoda, K. Onogi, H. Kamahori, C. Kobayashi, H. Endo, K. Miyaoka and K. Takahashi (2015). “The JRA-55 Reanalysis: General Specifications and Basic Characteristics”. *Journal of the Meteorological Society of Japan. Ser. II* 93.1, 5–48. DOI: [10.2151/jmsj.2015-001](https://doi.org/10.2151/jmsj.2015-001).
- Koutsoyiannis, D., D. Kozonis and A. Manetas (1998). “A mathematical framework for studying rainfall intensity-duration-frequency relationships”. *Journal of Hydrology* 206.1-2, 118–135. DOI: [10.1016/S0022-1694\(98\)00097-3](https://doi.org/10.1016/S0022-1694(98)00097-3).
- Kursinski, A. L. and X. Zeng (2006). “Areal estimation of intensity and frequency of summertime precipitation over a midlatitude region”. *Geophysical Research Letters* 33.22. DOI: [10.1029/2006gl027393](https://doi.org/10.1029/2006gl027393).
- Leduc, M., A. Mailhot, A. Frigon, J.-L. Martel, R. Ludwig, G. B. Brietzke, M. Giguere, F. Brissette, R. Turcotte, M. Braun and J. Scinocca (2019). “ClimEx project: a 50-member ensemble of climate change projections at 12-km resolution over Europe and northeastern North America with the Canadian Regional Climate Model (CRCM5)”. *Journal of Applied Meteorology and Climatology*. DOI: [10.1175/JAMC-D-18-0021.1](https://doi.org/10.1175/JAMC-D-18-0021.1).
- Liu, C., K. Ikeda, R. Rasmussen, M. Barlage, A. J. Newman, A. F. Prein, F. Chen, L. Chen, M. Clark, A. Dai, J. Dudhia, T. Eidhammer, D. Gochis, E. Gutmann, S. Kurkite, Y. Li, G. Thompson and D. Yates (2017). “Continental-scale convection-permitting modeling of the current and future climate of North America”. *Climate Dynamics* 49.1-2, 71–95. DOI: [10.1007/s00382-016-3327-9](https://doi.org/10.1007/s00382-016-3327-9).
- Lucas-Picher, P., R. Laprise and K. Winger (2017). “Evidence of added value in North American regional climate model hindcast simulations using ever-increasing horizontal resolutions”. *Climate Dynamics* 48.7-8, 2611–2633. DOI: [10.1007/s00382-016-3227-z](https://doi.org/10.1007/s00382-016-3227-z).
- Mantegna, G. A., C. J. White, T. A. Remenyi, S. P. Corney and P. Fox-Hughes (2017). “Simulating sub-daily Intensity-Frequency-Duration curves in Australia using a dynamical high-resolution regional climate model”. *Journal of Hydrology* 554. Supplement C, 277–291. DOI: [10.1016/j.jhydrol.2017.09.025](https://doi.org/10.1016/j.jhydrol.2017.09.025).
- Martynov, A., R. Laprise, L. Sushama, K. Winger, L. Separovic and B. Dugas (2013). “Reanalysis-driven climate simulation over CORDEX North America domain using the Canadian Regional Climate Model, version 5: model performance evaluation”. *Climate Dynamics* 41.11-12, 2973–3005. DOI: [10.1007/s00382-013-1778-9](https://doi.org/10.1007/s00382-013-1778-9).
- MDDELCC (n.b.). Données du Programme de surveillance du climat, Direction générale du suivi de l'état de l'environnement, Québec, Ministère du Développement Durable, de l'Environnement et de la Lutte contre les Changements Climatiques.
- Meinshausen, M., S. J. Smith, K. Calvin, J. S. Daniel, M. L. T. Kainuma, J.-F. Lamarque, K. Matsumoto, S. A. Montzka, S. C. B. Raper, K. Riahi, A. Thomson, G. J. M. Velders and D. P. P. v. Vuuren (2011). “The RCP greenhouse gas concentrations and their extensions from 1765 to 2300”. *Climatic Change* 109.1-2, 213. DOI: [10.1007/s10584-011-0156-z](https://doi.org/10.1007/s10584-011-0156-z).
- Menabde, M., A. Seed and G. Pegram (1999). “A simple scaling model for extreme rainfall”. *Water Resources Research* 35.1, 335–339.
- Mineo, C., E. Ridolfi, F. Napolitano and F. Russo (2018). “The areal reduction factor: A new analytical expression for the Lazio Region in central Italy”. *Journal of Hydrology* 560, 471–479. DOI: [10.1016/j.jhydrol.2018.03.033](https://doi.org/10.1016/j.jhydrol.2018.03.033).
- NERC (1975). Flood studies report. Vol. 2. UK Natural Environment Research Council London.

- NOAA (n.d.). 15 min precipitation data (15PD) and hourly precipitation data (HPD), Climate Data Online; editing status 2016-06-17; re3data.org - Registry of Research Data Repositories. last accessed: 2016-11-09. DOI: [10.17616/R32059](https://doi.org/10.17616/R32059).
- O-Gorman, P. A. (2015). "Precipitation Extremes Under Climate Change". *Curr Clim Change Rep* 1.2, 49–59. DOI: [10.1007/s40641-015-0009-3](https://doi.org/10.1007/s40641-015-0009-3).
- Omolayo, A. S. (1993). "On the transposition of areal reduction factors for rainfall frequency estimation". *Journal of Hydrology* 145.1, 191–205. DOI: [https://doi.org/10.1016/0022-1694\(93\)90227-Z](https://doi.org/10.1016/0022-1694(93)90227-Z).
- Panthou, G., T. Vischel, G. Quantin and G. Molinié (2014). "Characterising the space-time structure of rainfall in the Sahel with a view to estimating IDAF curves". *Hydrology and Earth System Sciences* 18.12, 5093–5107. DOI: [10.5194/hess-18-5093-2014](https://doi.org/10.5194/hess-18-5093-2014).
- Perkins, S. E., A. J. Pitman, N. J. Holbrook and J. McAneney (2007). "Evaluation of the AR4 climate models' simulated daily maximum temperature, minimum temperature, and precipitation over Australia using probability density functions". *Journal of climate* 20.17, 4356–4376.
- Prein, A. F., A. Gobiet, H. Truhetz, K. Keuler, K. Goergen, C. Teichmann, C. F. Maule, E. v. Meijgaard, D. M., G. Nikulin, R. Vautard, A. Colette, E. Kjellstrom and D. Jacob (2016). "Precipitation in the EURO-CORDEX 0.11° and 0.44° simulations: high resolution, high benefits?": *Climate Dynamics* 46.1-2, 383–412. DOI: [10.1007/s00382-015-2589-y](https://doi.org/10.1007/s00382-015-2589-y).
- Prein, A. F., W. Langhans, G. Fosser, A. Ferrone, N. Ban, K. Goergen, M. Keller, M. Tolle, O. Gutjahr, F. Feser, E. Brisson, S. Kollet, J. Schmidli, N. P. M. van Lipzig and R. Leung (2015). "A review on regional convection-permitting climate modeling: Demonstrations, prospects, and challenges". *Reviews of Geophysics* 53.2, 2014RG000475. DOI: [10.1002/2014RG000475](https://doi.org/10.1002/2014RG000475).
- Prein, A. F., C. Liu, K. Ikeda, R. Bullock, R. M. Rasmussen, G. J. Holland and M. Clark (2017). "Simulating North American mesoscale convective systems with a convection-permitting climate model". *Climate Dynamics*, 1–16. DOI: [10.1007/s00382-017-3993-2](https://doi.org/10.1007/s00382-017-3993-2).
- Rasmussen, K. L., A. F. Prein, R. M. Rasmussen, K. Ikeda and C. Liu (2017). "Changes in the convective population and thermodynamic environments in convection-permitting regional climate simulations over the United States". *Climate Dynamics*, 1–26. DOI: [10.1007/s00382-017-4000-7](https://doi.org/10.1007/s00382-017-4000-7).
- Rasmussen, R. and C. Liu (2017). "High Resolution WRF Simulations of the Current and Future Climate of North America". type: dataset. DOI: <https://doi.org/10.5065/D6V40SXP>.
- Rummukainen, M. (2016). "Added value in regional climate modeling". *Wiley Interdisciplinary Reviews: Climate Change* 7.1, 145–159. DOI: [10.1002/wcc.378](https://doi.org/10.1002/wcc.378).
- Salzen, K. von, J. F. Scinocca, N. A. McFarlane, J. Li, J. N. S. Cole, D. Plummer, D. Verseghy, M. C. Reader, X. Ma, M. Lazare and L. Solheim (2013). "The Canadian Fourth Generation Atmospheric Global Climate Model (CanAM4). Part I: Representation of Physical Processes". *Atmosphere-Ocean* 51.1, 104–125. DOI: [10.1080/07055900.2012.755610](https://doi.org/10.1080/07055900.2012.755610).
- Schneider, U., A. Becker, P. Finger, A. Meyer-Christoffer, M. Ziese and B. Rudolf (2014). "GPCC's new land surface precipitation climatology based on quality-controlled in situ data and its role in quantifying the global water cycle". *Theoretical and Applied Climatology* 115.1-2, 15–40.
- Sen, P. K. (1968). "Estimates of the Regression Coefficient Based on Kendall's Tau". *Journal of the American Statistical Association* 63.324, 1379–1389. DOI: [10.2307/2285891](https://doi.org/10.2307/2285891).
- Seneviratne, S. I., N. Nicholls, D. Easterling, C. Goodess, S. Kanae, J. Kossin, Y. Luo, J. Marengo, K. McInnes, M. Rahimi, et al. (2012). "Changes in climate extremes and their impacts on the natural physical environment". *Managing the risks of extreme events and disasters to advance climate change adaptation*, 109–230.
- Separovic, L., A. Alexandru, R. Laprise, A. Martynov, L. Sushama, K. Winger, K. Tete and M. Valin (2013). "Present climate and climate change over North America as simulated by the fifth-generation Canadian regional climate model". *Clim Dyn* 41.11-12, 3167–3201. DOI: [10.1007/s00382-013-1737-5](https://doi.org/10.1007/s00382-013-1737-5).
- Sigmond, M. and J. C. Fyfe (2016). "Tropical Pacific impacts on cooling North American winters". *Nature Climate Change* 6.10, 970–974. DOI: [10.1038/nclimate3069](https://doi.org/10.1038/nclimate3069).
- Sikorska, A. E. and J. Seibert (2016). "Value of different precipitation data for flood prediction in an alpine catchment: A Bayesian approach". DOI: [10.1016/j.jhydrol.2016.06.031](https://doi.org/10.1016/j.jhydrol.2016.06.031).
- Sivapalan, M. and G. Blöschl (1998). "Transformation of point rainfall to areal rainfall: Intensity-duration-frequency curves". *Journal of Hydrology* 204.1-4, 150–167. DOI: [10.1016/S0022-1694\(97\)00117-0](https://doi.org/10.1016/S0022-1694(97)00117-0).
- Skamarock, C., B. Klemp, J. Dudhia, O. Gill, D. Barker, G. Duda, X.-y. Huang, W. Wang and G. Powers (2008). "A Description of the Advanced Research WRF Version 3". DOI: [10.5065/D68S4MVH](https://doi.org/10.5065/D68S4MVH).
- Svensson, C. and D. A. Jones (2010). "Review of methods for deriving areal reduction factors". *Journal of Flood Risk Management* 3.3, 232–245. DOI: [10.1111/j.1753-318X.2010.01075.x](https://doi.org/10.1111/j.1753-318X.2010.01075.x).
- Tapiador, F. J., A. Navarro, V. Levizzani, E. Garcia-Ortega, G. J. Huffman, C. Kidd, P. A. Kucera, C. D. Kummerow, H. Masunaga, W. A. Petersen, R. Roca, J.-L. Sanchez, W.-K. Tao and F. J. Turk (2017). "Global precipitation measurements for validating climate models". *Atmospheric Research* 197. Supplement C, 1–20. DOI: [10.1016/j.atmosres.2017.06.021](https://doi.org/10.1016/j.atmosres.2017.06.021).
- Touma, D., A. M. Michalak, D. L. Swain and N. S. Diffenbaugh (2018). "Characterizing the Spatial Scales of Extreme Daily Precipitation in the United States".

- Journal of Climate* 31.19, 8023–8037. DOI: [10.1175/JCLI-D-18-0019.1](https://doi.org/10.1175/JCLI-D-18-0019.1).
- Trenberth, K. E., Y. Zhang and M. Gehne (2017). “Intermittency in Precipitation: Duration, Frequency, Intensity, and Amounts Using Hourly Data”. *Journal of Hydrometeorology* 18.5, 1393–1412. DOI: [10.1175/JHM-D-16-0263.1](https://doi.org/10.1175/JHM-D-16-0263.1).
- Tustison, B., D. Harris and E. Foufoula-Georgiou (2001). “Scale issues in verification of precipitation forecasts”. *Journal of Geophysical Research: Atmospheres* 106.D11, 11775–11784. DOI: [10.1029/2001JD900066](https://doi.org/10.1029/2001JD900066).
- Ushio, T., K. Sasashige, T. Kubota, S. Shige, K. Okamoto, K. Aonashi, T. Inoue, N. Takahashi, T. Iguchi, M. Kachi, R. Oki, T. Morimoto and Z.-I. Kawasaki (2009). “A Kalman Filter Approach to the Global Satellite Mapping of Precipitation (GSMaP) from Combined Passive Microwave and Infrared Radiometric Data”. *Journal of the Meteorological Society of Japan. Ser. II* 87A, 137–151. DOI: [10.2151/jmsj.87A.137](https://doi.org/10.2151/jmsj.87A.137).
- Veneziano, D. and A. Langousis (2010). “Scaling and fractals in hydrology”. *Advances in data-based approaches for hydrologic modeling and forecasting*. Sivakumar, Bellie and Berndtsson, Ronny. Singapore: World Scientific.
- Westra, S., H. J. Fowler, J. P. Evans, L. V. Alexander, P. Berg, F. Johnson, E. J. Kendon, G. Lenderink and N. M. Roberts (2014). “Future changes to the intensity and frequency of short-duration extreme rainfall”. *Reviews of Geophysics* 52.3, 2014RG000464. DOI: [10.1002/2014RG000464](https://doi.org/10.1002/2014RG000464).
- Whan, K. and F. Zwiers (2016). “Evaluation of extreme rainfall and temperature over North America in CanRCM4 and CRCM5”. *Climate Dynamics* 46.11-12, 3821–3843. DOI: [10.1007/s00382-015-2807-7](https://doi.org/10.1007/s00382-015-2807-7).
- Xie, P., M. Chen and W. Shi (2010). “CPC unified gauge-based analysis of global daily precipitation”. *Preprints, 24th Conf. on Hydrology, Atlanta, GA, Amer. Meteor. Soc.* Vol. 2.
- Xie, P., M. Chen, S. Yang, A. Yatagai, T. Hayasaka, Y. Fukushima and C. Liu (2007). “A Gauge-Based Analysis of Daily Precipitation over East Asia”. *Journal of Hydrometeorology* 8.3, 607–626. DOI: [10.1175/JHM583.1](https://doi.org/10.1175/JHM583.1).
- Xie, P. and R. J. Joyce (2014). “Integrating Information from Satellite Observations and Numerical Models for Improved Global Precipitation Analyses”. *Remote Sensing of the Terrestrial Water Cycle*. Ed. by V. Lakshmi, D. Alsdorf, r. Anderson, S. Biancamaria, M. Cosh, J. Entin, G. Huffman, W. Kustas, P. v. Oevelen, T. Painter, J. Parajka, t. Rodell and C. RÄE(Ediger. DOI: [10.1002/9781118872086.ch3](https://doi.org/10.1002/9781118872086.ch3). John Wiley & Sons, Inc, 43–59.
- Xie, P., R. Joyce, S. Wu, S.-H. Yoo, Y. Yarosh, F. Sun and R. Lin (2017). “Reprocessed, Bias-Corrected CMORPH Global High-Resolution Precipitation Estimates from 1998”. *Journal of Hydrometeorology* 18.6, 1617–1641. DOI: [10.1175/JHM-D-16-0168.1](https://doi.org/10.1175/JHM-D-16-0168.1).
- Xie, P. and A.-Y. Xiong (2011). “A conceptual model for constructing high-resolution gauge-satellite merged precipitation analyses”. *Journal of Geophysical Research: Atmospheres* 116.D21, D21106. DOI: [10.1029/2011JD016118](https://doi.org/10.1029/2011JD016118).

Article 3

Extreme precipitation under climate change: probability distributions, seasonality, and spatio-temporal scaling of sub-daily annual maxima.

Silvia Innocenti,¹ Alain Mailhot¹, Anne Frigon²,
Alex J. Cannon³, Martin Leduc²

1. Centre Eau-Terre-Environnement, INRS, Québec, Canada;
2. Consortium Ouranos, Montréal, Canada;
3. Climate Research Division, ECCC, Victoria, Canada.

Ready to be submitted.

Résumé

Il est attendu que le réchauffement climatique modifie l'intensité, la fréquence et la saisonnalité des précipitations extrêmes. Même la structure spatio-temporelle de ces événements de précipitation pourrait être modifiée, ce qui pourrait avoir des conséquences importantes sur les sociétés humaines et les écosystèmes locaux et régionaux. Dans le cadre de cette étude, l'évolution temporelle des précipitations projetées pour le climat futur a été analysée de manière à évaluer l'impact du réchauffement climatique sur les extrêmes journaliers et sous-journaliers pour différents horizons temporels.

À l'aide du grand ensemble de 50 simulations issues du Modèle Régional Canadien du Climat génération 5, (MRCC5), les distributions de probabilité, ainsi que les dates et les heures d'occurrence des Maxima Annuels (MA) de précipitation ont été analysées pour différentes échelles spatiales et pour des durées allant de 1 heure à 3 jours. La structure spatio-temporelle des quantiles de précipitation les plus extrêmes a ainsi été caractérisée.

Regrouper les données des 50 membres du grand ensemble MRCC5 a permis d'estimer les statistiques des MA sur des sous-périodes de quelques années (par exemple de 3 ou 7 ans). Les résultats ont souligné une augmentation critique des quantiles des MA de précipitation, et ce plus particulièrement pour les durées plus courtes et pour des longues périodes de retour. On notera également que des modifications importantes des lois d'échelle spatio-temporelle ainsi que des cycles annuels et journaliers ont été observées pour les extrêmes futurs.

Enfin, les analyses ont démontré que la définition des lois d'échelle spatio-temporelle avait le potentiel d'améliorer substantiellement l'estimation des caractéristiques les plus incertaines des MA (notamment les paramètres de forme des distributions de probabilité et les quantiles associés aux longues périodes de retour), en permettant en fait de regrouper les MA provenant de différentes durées et résolutions spatiales. En suggérant des modifications de queues des distributions des MA, les résultats soulignent aussi qu'une certaine prudence doit être observée quant à l'utilisation de méthodes basées sur l'hypothèse de stationnarité de la forme des distributions de probabilité des extrêmes de précipitations, ainsi que pour l'utilisation de longues séries pour l'estimation de la climatologie des MA de précipitations.

Abstract

Global warming is expected to produce important modifications in the intensity, frequency, and seasonality of extreme precipitation. The spatio-temporal structure of precipitation extremes is also expected to change in future climate, with possibly dramatic consequences for local and regional ecosystems and human societies. In the present study, the temporal evolution of simulated extreme precipitation was analyzed to assess how daily and sub-daily extremes respond to climate warming over different time-horizons. Using the recent 50 member Canadian RCM5 Large Ensemble (CRCM5-LE), the probability distributions, date and time of occurrences, and spatio-temporal structure of simulated Annual Maxima (AM) precipitation were analyzed at various spatial scales and for durations between 1 h and 3 days. Pooling data from the 50 CRCM-LE members allowed estimating AM statistics over short sub-periods of a few years (e.g., 3 or 7 years). Results underline the large increase in AM precipitation quantiles, and the relative increases are more important for shortest durations and longest return periods. Also, modifications in the spatio-temporal scaling properties, as well as in the annual and daily cycles emerged for projected extremes. Finally, the analyses demonstrated that AM pooling across various spatio-temporal scales improves the estimation of most uncertain AM characteristics. Accordingly, heavy-tail GEV distributions are expected to be more frequent in future climates. Some regions also showed a significant increase of GEV shape parameter values with time, which calls into question a familiar hypothesis usually adopted for climate change analysis of extreme precipitation.

3.1 Introduction

The impact of climate change on precipitations is a major issue in hydrological and climate science due to potential impacts these changes may have on natural ecosystems and socio-economic activities [Fischer and Knutti 2016]. Modifications in the probability distributions of precipitation are expected to occur at regional and local scales as a result of global warming because of the increased moisture holding capacity of a warmer atmosphere [Trenberth 2011; Westra et al. 2014]. According to these theoretical considerations, more intense and frequent precipitation extremes are expected, especially at sub-daily and sub-hourly temporal scales. Changes

in the seasonality and spatial distribution of extreme rainfall events may also be expected based on both thermodynamic considerations and possible changes in small and large scale dynamics [Dhakal et al. 2015; Skeeter et al. 2018; Touma et al. 2018].

Using historical records and simulations in historical climate, numerous studies supported these theoretical arguments, showing increases in the frequency and/or the intensification of daily and multi-daily precipitation extremes over the past decades at global and regional scales [e.g., Fischer and Knutti 2016; Barbero et al. 2017; Kendon et al. 2018]. Some evidence of changes in the duration and spatial characteristics of extreme rainfall events, such as the spatial extent

and auto-correlation structure, have also been reported [e.g., Wasko et al. 2016 for observed precipitation series; Li et al. 2015 and Guinard et al. 2015 for Regional Climate Model (RCM) simulations under future conditions; and Prein et al. 2017 for convection permitting RCM projections]. This has important implications for security issues, resource management, and infrastructure design since watershed and ecosystem response to extreme rainfall events is highly dependent on their spatial and temporal features [Mallakpour and Villarini 2017]. However, while there is a significant and growing literature on extreme precipitation intensity, fewer studies have jointly examined the future evolution of extreme precipitation characteristics such as duration, seasonality, timing, and spatial features [Wasko et al. 2016]. As a result the possible modifications of the spatiotemporal structure of extreme rainfall and the mechanisms driving these changes in a warming climate are not completely understood [Mallakpour and Villarini 2017; Dwyer and O’Gorman 2017; Touma et al. 2018].

Although there is a broad consensus that climate change particularly affects extremes at short duration and for long return periods [Westra et al. 2014; Kharin et al. 2018], modifications of sub-daily rainfall extremes are generally difficult to assess due to their high temporal and spatial variability [e.g., Barbero et al. 2017; Kendon et al. 2018] and the paucity of high-quality rainfall series [Westra et al. 2014].

Sparse gauge networks, short records, and measurement errors limit the possibility of assessing extreme spatiotemporal characteristics from observed rainfall series [Tapiador et al. 2017]. Also, uncertainties associated with the use of dynamical models [e.g., *structural modeling* and *tuning uncertainties* Tebaldi and Knutti 2007; Kendon et

al. 2017], to radiative forcing [e.g., *scenario uncertainties*; Hawkins and Sutton 2009], and possible biases arising from the relatively coarse resolution of state-of-the-art RCMs [e.g., Prein et al. 2015] should be accounted for when inferring rainfall extreme characteristics climate model simulations. Finally, the *natural climate variability* associated to the chaotic and nonlinear nature of the climate system may hide the temporal changes in precipitation extreme statistics due to a warming climate, especially at small spatiotemporal scales and for most extreme events [Hawkins 2011]. However, the impacts of these uncertainties on the spatiotemporal structure of rainfall extremes are difficult to evaluate, partly because they emerge at different time horizons and spatiotemporal scales [Fatichi et al. 2016 and references therein]. For instance, whereas model and scenario uncertainties play an important role for most climate variables for projections at the global scale and/or for centennial lead times, *internal variability* is expected to be the major source of uncertainty for precipitation, especially for the most extreme events and short time horizons [e.g., one decade or two; Hawkins and Sutton 2009; Hingray and Saïd 2014].

One way to assess the impact of internal variability on rainfall extreme estimation is done by generating initial-condition ensembles from a single climate model and a given radiative forcing scenario [e.g., Flato et al. 2013; Sanderson et al. 2018]. Ensemble members are thus created by applying minor perturbations to the initial state of the model simulation so that the different climate trajectories are surrogate representations of the climate natural variability [Deser et al. 2012]. Initial-condition ensembles have been therefore used for detecting and discriminating climate changes from natural variability in global

and regional climate extremes [e.g., Fyfe et al. 2017; Martel et al. 2018]. Nonetheless, the integration of natural variability into statistical projections of climate variables is still under development [Hingray and Saïd 2014].

In this study, a recent 50 member initial-condition large ensemble simulated by the 5th generation of the Canadian Regional Climate Model (CRCM5) [Martynov et al. 2013; Separovic et al. 2013] for the period 1950-2100 [Leduc et al. 2019], is used to investigate the multi-scale characteristics of extreme precipitation changes in a warming climate. The analysis focuses on the assessment of temporal changes in the extreme rainfall statistical properties, such as depth quantiles and date or time of extreme occurrence, at various spatial scales and for durations ranging from 1 h to 3 days. In this context, the salient question is that of examining sampling error effects on the spatiotemporal structure of simulated extreme by comparing the estimations of Annual Maxima (AM) precipitation statistics when series from various CRCM5 members are pooled [Li et al. 2019].

The paper is organized as follow. Section 3.2 introduces the CRCM5 large ensemble (CRCM5-LE) and Sec. 3.3.1 describes the extraction AM precipitation series at various spatiotemporal scales. Sections 3.3.2-3.3.3 outline the methodology used for pooling AM series from the various CRCM5-LE members and to assess the possible effects of climate change on rainfall extremes. The statistics characterizing the spatiotemporal structure of precipitation AM are described in Sec. 3.3.4-3.3.6. Results are presented and discussed in Sec. 3.4, while Sec. 3.5 provides a summary and presents the perspective for future works.

3.2 Data

The study is based on the integration of 50 members simulated at the 0.11° resolution (≈ 12 km) by the Canadian Regional Climate Model generation 5 (CRCM5) [Martynov et al. 2013; Separovic et al. 2013] over North East North America [Fig. 3.1] for the period 1950-2100 [Leduc et al. 2019].

The initial-condition CRCM5 large ensemble, hereinafter *CRCM5-LE*, was generated using the CanESM2-LE [Sigmond and Fyfe 2016; Fyfe et al. 2017]. The 50 independent CanESM2-LE simulations were simulated by the Canadian 4th generation Atmospheric Global Climate Model (CanESM2) [von Salzen et al. 2013; Arora et al. 2011] by applying random perturbations to the initial state of cloud-overlap parameters while all other simulation settings (e.g., forcing scenario) and model parameters remained unchanged [Fyfe et al. 2017]. For each member, the radiative forcing was prescribed as the observed concentrations of historical greenhouse gases, aerosol loadings, and land use emissions until 2005 and through the Representative Concentration Pathway 8.5 (RCP8.5) scenario thereafter [Meinshausen et al. 2011]

A spin up period of four years was discarded for each CRCM5-LE member series, resulting in 146 years of hourly precipitation available at 280×280 grid points over the 1954-2099 period. The reader can refer to Leduc et al. (2019) for additional details on experimental setup and the validation of *CRCM5-LE* monthly temperature and precipitation statistics.

Innocenti et al. (under review) evaluated the Canadian RCM performances in representing the extreme rainfall characteristics (including daily and annual cycles) at several spatiotemporal

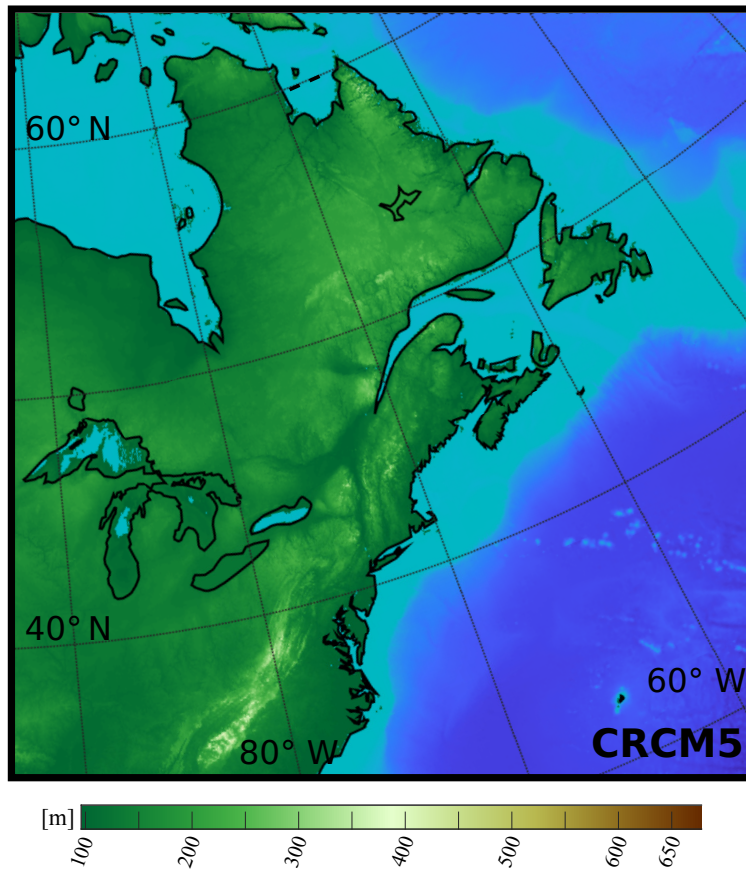


Figure 3.1: CRCM5-LE domain with topography.

scales by comparing CRCM5 simulations driven by the ERA-Interim reanalysis [Dee et al. 2011] to other simulated and observational gridded datasets. Their results showed an overall good agreement between ERA-Interim CRCM5 simulations and station quantiles at hourly time scale, while the model generally overestimated rainfall extreme quantiles at daily and longer durations. Interestingly ERA-Interim CRCM5 simulations also showed comparable performance than a high-resolution RCM [a convection-permitting WRF v3.4.1 simulation, Liu et al. 2017] and two observation-based datasets [the CMORPH, Xie et al. 2017, and the multi-source MSWEP dataset, Beck et al. 2017] for representing observed precipitation extreme annual and daily cycles. Finally, Innocenti et al. (under review) highlighted

that minor differences were found between the ERA-Interim CRCM5 simulations and *CRCM5-LE* diurnal cycles, while some dissimilarities were observed for AM annual cycles and sub-daily AM quantiles, especially in some areas of the domain.

3.3 Methods

3.3.1 Annual Maxima (AM) precipitation at various spatial and temporal scales

Annual Maximum (AM) precipitation series were extracted for each model grid box and for various spatiotemporal scales (r, d) . A moving window

was applied to grid box hourly precipitation series for each *CRCM5-LE* member, to construct precipitation series at durations $d = 1, 2, 3, 4, 6, 12, 18, 24, 36, 48, 60,$ and 72 h. As in Innocenti et al. (under review), grid box hourly precipitation series were also aggregated at six spatial scales using a fixed window in space ($r = 12, 24, \dots, 72$ km). Grids at scales $r > 12$ km were defined by considering non-overlapping grid boxes starting at the south-west corner of the native CRCM5 grid and moving toward the north-east corner of the domain. Grid boxes associated with the ocean and water bodies were removed, and series at coarser spatial scales were discarded if they included less than 75% native land grid boxes. Finally, AM precipitation series aggregated at each spatiotemporal scale (r, d) were extracted.

The dates and day time (starting hour at local time, UTC-5) of occurrence of AM were also extracted for each spatiotemporal scale, year, and grid box.

For the analysis of AM statistics, each native CRCM5 grid box was associated with the overlapping grid box at coarser spatial scales. Also, to reduce the computational time, the CRCM5 grid was under-sampled with ratio $1/4$, resulting in the selection of ≈ 11800 grid boxes randomly distributed over the CRCM5 North American domain. The strategy also reduced the number of neighboring grid points and therefore the spatial autocorrelation of computed statistics.

3.3.2 Pooling CRCM5-LE series

The probability of detecting changes in the time series of a given climatic variable X depends on the signal-to-noise ratio [Hawkins and Sutton 2012] which is a function of the magnitude of the

signal (e.g., the climatic trend of X), the series length, and the variability of X . Since time series of short-duration AM rainfall usually display large variability, the signal-to-noise is generally low at local spatial scales but can be enhanced by pooling AM series from several spatial and/or temporal scales [e.g., Innocenti et al. 2017], from various spatial locations [e.g., Shephard et al. 2014], and/or from several simulated series [e.g., Martel et al. 2018].

CRCM5-LE members represent 50 equiprobable climate realizations over the 1954-2099 period, providing for each year, spatiotemporal scale, and grid box 50 independent AM, as well as their corresponding date and time of occurrence. In order to reduce sampling errors on estimated AM characteristics, the 50 CRCM5-LE series were pooled over short sub-periods of 1, 3, and 7 years, hereinafter referred to as 1SP, 3SP, and 7SP. A schematic diagram showing the steps of this procedure for the 3SP case is provided in Fig. 3.2a-b.

3.3.3 Trend analysis for AM statistic series

Consider a time series \mathbf{Y}_t , where Y is one of the AM statistics defined in Sec.3.3.4-3.3.6 and the superscript t indicate the median year of a given 1SP, 3SP, or 7SP. For instance, $t = 1955$ for the first 3SP, as shown by the example in Fig. 3.2c.

The existence of significant monotonic trends for \mathbf{Y}_t was assessed using the rank-based variance-corrected Mann-Kendall (MK) [variance correction factor proposed by Yue and Wang 2004]. By modifying the variance of MK statistics, the corrected MK test accounts for the influence of serial correlations in \mathbf{Y}_t and reduce the probabil-

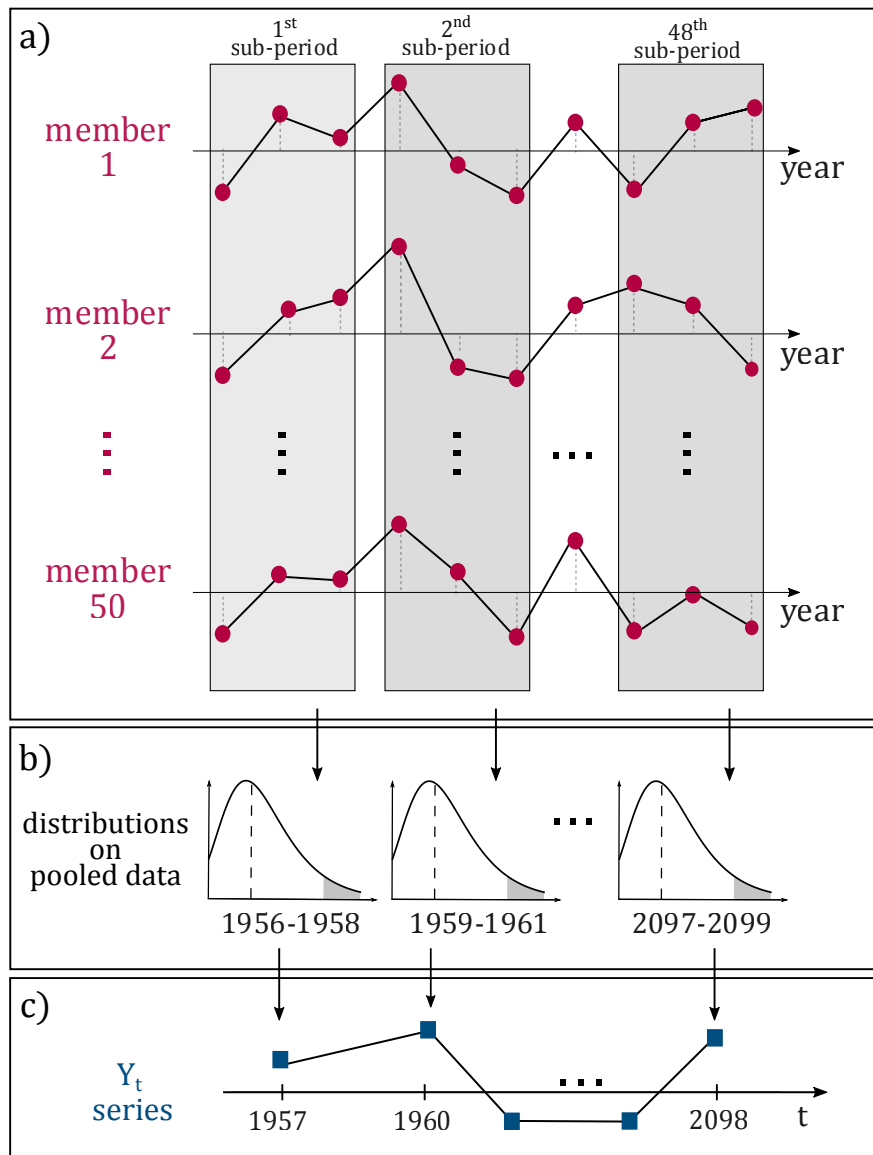


Figure 3.2: Pooling of AM precipitation series from the CRCM5-LE members: a) example for 3-years short sub-periods (3SP), b) AM probability distributions for each 3SP; and c) non-stationary time series of the Y_t statistics (e.g, 100-yr AM quantile for each 3SP t)

ity of false trend detections [Blain 2013]. For accounting the effects of CRCM5 grid box spatial dependence on MK results, the field significance of local tests was evaluated through a False Discovery Rate (FDR) approach [Wilks 2006]. Accordingly, the average fraction of false discoveries (i.e., of incorrect rejections of the MK null hypothesis made in the absence of a monotonic trend) over the total number of test rejections can

be guaranteed to be no greater than the global (field) significance level $\alpha_{glo} = 0.1$. The corresponding FDR global p value, p_{glo} , was computed using the Benjamini and Hochberg (1995) procedure and all local (grid box) tests yielding MK p values $p_{loc} \leq p_{glo}$ were considered significant. Field significance was considered to hold at the α_{glo} level if at least one local MK null hypothesis was rejected [Wilks 2006].

The magnitude of the significant temporal \mathbf{Y}_t trend was then estimated using the following log-linear model:

$$\ln(Y_t) = \alpha_Y + \beta_Y t, \quad (3.1)$$

where the subscript Y for α_Y and β_Y refers to the considered AM statistic.

For small values of β_Y , we have $e^{\beta_Y} \approx 1 + \beta_Y$. Hence, the slope of Eq. (3.1) represents the relative change of the Y_t statistics expected for a unit increase in t [Benoit 2011], namely the annual mean relative change of Y_t . Equivalently, $b_x = 10^3 \beta_Y$ approximates the mean decadal percent increase of Y_t and will be used as reference measure for the trend magnitude.

For statistics that can assume negative values [e.g., the shape GEV parameter; see Sect. 3.3.5], classical linear regression models were used to estimate the absolute magnitude of expected \mathbf{Y}_t trends. In this cases, the regression slope β_Y represents the absolute variation of Y_t expected for a unit increase in t , i.e. the expected annual variation of the statistic.

3.3.4 Statistical characterization of AM rainfall

Let $\mathbf{x}_t = (x_{1,t}, x_{2,t}, \dots, x_{i,t}, \dots, x_{n,t})$ be the sample of n AM pooled from the 50 CRCM5-LE members for the sub-period t , a given grid box s , and the spatiotemporal scale (r, d) . To simplify notation, grid box and and spatiotemporal scale subscripts are omitted, unless otherwise stated. Empirical AM quantiles, $x_{t,q}$, were estimated for each \mathbf{x}_t and various return periods q [yr] based on the Hazen plotting position [Cunnane 1978].

To investigate the spatial and temporal structure of the sampled extremes, the following log-log linear model was considered:

$$\ln\{x_{t,q}(r, d)\} = \alpha_{r,t} + (h_{0,t} + h_{1,t}r) \ln(d), \quad (3.2)$$

where $x_{t,q}(r, d)$ represents q -yr AM quantiles extracted at the spatiotemporal resolutions (r, d) for the sub-period t and the intercepts $\alpha_{r,t}$ represent estimates of $\ln\{x_{t,q}(r, 1h)\}$ for each $r = 12, 24, \dots, 72$ km. Note that, for simplicity, the index q for quantile orders have been omitted for $\alpha_{r,t}$, $h_{0,t}$, and $h_{1,t}$ parameters.

Eq.(3.2) is a synthetic expression that includes both the temporal scaling of AM quantiles at the point scale [Menabde et al. 1999; Casas-Castillo et al. 2018] (through the $h_{0,t}$ coefficient, hereinafter the *temporal scaling parameter*) and the sensitivity of AM temporal scaling to changes in the spatial scale (through $h_{1,t}$, hereinafter the *spatiotemporal scaling parameter*).

Previous investigations on the CRCM5-LE and other gridded datasets justify the choice of Eq.(3.2) [Innocenti et al. under review] and showed how it extends the classical *simple scaling* formulations [e.g., Gupta and Waymire 1990; Burlando and Rosso 1996] of Depth-Duration-Frequency (DDF) and Intensity-Duration-Frequency (IDF) curves which are widely used in hydrological and engineering applications [Koutsoyiannis et al. 1998]. Innocenti et al. (under review) also showed that $h_{1,t}$ can be interpreted as the change of AM quantile Areal-Reduction-Factors (ARFs) [Svensson and Jones 2010 and references therein] corresponding to changes in (r, d) for each sub-period t , i.e.:

$$\ln\{A_{t,q}(r, d)\} = \ln\{A_{t,q}(r, 1h)\} + h_{1,t} r \ln(d), \quad (3.3)$$

where $A_{t,q}(r, d) = x_{t,q}(r, d)/x_{t,q}(0, d)$ and $A_{t,q}(r, 1h) = x_{t,q}(r, 1h)/x_{t,q}(0, 1h)$ respectively represent the q -yr quantile ARFs for durations d and $1h$ at the spatial scale r and for the sub-period t .

As a result, the future evolution of the extreme precipitation spatiotemporal structure simulated by the CRCM5 can be assessed through the projected $h_{0,t}$ and $h_{1,t}$ values. For instance, previous studies stressed that temporal scaling parameters might change with time, questioning the adequacy of stationary frameworks classically used to estimate DDF and IDF slopes [e.g., Casas-Castillo et al. 2018 for observed rainfall extremes; Cannon and Innocenti 2018 for daily and sub-daily simulated AM]. Finally note that some authors underlined the presence of two temporal scaling regimes for short (e.g., hourly and sub-hourly) and long (e.g., daily and longer) durations [e.g., Ceresetti 2011; Eggert et al. 2015]. Different weather regimes that drive precipitation extremes at different spatiotemporal scales explain this result [Eggert et al. 2015; Innocenti et al. 2017]. Hence, the scaling properties of CRCM5-LE AM were separately investigated for *Short Duration* (SD, $1h \leq d < 6h$) and *Long Durations* (LD, $6h \leq d \leq 72h$), as in Innocenti et al. (under review).

3.3.5 Simple Scaling Generalized Extreme Value (SS-GEV) model

AM probability distributions were also assessed through the Generalized Extreme Value (GEV) distribution which is an appropriate model for extremes according to asymptotic results of the Extreme Value Theory (EVT) [Coles 2001]. Considering X_t to be the random variable for AM in

the \mathbf{x}_t sample, the GEV cumulative distribution function (cdf) for the sub-period t and a generic spatiotemporal scale can be written as:

$$F_t(x) = \exp \left\{ - \left[1 + \xi_t \left(\frac{x - \mu_t}{\sigma_t} \right) \right]^{-1/\xi_t} \right\}, \quad (3.4)$$

where $\xi_t \neq 0$, $-\infty < x \leq \mu_t - \sigma_t/\xi_t$ if $\xi_t < 0$ (bounded tail, Weibull) and $\mu_t - \sigma_t/\xi_t \leq x < +\infty$ if $\xi_t > 0$ (heavy tail, Fréchet). If $\xi_t = 0$ (Gumbel) Eq. (3.4) reduces to:

$$F_t(x) = \exp \left\{ - \exp - \left\{ \frac{x - \mu_t}{\sigma_t} \right\} \right\}, \quad (3.5)$$

where $-\infty < x < +\infty$. The parameters $\mu_t \in \mathbb{R}$, $\sigma_t > 0$, and ξ_t respectively represent the location, scale, and shape parameters of the distribution for the sub-period t . Since the shape parameter characterizes the distribution tail, an accurate estimation of ξ_t is critical to adequately assess extreme precipitation quantiles.

Uncertainties on ξ_t are important for short records [Koutsoyiannis 2004a and 2004b; Papalexiou et al. 2013] and various strategies to increase the sample size have been proposed to improve GEV parameter estimation [e.g., regional analysis, Hosking and Wallis 1997; or approaches combining AM series at different temporal scales, Blanchet et al. 2016]. In particular, temporal scaling relationships has been shown to be effective to increase the robustness of GEV estimation for station series [Innocenti et al. 2017]. Extending typical simple scaling GEV formulations [e.g., Panthou et al. 2014; Blanchet et al. 2016], the following expressions were thus considered for GEV parameters

at each spatiotemporal scale (r, d) :

$$\begin{aligned}\mu_t(r, d) &= d^{H_{t,r}} \mu_{t,r}^* \\ \sigma_t(r, d) &= d^{H_{t,r}} \sigma_{t,r}^*, \text{ and} \\ \xi_t(r, d) &= \xi_{t,r}^*\end{aligned}\quad (3.6)$$

where $H_{t,r}$, $r = 12, 24, \dots, 72\text{km}$, are generally referred to as *simple scaling exponents* and $\mu_{t,r}^*$, $\sigma_{t,r}^*$, and $\xi_{t,r}^*$ are the GEV parameters for the spatial scale r , the sub-period t , and the $d^* = 1\text{h}$ being used as reference duration. Distribution in Eq.(3.6) is hereinafter referred to as Simple Scaling GEV (SS-GEV) model.

Note that, according to Eq. (3.2) the SS-GEV simple scaling exponents should verify $H_{t,r} = h_{0,t} + h_{1,t}r$. However, while Eq.(3.2) may result in spatiotemporal scaling parameters that depend on the quantile return period q , the proposed SS-GEV model is based on unique $h_{0,t}$ and $h_{1,t}$ values estimated for each grid box and sub-period t (i.e., SS-GEV assumes scaling parameters to be independent of the return period).

Several methods can be considered for the estimation of the parameters $(H_{t,r}, \mu_{t,r}^*, \sigma_{t,r}^*, \xi_{t,r}^*)$ of the SS-GEV model over each sub-period t . The Nelder-Mead numerical approximation of the Maximum Likelihood (ML) estimate was used, considering Generalized Linear Model (GLM) formulations of the SS-GEV. To this end, the duration d was introduced as model covariate in SS-GEV probability distribution function (pdf) formulations [Coles 2001] as in temporal simple scaling expressions used in previous studies [e.g., Mélése et al. 2018 and references therein].

Likelihood-Ratio (LR) tests at the 0.05 significance level were also used to test the null hypothesis $\mathbf{H}_0 : \xi_t = 0$ for each t (Gumbel versus GEV distributions).

SS-GEV distribution parameters were estimated independently at each grid box and spatial scale r , i.e. assuming that AM extracted at different d are independent. This last assumption is not fully respected since AM occurring during the same year at different spatiotemporal scales may be associated to the same precipitation event or system. However, previous studies pointed out that the estimation is robust to likelihood misspecification and AM dependence [e.g., Blanchet et al. 2016; Mélése et al. 2018]. Also, to reduce computation time and improve convergence for GLM-ML optimizations, only durations $d = 1, 2, 3, 6, 24$, and 72 h were considered for GEV and SS-GEV estimation.

3.3.6 Characterization of AM annual and daily cycles

Descriptive statistics for annual and daily cycles of AM occurrences were assessed at the native CRCM5-LE spatial resolution ($r = 12\text{km}$) within the framework of circular statistics [Pewsey 2004], specifically developed for the analysis of periodic random variables. Within this framework, the date and time of the occurrence of AM for each spatiotemporal scale (r, d) are represented by angular variables (in radians) as [Berens 2009]:

$$\delta_{i,t} = \frac{2\pi z_{i,t}}{365} \quad \text{and} \quad \eta_{i,t} = \frac{2\pi w_{i,t}}{24} \quad (3.7)$$

where $z_{i,t}$ and $w_{i,t}$ respectively represent the day and the daily hour at which the i^{th} AM of the \mathbf{x}_t sample begins. Subscript for duration d has been omitted to simplify notation and leap years are not considered for variable $\delta_{i,t}$. A visual representation and an example for these variables are shown in Fig. 3.3.

Eq.(3.7) can then be used to measure the sample mean, variance, and shape of the AM annual and daily cycles. For instance, the mean date of AM occurrence can be determined for the sub-period t by averaging the cosine- and sine-component of the angular vectors $(\delta_{1,t}, \dots, \delta_{i,t}, \dots, \delta_{n,t})$:

$$\bar{\mathbf{u}}_t = [\bar{u}_{t,1}, \bar{u}_{t,2}], \quad (3.8)$$

where

$$\begin{aligned} \bar{u}_{t,1} &= \frac{1}{n} \sum_{i=1}^n \cos \delta_{i,t}, \\ \bar{u}_{t,2} &= \frac{1}{n} \sum_{i=1}^n \sin \delta_{i,t}. \end{aligned} \quad (3.9)$$

The mean angle, $\bar{\delta}_t$, can then be computed as:

$$\bar{\delta}_t = \tan^{-1} \left(\frac{\bar{u}_{t,2}}{\bar{u}_{t,1}} \right), \quad (3.10)$$

where \tan^{-1} is the four quadrant inverse tangent function. Equation 3.7 can then be used to estimate the corresponding \bar{z}_t [days].

The mean daily time of occurrence of AM can be estimated in a similar way considering mean vectors $\bar{\mathbf{v}}_t$ and corresponding angles $\bar{\eta}_t$ as shown in the examples of Fig. 3.3b.

If the $\delta_{i,t}$ or $\eta_{i,t}$ angles are uniformly distributed on the unit circle, the length of the resulting \mathbf{u}_t and \mathbf{v}_t vectors is 0, since sine and cosine distributions will be centered on 0. Conversely, if all AM occur at the same hour or on the same day, \mathbf{u}_t and \mathbf{v}_t will be unit vectors (i.e., $\|\bar{\mathbf{u}}_t\| = 1$ and $\|\bar{\mathbf{v}}_t\| = 1$). Hence, the length of the mean resultant vectors is a non-negative measure the circular dispersion of $\delta_{i,t}$ and $\eta_{i,t}$ values around their mean values, $\bar{\delta}_t$ and $\bar{\eta}_t$, for each sub-period t . The closer $\|\bar{\mathbf{u}}_t\|(\|\bar{\mathbf{v}}_t\|)$ value is to one, less dispersed are the AM occurrences concentrate around the mean date (time) direction.

With a similar approach it is also possible to define measures of circular symmetry, skewness, and higher order moments of circular probability distributions [Pewsey 2004]. The reader can refer to Berens (2009) for further details.

3.4 Results

Unless otherwise noted, only results for 3SP are presented since similar conclusions were reached for the 1SP and 7SP [the Supplementary material provides some examples for 1SP and 7SP results].

3.4.1 Projected changes in AM probability distributions

Figure 3.4 summarizes the main results for projected changes in empirical AM quantiles. Fig. 3.4a-b shows that hourly and daily AM quantiles increased for virtually all grid boxes. The MK null hypothesis of a non-significant trend was rejected for more than 98% grid boxes at the field significance level $\alpha_{glo} = 0.1$ (not shown). Also, while important increases appear during the 1990s for both hourly and daily 100-yr quantiles [Fig. 3.4a-b], trends were relatively stronger for sub-daily AM than for daily and longer durations [Fig. 3.4c].

Decadal percent variations of empirical AM quantiles were particularly important for $d \leq 3h$ with median $b_{x_t,q} \geq 3.3\%/10\text{-yr}$ for more than half of CRCM5 grid boxes at the hourly scale [Fig. 3.4c]. Estimated trends also displayed the largest spatial variability for $d = 1h$, as shown by the 10^{th} - 90^{th} and 25^{th} - 75^{th} quantile ranges in Fig. 3.4c. Finally, note that, while similar results were observed for shorter return periods, lower me-

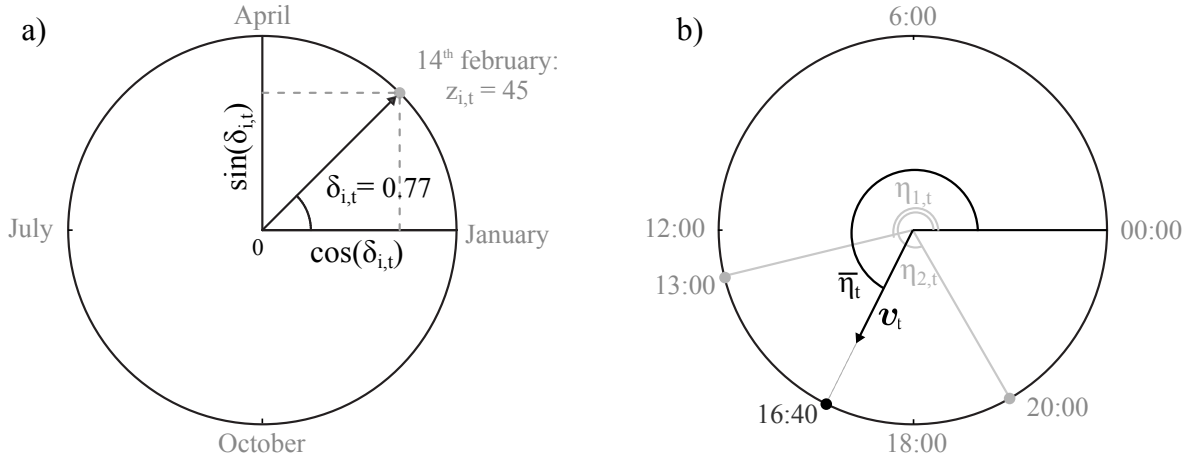


Figure 3.3: Angular representation of AM occurrences: a) example for an AM occurring on February 14th ($z_{i,t} = 45$); b) example of mean vector \bar{v}_t and mean angle $\bar{\eta}_t$ considering a first AM occurring at 13:00 (1:00pm, $w_{i,t} = 13$ and $\eta_{1,t} = 3.4$) and a second at 20:00 (8:00pm, $w_{i,t} = 20$) and $\eta_{1,t} = 5.23$.

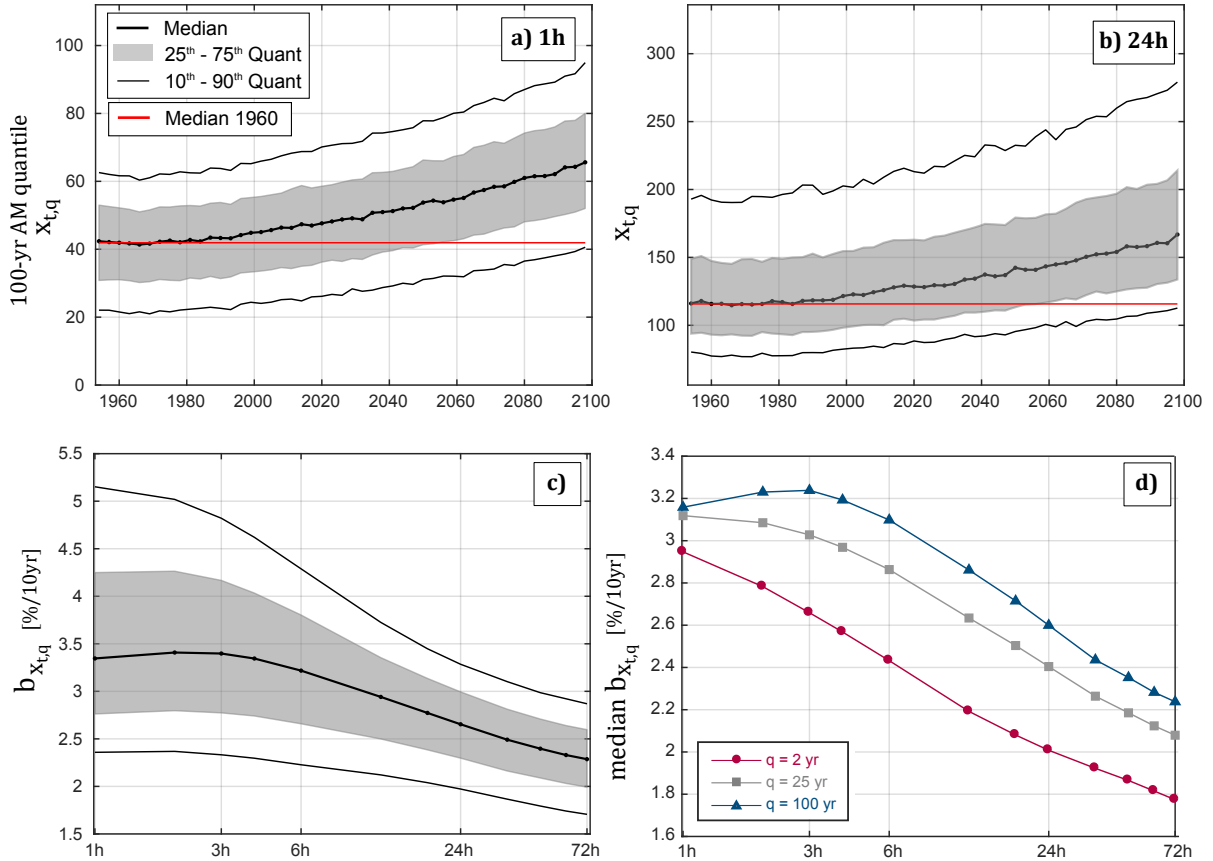


Figure 3.4: Temporal evolution of 3SP empirical quantiles at the model native spatial resolution ($r = 12\text{km}$): a)-b) distribution over CRCM5 grid boxes of the 100-yr AM quantiles, $x_{t,q}$, for each 3SP (x-axis) for a) $d = 1\text{h}$ and b) $d = 24\text{h}$; c) distribution over CRCM5 grid boxes of the expected decadal percent variation, $b_{x_{t,q}}$, of 100-yr AM quantiles; d) median over CRCM5 grid boxes of the projected decadal percent variation for 2-, 25-, and 100-yr quantiles.

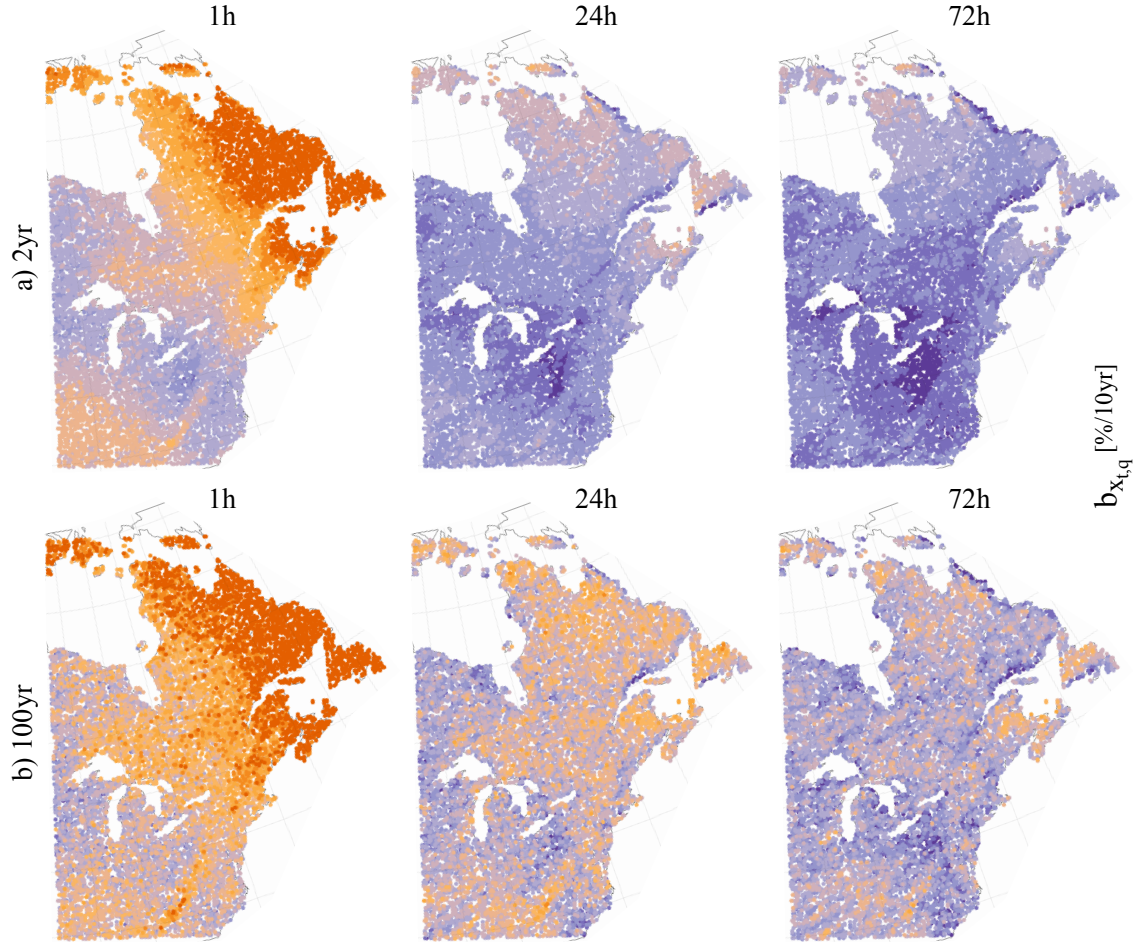


Figure 3.5: Spatial distribution of the expected decadal percent variation for 3SP AM quantiles: a) 2-yr and b) 100-yr empirical quantiles.

dian $b_{x,t,q}$ values were observed for $q = 2yr$ and $q = 25yr$ compared to 100-yr AM [Fig. 3.4c], meaning that more extreme AM are expected to experience larger relative increases in future climate.

Figure 3.5 shows that the largest decadal percent variations were generally obtained in the northeast portion of the domain, while a decreasing gradient was observed along the NE to SW axis, especially at the hourly time scale. For all durations and return periods, estimated trends over the Great Lake region and the southern Atlantic coast were generally small compared to south inland regions. Local differences between coastal

and inland grid box trends emerged in some cases over the North Atlantic coast for daily and longer durations [Fig. 3.5, 2nd and 3rd col.]. Due to the higher estimation uncertainty, larger spatial variability was observed for $b_{x,t,q}$ for 100-yr quantiles compared to shorter return periods, resulting in noisier maps and less obvious spatial structures, especially for daily and longer duration estimates.

GEV distribution parameters estimated through Eq.(3.4)-(3.5) are presented in Fig.3.6 for each 3SP and 7SP t (x-axis) and for $d = 1h, 3h, 24h,$ and $72h$ (for clarity, $72h$ is not shown in Fig. 3.6a). The comparison between 3SP and 7SP

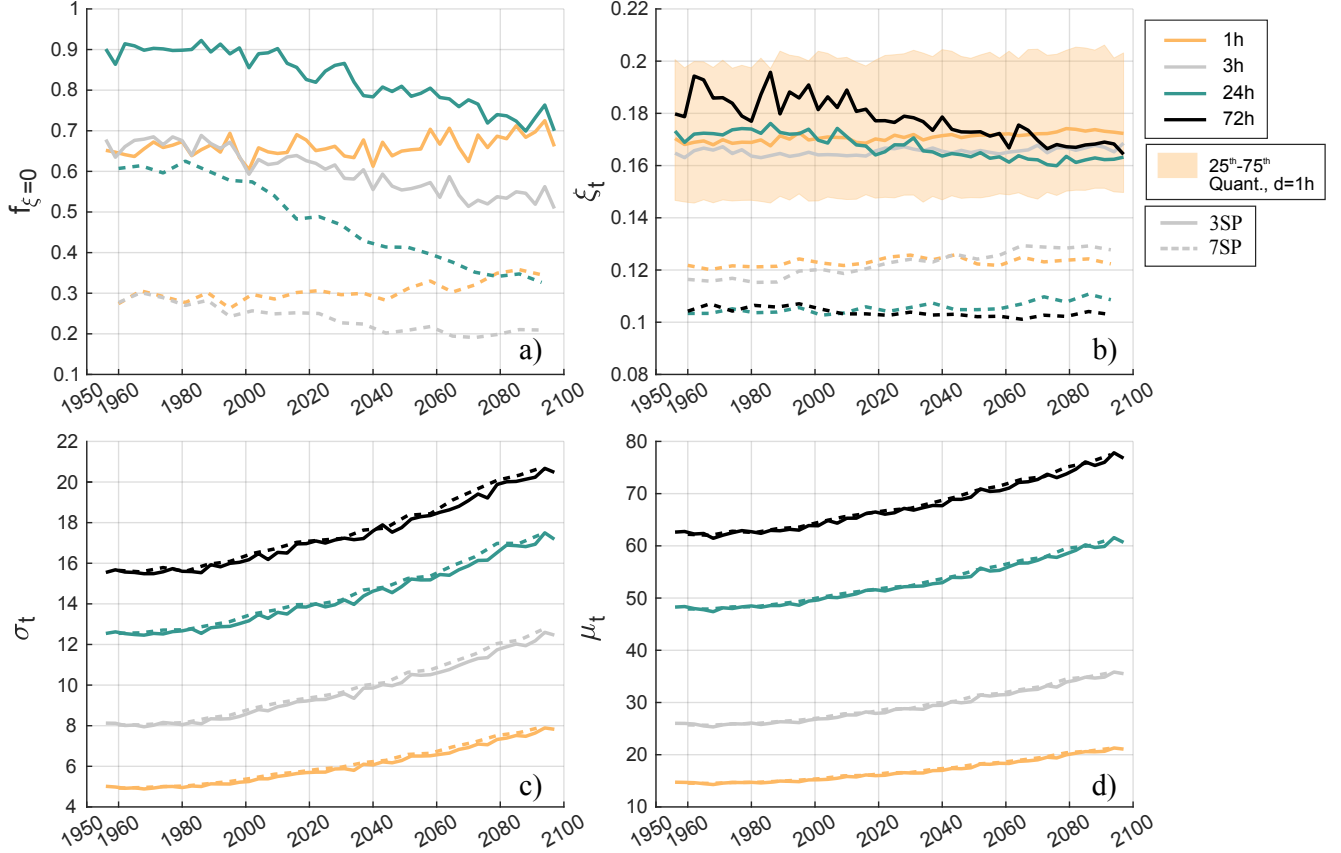


Figure 3.6: GEV estimation for each 3SP and 7SP period (x-axes): a) Proportion of grid boxes with shape parameter non-significantly different from 0 (Gumbel distribution) according to the LR test at the $\alpha_{glo} = 0.01$ FDR level; b) median over CRCM5 grid boxes of the GEV shape parameter (only grid boxes with $\xi_t > 0$ are considered; the yellow interval represents the 25th-75th quantile interval for 1h estimations); c)-d) median over CRCM5 grid boxes of GEV c) scale and d) location parameters (solid 3SP lines and dotted 7SP lines overlap for most sub-periods).

aims at evaluating the uncertainty on estimated GEV parameters and the impact of CRCM5-LE member pooling over sub-periods of various lengths.

The LR-tests assessing the significance of the ξ_t parameters showed that the Gumbel distribution ($\xi_t=0$) adequately represents the AM distributions for most of grid boxes when 3SP are considered [Fig.3.6a], especially for $d \geq 24h$. Also, the fraction $f_{\xi_t < 0}$ of grid boxes with significant and negative shape parameter (bounded tail distribution) was negligible ($f_{\xi_t < 0} < 8 * 10^{-3}$) for all considered durations and pooling sub-periods (not shown). Moreover, the fraction of model grid

boxes rejecting the LR H_0 clearly decreases with increasing t for all $d > 1h$ [Fig.3.6a]. This result was confirmed for 7SP, that presented $0.24 \leq f_{\xi_t=0} \leq 0.30$ ($0.57 \leq f_{\xi_t=0} \leq 0.62$) for 20th century sub-periods and $0.19 \leq f_{\xi_t=0} \leq 0.21$ ($0.32 \leq f_{\xi_t=0} \leq 0.41$) for $t > 2050$ for $d = 3h$ ($d = 24h$). This suggests that the large 3SP proportions of grid boxes with Gumbel distribution, were mainly due to the large estimation uncertainty on estimated GEV shape parameters. This uncertainty can in principle be reduced using larger samples (e.g., using 7SP).

Medians over the CRCM5 grid boxes of the estimated GEV parameter values are shown in Fig.

3.6b-d for 3SP and 7SP and several durations. For shape parameters, Fig. 3.6b, only considers grid boxes with $\xi_t > 0$. 3SP systematically displayed higher shape values than 7SP, with median positive ξ_t values distributed around $\xi_t \approx 0.17$. This result is consistent with typical GEV shape parameter values estimated from long recorded series (e.g., more than 100 years) presented in the literature [e.g., Koutsoyiannis 2004a and 2004; Ragulina and Reitan 2017 and references therein]. In these cases ξ ranged across positive values lower than ≈ 0.23 . Finally, note that for both 3SP and 7SP median ξ_t curves generally showed weak changes with time for all durations. Owing to the high uncertainty on estimated shape parameters, the fraction of grid boxes with statistically significant trends for ξ_t was generally negligible (e.g., lower than 1% for most durations, not shown). Conversely, most of grid boxes displayed statistically significant trends when considering statistics for the AM distribution shape characteristics that are less impacted by the sample size [e.g., the normalized dispersion coefficient σ_t/μ_t ; Fig. S1 in the supplementary material].

An important shift of AM distributions toward higher values is observed for all durations due to increase in median location parameters with t , while the increase of grid box median scale parameters corresponds to higher variability of AM precipitation in future climate [Fig. 3.6c-d]. According to the MK tests, μ_t and σ_t displayed significant increases for almost all grid boxes and durations. For both parameters, decadal percent variations showed low local variability, with spatial patterns similar to those of the 2-yr AM quantiles [e.g., Fig. S2 of the Supplementary material].

Finally, note that 3SP and 7SP estimates of μ_t and σ_t did not present any appreciable difference

[Fig. 3.6c-d], indicating that sample size has no impact on estimated values, contrary to shape parameter.

3.4.2 Projected changes in annual and daily cycles

Basic statistics for the dates of occurrence of hourly and daily AM are shown in Fig. 3.7 for each 3SP t . The $\bar{\delta}_t$ distributions over the CRCM5 grid boxes is represented for each t though the angular medians, that is the diameter that divides the unit circle into two equally sized groups of grid box $\bar{\delta}_t$ values. For each of these two groups, the angular median computation is then repeated to estimate *pseudo-quartiles* of the $\bar{\delta}_t$ distribution, i.e. angular measures that can be considered equivalent to 25th and 75th percentiles of the $\bar{\delta}_t$ distribution over CRCM5 grid boxes.

Fig.3.7a shows that hourly AM are generally concentrated in July, with $\bar{\delta}_t$ *pseudo-quartiles* taking values between the end of June and the beginning of August for all 3SP, while $\bar{\delta}_t$ values are more variable over summer months for $d = 24h$ [Fig.3.7c]. As expected, it could be shown that clear spatial distributions emerged for $\bar{\delta}_t$ each year, with evident influence of water bodies and oceans as well as marked latitudinal gradients [see, for instance, Fig. S3 of the Supplementary material]. Median $\bar{\delta}_t$ remained almost unchanged over time for both $d = 1h$ and $d = 24h$. However, at the end of the simulation period hourly and daily AM more frequently occur outside summer for some grid boxes, as the $\bar{\delta}_t$ *pseudo-quartile* interval become wider and asymmetrical with time, especially for $d = 24h$. In fact, daily and longer duration AM more frequently occur during winter and fall southern areas and grid boxes on the

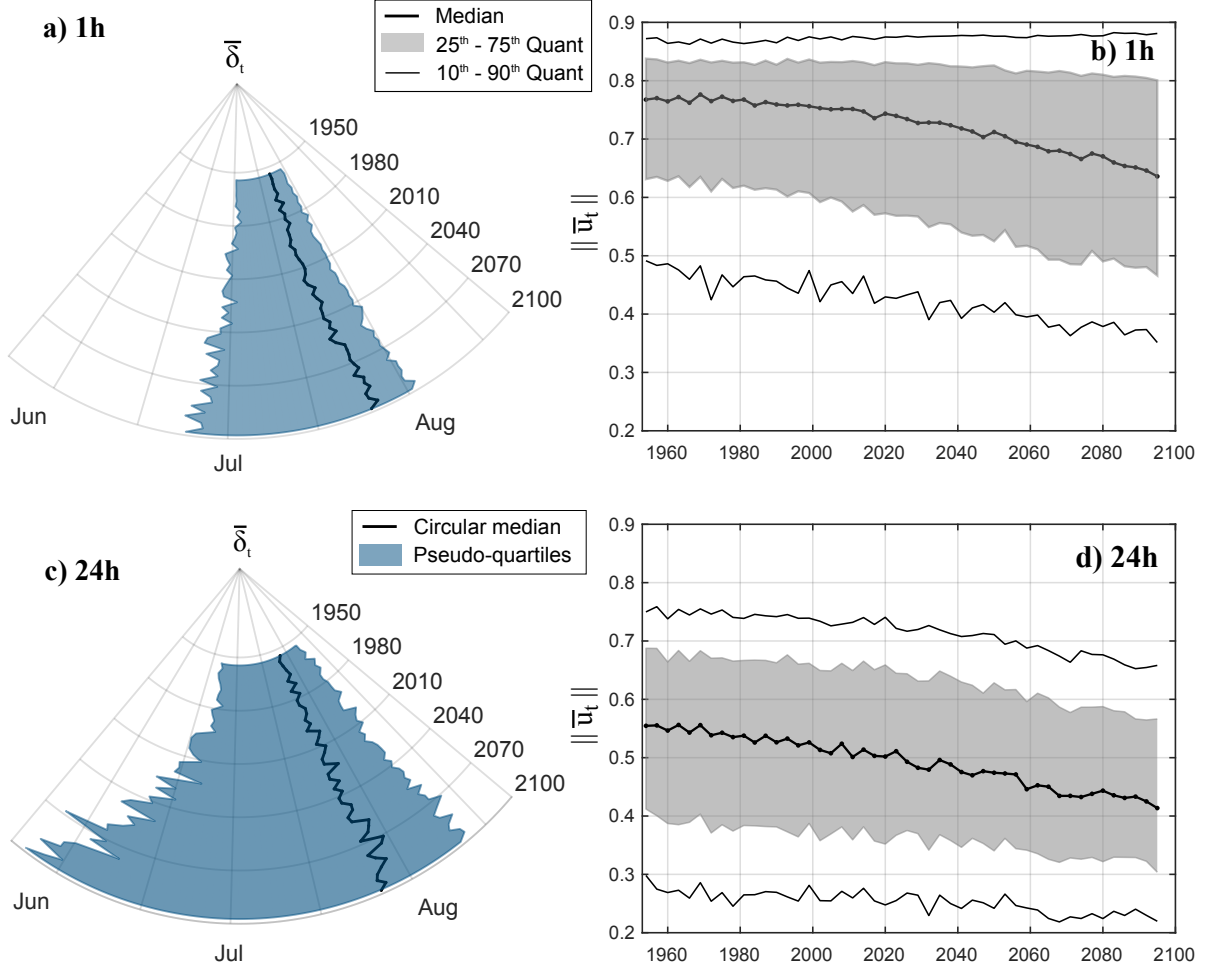


Figure 3.7: Distribution over CRCM5 grid boxes of the mean date of occurrences of AM (annual cycle) over each 3SP for a) $d = 1h$ and c) $d = 24h$ (for simplicity, axis have been rotated 90° , i.e. $\delta_t = 0$ at the top of each graph); distribution over CRCM5 grid boxes of the length of mean date vectors, $\|\bar{\mathbf{u}}_t\|$, for b) $d = 1h$ and d) $d = 24h$.

Great Lake and Atlantic coasts at the end of the 21st century, while in the southern continental areas annual peaks of daily AM are projected to occur more frequently during spring in future climate [see, for instance, Fig. S3 of the Supplementary material].

As expected, hourly extremes showed weaker seasonality than daily AM and annual cycles more peaked around their mean. In fact, larger $\|\bar{\mathbf{u}}_t\|$ values were observed for $d = 1h$ compared to $d = 24h$ [Fig. 3.7b-d], which indicates that the AM occurrence dates have less dispersed distributions for any given sub-period t . Also, the length

of mean vectors decreased in time for both hourly and daily AM, with significant $\|\bar{\mathbf{u}}_t\|$ trends detected at more than 75% of grid boxes for all durations and pooling strategies (not shown). This means that AM are expected to occur over a wider period of the year in future decades over most grid-boxes. Annual cycles of AM occurrences over many regions are therefore expected to be more dispersed around their mean values in a future warmer climate. Preliminary analyses on the circular skewness and kurtosis of $\delta_{i,t}$ values further supported this conclusion, as they showed a global tendency to more symmetric and less peaky grid

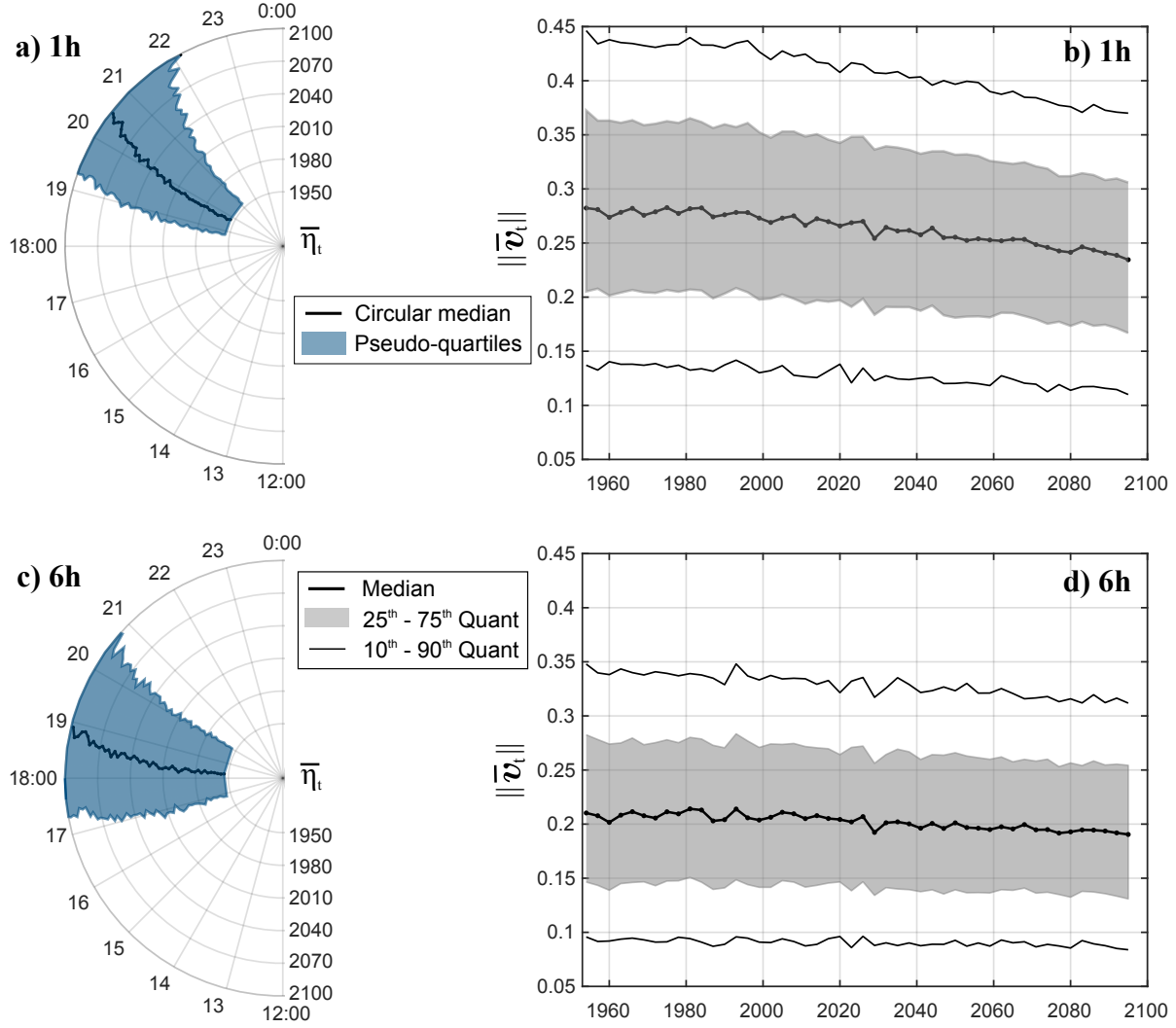


Figure 3.8: Distribution over CRCM5 grid boxes of the mean time of occurrences of AM (daily cycle) over each 3SP for a) $d = 1h$ and c) $d = 6h$ (for simplicity, axis have been rotated 90° , i.e. $\bar{\eta}_t = 0$ at the top of each graph, and time of the day is represented clockwise); distribution over CRCM5 grid boxes of the length of mean time vectors, $\|\bar{v}_t\|$, for b) $d = 1h$ and d) $d = 6h$.

box annual cycles, especially for sub-daily durations (not shown).

Important decreasing decadal percent variations were estimated for $\|\bar{\mathbf{u}}_t\|$ with different spatial patterns for different durations, with $b_{\|\bar{\mathbf{u}}_t\|} \leq -2\%/10yr$ ($b_{\|\bar{\mathbf{u}}_t\|} \leq -3\%/10yr$) for more than 20% of the grid boxes for hourly (daily) AM occurrences. Changes were generally more important in northern regions west of Great Lakes and coastal Atlantic areas, where the local temporal variability of AM occurrence dates is expected to

substantially change, especially for for daily and longer extremes [e.g., Fig. S4 of the Supplementary material].

Figure 3.8 shows the statistics for the daily cycles of AM occurrences for each 3SP. It shows that mean occurrences, $\bar{\eta}_t$, of hourly AM are concentrated between 19:00 and 21:00 for most of the grid boxes over the 1950-2000 period. During the following decades, hourly AM occur, on average, later in the evening. Similarly, for many grid boxes, mean occurrences of 6h AM generally

ranges between 17:00 and 20:00 for the 1950-2010 period, while a shift toward later mean daily time of occurrence is observed later in the 21st century [Fig. 3.8b].

For most grid boxes, however, the variability of $\eta_{i,t}$ within each sub-period was important, making it difficult the identification of a clear peak daily time of occurrence. This resulted in relatively small $\|\bar{\mathbf{v}}_t\|$ values (smaller than 0.5 for almost all grid boxes) which generally displayed significant decreasing trends for the shortest durations (e.g., for at least 50 % of grid boxes for $d \leq 3\text{h}$), especially in south-east areas (not shown). Hence, the times of occurrence of sub-daily AM were relatively evenly distributed over the 24-hour circle within each sub-period t and $\bar{\eta}_t$ is likely a poor approximation of the daily cycle mode, especially for the projected future climate.

3.4.3 Changes in AM spatiotemporal structure

Grid-box distribution of the estimated SD and LD scaling parameters [Eq. (3.2)] are shown in Fig. 3.9 for each 3SP. Confirming previous investigations on the spatiotemporal scaling of gridded datasets [Innocenti et al. [under review](#)], SD displays stronger scaling regimes (i.e. higher h_0 and h_1 values) than LD. This implies that changes in AM quantiles due to changes in the spatiotemporal scale (r, d) are more important for SD because short duration extremes are generated by spatially and temporally more heterogeneous weather systems.

Moreover, temporal scaling parameters decreased with t for both SD and LD [Fig. 3.9, 1st row]. This indicates that the changes of point-scale AM

quantiles across durations are expected to be less important in future climate than those observed in past periods. Similar results were also reported in previous studies [e.g., Cannon and Innocenti 2018 and references therein], that projected the increase of simple scaling exponents for rainfall intensity distributions or, equivalently, the change of IDF slopes towards more negative values. Note, in fact, that point-scale IDF slopes can be expressed as $h_0^{int} = h_0 - 1$, where h_0^{int} is the temporal scaling parameters for AM precipitation intensity. The projected decreases of h_0 in time may thus be explained by the relatively stronger intensification of short duration extremes compared to longer ones.

Increases of the spatiotemporal scaling parameter, $h_{1,t}$, were observed for the shortest return period, while trends are less obvious for $q \geq 25\text{-yr}$, especially for SD [Fig. 3.9, 2nd row]. Hence, the heterogeneity of the spatial characteristics of precipitation events producing AM is expected to increase in future decades, as higher h_1 values corresponds to larger variations of the ARFs [see Eq. (3.3)] for a specific change in the spatiotemporal scale (r, d) . Also, $h_{1,t}$ estimates showed higher local variability (not show) and larger temporal fluctuations than $h_{0,t}$ for $q \geq 25\text{-yr}$ [see, for instance, median curves in Fig. 3.9], suggesting that large uncertainty affect the spatiotemporal scaling estimation for relatively small samples, as previously found by Innocenti et al. ([under review](#)).

The analysis of the spatial distribution of scaling parameter trends revealed that important decadal percent variations were observed for both $h_{0,t}$ and $h_{1,t}$, especially in north-eastern areas, as shown in Fig. 3.10. For h_0 , significantly negative trends were observed for most of the grid boxes, with smallest changes (e.g., $0.3 \leq b_{h_{0,t}} \leq 0.$) found for

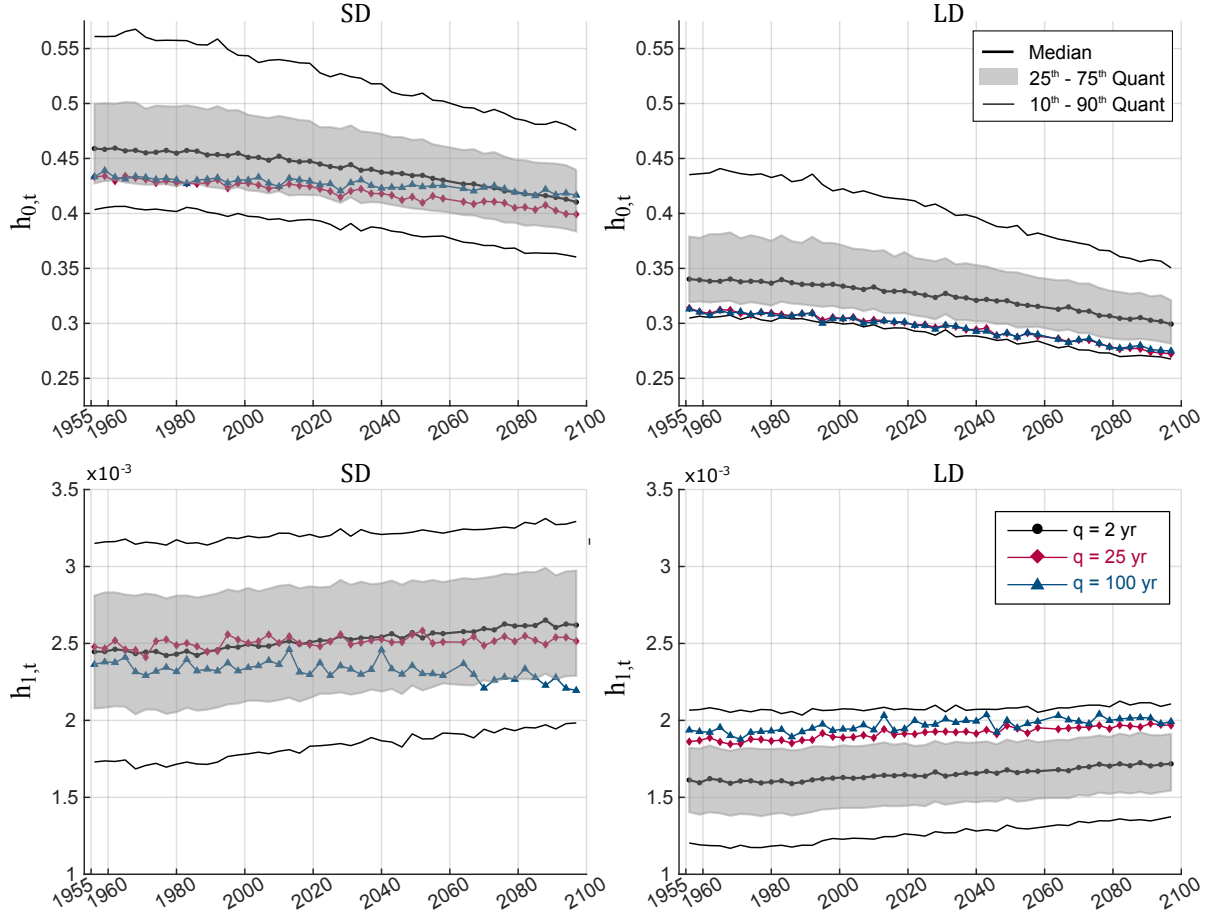


Figure 3.9: Distribution over CRCM5 grid boxes of temporal ($h_{0,t}$, 1st row) and spatiotemporal ($h_{1,t}$, 2nd row) scaling parameters for each 3SP period (x-axis) and for SD (left col.) and LD (right col.).

the Great Lake region and the southern Atlantic coast [Fig. 3.10, 1st row]. Significant trends were found for a smaller fraction of grid boxes for h_1 , while some differences emerged between northern (positive) and southern (negative and generally not significant) $b_{h_{1,t}}$ estimates, especially evident for SD [Fig. 3.10, 2nd row].

Note that, although the decadal percent variations for longer return periods were larger and characterized by similar spatial distributions than those presented in Fig. 3.10, the fraction of field significant trends for $q = 100\text{yr}$ was generally low (e.g., lower than 1%) for h_0 SD estimates and for h_1 (for both SD and LD). Moreover f_{H_1} slightly decreased when increasing the number of years

pooled within each sub-period (not shown). This underlines that changes in the spatiotemporal structure of projected AM distributions are more difficult to assess for more extreme quantiles, especially for the shortest durations, while the reduction of the scaling parameter series length due to the use of longer pooling periods (i.e. 3SP and 7SP) affects the power of the FDR MK test for trend detection.

SS-GEV estimated parameters are presented in Fig. 3.11 for each 3SP considering the reference duration $d^* = 1h$ for SD and $d^* = 24h$ for LD at the native CRCM5 spatial resolution ($r = 12\text{km}$). This figure confirms the statistically significant decrease of the temporal scaling parameter [Fig.

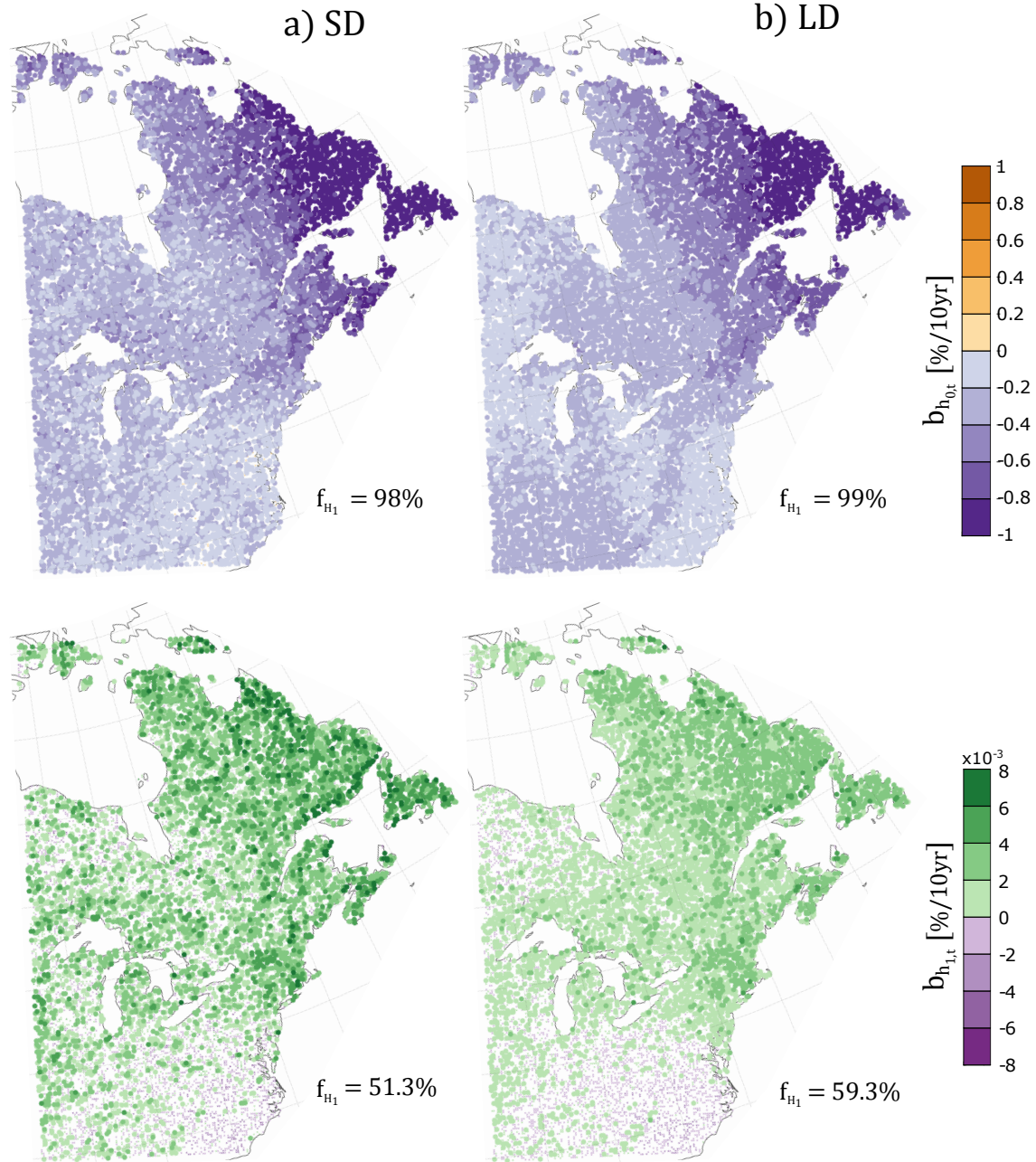


Figure 3.10: Spatial distribution of the expected decadal percent variation for 3SP scaling parameters $h_{0,t}$ (1st row; decreasing significant trends at the $\alpha_{glo} = 0.1$ FDR level) and $h_{1,t}$ (2nd row; increasing significant trends at the $\alpha_{glo} = 0.1$ FDR level) estimated for 2-yr quantiles for a) SD and b) LD. Smaller points represent grid boxes with no statically significant trend. The percentage f_{H1} of grid boxes with significant trend is indicated in each panel.

3.11a] and the increase of the scale and location SS-GEV parameters [Fig. 3.11c-d] with t that were suggested by results in previous sections for most of grid boxes. Results for coarser spatial scale (i.e. $r > 12\text{km}$) were consistent with these

estimates (not shown).

Moreover, Fig. 3.11 highlights four important results. First, the difference between short and long duration scaling regimes is important, as SD

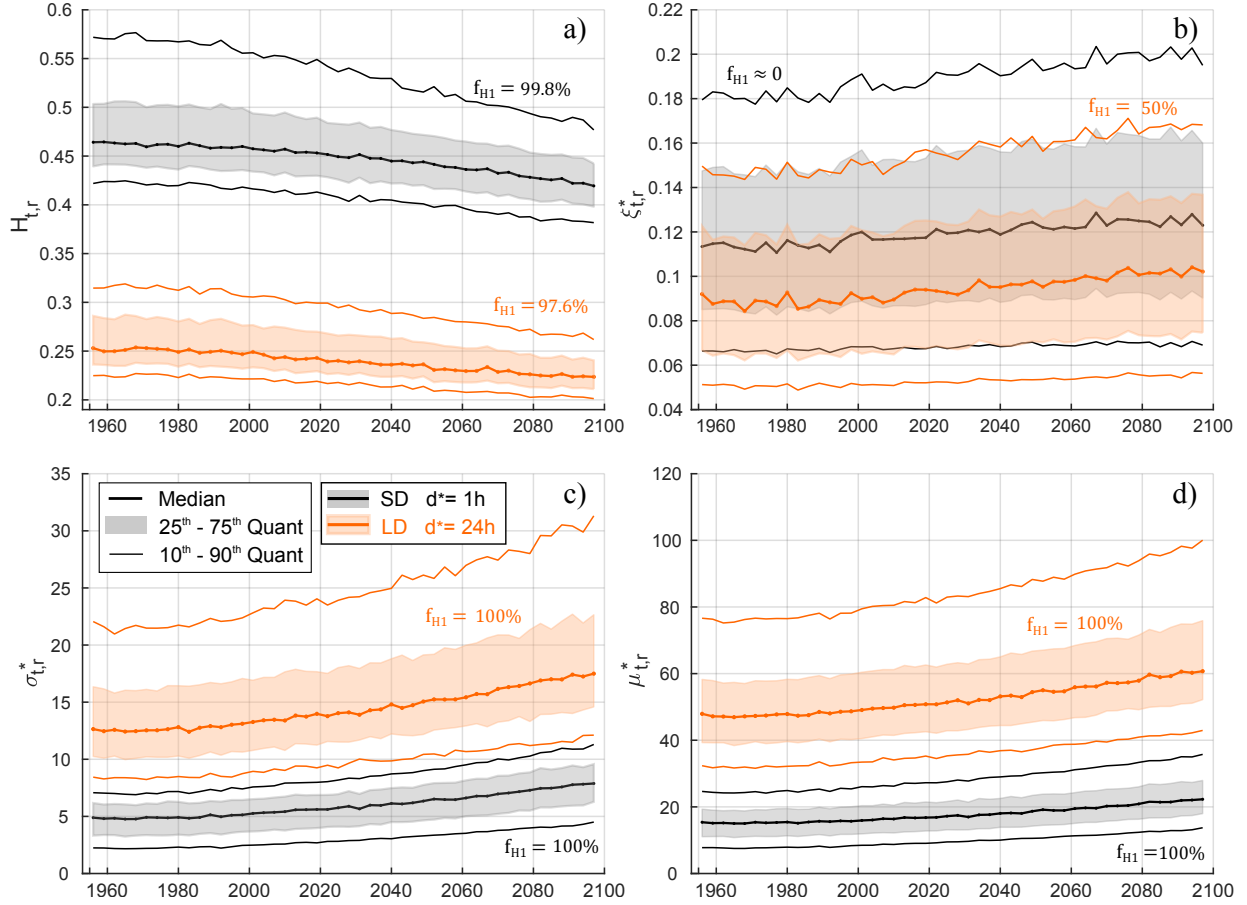


Figure 3.11: Distribution over CRCM5 grid boxes of SS-GEV parameters for the reference duration d^* at the native spatial resolution (i.e. $r = 12\text{km}$): a) temporal simple scaling exponent, $H_{t,r}$, b) shape, (only grid boxes with $\xi^* > 0$ are considered), c) scale, and d) location. The percentage f_{H1} of grid boxes with significant trend (MK test at the FDR $\alpha_{glo} = 0.1$ level) is reported in each panel.

scaling parameters take larger values than for LD [Fig. 3.11a].

Second, $H_{r,t}$ values estimated for $r = 12, 24, \dots, 72\text{km}$ verified, for each sub-period, the linear relationship $H_{t,r} = h_{0,t} + h_{1,t}r$ presented in Eq. (3.2) for empirical quantile scaling (not shown). Equally important, the scale and location SS-GEV parameters also varied linearly with r [e.g., Fig. S6 of the Supplementary material]. These linear relationships between the reference duration $\mu_{t,r}^*$ and $\sigma_{t,r}^*$ values and the spatial scales were statistically significant for most of grid boxes. However, higher uncertainty characterized the spatiotemporal scaling of the SS-GEV shape

estimates. It was therefore not possible to define a unique function for describing the dependence of $\xi_{t,r}^*$ on the spatial scale r for all grid boxes [see the examples in Fig. S6 of the Supplementary material].

Third, the SS-GEV distributions were mostly heavy tailed, with 3SP shape parameters being significantly positive for more than 72% and 59% of grid boxes for each t and for SD and LD respectively. The proportions of 3SP Gumbel distributions ($\xi_{t,r}^* = 0$) were considerably lower than the corresponding SD and LD proportions estimated for non scaling GEV models (e.g, $0.15 \leq f_{\xi_{t,r}^*=0} \leq 0.21$ for SD and

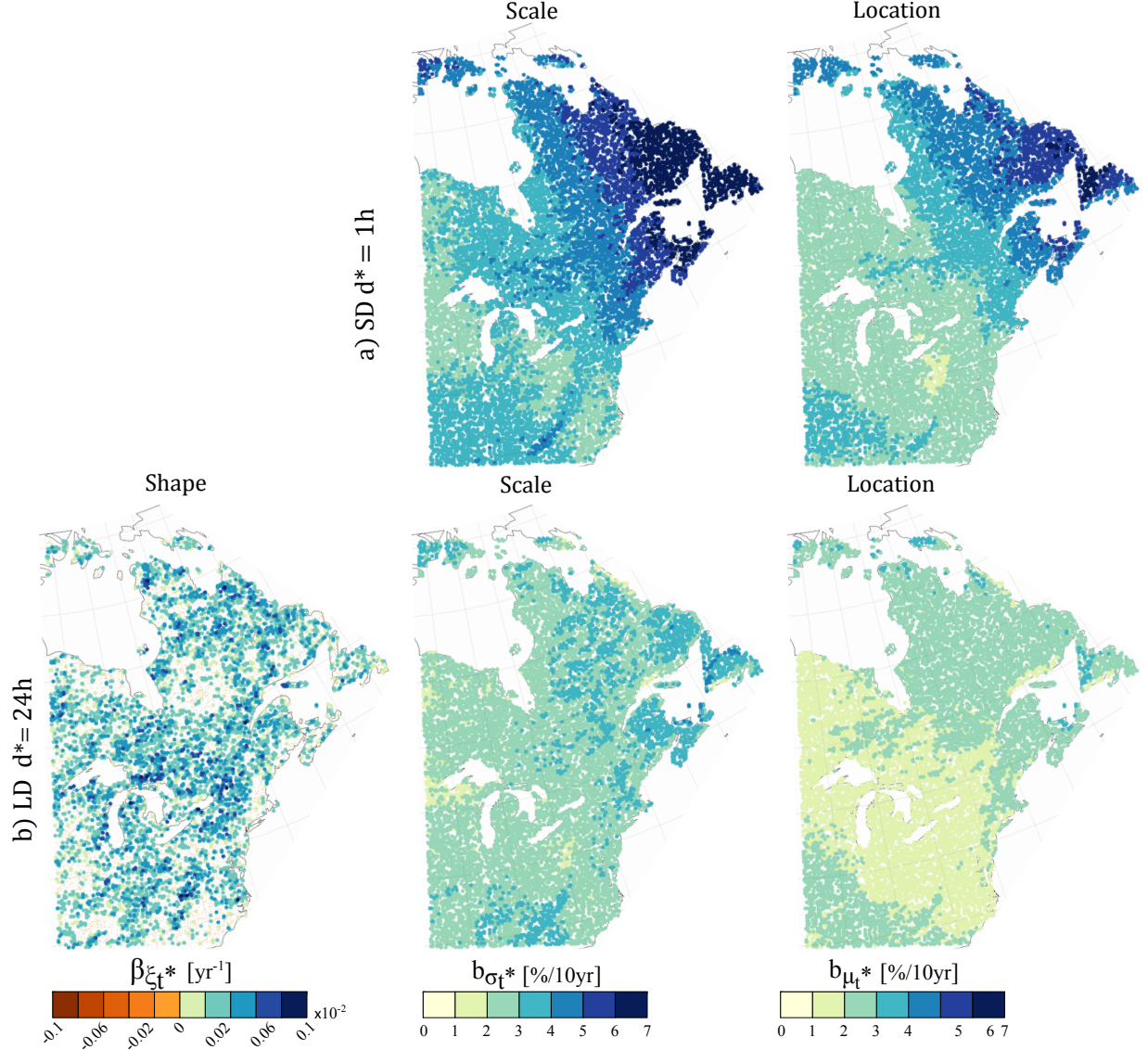


Figure 3.12: Spatial distribution of the decadal percent variation of SS-GEV parameters for a) SD ($d^* = 1h$) and b) LD ($d^* = 24h$) at the native spatial resolution (i.e. $r = 12km$): shape (1st col.; only LD estimations are shown, as SD virtually no significant trend was detected), scale (2nd col.), and location (3rd col.). Smaller points represent grid boxes with no statically significant trend (MK test at the FDR $\alpha_{glo} = 0.1$ level) .

$0.16 \leq f_{\xi_{t,r}=0} \leq 0.31$ for LD), and $f_{\xi_{t,r}=0}$ decreased with time, especially for LD [see Fig. S7 of the Supplementary material for examples on various spatial scales]. Moreover, while virtually no grid box rejected the FDR MK test null hypothesis for SD for all pooling strategies, statistically significant increasing trends were detected for the LD shape parameter values for 50.5%

of grid boxes [Fig. 3.11b for 3SP, while 50.7% and 42.0% of significantly increasing trend were detected for 1SP and 7SP respectively]. These results are particularly important since they suggest that crucial modifications can be expected for the characteristics of AM probability distribution tails, which have huge impacts on the statistical properties of more extreme AM quantiles.

Four, SD shape parameter values were larger than corresponding LD values for each 3SP for more 61% of grid boxes, as also shown by the SD and LD $\xi_{t,r}^*$ distributions [Fig. 3.11b; note that only $\xi_{t,r}^* > 0$ are considered in these figure]. Accordingly, SD extremes displayed heavier tailed distributions than longer duration AM, which is consistent with the hypothesis that links shape parameter changes to changes in the characteristics precipitation systems generating AM [Ragulina and Reitan 2017].

Figure 3.12 presents the spatial distribution of the temporal trends estimated at the native CRCM5 resolution for $\xi_{t,r}^*$, $\sigma_{t,r}^*$, and $\mu_{t,r}^*$. Decadal percent variations are shown for the scale and location parameters for SD ($d^* = 1\text{h}$) and LD ($d^* = 24\text{h}$), while the annual (absolute) variation $\beta_{\xi_{t,r}^*} [\text{yr}^{-1}]$ is considered for the SS-GEV shape for LD, virtually no significant trend having been detected for SD shape parameters. Trends estimated for $H_{r,t}$ are not shown, as consistent with results presented for empirical quantile in Fig. 3.9 and 3.10 [e.g., Fig. S8-S9 of the supplementary material].

As expected, the projected annual variations of SS-GEV shape parameters displayed a weaker spatial coherence than those estimated for the location and scale parameters. Decadal percent increases for $\sigma_{t,r}^*$, and $\mu_{t,r}^*$ were important in north-eastern regions for SD, while smaller increases (e.g. $\approx 2\%/10\text{-yr}$) were estimated in western areas. Also, smaller increases were observed over the North Atlantic and St-Lawrence gulf coasts for LD suggesting coastal effects for daily and longer duration AM trends [Fig. 3.12b]. Finally, note that $\sigma_{t,r}^*$ trends estimated in some areas were larger than those found for $\mu_{t,r}^*$ over corresponding grid boxes [e.g., over the Great Lake region for SD, Fig. 3.12a]. Standardized measures of AM distribution dispersion, such as the nor-

malized dispersion coefficient $\sigma_{t,r}^*/\mu_{t,r}^*$, are thus expected to increase in time, as suggested by Cannon and Innocenti (2018) in a recent study, and displayed significantly increasing trends for most of grid boxes [e.g., Fig. S10 of the Supplementary material]. However, high cross-correlation usually affect $\xi_{t,r}^*$ and $\sigma_{t,r}^*$ ML estimates and $\sigma_{t,r}^*/\mu_{t,r}^*$ trends may strongly depend on the temporal evolution of the SS-GEV shape parameter. Hence, the impacts of stationary and non-stationary assumptions for $\xi_{t,r}^*$ on the mentioned result should be further investigated.

Finally note that consistent results were also found for coarser spatial scale (i.e. $r > 12\text{km}$), despite the fact that the trend magnitude decreased with increasing r [e.g., Fig. S9-S10 of the Supplementary material].

3.5 Discussion and Conclusion

The spatiotemporal structure of precipitation extremes is expected to change with global warming, which can have dramatic impacts on the hydrological response of local and regional ecosystems. The projected changes in the statistical properties of sub-daily and daily precipitation extremes were investigated using the recently available initial-condition CRCM5-LE. Specifically, the impacts of global warming on AM probability distributions (empirical AM quantiles and GEV distribution parameters), annual and daily cycles (date and time of AM occurrences), and spatiotemporal structure (AM quantile and SS-GEV scaling) were considered.

The CRCM5-LE is constituted by 50 equiprobable climate realizations over the 1954-2099 period, that downscale at the 0.11° resolution the

CanESM2-LE (RCP8.5 forcing). Simulated grid box precipitation series were pooled over short sub-periods of 1, 3, and 7 years to create large samples that were used for estimating AM statistics at various spatial scales and durations (1h to 72h). For the spatiotemporal scaling, the analysis was conducted separately for SD ($1h \leq d < 6h$) and LD ($6h \leq d \leq 72h$) AM series. The significance and the magnitude of trends for extreme characteristics were assessed on the time series of AM quantiles, AM occurrence date and time statistics, and GEV and SS-GEV parameters.

Results globally confirmed the theoretical arguments pointing at the intensification of extreme precipitation over the study domain, with relatively stronger trends for short duration AM and more extreme events. This conclusion is consistent with previous analyses over North America [e.g., Mailhot et al. 2012, Kharin et al. 2018], and was highlighted by both the results on AM empirical quantiles and the analysis of their spatiotemporal scaling.

Increasing trends in AM empirical quantiles were observed for most grid boxes, and hourly AM decadal percent variations were larger than those estimated for daily AM. Trends were also more important for more extreme AM quantiles and northern grid boxes.

The empirical temporal scaling parameters $h_{0,t}$ displayed decreasing trends in time, which corresponds to a decrease in point-scale IDF slopes toward more negative values. The decadal percent variations of $h_{0,t}$ were statistically significant and negative for most grid boxes for 2-yr AM quantiles, for both SD and LD intervals, while for longer return periods field significant trends were only found for LD.

The estimated trends for spatiotemporal scaling parameters $h_{1,t}$ suggest that changes may be ex-

pected in the spatial structure of empirical AM quantiles in future climate. In particular, the variability of ARF values across the spatiotemporal scales (r, d) is projected to increase, as $h_{1,t}$ increased with time, especially for northern regions. However, large uncertainty affects $h_{1,t}$ estimation and projected trends were not significantly different from zero for most of the grid boxes when considering return periods $q \geq 25$ yr. Interestingly, SD showed larger but fewer significant decadal percent increases than LD.

No meaningful temporal change was observed for the mean date of AM occurrences for daily and sub-daily durations for most grid boxes. However, increasing seasonal variability of hourly and daily AM is expected in future decades, as the dates of AM occurrences are projected to be more dispersed around their summer peaks. Hence, more frequent warm meteorological conditions [e.g., Vincent et al. 2018] are likely to increase the probability of occurrence of intense precipitation events over an extended summer season. However, the temporal changes in annual peak dates and seasonal variability also showed a well defined spatial structure over the study domain for daily and longer durations, which suggests that different mechanisms may drive observed changes in different areas.

A small shift toward later mean time of occurrence was projected for future sub-daily AM, suggesting that their daily peak frequency of is expected to occur later in the evening compared to past climate. Basic considerations on projected temperature increases (e.g., higher evening and night temperatures or possible changes in the surface heat budget) could partly explain this result. However, various other factors and local and large-scale land-atmosphere feedbacks may influence this result [Lo et al. 2017 and references

therein].

Considering GEV and SS-GEV models, the fraction of grid boxes with heavy-tailed AM distributions was generally found to increase with time. In particular, increasing fractions of grid boxes with significant and positive shape parameters were found for SS-GEV for both SD and LD at the native CRCM5 spatial resolution. Classical GEV models (i.e., without scaling) presented similar results for all durations $d \geq 3h$, although the fraction of grid boxes with Gumbel distributions weakly increased in time for 1h AM. Accordingly, the assumption of Gumbel distributions ($\xi_t = 0$) is often inadequate in future climate for sub-daily AM and could lead to important underestimations of long return period quantiles.

Some evidence for statistically significant trends of the SS-GEV shape parameter values was also observed, with most of grid boxes displaying significant increases of ξ_t^* for LD. This result is important as it suggests that the assumption of a stationary GEV distribution shape parameter, often made because of the large uncertainties affecting its estimation [Katz 2013], may be inadequate for the analysis of daily and sub-daily AM. Limiting the range of possible changes detectable for AM distribution tails, the stationary hypothesis may thus affect the projected changes for other GEV distribution parameters (e.g., for the scale parameter) and/or more extreme precipitation quantiles. At the same time, however, weaker statistical evidence was found for trends in SD SS-GEV shape parameters and changes in longer return period quantiles were mainly observed through significant increases of the scale-location parameter ratios, $\sigma_{t,r}^*/\mu_{t,r}^*$. It is therefore more difficult to provide a robust assessment of extreme precipitation characteristics and their changes for the shortest durations, even when

data from various d and from different model members are pooled.

Considering the ensemble of these results caution is advised when using very long precipitation series for the assessment of climate change impacts on AM characteristics, as also suggested by DeGaetano and Castellano (2018). In fact, while there exists a clear advantage in using large samples of precipitation extremes for improving the estimation of most uncertain AM statistics (e.g., GEV shape distribution parameters or spatiotemporal scaling statistics), important non-stationarities characterize the AM probability distributions (e.g., changes in GEV location and scale parameters) over very short period of time (e.g., 10 years).

Future works should thus consider the possibility of introducing temporal trends in SS-GEV models (e.g., for spatiotemporal scaling and/or probability distribution parameters) and further explore the relationships between the SS-GEV parameters and the spatial scale at which precipitation extremes are extracted.

Moreover, it would be important to extend this study to higher-resolution climate model simulations in order to assess the possible impact of convection representation on the reported conclusion, especially those related to the diurnal cycle and short duration AM. In particular, the use of a large-ensemble from a parametrized RCM may in fact represent a strong constraint on the type of the detectable changes for precipitation characteristics, especially limiting the assessment of the nonstationarity of the extreme precipitation spatiotemporal structure.

Similarly, modifications in timing and seasonality of sub-daily extremes should be more thoughtfully analyzed to better understand the weather processes and climate feedbacks explaining the pro-

jected changes, while other RCM large ensembles should be considered to evaluate the impacts of models on these results.

As a final remark, the practical implications of the presented results need also to be further examined, as the consequences of the highlighted changes in IDF and IDA curve characteristics may be critical in terms of long- and mid-term infrastructure design and engineering practice [Mailhot and Duchesne 2010].

Acknowledgments Silvia Innocenti’s scholarship was partly provided by the Consortium OURANOS. The Discovery Grants Program from the Natural Science and Engineering Research Council of Canada also offered financial support for this project. The ClimEx project was financed by the Bavarian State Ministry for the Environment and Consumer Protection. CRCM5 simulations were run by SuperMUC supercomputer at Leibniz Supercomputing Centre (LRZ) of the Bavarian Academy of Sciences and Humanities and funded via the Gauss Centre for Supercomputing (GCS) by the German Federal Ministry of Education and Research and the Bavarian State Ministry of Education, Science and the Arts. The CRCM5 was developed by the ES-CER centre of Université du Québec à Montréal (UQAM) in collaboration with Environment and Climate Change Canada. The Canadian Centre for Climate Modelling and Analysis (CCCma) executed and made available the CanESM2-LE for the ClimEx project. We acknowledge the Canadian Sea Ice and Snow Evolution Network for proposing the simulations.

Data availability The CRCM5-LE dataset for the north eastern North America domain can be obtained upon request contacting Ouranos.

References

- Arora, V. K., J. F. Scinocca, G. J. Boer, J. R. Christian, K. L. Denman, G. M. Flato, V. V. Kharin, W. G. Lee and W. J. Merryfield (2011). “Carbon emission limits required to satisfy future representative concentration pathways of greenhouse gases”. *Geophysical Research Letters* 38.5, L05805. DOI: [10.1029/2010GL046270](https://doi.org/10.1029/2010GL046270).
- Barbero, R., H. J. Fowler, G. Lenderink and S. Blenkinsop (2017). “Is the intensification of precipitation extremes with global warming better detected at hourly than daily resolutions?”: *Geophysical Research Letters* 44.2, 2016GL071917. DOI: [10.1002/2016GL071917](https://doi.org/10.1002/2016GL071917).
- Beck, H. E., A. I. J. M. Van Dijk, V. Levizzani, J. Schellekens, D. G. Miralles, B. Martens and A. de Roo (2017). “MSWEP: 3-hourly 0.25° global gridded precipitation (1979–2015) by merging gauge, satellite, and reanalysis data”. *Hydrol. Earth Syst. Sci.* 21.1, 589–615. DOI: [10.5194/hess-21-589-2017](https://doi.org/10.5194/hess-21-589-2017).
- Benjamini, Y. and Y. Hochberg (1995). “Controlling the False Discovery Rate: A Practical and Powerful Approach to Multiple Testing”. *Journal of the Royal Statistical Society. Series B (Methodological)* 57.1, 289–300.
- Benoit, K. (2011). “Linear regression models with logarithmic transformations”. *London School of Economics, London* 22.1, 23–36.
- Berens, P. (2009). “CircStat: A MATLAB Toolbox for Circular Statistics | Berens | Journal of Statistical Software”. 31.10. DOI: [10.18637/jss.v031.i10](https://doi.org/10.18637/jss.v031.i10).
- Blain, G. C. (2013). “The modified Mann-Kendall test: on the performance of three variance correction approaches”. *Bragantia* 72.4, 416–425. DOI: [10.1590/brag.2013.045](https://doi.org/10.1590/brag.2013.045).
- Blanchet, J., D. Ceresetti, G. Molinié and J.-D. Creutin (2016). “A regional GEV scale-invariant framework for Intensity-Duration-Frequency analysis”. *Journal of Hydrology* 540, 82–95. DOI: [10.1016/j.jhydrol.2016.06.007](https://doi.org/10.1016/j.jhydrol.2016.06.007).
- Burlando, P. and R. Rosso (1996). “Scaling and multiscaling models of DDF for storm precipitations”. *Journal of Hydrology* 187, 45–64. DOI: [10.1016/S0022-1694\(96\)03086-7](https://doi.org/10.1016/S0022-1694(96)03086-7).
- Cannon, A. J. and S. Innocenti (2018). “Projected intensification of sub-daily and daily rainfall extremes in convection-permitting climate model simulations over North America: Implications for future Intensity-Duration-Frequency curves”. *Natural Hazards and*

- Earth System Sciences Discussions*, 1–29. DOI: <https://doi.org/10.5194/nhess-2018-290>.
- Casas-Castillo, M. C., A. Llabres-Brustenga, A. Rius, R. Rodriguez-Sola and X. Navarro (2018). “A single scaling parameter as a first approximation to describe the rainfall pattern of a place: application on Catalonia”. *Acta Geophysica*, 1–10. DOI: [10.1007/s11600-018-0122-5](https://doi.org/10.1007/s11600-018-0122-5).
- Ceresetti, D. (2011). “Structure spatio-temporelle des fortes précipitations: application à la région Cévennes-Vivarais”. PhD thesis. Université de Grenoble.
- Coles, S. G. (2001). *An Introduction to Statistical Modeling of Extreme Values*. London: Springer.
- Cunnane, C. (1978). “Unbiased plotting positions : A review”. *Journal of Hydrology* 37.3-4, 205–222. DOI: [10.1016/0022-1694\(78\)90017-3](https://doi.org/10.1016/0022-1694(78)90017-3).
- Dee, D. P., S. M. Uppala, A. J. Simmons, P. Berrisford, P. Poli, S. Kobayashi, U. Andrae, M. A. Balmaseda, G. Balsamo, P. Bauer, P. Bechtold, A. C. M. Beljaars, L. van de Berg, J. Bidlot, N. Bormann, C. Delsol, R. Dragani, M. Fuentes, A. J. Geer, L. Haimberger, S. B. Healy, H. Hersbach, E. V. Hólm, L. Isaksen, P. Kållberg, M. Köhler, M. Matricardi, A. P. McNally, B. M. Monge-Sanz, J.-J. Morcrette, B.-K. Park, C. Peubey, P. de Rosnay, C. Tavalato, J.-N. Thépaut and F. Vitart (2011). “The ERA-Interim reanalysis: configuration and performance of the data assimilation system”. *Quarterly Journal of the Royal Meteorological Society* 137.656, 553–597. DOI: [10.1002/qj.828](https://doi.org/10.1002/qj.828).
- DeGaetano, A. T. and C. Castellano (2018). “Selecting Time Series Length to Moderate the Impact of Nonstationarity in Extreme Rainfall Analyses”. *Journal of Applied Meteorology and Climatology* 57.10, 2285–2296. DOI: [10.1175/JAMC-D-18-0097.1](https://doi.org/10.1175/JAMC-D-18-0097.1).
- Deser, C., R. Knutti, S. Solomon and A. S. Phillips (2012). “Communication of the role of natural variability in future North American climate”. *Nature Climate Change* 2.11, 775–779. DOI: [10.1038/nclimate1562](https://doi.org/10.1038/nclimate1562).
- Dhakal, N., S. Jain, A. Gray, M. Dandy and E. Stancioff (2015). “Nonstationarity in seasonality of extreme precipitation: A nonparametric circular statistical approach and its application”. *Water Resources Research* 51.6, 4499–4515. DOI: [10.1002/2014WR016399](https://doi.org/10.1002/2014WR016399).
- Dwyer, J. G. and P. A. O’Gorman (2017). “Changing duration and spatial extent of midlatitude precipitation extremes across different climates”. *Geophys. Res. Lett.* 44.11, 2017GL072855. DOI: [10.1002/2017GL072855](https://doi.org/10.1002/2017GL072855).
- Eggert, B., P. Berg, J. O. Haerter, D. Jacob and C. Moseley (2015). “Temporal and spatial scaling impacts on extreme precipitation”. *Atmos. Chem. Phys.* 15.10, 5957–5971. DOI: [10.5194/acp-15-5957-2015](https://doi.org/10.5194/acp-15-5957-2015).
- Fatichi, S., V. Y. Ivanov, A. Paschalis, N. Peleg, P. Molnar, S. Rimkus, J. Kim, P. Burlando and E. Caporali (2016). “Uncertainty partition challenges the predictability of vital details of climate change”. *Earth’s Future* 4.5, 240–251. DOI: [10.1002/2015EF000336](https://doi.org/10.1002/2015EF000336).
- Fischer, E. M. and R. Knutti (2016). “Observed heavy precipitation increase confirms theory and early models”. *Nature Climate Change* 6.11, nclimate3110. DOI: [10.1038/nclimate3110](https://doi.org/10.1038/nclimate3110).
- Flato, G., J. Marotzke, B. Abiodun, P. Braconnot, S. C. Chou, W. Collins, P. Cox, F. Driouech, S. Emori, V. Eyring, et al. (2013). “Evaluation of climate models”. *Climate Change 2013: The Physical Science Basis. Contribution of Working Group I to the Fifth Assessment Report of the Intergovernmental Panel on Climate Change*. Cambridge University Press, 741–866.
- Fyfe, J. C., C. Derksen, L. Mudryk, G. M. Flato, B. D. Santer, N. C. Swart, N. P. Molotch, X. Zhang, H. Wan, V. K. Arora, J. Scinocca and Y. Jiao (2017). “Large near-term projected snowpack loss over the western United States”. *Nature Communications* 8, 14996. DOI: [10.1038/ncomms14996](https://doi.org/10.1038/ncomms14996).
- Guinard, K., A. Mailhot and D. Caya (2015). “Projected changes in characteristics of precipitation spatial structures over North America”. *International Journal of Climatology*, n/a–n/a. DOI: [10.1002/joc.4006](https://doi.org/10.1002/joc.4006).
- Gupta, V. K. and E. Waymire (1990). “Multiscaling properties of spatial rainfall and river flow distributions”. *Journal of Geophysical Research: Atmospheres* 95.D3, 1999–2009. DOI: [10.1029/JD095iD03p01999](https://doi.org/10.1029/JD095iD03p01999).
- Hawkins, E. and R. Sutton (2012). “Time of emergence of climate signals”. *Geophysical Research Letters* 39.1. DOI: [10.1029/2011GL050087](https://doi.org/10.1029/2011GL050087).
- Hawkins, E. (2011). “Our evolving climate: communicating the effects of climate variability”. *Weather* 66.7, 175–179. DOI: [10.1002/wea.761](https://doi.org/10.1002/wea.761).
- Hawkins, E. and R. Sutton (2009). “The Potential to Narrow Uncertainty in Regional Climate Predictions”. *Bulletin of the American Meteorological Society* 90.8, 1095–1107. DOI: [10.1175/2009BAMS2607.1](https://doi.org/10.1175/2009BAMS2607.1).
- Hingray, B. and M. Saïd (2014). “Partitioning Internal Variability and Model Uncertainty Components in a Multimember Multimodel Ensemble of Climate Projections”. *Journal of Climate* 27.17, 6779–6798. DOI: [10.1175/JCLI-D-13-00629.1](https://doi.org/10.1175/JCLI-D-13-00629.1).
- Hosking, J. R. M. and J. R. Wallis (1997). *Regional Frequency analysis: an approach based on L-moments*. Cambridge University Press.
- Innocenti, S., A. Mailhot and A. Frigon (2017). “Simple scaling of extreme precipitation in North America”. *Hydrol. Earth Syst. Sci.* 21.11, 5823–5846. DOI: [10.5194/hess-21-5823-2017](https://doi.org/10.5194/hess-21-5823-2017).
- Innocenti, S., A. Mailhot, A. Frigon, A. J. Cannon and M. Leduc (under review). “Observed and simulated precipitation over North East North-America: how do sub-daily extremes scale in space and time?”.
- Katz, R. W. (2013). “Statistical Methods for Nonstationary Extremes”. *Extremes in a Changing Climate*. Ed. by A. AghaKouchak, D. Easterling, K. Hsu, S. Schubert and S. Sorooshian. Water Science and Technology Library 65. Springer Netherlands, 15–37.
- Kendon, E. J., N. Ban, N. M. Roberts, H. J. Fowler, M. J. Roberts, S. C. Chan, J. P. Evans, G. Fos-

- ser and J. M. Wilkinson (2017). “Do Convection-Permitting Regional Climate Models Improve Projections of Future Precipitation Change?”. *Bulletin of the American Meteorological Society* 98.1, 79–93. DOI: [10.1175/BAMS-D-15-0004.1](https://doi.org/10.1175/BAMS-D-15-0004.1).
- Kendon, E. J., S. Blenkinsop and H. J. Fowler (2018). “When Will We Detect Changes in Short-Duration Precipitation Extremes?”. *Journal of Climate* 31.7, 2945–2964. DOI: [10.1175/JCLI-D-17-0435.1](https://doi.org/10.1175/JCLI-D-17-0435.1).
- Kharin, V. V., G. M. Flato, X. Zhang, N. P. Gillett, F. Zwiers and K. J. Anderson (2018). “Risks from Climate Extremes Change Differently from 1.5°C to 2.0°C Depending on Rarity”. *Earth’s Future* 6.5, 704–715. DOI: [10.1002/2018EF000813](https://doi.org/10.1002/2018EF000813).
- Koutsoyiannis, D. (2004a). “Statistics of extremes and estimation of extreme rainfall: I. Theoretical investigation”. *Hydrological Sciences Journal* 49.4. DOI: [10.1623/hysj.49.4.575.54430](https://doi.org/10.1623/hysj.49.4.575.54430).
- Koutsoyiannis, D. (2004b). “Statistics of extremes and estimation of extreme rainfall: II. Empirical investigation of long rainfall records”. *Hydrological Sciences Journal* 49.4. DOI: [10.1623/hysj.49.4.591.54424](https://doi.org/10.1623/hysj.49.4.591.54424).
- Koutsoyiannis, D., D. Kozonis and A. Manetas (1998). “A mathematical framework for studying rainfall intensity-duration-frequency relationships”. *Journal of Hydrology* 206.1-2, 118–135. DOI: [10.1016/S0022-1694\(98\)00097-3](https://doi.org/10.1016/S0022-1694(98)00097-3).
- Leduc, M., A. Mailhot, A. Frigon, J.-L. Martel, R. Ludwig, G. B. Brietzke, M. Giguere, F. Brissette, R. Turcotte, M. Braun and J. Scinocca (2019). “ClimEx project: a 50-member ensemble of climate change projections at 12-km resolution over Europe and northeastern North America with the Canadian Regional Climate Model (CRCM5)”. *Journal of Applied Meteorology and Climatology*. DOI: [10.1175/JAMC-D-18-0021.1](https://doi.org/10.1175/JAMC-D-18-0021.1).
- Li, C., F. Zwiers, X. Zhang and G. Li (2019). “How Much Information Is Required to Well Constrain Local Estimates of Future Precipitation Extremes?”. *Earth’s Future* 7.1, 11–24. DOI: [10.1029/2018EF001001](https://doi.org/10.1029/2018EF001001).
- Li, J., A. Sharma, F. Johnson and J. Evans (2015). “Evaluating the effect of climate change on areal reduction factors using regional climate model projections”. *Journal of Hydrology* 528, 419–434. DOI: [10.1016/j.jhydrol.2015.06.067](https://doi.org/10.1016/j.jhydrol.2015.06.067).
- Liu, C., K. Ikeda, R. Rasmussen, M. Barlage, A. J. Newman, A. F. Prein, F. Chen, L. Chen, M. Clark, A. Dai, J. Dudhia, T. Eidhammer, D. Gochis, E. Gutmann, S. Kurkite, Y. Li, G. Thompson and D. Yates (2017). “Continental-scale convection-permitting modeling of the current and future climate of North America”. *Climate Dynamics* 49.1-2, 71–95. DOI: [10.1007/s00382-016-3327-9](https://doi.org/10.1007/s00382-016-3327-9).
- Lo, M.-H., T.-H. Kuo, H.-W. Wey, C.-W. Lan and J.-P. Chen (2017). “Land Processes as the Forcing of Extremes”. *Climate Extremes*. American Geophysical Union (AGU), 75–92. DOI: [10.1002/9781119068020.ch5](https://doi.org/10.1002/9781119068020.ch5).
- Mailhot, A., I. Beauguard, G. Talbot, D. Caya and S. Biner (2012). “Future changes in intense precipitation over Canada assessed from multi-model NARCCAP ensemble simulations”. *International Journal of Climatology* 32.8, 1151–1163. DOI: [10.1002/joc.2343](https://doi.org/10.1002/joc.2343).
- Mailhot, A. and S. Duchesne (2010). “Design Criteria of Urban Drainage Infrastructures under Climate Change”. *Journal of Water Resources Planning and Management* 136.2, 201–208. DOI: [10.1061/\(ASCE\)WR.1943-5452.0000023](https://doi.org/10.1061/(ASCE)WR.1943-5452.0000023).
- Mallakpour, I. and G. Villarini (2017). “Analysis of changes in the magnitude, frequency, and seasonality of heavy precipitation over the contiguous USA”. *Theoretical and Applied Climatology* 130.1, 345–363. DOI: [10.1007/s00704-016-1881-z](https://doi.org/10.1007/s00704-016-1881-z).
- Martel, J.-L., A. Mailhot, F. Brissette and D. Caya (2018). “Role of Natural Climate Variability in the Detection of Anthropogenic Climate Change Signal for Mean and Extreme Precipitation at Local and Regional Scales”. *Journal of Climate* 31.11, 4241–4263. DOI: [10.1175/JCLI-D-17-0282.1](https://doi.org/10.1175/JCLI-D-17-0282.1).
- Martynov, A., R. Laprise, L. Sushama, K. Winger, L. Separovic and B. Dugas (2013). “Reanalysis-driven climate simulation over CORDEX North America domain using the Canadian Regional Climate Model, version 5: model performance evaluation”. *Climate Dynamics* 41.11-12, 2973–3005. DOI: [10.1007/s00382-013-1778-9](https://doi.org/10.1007/s00382-013-1778-9).
- Meinshausen, M., S. J. Smith, K. Calvin, J. S. Daniel, M. L. T. Kainuma, J.-F. Lamarque, K. Matsumoto, S. A. Montzka, S. C. B. Raper, K. Riahi, A. Thomson, G. J. M. Velders and D. P. P. v. Vuuren (2011). “The RCP greenhouse gas concentrations and their extensions from 1765 to 2300”. *Climatic Change* 109.1-2, 213. DOI: [10.1007/s10584-011-0156-z](https://doi.org/10.1007/s10584-011-0156-z).
- Mélèse, V., J. Blanchet and G. Molinié (2018). “Uncertainty estimation of Intensity–Duration–Frequency relationships: A regional analysis”. *Journal of Hydrology* 558, 579–591. DOI: [10.1016/j.jhydrol.2017.07.054](https://doi.org/10.1016/j.jhydrol.2017.07.054).
- Menabde, M., A. Seed and G. Pegram (1999). “A simple scaling model for extreme rainfall”. *Water Resources Research* 35.1, 335–339.
- Panthou, G., T. Vischel, T. Lebel, G. Quantin and G. Molinié (2014). “Characterising the space–time structure of rainfall in the Sahel with a view to estimating IDAF curves”. *Hydrology and Earth System Sciences* 18.12, 5093–5107. DOI: [10.5194/hess-18-5093-2014](https://doi.org/10.5194/hess-18-5093-2014).
- Papalexiou, S. M., D. Koutsoyiannis and C. Makropoulos (2013). “How extreme is extreme? An assessment of daily rainfall distribution tails”. *Hydrology and Earth System Sciences* 17.2, 851–862. DOI: [10.5194/hess-17-851-2013](https://doi.org/10.5194/hess-17-851-2013).
- Pewsey, A. (2004). “The large-sample joint distribution of key circular statistics”. *Metrika* 60.1, 25–32. DOI: [10.1007/s001840300294](https://doi.org/10.1007/s001840300294).
- Prein, A. F., W. Langhans, G. Fosser, A. Ferrone, N. Ban, K. Goergen, M. Keller, M. Tolle, O. Gutjahr, F. Feser, E. Brisson, S. Kollet, J. Schmidli, N. P. M. van Lipzig and R. Leung (2015). “A review on regional convection-permitting climate modeling:

- Demonstrations, prospects, and challenges”. *Reviews of Geophysics* 53.2, 2014RG000475. DOI: [10.1002/2014RG000475](https://doi.org/10.1002/2014RG000475).
- Prein, A. F., C. Liu, K. Ikeda, S. B. Trier, R. M. Rasmussen, G. J. Holland and M. P. Clark (2017). “Increased rainfall volume from future convective storms in the US”. *Nature Climate Change* 7.12, 880. DOI: [10.1038/s41558-017-0007-7](https://doi.org/10.1038/s41558-017-0007-7).
- Ragulina, G. and T. Reitan (2017). “Generalized extreme value shape parameter and its nature for extreme precipitation using long time series and the Bayesian approach”. *Hydrological Sciences Journal* 62.6, 863–879. DOI: [10.1080/02626667.2016.1260134](https://doi.org/10.1080/02626667.2016.1260134).
- Salzen, K. von, J. F. Scinocca, N. A. McFarlane, J. Li, J. N. S. Cole, D. Plummer, D. Versegny, M. C. Reader, X. Ma, M. Lazare and L. Solheim (2013). “The Canadian Fourth Generation Atmospheric Global Climate Model (CanAM4). Part I: Representation of Physical Processes”. *Atmosphere-Ocean* 51.1, 104–125. DOI: [10.1080/07055900.2012.755610](https://doi.org/10.1080/07055900.2012.755610).
- Sanderson, B. M., K. W. Oleson, W. G. Strand, F. Lehner and B. C. O’Neill (2018). “A new ensemble of GCM simulations to assess avoided impacts in a climate mitigation scenario”. *Climatic Change* 146.3, 303–318. DOI: [10.1007/s10584-015-1567-z](https://doi.org/10.1007/s10584-015-1567-z).
- Separovic, L., A. Alexandru, R. Laprise, A. Martynov, L. Sushama, K. Winger, K. Tete and M. Valin (2013). “Present climate and climate change over North America as simulated by the fifth-generation Canadian regional climate model”. *Clim Dyn* 41.11-12, 3167–3201. DOI: [10.1007/s00382-013-1737-5](https://doi.org/10.1007/s00382-013-1737-5).
- Shephard, M. W., E. Mekis, R. J. Morris, Y. Feng, X. Zhang, K. Kilcup and R. Fleetwood (2014). “Trends in Canadian Short-Duration Extreme Rainfall: Including an Intensity–Duration–Frequency Perspective”. *Atmosphere-Ocean* 52.5, 398–417. DOI: [10.1080/07055900.2014.969677](https://doi.org/10.1080/07055900.2014.969677).
- Sigmond, M. and J. C. Fyfe (2016). “Tropical Pacific impacts on cooling North American winters”. *Nature Climate Change* 6.10, 970–974. DOI: [10.1038/nclimate3069](https://doi.org/10.1038/nclimate3069).
- Skeeter, W. J., J. C. Senkbeil and D. J. Keellings (2018). “Spatial and temporal changes in the frequency and magnitude of intense precipitation events in the southeastern United States”. *International Journal of Climatology* 1.15. DOI: [10.1002/joc.5841](https://doi.org/10.1002/joc.5841).
- Svensson, C. and D. A. Jones (2010). “Review of methods for deriving areal reduction factors”. *Journal of Flood Risk Management* 3.3, 232–245. DOI: [10.1111/j.1753-318X.2010.01075.x](https://doi.org/10.1111/j.1753-318X.2010.01075.x).
- Tapiador, F. J., A. Navarro, V. Levizzani, E. Garcia-Ortega, G. J. Huffman, C. Kidd, P. A. Kucera, C. D. Kummerow, H. Masunaga, W. A. Petersen, R. Roca, J.-L. Sanchez, W.-K. Tao and F. J. Turk (2017). “Global precipitation measurements for validating climate models”. *Atmospheric Research* 197. Supplement C, 1–20. DOI: [10.1016/j.atmosres.2017.06.021](https://doi.org/10.1016/j.atmosres.2017.06.021).
- Tebaldi, C. and R. Knutti (2007). “The use of the multi-model ensemble in probabilistic climate projections”. *Philosophical Transactions of the Royal Society A: Mathematical, Physical and Engineering Sciences* 365.1857, 2053–2075. DOI: [10.1098/rsta.2007.2076](https://doi.org/10.1098/rsta.2007.2076).
- Touma, D., A. M. Michalak, D. L. Swain and N. S. Diefenbaugh (2018). “Characterizing the Spatial Scales of Extreme Daily Precipitation in the United States”. *Journal of Climate* 31.19, 8023–8037. DOI: [10.1175/JCLI-D-18-0019.1](https://doi.org/10.1175/JCLI-D-18-0019.1).
- Trenberth, K. E. (2011). “Changes in precipitation with climate change”. *Climate Research* 47.1, 123–138. DOI: [10.3354/cr00953](https://doi.org/10.3354/cr00953).
- Vincent, L. A., X. Zhang, É. Mekis, H. Wan and E. J. Bush (2018). “Changes in Canada’s Climate: Trends in Indices Based on Daily Temperature and Precipitation Data”. *Atmosphere-Ocean* 0.0, 1–18. DOI: [10.1080/07055900.2018.1514579](https://doi.org/10.1080/07055900.2018.1514579).
- Wasko, C., A. Sharma and S. Westra (2016). “Reduced spatial extent of extreme storms at higher temperatures”. *Geophysical Research Letters* 43.8, 4026–4032. DOI: [10.1002/2016GL068509](https://doi.org/10.1002/2016GL068509).
- Westra, S., H. J. Fowler, J. P. Evans, L. V. Alexander, P. Berg, F. Johnson, E. J. Kendon, G. Lenderink and N. M. Roberts (2014). “Future changes to the intensity and frequency of short-duration extreme rainfall”. *Reviews of Geophysics* 52.3, 2014RG000464. DOI: [10.1002/2014RG000464](https://doi.org/10.1002/2014RG000464).
- Wilks, D. S. (2006). “On “Field Significance” and the False Discovery Rate”. *Journal of Applied Meteorology and Climatology* 45.9, 1181–1189. DOI: [10.1175/JAM2404.1](https://doi.org/10.1175/JAM2404.1).
- Xie, P., R. Joyce, S. Wu, S.-H. Yoo, Y. Yarosh, F. Sun and R. Lin (2017). “Reprocessed, Bias-Corrected CMORPH Global High-Resolution Precipitation Estimates from 1998”. *Journal of Hydrometeorology* 18.6, 1617–1641. DOI: [10.1175/JHM-D-16-0168.1](https://doi.org/10.1175/JHM-D-16-0168.1).
- Yue, S. and C. Wang (2004). “The Mann-Kendall Test Modified by Effective Sample Size to Detect Trend in Serially Correlated Hydrological Series”. *Water Resources Management* 18.3, 201–218. DOI: [10.1023/B:WARM.0000043140.61082.60](https://doi.org/10.1023/B:WARM.0000043140.61082.60).

Part III

Conclusion

Conclusion

Precipitation extremes are highly variable in space and time as various physical processes are involved in their generation. Moreover, as global warming is expected to differently affect heavy precipitation at different spatial and temporal scales, important modifications in the spatio-temporal structure of precipitation are expected for future decades. Characterizing the spatial and temporal variability of precipitation extremes is challenging, especially considering the deficiencies and limitations in actual data. Equally important, large sampling errors affect the extreme estimations, making it difficult to achieve a complete and adequate statistical characterization of extreme precipitation.

The three articles that compose this thesis address these issues by applying a multi-scale analysis of precipitation framed within the scaling model theory. This chapter summarizes and discusses the main results presented in each paper.

6.1.1 Temporal Simple Scaling (SS) for station AM

The ability of temporal SS models to approximate the probability distribution of precipitation intensity extremes was assessed using meteorological station AMS for durations from 15 min to 7 days. Results suggest that SS represents a reasonable working hypothesis for estimating IDF curves, allowing a reduction of uncertainties in precipitation estimation. In particular, the analysis of temporal SS models for summer AM (i.e., from May to October) led to the following results and conclusions:

- i) The validity of the SS hypothesis was empirically confirmed for the majority of the *scaling intervals* (i.e. duration intervals) through the Moment Scaling Analysis (MSA). Then, two

Goodness-of-Fit (GOF) tests and the calculation of error measures (e.g., normalized RMSE) validated the use of SS models for approximating empirical AM distributions. The hypothesis of a scale invariance held for all scaling intervals spanning durations from 1 h to 7 days. Lower SS performance was observed for durations shorter than 1h, especially for long scaling intervals (e.g., scaling intervals that contain 18 or 24 durations). Note that the coarse measurement tip resolution of available 15PD series may partly explain this result as it is expected to affect both the SS estimation and the validation tools (e.g., GOF tests).

- ii) Exploring the variability of the SS exponent, H , over a wide range of scaling intervals allowed assessing the influence of dominant pluviometric regimes on scaling estimates. Moreover, the SS exponent values generally displayed a well-defined spatial distribution, although higher local variability was observed for some scaling intervals. Characteristic changes in H values over the scaling intervals were observed for six geographical regions characterized by different precipitation regimes according to the Bukovsky (2012) classification. This suggests that both local geographical characteristics (e.g., topography or coastal effects) and large scale forcings (e.g., general circulation patterns) have an impact on estimated AM scaling.

H values generally ranged between 0.35 and 0.95, with weakest scaling regimes (i.e. lowest H values for precipitation intensity) typically found for sub-hourly duration intervals and along the west coast of the continent. Hence, for these scaling intervals and climatic areas, AM are likely generated by homogeneous weather processes across different durations. In the interior and southern areas of the continent, a more important shift from weaker to stronger scaling regimes (i.e., smaller to larger H values) was observed for increasing durations, with highest H values found for scaling intervals containing durations from ≈ 12 h to 2days. This indicates that important changes occur in AM intensity distribution moments and, thus, in extreme precipitation features for these ranges of durations. For scaling intervals of durations longer than a few days, H converges to ≈ 0.7 for most of the stations, except those on the Pacific coast.

- iii) The advantages of introducing the SS property in parametric distribution models were highlighted by comparing the performance of SS-GEV and classical (i.e. non-SS) GEV estimations for approximating AM quantiles. More evidence for positive GEV shape parameter (heavy tailed distributions) was found for SS-GEV compared to non-SS models. Pooling data under the scale-invariance hypothesis may thus allow a better assessment of ξ and a more reliable sta-

tistical inference for AM distributions. Also, heavy-tailed SS-GEV models displayed smaller errors (e.g., smaller RMSE between parametric and empirical AM quantiles) than non-SS GEV for scaling intervals that respected the MSA conditions. This suggests that, if the scaling interval (i.e., the range of durations across which the SS hypothesis is used) is adequately selected, the SS allows a better assessment of the GEV shape parameter and errors in IDF estimates can be overall reduced.

Note, however, that some important uncertainties remain in the estimation of SS-GEV parameters, especially for ξ . Also, limited applicability of SS models was observed for sub-hourly duration intervals and some specific regions (e.g., the Pacific South-West). Despite these specific cases, SS models appeared to be an interesting approach for reducing uncertainties in precipitation quantiles and IDF estimates. To this end, the spatial distribution of the scaling exponent and its dependency on climatology should also be considered when constructing SS IDF curves.

6.1.2 Spatio-temporal structure of AM in gridded datasets

This study had two main objectives. First, it aimed at comparing the representation of sub-daily and daily AM characteristics from various simulated and observational gridded datasets: precipitation series from meteorological station records, the CMORPH bias-corrected satellite dataset, the MSWEP multi-source dataset, and two RCM simulations driven by the ERA-Interim reanalysis, one from the convection-permitting WRF model and one from the CRCM5. The focus was on the evaluation of CRCM5 simulations before proceeding to the analysis of CRCM5-LE projections in future climate (Article 3). Second, it aimed to develop an analytical expression of the scaling relationship for describing AM probability distribution changes across various temporal and spatial scales.

To this end, AM were extracted for durations ranging from 1 h to 3 days and various spatial scales defined according to the native grid resolution of each gridded dataset. Then AM empirical quantiles, AM annual and diurnal cycles, and temporal scaling estimates were compared to the corresponding statistics computed for meteorological stations. The following conclusions were drawn from this analysis.

- i) At their native spatial resolutions, ERA-Interim driven CRCM5 and WRF simulations adequately reproduced short-duration (e.g., $d < 3\text{h}$) station AM quantiles. At daily and longer durations, the ERA-interim driven CRCM5 simulation significantly overestimated AM quantiles for most stations. Moreover, the two RCM simulations adequately reproduced the observed AM annual and daily cycles, although some discrepancies emerged for daily peaks of hourly AM frequencies.
- ii) Several issues were identified for CMORPH AM estimates in northern regions and during winter, confirming biases and uncertainties in cold conditions already mentioned in previous studies for this dataset [Xie and Joyce 2014; Trenberth et al. 2017]. However, AM quantiles were well approximated from CMORPH series in southern areas for daily and longer durations. MSWEP outperformed other datasets for the approximation of daily and longer AM distributions, but its coarse temporal resolution (i.e. $d_0 = 3\text{h}$) prevents assessing sub-daily extreme precipitation characteristics.
- iii) Consistent with station SS estimates, the interval of short durations (SD, $d < 6\text{h}$) was associated with stronger(weaker) AM depth(intensity) scaling regimes than the long duration interval (LD, $d \geq 6\text{h}$). Interestingly, for each dataset, estimated SS exponent values were found to linearly increase with the spatial scale, and the finest spatial resolution dataset, WRF, displayed the steepest increases.
- iv) The linearity of temporal SS exponents on the spatial scale was used to define a simple Spatio-Temporal Scaling (STS) relationship describing the variation of AM quantiles across the considered spatial and temporal scales.

High uncertainty affected local STS estimates (i.e. for a single grid box), especially for longest return periods and LD extremes, despite the STS validity at the regional scale (i.e. when estimated for the spatial average of SS exponents over all available locations). This result was attributed to the high sampling errors affecting AM empirical quantiles for the available relatively short precipitation series. Also, post-processing methods applied for MSWEP and CMORPH seemed to affect the STS properties of AM for these datasets. Pooling AMS from various CRCM5-LE members reduced sampling errors and the local uncertainty of STS estimates, validating STS models for most of the grid boxes and all quantile return periods.

According to these results, gridded dataset precipitation series at various spatial scales could in principle be used to efficiently estimate point-scale IDF curves and ARFs at locations where no sub-daily station records are available. Based on the linearity of SS exponents, the proposed STS model defines the statistical spatio-temporal structure of AM considering only two parameters: the temporal scaling exponent, h_0 , extrapolated at the point scale resolution (i.e. $r = 0$), and the spatio-temporal scaling parameter h_1 , which represents the sensitivity of quantile ARFs to changes in the spatio-temporal scale (r, d) . Despite the high local variability of h_1 estimates, the distributions of the two STS parameters over the study domain displayed a strong spatial coherence, with main patterns likely associated with local geo-climatic characteristics (e.g., topography features) and predominant precipitation regimes.

6.1.3 Evolution of the spatio-temporal structure of AM in time

Although there is a broad consensus that CC not only affects the frequency and intensity of heavy precipitation events, the assessment of temporal modifications in extreme precipitation characteristics such as their duration, seasonality, and spatial extent has received less attention in the literature. Our third analysis thus examined the temporal evolution of the multi-scale characteristics of AM based on CRCM5-LE simulations for the 1954-2099 period. The following main results were found:

- i) The analysis of the pooled AM from the 50 CRCM5-LE members showed a significant intensification of extreme precipitation quantiles for almost all grid boxes of the CRCM5 North American domain. This confirms the theoretical arguments mentioned in the literature stating that relatively stronger increases should be observed for short durations extremes and for long return periods (i.e., more extreme events).
- ii) Using the STS model, some modifications of the spatio-temporal structure of AM distributions were highlighted by the significant decreasing trends observed for the extrapolated SS exponent, h_0 . This confirms that shorter duration extremes will experience higher increases than long duration AM quantiles, and that station IDF slope values are expected to tend towards more negative values in a warming climate. Significant increases of the spatio-temporal scaling parameter, h_1 , were also found for many grid boxes. This implies that the ARF variability across the considered spatio-temporal scales is expected to increase with time. However, less evidence for the non-stationarity of the h_0 and h_1 scaling parameters was found for more

extreme AM, especially for the SD interval (i.e. $d < 6\text{h}$). As previously suggested, a possible explanation for these results is that high uncertainty affects the STS estimation for long return period AM quantiles.

- iii) Evidence of important changes of AM distribution tail characteristics emerged when considering SS-GEV models. On one hand, the proportion of grid boxes with a positive SS-GEV shape parameter (heavy-tailed distribution) increased substantially over time for both SD and LD. This implies that the use of Gumbel (i.e. light tail) distributions in future climate is likely to critically underestimate long return period quantiles for sub-daily and daily AM. On the other hand, SS-GEV shape parameters were found to significantly increase for most of grid boxes for LD while little evidence for a significant ξ increase emerged for SD. Also, the proportion of grid boxes with significant ξ trends was lower than the proportions of those with trends for the other SS-GEV parameters and for other measures of AM distribution dispersion, such as the normalized dispersion coefficient σ/μ , due to the high uncertainty that affects GEV shape parameter estimation. These results are particularly important since they highlight crucial modifications in the statistical properties of the most extremes precipitation with climate change. However, this also underline that it is more difficult to achieve a robust assessment of temporal changes in extreme precipitation characteristics for durations shorter than 6h and more rare extremes, event when AM observations from various durations and multiple RCM simulations are pooled under the SS hypothesis.
- iv) Finally, two fundamental changes are to be expected for the annual and daily cycles of AM occurrences according to CRCM5-LE simulations. First, hourly and daily AM are expected to occur over an extended period of the year in future climate, especially in some specific regions of the study domain (e.g., the southern areas between Appalachians mountains and the Atlantic coast). Second, the mean daily time of AM occurrence is expected to occur later in the evening for sub-hourly AM relative to past climate. Although many factors could drive these changes, more frequent and more intense warm meteorological conditions can basically explain these results.

In summary, STS models and pooled CRCM5-LE series seem to be effective methods for estimating the temporal evolution of crucial AM statistics, related to the tail of the AM probability distribution and the spatio-temporal scaling of the extremes. The reported results stress the importance of reconsidering some hypotheses often used in AM precipitation analysis. For instance, important

non-stationarity emerged for AM distributions even over relatively short time periods (e.g., 10 or 20 years), which are commonly used as reference climate periods in applications. Similarly, the assumption of a Gumbel distribution and/or stationary shape parameter GEV may led to important underestimations of projected changes for the more extreme precipitation events.

6.2 Original contributions

This thesis brought various original contributions. Applying an extensive validation of SS models over a large dataset of recorded precipitation series covering North America, the present study has allowed an unprecedented and systematic comparison of SS estimations across various duration ranges and for regions characterized by different climatological characteristics. The comparison of these results with previous studies has deepened the knowledge about the scale-invariant properties of extreme precipitation and provided new insights about the influence of regional precipitation features on estimated scaling regimes. Similarly, the assessment of SS estimates from various simulated and observationally-based datasets with different temporal, spatial, and measurement resolutions has allowed a more accurate description of the effects of dataset characteristics on precipitation scaling. Despite having been previously mentioned in some previous studied, the impacts of these characteristics on extreme precipitation scaling had not yet been thoroughly described in the literature.

New methodological developments were proposed for the assessment of scaling properties across various spatial scales. This allowed the integration of a spatial component in the scaling relationships and the definition of a spatio-temporal scaling model that describes AM quantile variability over a wide range of spatio-temporal scales. Though this method should be more extensively validated, it opens up to the possibility of estimating point-scale IDF curves and ARFs from precipitation series available at coarser resolutions over regular grids.

Finally, the use of the recently produced CRCM5-LE has allowed assessing the temporal evolution of AM characteristics using series of unprecedented length and testing the validity of STS models at local scale with consistently reduced sampling errors. Temporal changes of AM characteristics were studied with a straightforward methodological approach based on the construction of large samples of AM extracted over consecutive sub-periods of a few years. This permitted the investigation of

AM distribution changes in a transient climate. The results give a more complete and statistically consistent portrait of CC impacts on precipitation extremes relative to the classical period-by-period comparison of precipitation distributions between an historical reference period and one or many future periods.

6.3 Limitations and perspective on future works

Three major limitations must be stressed. First, SS models showed limited applicability for sub-hourly durations and some specific regions (e.g., the Pacific South-West), but the source of this deviation from the scale-invariance hypothesis was not investigated. Many factors and some methodological choices may have impacted these results. For instance, limiting the analysis to summer AM may have caused important heavy precipitation events to be neglected for some specific durations, especially for the southern US West Coast, where daily extremes are generally expected to occur during winter [Mallakpour and Villarini 2017].

Second, the analysis of STS parameters and their temporal trends highlighted some differences between the scaling properties of short and long return period quantiles. Further investigation should thus clarify whether these results are due to the higher estimation uncertainty of more extreme AM quantiles or if different STS regimes characterize quantiles of different orders. In the latter case, the possibility of modeling the scaling exponent as a function of the quantile order (e.g., using multiscaling frameworks for IDF) should be investigated.

Third, the proposed STS model should be carefully compared with other methods for approximating local scale AM distribution parameters (e.g., classical statistical downscaling methods) in order to evaluate their performance in IDF estimation and for downscaling AM distributions from precipitation series available at coarse spatial scales.

Considering these limitations and our general results, a more comprehensive assessment of the statistical uncertainty of the STS estimation is recommended. The analysis of seasonal AM scaling should also be considered to evaluate possible biases and sampling errors that may affect SS-IDF estimation based on datasets with limited coverage and/or possible seasonal biases. Also, any future extension of this study should investigate the possibility of introducing spatial information and

temporal trends in scaling and SS-GEV models [e.g., by considering models with non-stationary parameters in space and/or in time; Blanchet et al. 2018; Li et al. 2019]. Similarly, the relationships between GEV and SS-GEV parameters for AM distributions estimated at different spatial scales should be further investigated. In particular, it would be important to assess the possibility of defining analytical IDAF relationships based on the SS-GEV models and evaluate their consistency with other semi-empirical relationships proposed in the literature for observed datasets [e.g., De Michele et al. 2001; Panthou et al. 2014; Overeem et al. 2010]. Finally, note that it would be interesting to extend the study to geographical regions which are well covered by high density recording network (e.g., Europe) and/or characterized by different precipitation regimes. Other simulated RCM ensembles could be considered to further evaluate the spatial variability and the representativeness of the presented results. For instance, the analysis of high-resolution convection-permitting RCM large ensembles, when available, could help to characterize the causes of the deviation from scale-invariance that have been observed for short duration extremes and in some other specific cases. Equally important, this would allow to evaluate the impact of convection parametrization on the changes in time reported for short duration extreme distribution and scaling estimates.

Bibliography

- Abramowitz, G., N. Herger, E. Gutmann, D. Hammerling, R. Knutti, M. Leduc, R. Lorenz, R. Pincus and G. A. Schmidt (2019). “ESD Reviews: Model dependence in multi-model climate ensembles: weighting, sub-selection and out-of-sample testing”. *Earth System Dynamics* 10.1, 91–105. DOI: <https://doi.org/10.5194/esd-10-91-2019>.
- Adam, J. C. and D. P. Lettenmaier (2003). “Adjustment of global gridded precipitation for systematic bias”. *Journal of Geophysical Research: Atmospheres* 108.D9, 4257. DOI: [10.1029/2002JD002499](https://doi.org/10.1029/2002JD002499).
- AghaKouchak, A., A. Mehran, H. Norouzi and A. Behrangi (2012). “Systematic and random error components in satellite precipitation data sets”. *Geophysical Research Letters* 39.9, L09406. DOI: [10.1029/2012GL051592](https://doi.org/10.1029/2012GL051592).
- Akinremi, O. O., S. M. McGinn and H. W. Cutforth (1999). “Precipitation Trends on the Canadian Prairies*”. *Journal of Climate* 12.10, 2996–3003. DOI: [10.1175/1520-0442\(1999\)012<2996:PTOTCP>2.0.CO;2](https://doi.org/10.1175/1520-0442(1999)012<2996:PTOTCP>2.0.CO;2).
- Albeverio, S., V. Jentsch and H. Kantz, eds. (2006). *Extreme Events in Nature and Society*. The Frontiers Collection. Berlin Heidelberg: Springer-Verlag.
- Alexander, L. V., X. Zhang, T. C. Peterson, J. Caesar, B. Gleason, A. M. G. Klein Tank, M. Haylock, D. Collins, B. Trewin, F. Rahimzadeh, A. Tagipour, K. Rupa Kumar, J. Revadekar, G. Griffiths, L. Vincent, D. B. Stephenson, J. Burn, E. Aguilar, M. Brunet, M. Taylor, M. New, P. Zhai, M. Rusticucci and J. L. Vazquez-Aguirre (2006). “Global observed changes in daily climate extremes of temperature and precipitation”. *Journal of Geophysical Research* 111.D5. DOI: [10.1029/2005jd006290](https://doi.org/10.1029/2005jd006290).
- Alila, Y. (2000). “Regional rainfall depth-duration-frequency equations for Canada”. *Water Resources Research* 36.7, 1767–1778. DOI: [10.1029/2000WR900046](https://doi.org/10.1029/2000WR900046).
- Allen, R. J. and A. T. DeGaetano (2005). “Considerations for the use of radar-derived precipitation estimates in determining return intervals for extreme areal precipitation amounts”. *Journal of Hydrology* 315.1-4, 203–219. DOI: [10.1016/j.jhydro.2005.03.028](https://doi.org/10.1016/j.jhydro.2005.03.028).
- Arora, V. K., J. F. Scinocca, G. J. Boer, J. R. Christian, K. L. Denman, G. M. Flato, V. V. Kharin, W. G. Lee and W. J. Merryfield (2011). “Carbon emission limits required to satisfy future representative concentration pathways of greenhouse gases”. *Geophysical Research Letters* 38.5, L05805. DOI: [10.1029/2010GL046270](https://doi.org/10.1029/2010GL046270).
- Arritt, R. W. and M. Rummukainen (2010). “Challenges in Regional-Scale Climate Modeling”. *Bulletin of the American Meteorological Society* 92.3, 365–368. DOI: [10.1175/2010BAMS2971.1](https://doi.org/10.1175/2010BAMS2971.1).
- Austin, P. M. and R. A. Houze (1972). “Analysis of the Structure of Precipitation Patterns in New England”. *Journal of Applied Meteorology* 11.6, 926–935. DOI: [10.1175/1520-0450\(1972\)011<0926:AOTSOP>2.0.CO;2](https://doi.org/10.1175/1520-0450(1972)011<0926:AOTSOP>2.0.CO;2).
- Azzalini, A. (1996). *Statistical Inference Based on the likelihood*. CRC Press.
- Bacchi, B. and R. Ranzi (1996). “On the derivation of the areal reduction factor of storms”. *Atmospheric Research*. Closing the gap between theory and practice in urban rainfall applications 42.1-4, 123–135. DOI: [10.1016/0169-8095\(95\)00058-5](https://doi.org/10.1016/0169-8095(95)00058-5).
- Ban, N., J. Schmidli and C. Schär (2014). “Evaluation of the convection-resolving regional climate modeling approach in decade-long simulations”. *Journal of Geophysical Research: Atmospheres* 119.13, 7889–7907. DOI: [10.1002/2014JD021478](https://doi.org/10.1002/2014JD021478).
- Ban, N., J. Schmidli and C. Schär (2015). “Heavy precipitation in a changing climate: Does short-term summer precipitation increase faster?”. *Geophysical Research Letters* 42.4, 2014GL062588. DOI: [10.1002/2014GL062588](https://doi.org/10.1002/2014GL062588).
- Bara, M., S. Kohnová, L. Gaál, J. Szolgay and K. Hlavcová (2009). “Estimation of IDF curves of extreme rainfall by simple scaling in Slovakia”. *Contributions to Geophysics and Geodesy* 39.3, 187–206.
- Barbero, R., H. J. Fowler, G. Lenderink and S. Blenkinsop (2017). “Is the intensification of precipitation extremes with global warming better detected at hourly than daily resolutions?”. *Geophysical Research Letters* 44.2, 2016GL071917. DOI: [10.1002/2016GL071917](https://doi.org/10.1002/2016GL071917).

- Beck, H. E., A. I. J. M. Van Dijk, V. Levizzani, J. Schellekens, D. G. Miralles, B. Martens and A. de Roo (2017a). “MSWEP: 3-hourly 0.25° global gridded precipitation (1979–2015) by merging gauge, satellite, and reanalysis data”. *Hydrol. Earth Syst. Sci.* 21.1, 589–615. DOI: [10.5194/hess-21-589-2017](https://doi.org/10.5194/hess-21-589-2017).
- Beck, H. E., N. Vergopolan, M. Pan, V. Levizzani, A. I. J. M. van Dijk, G. Weedon, L. Brocca, F. Pappenberger, G. J. Huffman and E. F. Wood (2017b). “Global-scale evaluation of 23 precipitation datasets using gauge observations and hydrological modeling”. *Hydrol. Earth Syst. Sci. Discuss.* 2017, 1–23. DOI: [10.5194/hess-2017-508](https://doi.org/10.5194/hess-2017-508).
- Bendjoudi, H., P. Hubert, D. Schertzer and S. Lovejoy (1997). “Interprétation multifractale des courbes intensité-durée-fréquence des précipitations”. *Comptes Rendus de l’Académie des Sciences-Series IIA-Earth and Planetary Science* 325.5, 323–326.
- Bernard, M. M. (1932). “Formulas For Rainfall Intensities of Long Duration”. *Transactions of the American Society of Civil Engineers* 96.1, 592–606.
- Berne, A. and W. F. Krajewski (2013). “Radar for hydrology: Unfulfilled promise or unrecognized potential?”. *Advances in Water Resources*. 35th Year Anniversary Issue 51, 357–366. DOI: [10.1016/j.advwatres.2012.05.005](https://doi.org/10.1016/j.advwatres.2012.05.005).
- Blanchet, J., D. Ceresetti, G. Molinié and J.-D. Creutin (2016). “A regional GEV scale-invariant framework for Intensity-Duration-Frequency analysis”. *Journal of Hydrology* 540, 82–95. DOI: [10.1016/j.jhydrol.2016.06.007](https://doi.org/10.1016/j.jhydrol.2016.06.007).
- Blanchet, J. and M. Lehning (2010). “Mapping snow depth return levels: smooth spatial modeling versus station interpolation”. *Hydrology and Earth System Sciences* 14.12, 2527–2544. DOI: [10.5194/hess-14-2527-2010](https://doi.org/10.5194/hess-14-2527-2010).
- Blanchet, J., C. Marty and M. Lehning (2009). “Extreme value statistics of snowfall in the Swiss Alpine region”. *WATER RESOURCES RESEARCH* 45.5. DOI: [10.1029/2009WR007916](https://doi.org/10.1029/2009WR007916).
- Blanchet, J., G. Molinié and J. Touati (2018). “Spatial analysis of trend in extreme daily rainfall in southern France”. *Climate Dynamics* 51.3, 799–812. DOI: [10.1007/s00382-016-3122-7](https://doi.org/10.1007/s00382-016-3122-7).
- Blöschl, G. and M. Sivapalan (1995). “Scale issues in hydrological modelling: A review”. *Hydrological Processes* 9, 251–290. DOI: [10.1002/hyp.3360090305](https://doi.org/10.1002/hyp.3360090305).
- Borga, M., C. Vezzani and G. Dalla Fontana (2005). “Regional rainfall depth-duration-frequency equations for an alpine region”. *Natural Hazards* 36.1-2, 221–235.
- Boukhelifa, M., M. Meddi and E. Gaume (2018). “Integrated Bayesian Estimation of Intensity-Duration-Frequency Curves: Consolidation and Extensive Testing of a Method”. *Water Resources Research* 0.0. DOI: [10.1029/2018WR023366](https://doi.org/10.1029/2018WR023366).
- Brisson, E., M. Demuzere and N. Van Lipzig (2015). “Modelling strategies for performing convection-permitting climate simulations”. *Meteorologische Zeitschrift* 25.2, 149–163. DOI: [10.1127/metz/2015/0598](https://doi.org/10.1127/metz/2015/0598).
- Buishand, T. A. (1991). “Extreme rainfall estimation by combining data from several sites”. *Hydrological Sciences Journal* 36.4, 345–365. DOI: [10.1080/02626669109492519](https://doi.org/10.1080/02626669109492519).
- Bukovsky, M. S. (2012). “Masks for the Bukovsky regionalization of North America, Regional Integrated Sciences Collective”. *Institute for Mathematics Applied to Geosciences, National Center for Atmospheric Research, Boulder, CO. Downloaded (2015): 05-08*. 06–18.
- Burlando, P. and R. Rosso (1996). “Scaling and multiscaling models of DDF for storm precipitations”. *Journal of Hydrology* 187, 45–64. DOI: [10.1016/S0022-1694\(96\)03086-7](https://doi.org/10.1016/S0022-1694(96)03086-7).
- Cannon, A. J. and S. Innocenti (2018). “Projected intensification of sub-daily and daily rainfall extremes in convection-permitting climate model simulations over North America: Implications for future Intensity-Duration-Frequency curves”. *Natural Hazards and Earth System Sciences Discussions*, 1–29. DOI: <https://doi.org/10.5194/nhess-2018-290>.
- Casas-Castillo, M. C., A. Llabres-Brustenga, A. Rius, R. Rodriguez-Sola and X. Navarro (2018). “A single scaling parameter as a first approximation to describe the rainfall pattern of a place: application on Catalonia”. *Acta Geophysica*, 1–10. DOI: [10.1007/s11600-018-0122-5](https://doi.org/10.1007/s11600-018-0122-5).
- Castro, J. J., A. A. Cârsteanu and C. G. Flores (2004). “Intensity–duration–area–frequency functions for precipitation in a multifractal framework”. *Physica A: Statistical Mechanics and its Applications*. Proceedings of the conference A Nonlinear World: the Real World, 2nd International Conference on Frontier Science 338.1–2, 206–210. DOI: [10.1016/j.physa.2004.02.043](https://doi.org/10.1016/j.physa.2004.02.043).
- Cavicchia, L., E. Scocciarro, S. Gualdi, P. Marson, B. Ahrens, S. Berthou, D. Conte, A. Dell’Aquila, P. Drobinski, V. Djurdjevic, C. Dubois, C. Gallardo, L. Li, P. Oddo, A. Sanna and C. Torma (2016). “Mediterranean extreme precipitation: a multi-model assessment”. *Climate Dynamics*, 1–13. DOI: [10.1007/s00382-016-3245-x](https://doi.org/10.1007/s00382-016-3245-x).
- Ceresetti, D., G. Molinié and J.-D. Creutin (2010). “Scaling properties of heavy rainfall at short duration: A regional analysis”. *Water Resources Research* 46.9. W09531, n/a–n/a. DOI: [10.1029/2009WR008603](https://doi.org/10.1029/2009WR008603).
- Ceresetti, D. (2011). “Structure spatio-temporelle des fortes précipitations: application à la région Cévennes-Vivarais”. PhD thesis. Université de Grenoble.
- Chen, M., H. Mao, R. Talbot and D. Pollard (2005). “Changes in precipitation characteristics over North America for doubled CO₂”. *Geophysical Research Letters* 32.19, L19716. DOI: [10.1029/2005GL024535](https://doi.org/10.1029/2005GL024535).

- Chen, M., W. Shi, P. Xie, V. Silva, V. E. Kousky, R. Wayne Higgins and J. E. Janowiak (2008). “Assessing objective techniques for gauge-based analyses of global daily precipitation”. *Journal of Geophysical Research: Atmospheres* 113.D4.
- Chow, V. T., D. R. Maidment, L. W. Mays, V. T. Chow, D. R. Maidment and L. W. Mays (1988). “Applied Hydrology”. *McGraw-Hill Series in Water Resources and Environmental Engineering*.
- Chow, V. T. (1951). “A general formula for hydrologic frequency analysis”. *Transactions, American Geophysical Union* 32.2, 231. DOI: [10.1029/TR032i002p00231](https://doi.org/10.1029/TR032i002p00231).
- Coles, S. G. (2001). *An Introduction to Statistical Modeling of Extreme Values*. London: Springer.
- Coles, S. G. and J. A. Tawn (1996). “Modelling Extremes of the Areal Rainfall Process”. *Journal of the Royal Statistical Society. Series B (Methodological)* 58.2, 329–347.
- Coles, S., J. Heffernan and J. Tawn (1999). “Dependence Measures for Extreme Value Analyses”. *Extremes* 2.4, 339–365. DOI: [10.1023/A:1009963131610](https://doi.org/10.1023/A:1009963131610).
- Collins, M., R. Knutti, J. M. Arblaster, J.-L. Dufresne, T. Fichet, P. Friedlingstein, X. Gao, W. J. Gutowski, T. Johns, G. Krinner, et al. (2013). “Long-term climate change: projections, commitments and irreversibility”. *Climate Change 2013: The Physical Science Basis. Contribution of Working Group I to the Fifth Assessment Report of the Intergovernmental Panel on Climate Change*. Cambridge University Press. Cambridge, United Kingdom and New York, \{\{NY\}\}, \{\{USA\}\}: Stocker, T.F., D. Qin, G.-K. Plattner, M. Tignor, S.K. Allen, J. Boschung, A. Nauels, Y. Xia, V. Bex and P.M. Midgley.
- Cooley, D. (2013). “Return Periods and Return Levels Under Climate Change”. *Extremes in a Changing Climate*. Ed. by A. AghaKouchak, D. Easterling, K. Hsu, S. Schubert and S. Sorooshian. Water Science and Technology Library 65. Springer Netherlands, 97–114.
- Cooley, D., D. Nychka and P. Naveau (2007). “Bayesian Spatial Modeling of Extreme Precipitation Return Levels”. *Journal of the American Statistical Association* 102.479, 824–840. DOI: [10.1198/016214506000000780](https://doi.org/10.1198/016214506000000780).
- CSA (2012). Development, interpretation and use of rainfall intensity-duration-frequency (IDF) information: Guideline for Canadian water resources practitioners. Tech. rep. Canadian Standard Association, Tech. Rep. PLUS 4013, Mississauga, Ontario, 2nd ed. 214.
- Cunnane, C. (1978). “Unbiased plotting positions : A review”. *Journal of Hydrology* 37.3-4, 205–222. DOI: [10.1016/0022-1694\(78\)90017-3](https://doi.org/10.1016/0022-1694(78)90017-3).
- Dai, A. (2006). “Precipitation Characteristics in Eighteen Coupled Climate Models”. *Journal of Climate* 19.18, 4605–4630. DOI: [10.1175/JCLI3884.1](https://doi.org/10.1175/JCLI3884.1).
- Dai, A., R. M. Rasmussen, C. Liu, K. Ikeda and A. F. Prein (2017). “A new mechanism for warm-season precipitation response to global warming based on convection-permitting simulations”. *Climate Dynamics*, 1–26. DOI: [10.1007/s00382-017-3787-6](https://doi.org/10.1007/s00382-017-3787-6).
- Daly, C., M. Halbleib, J. I. Smith, W. P. Gibson, M. K. Doggett, G. H. Taylor, J. Curtis and P. P. Pasteris (2008). “Physiographically sensitive mapping of climatological temperature and precipitation across the conterminous United States”. *International Journal of Climatology* 28.15, 2031–2064. DOI: [10.1002/joc.1688](https://doi.org/10.1002/joc.1688).
- De Michele, C., N. T. Kottegoda and R. Rosso (2002). “IDAF curves extreme storm rainfall a scaling approach”. *Water Science & Technol* 45.2, 83–90.
- De Michele, C., N. T. Kottegoda and R. Rosso (2001). “The derivation of areal reduction factor of storm rainfall from its scaling properties”. *Water Resources Research* 37.12, 3247–3252. DOI: [10.1029/2001wr000346](https://doi.org/10.1029/2001wr000346).
- Dee, D. P., S. M. Uppala, A. J. Simmons, P. Berrisford, P. Poli, S. Kobayashi, U. Andrae, M. A. Balmaseda, G. Balsamo, P. Bauer, P. Bechtold, A. C. M. Beljaars, L. van de Berg, J. Bidlot, N. Bormann, C. Delsol, R. Dragani, M. Fuentes, A. J. Geer, L. Haimberger, S. B. Healy, H. Hersbach, E. V. Hólm, L. Isaksen, P. Kållberg, M. Köhler, M. Matricardi, A. P. McNally, B. M. Monge-Sanz, J.-J. Morcrette, B.-K. Park, C. Peubey, P. de Rosnay, C. Tavolato, J.-N. Thépaut and F. Vitart (2011). “The ERA-Interim reanalysis: configuration and performance of the data assimilation system”. *Quarterly Journal of the Royal Meteorological Society* 137.656, 553–597. DOI: [10.1002/qj.828](https://doi.org/10.1002/qj.828).
- Deser, C., R. Knutti, S. Solomon and A. S. Phillips (2012a). “Communication of the role of natural variability in future North American climate”. *Nature Climate Change* 2.11, 775–779. DOI: [10.1038/nclimate1562](https://doi.org/10.1038/nclimate1562).
- Deser, C., A. Phillips, V. Bourdette and H. Teng (2012b). “Uncertainty in climate change projections: the role of internal variability”. *Climate Dynamics* 38.3-4, 527–546. DOI: [10.1007/s00382-010-0977-x](https://doi.org/10.1007/s00382-010-0977-x).
- Devine, K. A. and É. Mekis (2008). “Field accuracy of Canadian rain measurements”. *Atmosphere-Ocean* 46.2, 213–227. DOI: [10.3137/ao.460202](https://doi.org/10.3137/ao.460202).
- Dittus, A. J., D. J. Karoly, S. C. Lewis and L. V. Alexander (2015). “A Multiregion Assessment of Observed Changes in the Areal Extent of Temperature and Precipitation Extremes”. *Journal of Climate* 28.23, 9206–9220. DOI: [10.1175/JCLI-D-14-00753.1](https://doi.org/10.1175/JCLI-D-14-00753.1).
- Donat, M. G., L. V. Alexander, H. Yang, I. Durre, R. Vose, R. J. H. Dunn, K. M. Willett, E. Aguilar, M. Brunet, J. Caesar, B. Hewitson, C. Jack, A. M. G. Klein Tank, A. C. Kruger, J. Marengo, T. C. Peterson, M. Renom, C. Oria Rojas, M. Rusticucci, J. Salinger, A. S. Elrayah, S. S. Sekele, A. K. Srivastava, B. Trewin, C. Villarroya, L. A.

- Vincent, P. Zhai, X. Zhang and S. Kitching (2013). “Updated analyses of temperature and precipitation extreme indices since the beginning of the twentieth century: The HadEX2 dataset”. *Journal of Geophysical Research: Atmospheres* 118.5, 2098–2118. DOI: [10.1002/jgrd.50150](https://doi.org/10.1002/jgrd.50150).
- Drobinski, P., N. D. Silva, G. Panthou, S. Bastin, C. Muller, B. Ahrens, M. Borga, D. Conte, G. Fosser, F. Giorgi, I. GEttler, V. Kotroni, L. Li, E. Morin, B. ˆAnol, P. Quintana-Segui, R. Romera and C. Z. Torma (2016). “Scaling precipitation extremes with temperature in the Mediterranean: past climate assessment and projection in anthropogenic scenarios”. *Climate Dynamics*, 1–21. DOI: [10.1007/s00382-016-3083-x](https://doi.org/10.1007/s00382-016-3083-x).
- Dubrulle, B., F. Graner and D. Sornette (1997). *Scale Invariance and Beyond*. Les Houches Workshop, March 10-14, 1997. Les Ulis, France: EDP Sciences.
- Dunkerley, D. (2008). “Identifying individual rain events from pluviograph records: a review with analysis of data from an Australian dryland site”. *Hydrological Processes* 22.26, 5024–5036. DOI: [10.1002/hyp.7122](https://doi.org/10.1002/hyp.7122).
- Dwyer, J. G. and P. A. O’Gorman (2017). “Changing duration and spatial extent of midlatitude precipitation extremes across different climates”. *Geophys. Res. Lett.* 44.11, 2017GL072855. DOI: [10.1002/2017GL072855](https://doi.org/10.1002/2017GL072855).
- Easterling, D. R. K. (2017). “Climate Science Special Report: Fourth National Climate Assessment, Vol I. Ch. 7: Precipitation Change in the United States”. Vol. Vol I. GSFC-E-DAA-TN49608. U.S. Global Change Research Program, 207–230.
- Easterling, D. R., J. L. Evans, P. Y. Groisman, T. R. Karl, K. E. Kunkel and P. Ambenje (2000a). “Observed Variability and Trends in Extreme Climate Events: a Brief Review”. *Bulletin of the American Meteorological Society* 81.3.
- Easterling, D. R., G. A. Meehl, C. Parmesan, S. A. Changnon, T. R. Karl and L. O. Mearns (2000b). “Climate Extremes: Observations, Modeling, and Impacts”. *Science* 289.5487, 2068–2074. DOI: [10.1126/science.289.5487.2068](https://doi.org/10.1126/science.289.5487.2068).
- Eggert, B., P. Berg, J. O. Haerter, D. Jacob and C. Moseley (2015). “Temporal and spatial scaling impacts on extreme precipitation”. *Atmos. Chem. Phys.* 15.10, 5957–5971. DOI: [10.5194/acp-15-5957-2015](https://doi.org/10.5194/acp-15-5957-2015).
- Field, C. B., V. R. Barros, D. J. Dokken, K. J. Mach, M. D. Mastrandrea, T. E. Bilir, M. Chatterjee, K. L. Ebi, Y. O. Estrada and R. C. Genova (2014). IPCC, 2014: Climate change 2014: Impacts, adaptation, and vulnerability. Part A: Global and sectoral aspects. Contribution of working group II to the fifth assessment report of the intergovernmental panel on climate change. Cambridge University Press, Cambridge, United Kingdom and New York, NY, USA.
- Fischer, E. M. and R. Knutti (2016). “Observed heavy precipitation increase confirms theory and early models”. *Nature Climate Change* 6.11, nclimate3110. DOI: [10.1038/nclimate3110](https://doi.org/10.1038/nclimate3110).
- Fisher, R. A. and L. H. C. Tippett (1928). “Limiting forms of the frequency distribution of the largest or smallest member of a sample”. *Mathematical Proceedings of the Cambridge Philosophical Society* 24.02, 180–190. DOI: [10.1017/S0305004100015681](https://doi.org/10.1017/S0305004100015681).
- Fix, M. J., D. Cooley, S. R. Sain and C. Tebaldi (2018). “A comparison of U.S. precipitation extremes under RCP8.5 and RCP4.5 with an application of pattern scaling”. *Climatic Change* 146.3, 335–347. DOI: [10.1007/s10584-016-1656-7](https://doi.org/10.1007/s10584-016-1656-7).
- Flato, G., J. Marotzke, B. Abiodun, P. Braconnot, S. C. Chou, W. Collins, P. Cox, F. Driouech, S. Emori, V. Eyring, et al. (2013). “Evaluation of climate models”. *Climate Change 2013: The Physical Science Basis. Contribution of Working Group I to the Fifth Assessment Report of the Intergovernmental Panel on Climate Change*. Cambridge University Press, 741–866.
- Fyfe, J. C., C. Derksen, L. Mudryk, G. M. Flato, B. D. Santer, N. C. Swart, N. P. Molotch, X. Zhang, H. Wan, V. K. Arora, J. Scinocca and Y. Jiao (2017). “Large near-term projected snowpack loss over the western United States”. *Nature Communications* 8, 14996. DOI: [10.1038/ncomms14996](https://doi.org/10.1038/ncomms14996).
- Gadian, A. M., A. M. Blyth, C. L. Bruyere, R. R. Burton, J. M. Done, J. Groves, G. Holland, S. D. Mobbs, J. Thielendel Pozo, M. R. Tye and J. L. Warner (2017). “A case study of possible future summer convective precipitation over the UK and Europe from a regional climate projection”. *International Journal of Climatology*.
- Galmarini, S., I. Kioutsioukis, E. Solazzo, U. Alyuz, A. Balzarini, R. Bellasio, A. M. K. Benedictow, R. Bianconi, J. Bieser, J. Brandt, J. H. Christensen, A. Colette, G. Curci, Y. Davila, X. Dong, J. Flemming, X. Francis, A. Fraser, J. Fu, D. K. Henze, C. Hogrefe, U. Im, M. Garcia Vivanco, P. Jimenez-Guerrero, J. E. Jonson, N. Kitwiroon, A. Manders, R. Mathur, L. Palacios-Pena, G. Pirovano, L. Pozzoli, M. Prank, M. Schultz, R. S. Sokhi, K. Sudo, P. Tuccella, T. Takemura, T. Sekiya and A. Unal (2018). “Two-scale multi-model ensemble: is a hybrid ensemble of opportunity telling us more?”: *Atmospheric Chemistry and Physics* 18.12, 8727–8744. DOI: <https://doi.org/10.5194/acp-18-8727-2018>.
- Gervais, M., J. R. Gyakum, E. Atallah, L. B. Tremblay and R. B. Neale (2014a). “How Well Are the Distribution and Extreme Values of Daily Precipitation over North America Represented in the Community Climate System Model? A Comparison to Reanalysis, Satellite, and Gridded Station Data”. *Journal of Climate* 27.14, 5219–5239. DOI: [10.1175/jcli-d-13-00320.1](https://doi.org/10.1175/jcli-d-13-00320.1).

- Gervais, M., L. B. Tremblay, J. R. Gyakum and E. Atallah (2014b). “Representing Extremes in a Daily Gridded Precipitation Analysis over the United States: Impacts of Station Density, Resolution, and Gridding Methods”. *Journal of Climate* 27.14, 5201–5218. DOI: [10.1175/jcli-d-13-00319.1](https://doi.org/10.1175/jcli-d-13-00319.1).
- Gilleland, E. and R. W. Katz (2006). “Analyzing seasonal to interannual extreme weather and climate variability with the extremes toolkit”. *18th Conference on Climate Variability and Change, 86th American Meteorological Society (AMS) Annual Meeting*. Vol. 29.
- Giorgi, F., E. S. Im, E. Coppola, N. S. Diffenbaugh, X. J. Gao, L. Mariotti and Y. Shi (2011). “Higher Hydroclimatic Intensity with Global Warming”. *Journal of Climate* 24.20, 5309–5324. DOI: [10.1175/2011jcli3979.1](https://doi.org/10.1175/2011jcli3979.1).
- Gnedenko, B. (1943). “Sur La Distribution Limite Du Terme Maximum D’Une Serie Aleatoire”. *Annals of Mathematics*. Second Series 44.3, 423–453. DOI: [10.2307/1968974](https://doi.org/10.2307/1968974).
- Greenwood, J. A., J. M. Landwehr, N. C. Matalas and J. R. Wallis (1979). “Probability weighted moments: definition and relation to parameters of several distributions expressible in inverse form”. *Water Resources Research* 15.5, 1049–1054.
- Groisman, P. Y. and D. R. Legates (1994). “The Accuracy of United States Precipitation Data”. *Bulletin of the American Meteorological Society* 75.2, 215–227. DOI: [10.1175/1520-0477\(1994\)075<0215:TA0USP>2.0.CO;2](https://doi.org/10.1175/1520-0477(1994)075<0215:TA0USP>2.0.CO;2).
- Guinard, K., A. Mailhot and D. Caya (2015). “Projected changes in characteristics of precipitation spatial structures over North America”. *International Journal of Climatology*, n/a–n/a. DOI: [10.1002/joc.4006](https://doi.org/10.1002/joc.4006).
- Gumbel, E. J. (1958). *Statistics of Extremes*. New York, Columbia University Press.
- Gumbel, E. J. (1941). “The return period of flood flows”. *The annals of mathematical statistics* 12.2, 163–190.
- Gupta, V. K. and E. Waymire (1990). “Multiscaling properties of spatial rainfall and river flow distributions”. *Journal of Geophysical Research: Atmospheres* 95.D3, 1999–2009. DOI: [10.1029/JD095iD03p01999](https://doi.org/10.1029/JD095iD03p01999).
- Gutowski, W. J., E. S. Takle, K. A. Kozak, J. C. Patton, R. W. Arritt and J. H. Christensen (2007). “A Possible Constraint on Regional Precipitation Intensity Changes under Global Warming”. *Journal of Hydrometeorology* 8.6, 1382–1396. DOI: [10.1175/2007JHM817.1](https://doi.org/10.1175/2007JHM817.1).
- Gutowski, W. J., R. W. Arritt, S. Kawazoe, D. M. Flory, E. S. Takle, S. Biner, D. Caya, R. G. Jones, R. Laprise, L. R. Leung, L. O. Mearns, W. Moufouma-Okia, A. M. B. Nunes, Y. Qian, J. O. Roads, L. C. Sloan and M. A. Snyder (2010). “Regional Extreme Monthly Precipitation Simulated by NARCCAP RCMs”. *Journal of Hydrometeorology* 11.6, 1373–1379. DOI: [10.1175/2010JHM1297.1](https://doi.org/10.1175/2010JHM1297.1).
- Hand, W. H., N. I. Fox and C. G. Collier (2004). “A study of twentieth-century extreme rainfall events in the United Kingdom with implications for forecasting”. *Meteorological Applications* 11.1, 15–31. DOI: [10.1017/S1350482703001117](https://doi.org/10.1017/S1350482703001117).
- Hartmann, D. L., A. M. G. Klein Tank, M. Ruscicucci, L. V. Alexander, B. Broenniman, Y. Charabi, F. J. Dentener, E. J. Dlugokencky, D. R. Easterling, A. Kaplan, B. J. Soden, P. W. Thorne, M. Wild, P. M. Zhai and E. C. Kent (2013). “Observations: Atmosphere and Surface”. *Climate Change 2013: The Physical Science Basis. Contribution of Working Group I to the Fifth Assessment Report of the Intergovernmental Panel on Climate Change*. Ed. by T. F. Stocker, D. Qin, G.-K. Plattner, M. Tignor, S. K. Allen, J. Boschung, A. Nauels, Y. Xia, V. Bex and P. M. Midgley. Cambridge, United Kindom and New York, NY, USA: Cambridge University Press, 159–254.
- Hartmann, D. L. (2015). *Global Physical Climatology*. Google-Books-ID: RsScBAAAQBAJ. Newnes.
- Hawkins, E. (2011). “Our evolving climate: communicating the effects of climate variability”. *Weather* 66.7, 175–179. DOI: [10.1002/wea.761](https://doi.org/10.1002/wea.761).
- Hawkins, E. and R. Sutton (2009). “The Potential to Narrow Uncertainty in Regional Climate Predictions”. *Bulletin of the American Meteorological Society* 90.8, 1095–1107. DOI: [10.1175/2009BAMS2607.1](https://doi.org/10.1175/2009BAMS2607.1).
- Haylock, M. R., N. Hofstra, A. M. G. Klein Tank, E. J. Klok, P. D. Jones and M. New (2008). “A European daily high-resolution gridded data set of surface temperature and precipitation for 1950–2006”. *Journal of Geophysical Research* 113.D20. DOI: [10.1029/2008jd010201](https://doi.org/10.1029/2008jd010201).
- Herold, N., A. Behrangi and L. V. Alexander (2017). “Large uncertainties in observed daily precipitation extremes over land”. *Journal of Geophysical Research: Atmospheres* 122.2, 2016JD025842. DOI: [10.1002/2016JD025842](https://doi.org/10.1002/2016JD025842).
- Hingray, B. and M. Saïd (2014). “Partitioning Internal Variability and Model Uncertainty Components in a Multi-member Multimodel Ensemble of Climate Projections”. *Journal of Climate* 27.17, 6779–6798. DOI: [10.1175/JCLI-D-13-00629.1](https://doi.org/10.1175/JCLI-D-13-00629.1).
- Hoerling, M., J. Eischeid, J. Perlwitz, X.-W. Quan, K. Wolter and L. Cheng (2016). “Characterizing Recent Trends in U.S. Heavy Precipitation”. *Journal of Climate* 29.7, 2313–2332. DOI: [10.1175/JCLI-D-15-0441.1](https://doi.org/10.1175/JCLI-D-15-0441.1).
- Hofstra, N., M. Haylock, M. New, P. Jones and C. Frei (2008). “Comparison of six methods for the interpolation of daily, European climate data”. *Journal of Geophysical Research: Atmospheres* 113.D21, D21110. DOI: [10.1029/2008JD010100](https://doi.org/10.1029/2008JD010100).
- Hofstra, N., M. New and C. McSweeney (2009). “The influence of interpolation and station network density on the distributions and trends of climate variables in gridded daily data”. *Climate Dynamics* 35.5, 841–858. DOI: [10.1007/s00382-009-0698-1](https://doi.org/10.1007/s00382-009-0698-1).

- Hoogewind, K. A., M. E. Baldwin and R. J. Trapp (2017). “The Impact of Climate Change on Hazardous Convective Weather in the United States: Insight from High-Resolution Dynamical Downscaling”. *Journal of Climate*. DOI: [10.1175/JCLI-D-16-0885.1](https://doi.org/10.1175/JCLI-D-16-0885.1).
- Hosking, J. R. M., J. R. Wallis and E. F. Wood (1985). “Estimation of the generalized extreme-value distribution by the method of probability-weighted moments”. *Technometrics* 27.3, 251–261.
- Hosking, J. R. M. and J. R. Wallis (1997). *Regional Frequency analysis: an approach based on L-moments*. Cambridge University Press.
- Houze, R. A. (1981). “Structures of atmospheric precipitation systems: A global survey”. *Radio Science* 16.5, 671–689. DOI: [10.1029/RS016i005p00671](https://doi.org/10.1029/RS016i005p00671).
- Huang, H., J. M. Winter, E. C. Osterberg, R. M. Horton and B. Beckage (2017). “Total and Extreme Precipitation Changes over the Northeastern United States”. *Journal of Hydrometeorology* 18.6, 1783–1798. DOI: [10.1175/JHM-D-16-0195.1](https://doi.org/10.1175/JHM-D-16-0195.1).
- Hubert, P. and H. Bendjoudi (1996). “Introduction à l’étude des longues séries pluviométriques”. *XIIème journées hydrologiques de l’Orstom*, 10–11.
- Huffman, G. J., D. T. Bolvin, E. J. Nelkin, D. B. Wolff, R. F. Adler, G. Gu, Y. Hong, K. P. Bowman and E. F. Stocker (2007). “The TRMM Multisatellite Precipitation Analysis (TMPA): Quasi-Global, Multiyear, Combined-Sensor Precipitation Estimates at Fine Scales”. *Journal of Hydrometeorology* 8.1, 38–55. DOI: [10.1175/JHM560.1](https://doi.org/10.1175/JHM560.1).
- Innocenti, S., A. Mailhot and A. Frigon (2017). “Simple scaling of extreme precipitation in North America”. *Hydrol. Earth Syst. Sci.* 21.11, 5823–5846. DOI: [10.5194/hess-21-5823-2017](https://doi.org/10.5194/hess-21-5823-2017).
- IPCC (2013). IPCC, 2013: Annexe III, Glossary. Stocker, T.F., D. Qin, G.-K. Plattner, M. Tignor, S.K. Allen, J. Boschung, A. Nauels, Y. Xia, V. Bex and P.M. Midgley (eds.) *Climate Change 2013: The physical Science Basis. Contribution of Working Group I to the Fifth Assessment Report of the Intergovernmental Panel On Climate Change*. Cambridge, United Kingdom and New York, NY, USA: Cambridge University Press.
- Jalbert, J., A.-C. Favre, C. Bélisle, J.-F. Angers and D. Paquin (2015). “Canadian RCM Projected Transient Changes to Precipitation Occurrence, Intensity, and Return Level over North America”. *Journal of Climate* 28.17, 6920–6937. DOI: [10.1175/JCLI-D-14-00360.1](https://doi.org/10.1175/JCLI-D-14-00360.1).
- Joyce, R. J., J. E. Janowiak, P. A. Arkin and P. Xie (2004). “CMORPH: A Method that Produces Global Precipitation Estimates from Passive Microwave and Infrared Data at High Spatial and Temporal Resolution”. *Journal of Hydrometeorology* 5.3, 487–503. DOI: [10.1175/1525-7541\(2004\)005<0487:CAMTPG>2.0.CO;2](https://doi.org/10.1175/1525-7541(2004)005<0487:CAMTPG>2.0.CO;2).
- Karl, T. R. and R. W. Knight (1998). “Secular Trends of Precipitation Amount, Frequency, and Intensity in the United States”. *Bulletin of the American Meteorological Society* 79.2, 231–241. DOI: [10.1175/1520-0477\(1998\)079<0231:STOPAF>2.0.CO;2](https://doi.org/10.1175/1520-0477(1998)079<0231:STOPAF>2.0.CO;2).
- Katz, R. W., M. Parlange and P. Naveau (2002). “Statistics of extremes in hydrology”. *Advances in Water Resources* 25, 1287–1304.
- Katz, R. W. (2013). “Statistical Methods for Nonstationary Extremes”. *Extremes in a Changing Climate*. Ed. by A. AghaKouchak, D. Easterling, K. Hsu, S. Schubert and S. Sorooshian. Water Science and Technology Library 65. Springer Netherlands, 15–37.
- Kendon, E. J., N. Ban, N. M. Roberts, H. J. Fowler, M. J. Roberts, S. C. Chan, J. P. Evans, G. Fosser and J. M. Wilkinson (2017). “Do Convection-Permitting Regional Climate Models Improve Projections of Future Precipitation Change?”. *Bulletin of the American Meteorological Society* 98.1, 79–93. DOI: [10.1175/BAMS-D-15-0004.1](https://doi.org/10.1175/BAMS-D-15-0004.1).
- Kendon, E. J., S. Blenkinsop and H. J. Fowler (2018). “When Will We Detect Changes in Short-Duration Precipitation Extremes?”. *Journal of Climate* 31.7, 2945–2964. DOI: [10.1175/JCLI-D-17-0435.1](https://doi.org/10.1175/JCLI-D-17-0435.1).
- Kharin, V. V., G. M. Flato, X. Zhang, N. P. Gillett, F. Zwiers and K. J. Anderson (2018). “Risks from Climate Extremes Change Differently from 1.5°C to 2.0°C Depending on Rarity”. *Earth’s Future* 6.5, 704–715. DOI: [10.1002/2018EF000813](https://doi.org/10.1002/2018EF000813).
- Kharin, V. V., F. W. Zwiers, X. Zhang and M. Wehner (2013). “Changes in temperature and precipitation extremes in the CMIP5 ensemble”. *Climatic Change* 119.2, 345–357. DOI: [10.1007/s10584-013-0705-8](https://doi.org/10.1007/s10584-013-0705-8).
- Kidd, C., A. Becker, G. J. Huffman, C. L. Muller, P. Joe, G. Skofronick-Jackson and D. B. Kirschbaum (2016). “So, How Much of the Earth’s Surface Is Covered by Rain Gauges?”. *Bulletin of the American Meteorological Society* 98.1, 69–78. DOI: [10.1175/BAMS-D-14-00283.1](https://doi.org/10.1175/BAMS-D-14-00283.1).
- Knutti, R. (2018). “Climate Model Confirmation: From Philosophy to Predicting Climate in the Real World”. *Climate Modelling: Philosophical and Conceptual Issues*. Ed. by E. A. Lloyd and E. Winsberg. Cham: Springer International Publishing, 325–359. DOI: [10.1007/978-3-319-65058-6_11](https://doi.org/10.1007/978-3-319-65058-6_11).
- Knutti, R., R. Furrer, C. Tebaldi, J. Cermak and G. A. Meehl (2010). “Challenges in Combining Projections from Multiple Climate Models”. *Journal of Climate* 23.10, 2739–2758. DOI: [10.1175/2009JCLI3361.1](https://doi.org/10.1175/2009JCLI3361.1).
- Kobayashi, S., Y. Ota, Y. Harada, A. Ebata, M. Moriya, H. Onoda, K. Onogi, H. Kamahori, C. Kobayashi, H. Endo, K. Miyaoka and K. Takahashi (2015). “The JRA-55 Reanalysis: General Specifications and Basic Characteristics”. *Journal of the Meteorological Society of Japan. Ser. II* 93.1, 5–48. DOI: [10.2151/jmsj.2015-001](https://doi.org/10.2151/jmsj.2015-001).

- Kochendorfer, J., R. Rasmussen, M. Wolff, B. Baker, M. E. Hall, T. Meyers, S. Landolt, A. Jachcik, K. Isaksen, R. Brækkan and R. Leeper (2017). “The quantification and correction of wind-induced precipitation measurement errors”. *Hydrology and Earth System Sciences* 21.4, 1973–1989. DOI: <https://doi.org/10.5194/hess-21-1973-2017>.
- Kolmogorov, A. N. (1941). “The local structure of turbulence in incompressible viscous fluid for very large Reynolds numbers”. *Dokl. Akad. Nauk SSSR*. Vol. 30, 299–303.
- Koutsoyiannis, D. (2004a). “Statistics of extremes and estimation of extreme rainfall: I. Theoretical investigation”. *Hydrological Sciences Journal* 49.4. DOI: [10.1623/hysj.49.4.575.54430](https://doi.org/10.1623/hysj.49.4.575.54430).
- Koutsoyiannis, D. (2004b). “Statistics of extremes and estimation of extreme rainfall: II. Empirical investigation of long rainfall records”. *Hydrological Sciences Journal* 49.4. DOI: [10.1623/hysj.49.4.591.54424](https://doi.org/10.1623/hysj.49.4.591.54424).
- Koutsoyiannis, D. (2006). “An entropic-stochastic representation of rainfall intermittency: The origin of clustering and persistence”. *Water Resources Research* 42.1, W01401. DOI: [10.1029/2005WR004175](https://doi.org/10.1029/2005WR004175).
- Koutsoyiannis, D., D. Kozonis and A. Manetas (1998). “A mathematical framework for studying rainfall intensity-duration-frequency relationships”. *Journal of Hydrology* 206.1-2, 118–135. DOI: [10.1016/S0022-1694\(98\)00097-3](https://doi.org/10.1016/S0022-1694(98)00097-3).
- Kunkel, K. E. (2013). “Uncertainties in Observed Changes in Climate Extremes”. *Extremes in a Changing Climate*. Ed. by A. AghaKouchak, D. Easterling, K. Hsu, S. Schubert and S. Sorooshian. Water Science and Technology Library 65. Springer Netherlands, 287–307.
- Kunkel, K. E., T. R. Karl, H. Brooks, J. Kossin, J. H. Lawrimore, D. Arndt, L. Bosart, D. Changnon, S. L. Cutter, N. Doesken, K. Emanuel, P. Y. Groisman, R. W. Katz, T. Knutson, J. O’Brien, C. J. Paciorek, T. C. Peterson, K. Redmond, D. Robinson, J. Trapp, R. Vose, S. Weaver, M. Wehner, K. Wolter and D. Wuebbles (2013). “Monitoring and Understanding Trends in Extreme Storms: State of Knowledge”. *Bulletin of the American Meteorological Society* 94.4, 499–514. DOI: [10.1175/bams-d-11-00262.1](https://doi.org/10.1175/bams-d-11-00262.1).
- Lebel, T. and J. P. Laborde (1988). “A geostatistical approach for areal rainfall statistics assessment”. *Stochastic Hydrology and Hydraulics* 2.4, 245–261. DOI: [10.1007/BF01544039](https://doi.org/10.1007/BF01544039).
- Leduc, M., A. Mailhot, A. Frigon, J.-L. Martel, R. Ludwig, G. B. Brietzke, M. Giguere, F. Brissette, R. Turcotte, M. Braun and J. Scinocca (2019). “ClimEx project: a 50-member ensemble of climate change projections at 12-km resolution over Europe and northeastern North America with the Canadian Regional Climate Model (CRCM5)”. *Journal of Applied Meteorology and Climatology*. DOI: [10.1175/JAMC-D-18-0021.1](https://doi.org/10.1175/JAMC-D-18-0021.1).
- Lenderink, G., R. Barbero, J. M. Loriaux and H. J. Fowler (2017). “Super-Clausius–Clapeyron Scaling of Extreme Hourly Convective Precipitation and Its Relation to Large-Scale Atmospheric Conditions”. *Journal of Climate* 30.15, 6037–6052. DOI: [10.1175/JCLI-D-16-0808.1](https://doi.org/10.1175/JCLI-D-16-0808.1).
- Li, C., F. Zwiers, X. Zhang and G. Li (2019). “How Much Information Is Required to Well Constrain Local Estimates of Future Precipitation Extremes?”. *Earth’s Future* 7.1, 11–24. DOI: [10.1029/2018EF001001](https://doi.org/10.1029/2018EF001001).
- Li, J., A. Sharma, F. Johnson and J. Evans (2015). “Evaluating the effect of climate change on areal reduction factors using regional climate model projections”. *Journal of Hydrology* 528, 419–434. DOI: [10.1016/j.jhydrol.2015.06.067](https://doi.org/10.1016/j.jhydrol.2015.06.067).
- Liu, C., K. Ikeda, R. Rasmussen, M. Barlage, A. J. Newman, A. F. Prein, F. Chen, L. Chen, M. Clark, A. Dai, J. Dudhia, T. Eidhammer, D. Gochis, E. Gutmann, S. Kurkute, Y. Li, G. Thompson and D. Yates (2017). “Continental-scale convection-permitting modeling of the current and future climate of North America”. *Climate Dynamics* 49.1-2, 71–95. DOI: [10.1007/s00382-016-3327-9](https://doi.org/10.1007/s00382-016-3327-9).
- Liu, C., K. Ikeda, G. Thompson, R. Rasmussen and J. Dudhia (2011). “High-Resolution Simulations of Wintertime Precipitation in the Colorado Headwaters Region: Sensitivity to Physics Parameterizations”. *Monthly Weather Review* 139.11, 3533–3553. DOI: [10.1175/MWR-D-11-00009.1](https://doi.org/10.1175/MWR-D-11-00009.1).
- Lovejoy, S. (1982). “Area-perimeter relation for rain and cloud areas”. *Science* 216.4542, 185–187.
- Lovejoy, S. and B. B. Mandelbrot (1985). “Fractal properties of rain, and a fractal model”. *Tellus A* 37.3, 209–232.
- Lovejoy, S. and D. Schertzer (1985). “Generalized Scale Invariance in the Atmosphere and Fractal Models of Rain”. *Water Resources Research* 21.8, 1233–1250. DOI: [10.1029/WR021i008p01233](https://doi.org/10.1029/WR021i008p01233).
- Lucas-Picher, P., R. Laprise and K. Winger (2017). “Evidence of added value in North American regional climate model hindcast simulations using ever-increasing horizontal resolutions”. *Climate Dynamics* 48.7-8, 2611–2633. DOI: [10.1007/s00382-016-3227-z](https://doi.org/10.1007/s00382-016-3227-z).
- Mahoney, K., M. A. Alexander, G. Thompson, J. J. Barsugli and J. D. Scott (2012). “Changes in hail and flood risk in high-resolution simulations over Colorado’s mountains”. *Nature Climate Change* 2.2, 125. DOI: [10.1038/nclimate1344](https://doi.org/10.1038/nclimate1344).
- Mahoney, K., M. Alexander, J. D. Scott and J. Barsugli (2013). “High-Resolution Downscaled Simulations of Warm-Season Extreme Precipitation Events in the Colorado Front Range under Past and Future Climates”. *J. Climate* 26.21, 8671–8689. DOI: [10.1175/JCLI-D-12-00744.1](https://doi.org/10.1175/JCLI-D-12-00744.1).
- Mailhot, A., I. Beauregard, G. Talbot, D. Caya and S. Biner (2012). “Future changes in intense precipitation over Canada assessed from multi-model NARCCAP ensemble simulations”. *International Journal of Climatology* 32.8, 1151–1163. DOI: [10.1002/joc.2343](https://doi.org/10.1002/joc.2343).

- Mailhot, A. and S. Duchesne (2010). “Design Criteria of Urban Drainage Infrastructures under Climate Change”. *Journal of Water Resources Planning and Management* 136.2, 201–208. DOI: [10.1061/\(ASCE\)WR.1943-5452.0000023](https://doi.org/10.1061/(ASCE)WR.1943-5452.0000023).
- Mailhot, A. and G. Talbot (2011). *Mise À Jour Des Estimateurs Intensité-Durée-Fréquence (idf) Pour Le Sud-Québec Tome I – Données Et Méthodes*. Tech. rep. Tome I. Quebec Canada: Institut national de la recherche scientifique INRS-Eau, Terre et Environnement.
- Mallakpour, I. and G. Villarini (2017). “Analysis of changes in the magnitude, frequency, and seasonality of heavy precipitation over the contiguous USA”. *Theoretical and Applied Climatology* 130.1, 345–363. DOI: [10.1007/s00704-016-1881-z](https://doi.org/10.1007/s00704-016-1881-z).
- Mandelbrot, B. B. (1977). “Les Objects Fractals: Forme, Chance, Dimensions”. *Hasard et Dimension*, Flammarion, Paris.
- Mantegna, G. A., C. J. White, T. A. Remenyi, S. P. Corney and P. Fox-Hughes (2017). “Simulating sub-daily Intensity-Frequency-Duration curves in Australia using a dynamical high-resolution regional climate model”. *Journal of Hydrology* 554.Supplement C, 277–291. DOI: [10.1016/j.jhydrol.2017.09.025](https://doi.org/10.1016/j.jhydrol.2017.09.025).
- Martel, J.-L., A. Mailhot, F. Brissette and D. Caya (2018). “Role of Natural Climate Variability in the Detection of Anthropogenic Climate Change Signal for Mean and Extreme Precipitation at Local and Regional Scales”. *Journal of Climate* 31.11, 4241–4263. DOI: [10.1175/JCLI-D-17-0282.1](https://doi.org/10.1175/JCLI-D-17-0282.1).
- Martynov, A., R. Laprise, L. Sushama, K. Winger, L. Separovic and B. Dugas (2013). “Reanalysis-driven climate simulation over CORDEX North America domain using the Canadian Regional Climate Model, version 5: model performance evaluation”. *Climate Dynamics* 41.11-12, 2973–3005. DOI: [10.1007/s00382-013-1778-9](https://doi.org/10.1007/s00382-013-1778-9).
- McPhillips, L. E., H. Chang, M. V. Chester, Y. Depietri, E. Friedman, N. B. Grimm, J. S. Kominoski, T. McPhearson, P. Méndez-Lázaro, E. J. Rosi and J. Shafiei Shiva (2018). “Defining Extreme Events: A Cross-Disciplinary Review”. *Earth’s Future* 6.3, 441–455. DOI: [10.1002/2017EF000686](https://doi.org/10.1002/2017EF000686).
- Mearns, L. O., M. Bukovsky, S. C. Pryor and V. Magaña (2018). “Downscaling of Climate Information”. *Climate Modelling*. Palgrave Macmillan, Cham, 199–269. DOI: [10.1007/978-3-319-65058-6_8](https://doi.org/10.1007/978-3-319-65058-6_8).
- Mearns, L. O., W. J. Gutowski, R. Jones, L. Y. Leung, S. McGinnis, A. M. B. Nunes and Y. Qian (2007). “The North American regional climate change assessment program dataset”. *National Center for atmospheric research earth system grid data portal*, Boulder, CO. Data downloaded, 01–03. DOI: [doi:10.5065/D6RN35ST](https://doi.org/10.5065/D6RN35ST).
- Mearns, L. O., W. Gutowski, R. Jones, R. Leung, S. McGinnis, A. Nunes and Y. Qian (2009). “A Regional Climate Change Assessment Program for North America”. *Eos, Transactions American Geophysical Union* 90.36, 311–311. DOI: [10.1029/2009E0360002](https://doi.org/10.1029/2009E0360002).
- Meinshausen, M., S. J. Smith, K. Calvin, J. S. Daniel, M. L. T. Kainuma, J.-F. Lamarque, K. Matsumoto, S. A. Montzka, S. C. B. Raper, K. Riahi, A. Thomson, G. J. M. Velders and D. P. P. v. Vuuren (2011). “The RCP greenhouse gas concentrations and their extensions from 1765 to 2300”. *Climatic Change* 109.1-2, 213. DOI: [10.1007/s10584-011-0156-z](https://doi.org/10.1007/s10584-011-0156-z).
- Mekis, E. and L. A. Vincent (2011). “An Overview of the Second Generation Adjusted Daily Precipitation Dataset for Trend Analysis in Canada”. *Atmosphere-Ocean* 49.2, 163–177. DOI: [10.1080/07055900.2011.583910](https://doi.org/10.1080/07055900.2011.583910).
- Mélèse, V., J. Blanchet and G. Molinié (2018). “Uncertainty estimation of Intensity–Duration–Frequency relationships: A regional analysis”. *Journal of Hydrology* 558, 579–591. DOI: [10.1016/j.jhydrol.2017.07.054](https://doi.org/10.1016/j.jhydrol.2017.07.054).
- Melillo, J. M., T. C. Richmond and G. W. Yohe (2014). “Climate Change Impacts in the United States: The Third National Climate Assessment”. *US Global Change Research Program*.
- Menabde, M., A. Seed and G. Pegram (1999). “A simple scaling model for extreme rainfall”. *Water Resources Research* 35.1, 335–339.
- Metcalf, J. R., B. Routledge and K. Devine (1997). “Rainfall Measurement in Canada: Changing Observational Methods and Archive Adjustment Procedures”. *Journal of Climate* 10.1, 92–101. DOI: [10.1175/1520-0442\(1997\)010<0092:RMICCO>2.0.CO;2](https://doi.org/10.1175/1520-0442(1997)010<0092:RMICCO>2.0.CO;2).
- Min, S.-K., X. Zhang, F. W. Zwiers and G. C. Hegerl (2011). “Human contribution to more-intense precipitation extremes”. *Nature* 470.7334, 378–381. DOI: [10.1038/nature09763](https://doi.org/10.1038/nature09763).
- Mineo, C., E. Ridolfi, F. Napolitano and F. Russo (2018). “The areal reduction factor: A new analytical expression for the Lazio Region in central Italy”. *Journal of Hydrology* 560, 471–479. DOI: [10.1016/j.jhydrol.2018.03.033](https://doi.org/10.1016/j.jhydrol.2018.03.033).
- Mladjic, B., L. Sushama, M. N. Khaliq, R. Laprise, D. Caya and R. Roy (2011). “Canadian RCM Projected Changes to Extreme Precipitation Characteristics over Canada”. *Journal of Climate* 24.10, 2565–2584. DOI: [10.1175/2010JCLI3937.1](https://doi.org/10.1175/2010JCLI3937.1).
- Musy, A. and V. Laglaine (2005). “Hydrologie générale”. *Section SIE et GC. 4^{ème} semestre*.
- Myhre, G., D. Shindell, F. Bréon, W. Collins, J. Fuglestedt, J. Huang, D. Koch, J. Lamarque, D. Lee, B. Mendoza, et al. (2013). “Anthropogenic and natural radiative forcing”. *Climate Change 2013: The Physical Science Basis. Contribution of Working Group I to the Fifth Assessment Report of the Intergovernmental Panel on Climate Change ed TF Stocker, D Qin, GK Plattner, M Tignor, SK Allen, J Boschung, A Nauels, Y Xia, V Bex and PM Midgley*. New York: Cambridge University Press.

- Nakicenovic, N. and R. Swart (2000). “Special Report on Emissions Scenarios”. *Special Report on Emissions Scenarios*, Edited by Nebojsa Nakicenovic and Robert Swart, pp. 612. ISBN 0521804930. Cambridge, UK: Cambridge University Press, July 2000. Vol. -1.
- Naveau, P., A. Ribes, F. Zwiers, A. Hannart, A. Tuel and P. Yiou (2018). “Revising Return Periods for Record Events in a Climate Event Attribution Context”. *Journal of Climate* 31.9, 3411–3422. DOI: [10.1175/JCLI-D-16-0752.1](https://doi.org/10.1175/JCLI-D-16-0752.1).
- NCDC (2003). Data Set 3240 (DSI-3240). Hourly Precipitation Data. Tech. rep. Asheville, NC, USA: National Climatic Data Center.
- NERC (1975). Flood studies report. Vol. 2. UK Natural Environment Research Council London.
- Nhat, L. M., Y. Tachikawa, T. Sayama and K. Takara (2007). “A Simple Scaling Characteristics of Rainfall in Time and Space to Derive Intensity Duration Frequency Relationships”. 51, 73–78. DOI: [10.2208/probe.51.73](https://doi.org/10.2208/probe.51.73).
- Olsson, J., V. P. Singh and K. Jinno (1999). “Effect of spatial averaging on temporal statistical and scaling properties of rainfall”. *Journal of Geophysical Research: Atmospheres* 104.D16, 19117–19126. DOI: [10.1029/1999JD900271](https://doi.org/10.1029/1999JD900271).
- Omolayo, A. S. (1993). “On the transposition of areal reduction factors for rainfall frequency estimation”. *Journal of Hydrology* 145.1, 191–205. DOI: [https://doi.org/10.1016/0022-1694\(93\)90227-Z](https://doi.org/10.1016/0022-1694(93)90227-Z).
- Overeem, A., T. A. Buishand, I. Holleman and R. Uijlenhoet (2010). “Extreme value modeling of areal rainfall from weather radar”. *Water Resources Research* 46.9, W09514. DOI: [10.1029/2009WR008517](https://doi.org/10.1029/2009WR008517).
- Overeem, A., I. Holleman and A. Buishand (2009). “Derivation of a 10-Year Radar-Based Climatology of Rainfall”. *Journal of Applied Meteorology and Climatology* 48.7, 1448–1463. DOI: [10.1175/2009JAMC1954.1](https://doi.org/10.1175/2009JAMC1954.1).
- Panthou, G., T. Vischel, T. Lebel, J. Blanchet, G. Quantin and A. Ali (2012). “Extreme rainfall in West Africa: A regional modeling”. *Water Resources Research* 48.8, n/a–n/a. DOI: [10.1029/2012wr012052](https://doi.org/10.1029/2012wr012052).
- Panthou, G., T. Vischel, T. Lebel, G. Quantin and G. Molinié (2014). “Characterising the space–time structure of rainfall in the Sahel with a view to estimating IDAF curves”. *Hydrology and Earth System Sciences* 18.12, 5093–5107. DOI: [10.5194/hess-18-5093-2014](https://doi.org/10.5194/hess-18-5093-2014).
- Papalexiou, S. M., D. Koutsoyiannis and C. Makropoulos (2013). “How extreme is extreme? An assessment of daily rainfall distribution tails”. *Hydrology and Earth System Sciences* 17.2, 851–862. DOI: [10.5194/hess-17-851-2013](https://doi.org/10.5194/hess-17-851-2013).
- Papalexiou, S. M. and D. Koutsoyiannis (2013a). “Battle of extreme value distributions: A global survey on extreme daily rainfall”. *Water Resources Research* 49.1, 187–201. DOI: [10.1029/2012WR012557](https://doi.org/10.1029/2012WR012557).
- Papalexiou, S. M. and D. Koutsoyiannis (2013b). “Battle of extreme value distributions: A global survey on extreme daily rainfall”. *Water Resources Research* 49.1, 187–201. DOI: [10.1029/2012WR012557](https://doi.org/10.1029/2012WR012557).
- Parker, W. S. (2016). “Reanalyses and Observations: What’s the difference?”: *Bulletin of the American Meteorological Society*. DOI: [10.1175/BAMS-D-14-00226.1](https://doi.org/10.1175/BAMS-D-14-00226.1).
- Pendergrass, A. G. (2018). “What precipitation is extreme?”: *Science* 360.6393, 1072–1073. DOI: [10.1126/science.aat1871](https://doi.org/10.1126/science.aat1871).
- Plummer, D. A., D. Caya, A. Frigon, H. Côté, M. Giguère, D. Paquin, S. Biner, R. Harvey and R. de Elia (2006). “Climate and Climate Change over North America as Simulated by the Canadian RCM”. *Journal of Climate* 19.13, 3112–3132. DOI: [10.1175/JCLI3769.1](https://doi.org/10.1175/JCLI3769.1).
- Prein, A. F., A. Gobiet, H. Truhetz, K. Keuler, K. Goergen, C. Teichmann, C. F. Maule, E. v. Meijgaard, D. M., G. Nikulin, R. Vautard, A. Colette, E. Kjellstrom and D. Jacob (2016). “Precipitation in the EURO-CORDEX 0.11° and 0.44° simulations: high resolution, high benefits?”: *Climate Dynamics* 46.1-2, 383–412. DOI: [10.1007/s00382-015-2589-y](https://doi.org/10.1007/s00382-015-2589-y).
- Prein, A. F., W. Langhans, G. Fossier, A. Ferrone, N. Ban, K. Goergen, M. Keller, M. Tolle, O. Gutjahr, F. Feser, E. Brisson, S. Kollet, J. Schmidli, N. P. M. van Lipzig and R. Leung (2015). “A review on regional convection-permitting climate modeling: Demonstrations, prospects, and challenges”. *Reviews of Geophysics* 53.2, 2014RG000475. DOI: [10.1002/2014RG000475](https://doi.org/10.1002/2014RG000475).
- Prein, A. F., C. Liu, K. Ikeda, R. Bullock, R. M. Rasmussen, G. J. Holland and M. Clark (2017a). “Simulating North American mesoscale convective systems with a convection-permitting climate model”. *Climate Dynamics*, 1–16. DOI: [10.1007/s00382-017-3993-2](https://doi.org/10.1007/s00382-017-3993-2).
- Prein, A. F., C. Liu, K. Ikeda, S. B. Trier, R. M. Rasmussen, G. J. Holland and M. P. Clark (2017b). “Increased rainfall volume from future convective storms in the US”. *Nature Climate Change* 7.12, 880. DOI: [10.1038/s41558-017-0007-7](https://doi.org/10.1038/s41558-017-0007-7).
- Ragulina, G. and T. Reitan (2017). “Generalized extreme value shape parameter and its nature for extreme precipitation using long time series and the Bayesian approach”. *Hydrological Sciences Journal* 62.6, 863–879. DOI: [10.1080/02626667.2016.1260134](https://doi.org/10.1080/02626667.2016.1260134).
- Rasmussen, K. L., A. F. Prein, R. M. Rasmussen, K. Ikeda and C. Liu (2017). “Changes in the convective population and thermodynamic environments in convection-permitting regional climate simulations over the United States”. *Climate Dynamics*, 1–26. DOI: [10.1007/s00382-017-4000-7](https://doi.org/10.1007/s00382-017-4000-7).
- Rasmussen, R., K. Ikeda, C. Liu, D. Gochis, M. Clark, A. Dai, E. Gutmann, J. Dudhia, F. Chen, M. Barlage, D. Yates and G. Zhang (2014). “Climate Change Impacts on the Water Balance of the Colorado Headwaters: High-

- Resolution Regional Climate Model Simulations”. *Journal of Hydrometeorology* 15.3, 1091–1116. DOI: [10.1175/JHM-D-13-0118.1](https://doi.org/10.1175/JHM-D-13-0118.1).
- Rasmussen, R., C. Liu, K. Ikeda, D. Gochis, D. Yates, F. Chen, M. Tewari, M. Barlage, J. Dudhia, W. Yu, K. Miller, K. Arsenault, V. Grubisic, G. Thompson and E. Gutmann (2011). “High-Resolution Coupled Climate Runoff Simulations of Seasonal Snowfall over Colorado: A Process Study of Current and Warmer Climate”. *Journal of Climate* 24.12, 3015–3048. DOI: [10.1175/2010JCLI3985.1](https://doi.org/10.1175/2010JCLI3985.1).
- Rienecker, M. M., M. J. Suarez, R. Gelaro, R. Todling, J. Bacmeister, E. Liu, M. G. Bosilovich, S. D. Schubert, L. Takacs, G.-K. Kim, S. Bloom, J. Chen, D. Collins, A. Conaty, A. da Silva, W. Gu, J. Joiner, R. D. Koster, R. Lucchesi, A. Molod, T. Owens, S. Pawson, P. Pegion, C. R. Redder, R. Reichle, F. R. Robertson, A. G. Ruddick, M. Sienkiewicz and J. Woollen (2011). “MERRA: NASA’s Modern-Era Retrospective Analysis for Research and Applications”. *Journal of Climate* 24.14, 3624–3648. DOI: [10.1175/JCLI-D-11-00015.1](https://doi.org/10.1175/JCLI-D-11-00015.1).
- Riette, S. and D. Caya (2002). Sensitivity of short simulations to the various parameters in the new CRCM spectral nudging.
- Rodriguez-Iturbe, I., V. K. Gupta and E. Waymire (1984). “Scale considerations in the modeling of temporal rainfall”. *Water Resources Research* 20.11, 1611–1619.
- Rodriguez-Iturbe, I. and J. M. Mejía (1974). “On the transformation of point rainfall to areal rainfall”. *Water Resources Research* 10.4, 729–735. DOI: [10.1029/WR010i004p00729](https://doi.org/10.1029/WR010i004p00729).
- Rootzén, H. and R. W. Katz (2013). “Design Life Level: Quantifying risk in a changing climate”. *Water Resources Research* 49.9, 5964–5972. DOI: [10.1002/wrcr.20425](https://doi.org/10.1002/wrcr.20425).
- Rummukainen, M. (2016). “Added value in regional climate modeling”. *Wiley Interdisciplinary Reviews: Climate Change* 7.1, 145–159. DOI: [10.1002/wcc.378](https://doi.org/10.1002/wcc.378).
- Salzen, K. von, J. F. Scinocca, N. A. McFarlane, J. Li, J. N. S. Cole, D. Plummer, D. Verseghy, M. C. Reader, X. Ma, M. Lazare and L. Solheim (2013). “The Canadian Fourth Generation Atmospheric Global Climate Model (CanAM4). Part I: Representation of Physical Processes”. *Atmosphere-Ocean* 51.1, 104–125. DOI: [10.1080/07055900.2012.755610](https://doi.org/10.1080/07055900.2012.755610).
- Sanderson, B. M., K. W. Oleson, W. G. Strand, F. Lehner and B. C. O’Neill (2018). “A new ensemble of GCM simulations to assess avoided impacts in a climate mitigation scenario”. *Climatic Change* 146.3, 303–318. DOI: [10.1007/s10584-015-1567-z](https://doi.org/10.1007/s10584-015-1567-z).
- Sane, Y., G. Panthou, A. Bodian, T. Vischel, T. Lebel, H. Dacosta, G. Quantin, C. Wilcox, O. Ndiaye, A. Diongue-Niang and M. Diop Kane (2018). “Intensity–duration–frequency (IDF) rainfall curves in Senegal”. *Natural Hazards and Earth System Sciences* 18.7, 1849–1866. DOI: <https://doi.org/10.5194/nhess-18-1849-2018>.
- Sarhadi, A. and E. D. Soulis (2017). “Time-varying extreme rainfall intensity-duration-frequency curves in a changing climate”. *Geophysical Research Letters*, 2016GL072201. DOI: [10.1002/2016GL072201](https://doi.org/10.1002/2016GL072201).
- Schertzer, D. and S. Lovejoy (1987). “Physical modeling and analysis of rain and clouds by anisotropic scaling multiplicative processes”. *Journal of Geophysical Research: Atmospheres* 92.D8, 9693–9714. DOI: [10.1029/JD092iD08p09693](https://doi.org/10.1029/JD092iD08p09693).
- Schneider, U., A. Becker, P. Finger, A. Meyer-Christoffer, M. Ziese and B. Rudolf (2014). “GPCC’s new land surface precipitation climatology based on quality-controlled in situ data and its role in quantifying the global water cycle”. *Theoretical and Applied Climatology* 115.1-2, 15–40.
- Scinocca, J. F., V. V. Kharin, Y. Jiao, M. W. Qian, M. Lazare, L. Solheim, G. M. Flato, S. Biner, M. Desgagne and B. Dugas (2016). “Coordinated Global and Regional Climate Modeling”. *Journal of Climate* 29.1, 17–35. DOI: [10.1175/JCLI-D-15-0161.1](https://doi.org/10.1175/JCLI-D-15-0161.1).
- Seneviratne, S. I., N. Nicholls, D. Easterling, C. Goodess, S. Kanae, J. Kossin, Y. Luo, J. Marengo, K. McInnes, M. Rahimi, et al. (2012). “Changes in climate extremes and their impacts on the natural physical environment”. *Managing the risks of extreme events and disasters to advance climate change adaptation*, 109–230.
- Separovic, L., A. Alexandru, R. Laprise, A. Martynov, L. Sushama, K. Winger, K. Tete and M. Valin (2013). “Present climate and climate change over North America as simulated by the fifth-generation Canadian regional climate model”. *Clim Dyn* 41.11-12, 3167–3201. DOI: [10.1007/s00382-013-1737-5](https://doi.org/10.1007/s00382-013-1737-5).
- Separovic, L., R. d. Elia and R. Laprise (2012). “Impact of spectral nudging and domain size in studies of RCM response to parameter modification”. *Climate Dynamics* 38.7-8, 1325–1343. DOI: [10.1007/s00382-011-1072-7](https://doi.org/10.1007/s00382-011-1072-7).
- Sevruk, B., M. Ondrás and B. Chvíla (2009). “The WMO precipitation measurement intercomparisons”. *Atmospheric Research*. 7th International Workshop on Precipitation in Urban Areas 7th International Workshop on Precipitation in Urban Areas 92.3, 376–380. DOI: [10.1016/j.atmosres.2009.01.016](https://doi.org/10.1016/j.atmosres.2009.01.016).
- Shephard, M. W., E. Mekis, R. J. Morris, Y. Feng, X. Zhang, K. Kilcup and R. Fleetwood (2014). “Trends in Canadian Short-Duration Extreme Rainfall: Including an Intensity–Duration–Frequency Perspective”. *Atmosphere-Ocean* 52.5, 398–417. DOI: [10.1080/07055900.2014.969677](https://doi.org/10.1080/07055900.2014.969677).
- Sigmond, M. and J. C. Fyfe (2016). “Tropical Pacific impacts on cooling North American winters”. *Nature Climate Change* 6.10, 970–974. DOI: [10.1038/nclimate3069](https://doi.org/10.1038/nclimate3069).
- Sivapalan, M. and G. Blöschl (1998). “Transformation of point rainfall to areal rainfall: Intensity-duration-frequency curves”. *Journal of Hydrology* 204.1-4, 150–167. DOI: [10.1016/S0022-1694\(97\)00117-0](https://doi.org/10.1016/S0022-1694(97)00117-0).

- Skamarock, C., B. Klemp, J. Dudhia, O. Gill, D. Barker, G. Duda, X.-y. Huang, W. Wang and G. Powers (2008). “A Description of the Advanced Research WRF Version 3”. DOI: [10.5065/D68S4MVH](https://doi.org/10.5065/D68S4MVH).
- Skeeter, W. J., J. C. Senkbeil and D. J. Keellings (2018). “Spatial and temporal changes in the frequency and magnitude of intense precipitation events in the southeastern United States”. *International Journal of Climatology* 1.15. DOI: [10.1002/joc.5841](https://doi.org/10.1002/joc.5841).
- Stephens, G. L., T. L’Ecuyer, R. Forbes, A. Gettelmen, J.-C. Golaz, A. Bodas-Salcedo, K. Suzuki, P. Gabriel and J. Haynes (2010). “Dreary state of precipitation in global models”. *Journal of Geophysical Research: Atmospheres* 115.D24. DOI: [10.1029/2010JD014532](https://doi.org/10.1029/2010JD014532).
- Stephenson, D. B., H. F. Diaz and R. J. Murnane (2008). Definition, diagnosis, and origin of extreme weather and climate events. Vol. 348. Cambridge University Press: New York.
- Stone, D. A., A. J. Weaver and F. W. Zwiers (2000). “Trends in Canadian precipitation intensity”. *Atmosphere-Ocean* 38.2, 321–347. DOI: [10.1080/07055900.2000.9649651](https://doi.org/10.1080/07055900.2000.9649651).
- Stott, P. A., N. P. Gillett, G. C. Hegerl, D. J. Karoly, D. A. Stone, X. Zhang and F. Zwiers (2010). “Detection and attribution of climate change: a regional perspective”. *Wiley Interdisciplinary Reviews: Climate Change* 1.2, 192–211. DOI: [10.1002/wcc.34](https://doi.org/10.1002/wcc.34).
- Sunyer, M. A., J. Luchner, C. Onof, H. Madsen and K. Arnbjerg-Nielsen (2016). “Assessing the importance of spatio-temporal RCM resolution when estimating sub-daily extreme precipitation under current and future climate conditions: SUB-DAILY EXTREME PRECIPITATION FROM RCM”. *International Journal of Climatology*. DOI: [10.1002/joc.4733](https://doi.org/10.1002/joc.4733).
- Svensson, C. and D. A. Jones (2010). “Review of methods for deriving areal reduction factors”. *Journal of Flood Risk Management* 3.3, 232–245. DOI: [10.1111/j.1753-318X.2010.01075.x](https://doi.org/10.1111/j.1753-318X.2010.01075.x).
- Tapiador, F. J., A. Navarro, V. Levizzani, E. Garcia-Ortega, G. J. Huffman, C. Kidd, P. A. Kucera, C. D. Kummerow, H. Masunaga, W. A. Petersen, R. Roca, J.-L. Sanchez, W.-K. Tao and F. J. Turk (2017). “Global precipitation measurements for validating climate models”. *Atmospheric Research* 197. Supplement C, 1–20. DOI: [10.1016/j.atmosres.2017.06.021](https://doi.org/10.1016/j.atmosres.2017.06.021).
- Taylor, K. E., R. J. Stouffer and G. A. Meehl (2011). “An Overview of CMIP5 and the Experiment Design”. *Bulletin of the American Meteorological Society* 93.4, 485–498. DOI: [10.1175/BAMS-D-11-00094.1](https://doi.org/10.1175/BAMS-D-11-00094.1).
- Tebaldi, C. and R. Knutti (2007). “The use of the multi-model ensemble in probabilistic climate projections”. *Philosophical Transactions of the Royal Society A: Mathematical, Physical and Engineering Sciences* 365.1857, 2053–2075. DOI: [10.1098/rsta.2007.2076](https://doi.org/10.1098/rsta.2007.2076).
- Teegavarapu, R. S. V. (2012). Floods in a Changing Climate: Extreme Precipitation. Cambridge University Press, 1–289.
- Tessier, Y., S. Lovejoy and D. Schertzer (1993). “Universal Multifractals: Theory and observations for rain and clouds”. *J. Appl. Meteorol.*, 32, 223–250 32, 223–250.
- Thompson, D. W. J., E. A. Barnes, C. Deser, W. E. Foust and A. S. Phillips (2015). “Quantifying the Role of Internal Climate Variability in Future Climate Trends”. *Journal of Climate* 28.16, 6443–6456. DOI: [10.1175/JCLI-D-14-00830.1](https://doi.org/10.1175/JCLI-D-14-00830.1).
- Toreti, A., P. Naveau, M. Zampieri, A. Schindler, E. Scoccimarro, E. Xoplaki, H. A. Dijkstra, S. Gualdi and J. Luterbacher (2013). “Projections of global changes in precipitation extremes from Coupled Model Intercomparison Project Phase 5 models”. *Geophysical Research Letters* 40.18, 4887–4892. DOI: [10.1002/grl.50940](https://doi.org/10.1002/grl.50940).
- Touma, D., A. M. Michalak, D. L. Swain and N. S. Diffenbaugh (2018). “Characterizing the Spatial Scales of Extreme Daily Precipitation in the United States”. *Journal of Climate* 31.19, 8023–8037. DOI: [10.1175/JCLI-D-18-0019.1](https://doi.org/10.1175/JCLI-D-18-0019.1).
- Trenberth, K. E. (2011). “Changes in precipitation with climate change”. *Climate Research* 47.1, 123–138. DOI: [10.3354/cr00953](https://doi.org/10.3354/cr00953).
- Trenberth, K. E., A. Dai, R. M. Rasmussen and D. B. Parsons (2003). “The Changing Character of Precipitation”. *Bulletin of the American Meteorological Society* 84.9, 1205–1217. DOI: [10.1175/bams-84-9-1205](https://doi.org/10.1175/bams-84-9-1205).
- Trenberth, K. E., Y. Zhang and M. Gehne (2017). “Intermittency in Precipitation: Duration, Frequency, Intensity, and Amounts Using Hourly Data”. *Journal of Hydrometeorology* 18.5, 1393–1412. DOI: [10.1175/JHM-D-16-0263.1](https://doi.org/10.1175/JHM-D-16-0263.1).
- Tustison, B., D. Harris and E. Foufoula-Georgiou (2001). “Scale issues in verification of precipitation forecasts”. *Journal of Geophysical Research: Atmospheres* 106.D11, 11775–11784. DOI: [10.1029/2001JD900066](https://doi.org/10.1029/2001JD900066).
- Uppala, S. M., P. W. Kållberg, A. J. Simmons, U. Andrae, V. D. C. Bechtold, M. Fiorino, J. K. Gibson, J. Haseler, A. Hernandez, G. A. Kelly, X. Li, K. Onogi, S. Saarinen, N. Sokka, R. P. Allan, E. Andersson, K. Arpe, M. A. Balmaseda, A. C. M. Beljaars, L. V. D. Berg, J. Bidlot, N. Bormann, S. Caires, F. Chevallier, A. Dethof, M. Dragosavac, M. Fisher, M. Fuentes, S. Hagemann, E. Hólm, B. J. Hoskins, L. Isaksen, P. A. E. M. Janssen, R. Jenne, A. P. McNally, J. F. Mahfouf, J. J. Morcrette, N. A. Rayner, R. W. Saunders, P. Simon, A. Sterl, K. E. Trenberth, A. Untch, D. Vasiljevic, P. Viterbo and J. Woollen (2005). “The ERA-40 re-analysis”. *Quarterly Journal of the Royal Meteorological Society* 131.612, 2961–3012. DOI: [10.1256/qj.04.176](https://doi.org/10.1256/qj.04.176).
- Ushio, T., K. Sasashige, T. Kubota, S. Shige, K. Okamoto, K. Aonashi, T. Inoue, N. Takahashi, T. Iguchi, M. Kachi, R. Oki, T. Morimoto and Z.-I. Kawasaki (2009). “A Kalman Filter Approach to the Global Satellite Mapping

- of Precipitation (GSMaP) from Combined Passive Microwave and Infrared Radiometric Data”. *Journal of the Meteorological Society of Japan. Ser. II* 87A, 137–151. DOI: [10.2151/jmsj.87A.137](https://doi.org/10.2151/jmsj.87A.137).
- Van de Vyver, H. (2012). “Spatial regression models for extreme precipitation in Belgium”. *Water Resources Research* 48.9, n/a–n/a. DOI: [10.1029/2011wr011707](https://doi.org/10.1029/2011wr011707).
- Van Vuuren, D. P., J. Edmonds, M. Kainuma, K. Riahi, A. Thomson, K. Hibbard, G. C. Hurtt, T. Kram, V. Krey, J.-F. Lamarque, et al. (2011). “The representative concentration pathways: an overview”. *Climatic Change* 109, 5–31.
- Varin, C., N. M. Reid and D. (Firth (2011). “An overview of composite likelihood methods”. *Statistica Sinica* Vol.21.No.1, 5–42.
- Vecchi, G. A. and B. J. Soden (2007). “Global Warming and the Weakening of the Tropical Circulation”. *Journal of Climate* 20.17, 4316–4340. DOI: [10.1175/JCLI4258.1](https://doi.org/10.1175/JCLI4258.1).
- Veneziano, D. and P. Furcolo (2002). “Multifractality of rainfall and scaling of intensity-duration-frequency curves”. *Water Resources Research* 38.12, 1306. DOI: [10.1029/2001WR000372](https://doi.org/10.1029/2001WR000372).
- Veneziano, D. and A. Langousis (2005). “The areal reduction factor: A multifractal analysis”. *Water Resources Research* 41.7, W07008. DOI: [10.1029/2004WR003765](https://doi.org/10.1029/2004WR003765).
- Veneziano, D., C. Lepore, A. Langousis and P. Furcolo (2007). “Marginal methods of intensity-duration-frequency estimation in scaling and nonscaling rainfall”. *Water Resources Research* 43.10, n/a–n/a. DOI: [10.1029/2007wr006040](https://doi.org/10.1029/2007wr006040).
- Veneziano, D. and S. Yoon (2013). “Rainfall extremes, excesses, and intensity-duration-frequency curves: A unified asymptotic framework and new nonasymptotic results based on multifractal measures”. *Water Resources Research* 49.7, 4320–4334. DOI: [10.1002/wrcr.20352](https://doi.org/10.1002/wrcr.20352).
- Venugopal, V., E. Foufoula-Georgiou and V. Sapozhnikov (1999). “Evidence of dynamic scaling in space-time rainfall”. *Journal of Geophysical Research* 104.D24, 31, 599–31, 610. DOI: [10.1029/1999jd900437](https://doi.org/10.1029/1999jd900437).
- Vincent, L. A., X. Zhang, É. Mekis, H. Wan and E. J. Bush (2018). “Changes in Canada’s Climate: Trends in Indices Based on Daily Temperature and Precipitation Data”. *Atmosphere-Ocean* 0.0, 1–18. DOI: [10.1080/07055900.2018.1514579](https://doi.org/10.1080/07055900.2018.1514579).
- Vincent, L. A. and E. Mekis (2006). “Changes in daily and extreme temperature and precipitation indices for Canada over the twentieth century”. *Atmosphere-Ocean* 44.2, 177–193.
- Von Mises, R. (1936). “La distribution de la plus grande de n valeurs”. *Rev. math. Union interbalcanique* 1.1.
- Wasko, C., A. Sharma and S. Westra (2016). “Reduced spatial extent of extreme storms at higher temperatures”. *Geophysical Research Letters* 43.8, 4026–4032. DOI: [10.1002/2016GL068509](https://doi.org/10.1002/2016GL068509).
- Wazneh, H., M. A. Arain and P. Coulibaly (2017). “Historical Spatial and Temporal Climate Trends in Southern Ontario, Canada”. *Journal of Applied Meteorology and Climatology* 56.10, 2767–2787. DOI: [10.1175/JAMC-D-16-0290.1](https://doi.org/10.1175/JAMC-D-16-0290.1).
- Wehner, M. F. (2013). “Very extreme seasonal precipitation in the NARCCAP ensemble: model performance and projections”. *Climate Dynamics* 40.1, 59–80. DOI: [10.1007/s00382-012-1393-1](https://doi.org/10.1007/s00382-012-1393-1).
- Westra, S., H. J. Fowler, J. P. Evans, L. V. Alexander, P. Berg, F. Johnson, E. J. Kendon, G. Lenderink and N. M. Roberts (2014). “Future changes to the intensity and frequency of short-duration extreme rainfall”. *Reviews of Geophysics* 52.3, 2014RG000464. DOI: [10.1002/2014RG000464](https://doi.org/10.1002/2014RG000464).
- WMO (2008). Guide to Meteorological Instruments and Methods of Observation. Tech. rep. 8. Geneva: WMO.
- Woodhams, B. J., C. E. Birch, J. H. Marsham, C. L. Bain, N. M. Roberts and D. F. A. Boyd (2018). “What Is the Added Value of a Convection-Permitting Model for Forecasting Extreme Rainfall over Tropical East Africa?”. *Monthly Weather Review* 146.9, 2757–2780. DOI: [10.1175/MWR-D-17-0396.1](https://doi.org/10.1175/MWR-D-17-0396.1).
- Wright, D. B., D. B. Kirschbaum and S. Yatheendradas (2017). “Satellite Precipitation Characterization, Error Modeling, and Error Correction Using Censored Shifted Gamma Distributions”. *Journal of Hydrometeorology* 18.10, 2801–2815. DOI: [10.1175/JHM-D-17-0060.1](https://doi.org/10.1175/JHM-D-17-0060.1).
- Xie, P., M. Chen and W. Shi (2010). “CPC unified gauge-based analysis of global daily precipitation”. *Preprints, 24th Conf. on Hydrology, Atlanta, GA, Amer. Meteor. Soc.* Vol. 2.
- Xie, P., M. Chen, S. Yang, A. Yatagai, T. Hayasaka, Y. Fukushima and C. Liu (2007). “A Gauge-Based Analysis of Daily Precipitation over East Asia”. *Journal of Hydrometeorology* 8.3, 607–626. DOI: [10.1175/JHM583.1](https://doi.org/10.1175/JHM583.1).
- Xie, P. and R. J. Joyce (2014). “Integrating Information from Satellite Observations and Numerical Models for Improved Global Precipitation Analyses”. *Remote Sensing of the Terrestrial Water Cycle*. Ed. by V. Lakshmi, D. Alsdorf, r. Anderson, S. Biancamaria, M. Cosh, J. Entin, G. Huffman, W. Kustas, P. v. Oevelen, T. Painter, J. Parajka, t. Rodell and C. RÄEdiger. DOI: [10.1002/9781118872086.ch3](https://doi.org/10.1002/9781118872086.ch3). John Wiley & Sons, Inc, 43–59.
- Xie, P., R. Joyce, S. Wu, S.-H. Yoo, Y. Yarosh, F. Sun and R. Lin (2017). “Reprocessed, Bias-Corrected CMORPH Global High-Resolution Precipitation Estimates from 1998”. *Journal of Hydrometeorology* 18.6, 1617–1641. DOI: [10.1175/JHM-D-16-0168.1](https://doi.org/10.1175/JHM-D-16-0168.1).
- Xie, P. and A.-Y. Xiong (2011). “A conceptual model for constructing high-resolution gauge-satellite merged precipitation analyses”. *Journal of Geophysical Research: Atmospheres* 116.D21, D21106. DOI: [10.1029/2011JD016118](https://doi.org/10.1029/2011JD016118).

- Ye, L., L. S. Hanson, P. Ding, D. Wang and R. M. Vogel (2018). “The Probability Distribution of Daily Precipitation at the Point and Catchment Scales in the United States”. *Hydrology and Earth System Sciences Discussions*, 1–28. DOI: <https://doi.org/10.5194/hess-2018-85>.
- Ylhaisi, J. (2014). “Limitations of climate model simulations to support climate change adaptation”. Doctoral dissertation. University of Helsinki, Faculty of Science, Department of Physics, Division of atmospheric sciences.
- Yu, P.-S., T.-C. Yang and C.-S. Lin (2004). “Regional rainfall intensity formulas based on scaling property of rainfall”. *Journal of Hydrology* 295.1-4, 108–123. DOI: [10.1016/j.jhydrol.2004.03.003](https://doi.org/10.1016/j.jhydrol.2004.03.003).
- Zadra, A., D. Caya, J. CÅŽtÅ©, B. Dugas, C. Jones, R. Laprise, K. Winger and L.-P. Caron (2008). “The next Canadian regional climate model”. *Phys Can* 64.2, 75–83.
- Zhang, X., W. D. Hogg and É. Mekis (2001). “Spatial and Temporal Characteristics of Heavy Precipitation Events over Canada”. *Journal of Climate* 14.9, 1923–1936. DOI: [10.1175/1520-0442\(2001\)014<1923:SATCOH>2.0.CO;2](https://doi.org/10.1175/1520-0442(2001)014<1923:SATCOH>2.0.CO;2).
- Zhang, X., L. A. Vincent, W. Hogg and A. Niitsoo (2000). “Temperature and precipitation trends in Canada during the 20th century”. *Atmosphere-Ocean* 38.3, 395–429. DOI: [10.1080/07055900.2000.9649654](https://doi.org/10.1080/07055900.2000.9649654).
- Zhang, X. and F. W. Zwiers (2013). “Statistical Indices for the Diagnosing and Detecting Changes in Extremes”. *Extremes in a Changing Climate*. Ed. by A. AghaKouchak, D. Easterling, K. Hsu, S. Schubert and S. Sorooshian. Water Science and Technology Library 65. Springer Netherlands, 1–14.

Part IV

Appendix

Appendix A:

GEV parameter estimation

Two common estimation methods for the Generalized Extreme Value (GEV) distribution are described: the Maximum Likelihood (ML) method [Azzalini 1996; Coles 2001] and the Probability Weighted Moment (PWM) method [Greenwood et al. 1979; Hosking et al. 1985].

A.1 Maximum Likelihood (ML) estimation

Consider a random variable X described by the probability density function $f(x; \boldsymbol{\vartheta})$, where $f(\cdot)$ is a function known except that for the values of the parameters in the vector $\boldsymbol{\vartheta}$. Once a sample $\boldsymbol{x} = (x_1, x_2, \dots, x_N)$ of i.i.d. realizations of X has been observed, $f(x; \boldsymbol{\vartheta})$ depends only on $\boldsymbol{\vartheta}$. The probability of the observed sample considered as a function of $\boldsymbol{\vartheta}$ defines the *likelihood function* $L(\boldsymbol{\vartheta})$ [Azzalini 1996]:

$$L(\boldsymbol{\vartheta}|\boldsymbol{x}) = \prod_{i=1}^n f(x_i; \boldsymbol{\vartheta}). \quad (\text{A.1})$$

Since $L(\boldsymbol{\vartheta}|\boldsymbol{x})$ is a non-negative quantity, we usually refer to the *log-likelihood function*, defined as the logarithm of $L(\boldsymbol{\vartheta}|\boldsymbol{x})$: $\ell(L(\boldsymbol{\vartheta}|\boldsymbol{x})) = \log L(\boldsymbol{\vartheta}|\boldsymbol{x})$.

Under the assumption that $X \sim GEV(\boldsymbol{\vartheta})$, the log-likelihood function for the GEV parameters is [Coles 2001]:

$$\ell(\boldsymbol{\vartheta}|\boldsymbol{x}) = -N \ln \sigma - \left(\frac{1}{\xi} + 1 \right) \sum_i^N \ln \left[1 + \frac{\xi}{\sigma} (x_i - \mu) \right] - \sum_i^N \left[1 + \frac{\xi}{\sigma} (x_i - \mu) \right]^{-1/\xi} \quad (\text{A.2})$$

Eq.(A.2) is valid under the constraint $1 + \xi \left(\frac{x_i - \mu}{\sigma} \right) > 0$ and when $\xi \neq 0$. The expression of the log-likelihood for $\xi = 0$ can be obtained by simply replacing $f(x)$ in Eq.(A.1) by the Gumbel probability distribution function.

The maximization of Eq.(A.2) with respect to the vector of parameter $\boldsymbol{\vartheta} = (\mu, \sigma, \xi)$ provides the ML estimations of GEV distribution parameters. Although this maximization has no analytical solutions,

many numerical optimization techniques can be used to solve the equation system of first-order partial derivatives of Eq.(A.2) with respect of each unknown parameter in ϑ .

ML inference for models with covariates

In applications, BM assumptions might be unrealistic because of the presence of trends, seasonality, or other characteristic pattern of X . A simple way to deal with these patterns in the observed \mathbf{x} is to express distribution parameters as function of covariates [Coles 2001]. Consider ϑ to indicate either μ , σ , or ξ of a GEV. The dependence of X on the covariates $\mathbf{Y} = [Y_1, Y_2, \dots, Y_p]$ can be accounted for by expressing each ϑ as a function of some or all the Y_j , $j = 1, 2, \dots, p$: $\vartheta(\mathbf{Y}) = g(Y_1, Y_2, \dots, Y_p)$. A common choice is to simply use a linear relationships [Coles 2001; Katz 2013]:

$$\vartheta(\mathbf{Y}) = \beta_0 + \beta_1 Y_1 + \beta_2 Y_2 + \dots + \beta_p Y_p, \quad (\text{A.3})$$

but any functional expression $g(\mathbf{Y})$ can be theoretically used. β represents the set of parameters involved in the expression of $g(\cdot)$ for each ϑ . Each Y_j , for example, may represent the time or a geographical coordinate if we are interested in modeling temporal and spatial patterns of X , respectively [e.g., Katz et al. 2002; Blanchet and Lehning 2010]. Other covariates in climatological applications could also be used to model the effects of atmospheric oscillations and climate cycles on extremes [e.g., Gilleland and Katz 2006].

As a result $X \sim GEV \{\mu(\mathbf{Y}), \sigma(\mathbf{Y}), \xi(\mathbf{Y})\}$, and its log-likelihood can be written as:

$$\begin{aligned} \ell(\beta|\mathbf{x}, \mathbf{y}) &= -N \ln \sigma(\mathbf{y}; \beta) - \left(\frac{1}{\xi(\mathbf{y}; \beta)} + 1 \right) \sum_i^N \ln \left[1 + \frac{\xi(\mathbf{y}; \beta)}{\sigma(\mathbf{y}; \beta)} (x_i - \mu(\mathbf{y}; \beta)) \right] \\ &\quad - \sum_i^N \left[1 + \frac{\xi(\mathbf{y}; \beta)}{\sigma(\mathbf{y}; \beta)} (x_i - \mu(\mathbf{y}; \beta)) \right]^{-1/\xi(\mathbf{y}; \beta)} \end{aligned} \quad (\text{A.4})$$

where β represents the vector of all parameters involved in the specification of $\mu(\mathbf{Y})$, $\sigma(\mathbf{Y})$, and $\xi(\mathbf{Y})$, and \mathbf{y} is the matrix with column j equals to the N observed values $y_{1,j}, y_{2,j}, \dots, y_{N,j}$ of the j^{th} covariate Y_j .

Maximization of Eq.(A.4) with respect of β yields the ML estimates of the parameters. Standard techniques also can be used to estimate standard errors and confidence intervals for parameters and quantiles [Coles 2001].

Note that, in many applications Eq.(A.4) is a misspecified expression of the log-likelihood. For instance, it considers block maxima as being independent once the effect of the covariates is taken into account (when specifying their joint distribution), while the may be a simplified hypothesis for

the model. For example, for spatial GEV models¹ [e.g., Buishand 1991; Blanchet and Lehning 2010], AM observed at several locations s for a give year may not be independent. Similarly, scaling GEV models [Sec. 4.2.3] involve AM observed at different scales which may be generated by te same precipitation event, and thus be dependent between each other. However, the method is applicable if we are not interested to explicitly model the dependency structure between observations and if the misspecification is not too restrictive. Asymptotic properties of the ML estimator β_{ML} are available from the theory of *composite likelihood* [Varin et al. 2011].

A.2 Probability Weighted Moment (PWM) estimation

The Probability Weighted Moment (PWM) method [Greenwood et al. 1979] is equivalent to the L-Moment (LM) method which has been widely used for the estimation of GEV parameters since its introduction in the EVT due to Hosking et al. (1985). L-moments are defined as the expectation of linear combinations of order statistics of the target variable. As ordinary moments, L-moments provide measures of the X probability distribution characteristics, such as location, dispersion, skewness, and kurtosis, but they are computed from the ordered data sample. They have the advantage of being more robust than conventional moments on small data samples and in the presence of outliers.

L-moment GEV parameter estimators, in the case that $-0.5 < \xi < 0.5$, can be written as [Hosking et al. 1985]:

$$\hat{\xi} = -7.859c - 2.9554c^2 \quad (\text{A.5})$$

$$\hat{\sigma} = \frac{l_2 \hat{\xi}}{(1 - 2^{\hat{\xi}})\Gamma(1 - \hat{\xi})} \quad (\text{A.6})$$

$$\hat{\mu} = l_1 + \frac{\hat{\sigma}}{\hat{\xi}} \left[1 - \Gamma(1 - \hat{\xi}) \right] \quad (\text{A.7})$$

where

$$c = \frac{2}{3 + t_3} - \frac{\ln 2}{\ln 3} \quad (\text{A.8})$$

and $t_3 = l_3/l_2$, and l_1, l_2, l_3 represents, respectively, the sample L-moments of order 1, 2, and 3. Sample L-moments can be define from the r-order Probability Weighted Moments β_r [Greenwood

¹Note that, these models have been designated by different names, each of them indicating an essential characteristic of the technique. Blanchet and Lehning (2010), for instance, referred to them as *smooth-GEV model*, pointing out the difference with interpolation strategies; while the latter locally approximate the value of each ϑ , the smooth GEV estimates the parameters as a smooth function of space directly from the original AMS. Panthou et al. (2012), using the expression *Spatial Maximum Likelihood Estimation (SMLE)*, underlined the fact that the model is based on the ML estimation of the ϑ . Finally, and other authors, using more generic names such as *Spatial GEV Regression* [Van de Vyver 2012] or *Hierarchical GEV* [Katz et al. 2002]. stressed the way how the spatial component is introduced in the model.

et al. 1979, Hosking et al. 1985]:

$$\beta_r = E[X \{F(X)\}^r], \quad r = 1, 2, \dots \quad (\text{A.9})$$

Given an observed i.i.d. sample $\mathbf{x} = (x_1, x_2, \dots, x_N)$ of X having cumulative distribution function $F(x)$, an unbiased estimation of β_r is [Hosking et al. 1985]:

$$b_r = \frac{1}{N} \sum_{i=r+1}^N \frac{(i-1)(i-2)\dots(i-r)}{(N-1)(N-2)\dots(N-r)} x_{(i)} \quad (\text{A.10})$$

where $x_{(i)}$ is the i^{th} order statistic of \mathbf{x} and with

$$b_0 = \frac{1}{N} \sum_{i=1}^N x_i \quad (\text{A.11})$$

The corresponding estimators of the first three L-moments are:

$$\hat{l}_1 = b_0 \quad (\text{A.12})$$

$$\hat{l}_2 = 2b_1 - b_0 \quad (\text{A.13})$$

$$\hat{l}_3 = 6b_2 - 6b_1 + b_0 \quad (\text{A.14})$$

Hosking et al. (1985) demonstrated the asymptotic normality of PWM estimators and derived GEV parameters standard errors useful for the construction of confidence intervals whenever $\xi < 1/2$. They further indicated that asymptotic theory works well for sample sizes of 50 or larger. When a PWM approach is adopted, confidence intervals for GEV quantiles are generally obtained from return levels expressions based on frequency factors [Chow 1951] or through the use of resampling techniques.

Supplementary Material of "Simple Scaling of extreme precipitation in North America"

S. Innocenti¹, A. Mailhot¹, and A. Frigon²

1. Centre Eau-Terre-Environnement, INRS, Québec, Canada;

2. Consortium Ouranos, Montréal, Canada.

Available online at:

<https://doi.org/10.5194/hess-21-5823-2017-supplement>.

Introduction

This supporting information presents some extended results and describes in more details some methodological developments. It is structured as follows. Table S1 lists in alphabetic order the recurrent acronyms used in text. Figure S1 displays the station locations and the median of the distribution of the annual maximum precipitation for various durations considered in the study. Figures S2 and S3 show results for the SS model validation (Slope and GOF tests) when AMS are pooled according to the instrument and temporal resolution. Section S1 briefly describes these figures. Figure S4 presents the results of the cross-validation experiment for the SS model (Slope and GOF tests) for each duration and scaling interval. Figures S5 and S6 present, respectively, the regional distribution of the mean number of events per year, \bar{N}_{eve} , and the mean wet time, \bar{T}_{wet} , of these events for each 6-duration scaling interval. The detailed definition of \bar{N}_{eve} and \bar{T}_{wet} is given in Sect. S2. Finally, Fig. S9 to S17, extend to longer scaling intervals the analysis presented in Sect. 4.3 (Regional analysis) and Sect. 5.2 (SS-GEV model evaluation) for 6-duration scaling intervals.

Section S1: Details on Fig. 2 and 3

Figures S2 and S3 show the results of the Slope and GOF tests applied at the 0.05 significance level when AMS are pooled according to the instrument and temporal resolution of the recording station. Each of the 12 matrices of these figures represents the proportion of valid SS stations [see the definition of valid SS station in Sect. 4.1 and in Fig. 1 (e) of the paper] for each duration (vertical axis) and scaling intervals (horizontal axis).

Each grid-box of the heatmaps is divided in two triangles. Upper triangles in Fig. S2 correspond to the fraction of AMS having instrument resolution < 2.54 mm, while lower triangles correspond to AMS with instrument resolution of 2.54 mm. Tip resolution at each station is defined as the minimum non-zero recorded value. Tip resolution at stations having both DPDM and HCPD series, or both 15PD and HPD series, was defined as the maximum value between the resolutions of these two series.

Upper triangles in Fig. S3 correspond to the fraction of AMS constructed from both HPD and 15PD series, or both HCPD and DMPD series (i.e. with temporal resolution ≤ 1 h). Lower triangles correspond to the fraction of AMS estimated from hourly series only (series constructed from HCPD or HPD series, i.e. a 1h temporal resolution).

White triangles in Fig. S2 and S3 indicate non-significant differences between upper and lower triangle proportions. Tests on proportion differences were applied at significance level 0.05 without accounting for the spatial autocorrelation among stations.

Section S2: Definition of \bar{N}_{eve} and \bar{T}_{wet} for the events sampled within each scaling interval

To provide deeper insights about regional features of precipitation associated with specific scaling regimes, two variables related to the precipitation events observed within AMS were also analyzed: the mean number of events per year, \bar{N}_{eve} , and the mean wet time per event, \bar{T}_{wet} , contributing to AMS within each scaling interval.

For a given year and station, annual maxima associated to different durations of a given scaling interval were considered to belong to the same precipitation event if the time intervals over which they occurred overlapped [see Fig. S5 (g); in this example 3, 4, and 5 h annual maxima are associated with the first event while 1, 2, and 6 h annual maxima are associated to the second event]. The mean number of events at each station was then computed:

$$\bar{N}_{eve} = \frac{1}{n} \sum_i^n N_{eve,i} \quad (\text{S1 .1})$$

with $N_{eve,i}$ the number of non-overlapping time intervals, i.e. the number of different events contributing to AMS during the i^{th} year of record. The distribution of \bar{N}_{eve} values within each region is presented in Fig. S5.

For each station, the mean wet time, \bar{T}_{wet} [hours], of events sampled within each scaling interval was computed as:

$$\bar{T}_{wet} = n_E^{-1} \sum_e^{n_E} T_{wet,e} \quad (\text{S2})$$

with n_E the total number of events e sampled by the annual maxima precipitation series in the scaling interval [see Sect. 4.3 of the article for the definition of each event]. $T_{wet,e}$ is the wet time of the e^{th} event:

$$T_{wet,e} = W_e T_e \quad (\text{S2})$$

where W_e is the fraction of event time steps during which positive precipitation depths were recorded, and T_e is the total event duration (in hours).

Figure S6 displays the distribution over valid SS stations of \bar{T}_{wet} within each region [Fig. S6 (a) to (f)] and one example of calculation of $T_{wet,e}$ and \bar{T}_{wet} [Fig. S6 (g)].

Table S1 .1: List of the relevant acronyms recurring in the manuscript.

| | |
|---|--|
| AD: Anderson Darling <i>test</i> | KS: Kolmogorov-Smirnov <i>test</i> |
| AMS: Annual Maxima Series | ML: Maximum-Likelihood <i>estimation</i> |
| GEV: Generalized Extreme Value <i>distribution</i> | MS: Multiscaling |
| GOF: Goodness-Of-Fit <i>test</i> | MSA: Moment Scaling Analysis |
| IQR: Interquartile Range | PWM: Probability Weighted Moments <i>estimation</i> |
| IDF: Intensity-Duration-Frequency <i>curve</i> | SS: Simple Scaling |

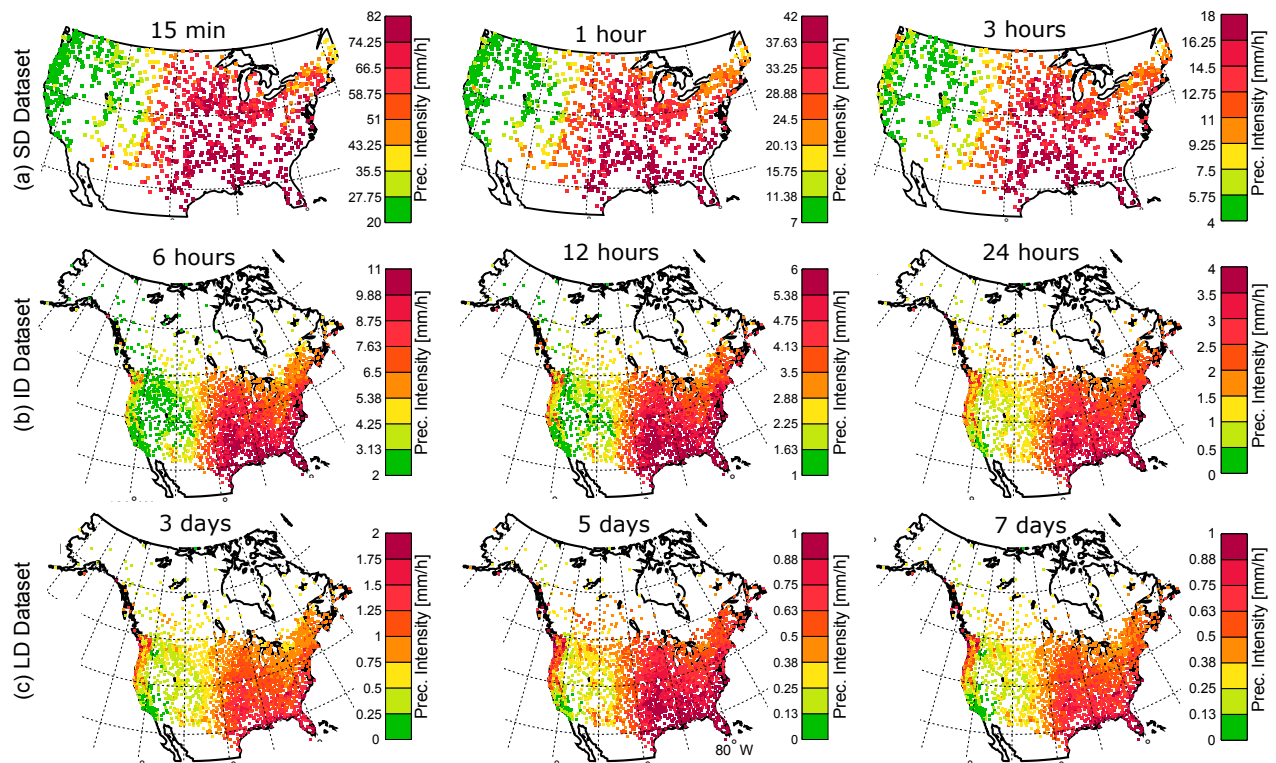


Figure S1: Spatial distribution of the median precipitation intensity for: (a) 15 min, 1 h, and 3 h in the SD dataset, (b) 6 h, 12 h, and 24 h in the ID dataset, and (c) 3days, 5days, and 7days in the LD datasets.

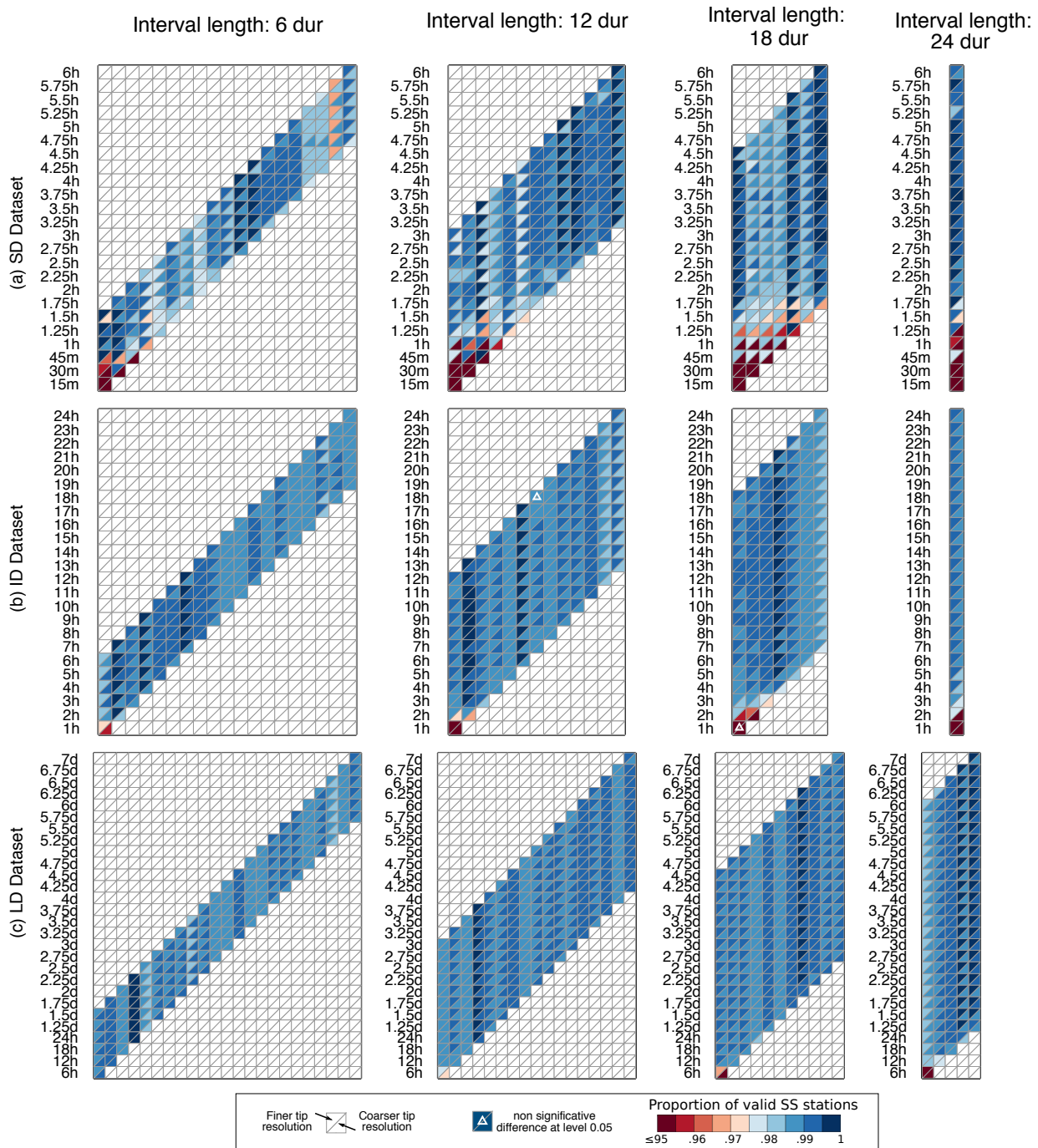


Figure S2: Proportion of valid SS stations for each duration and scaling interval for the SD, ID, and LD datasets [row (a), (b), and (c) respectively] when accounting for series instrument resolutions. Upper triangles correspond to the fraction of AMS having instrument resolution < 2.54 mm, while lower triangles correspond to AMS with instrument resolution of 2.54 mm. White triangles indicate non-significant differences between upper and lower triangle proportions. See Sect. S1 for details.

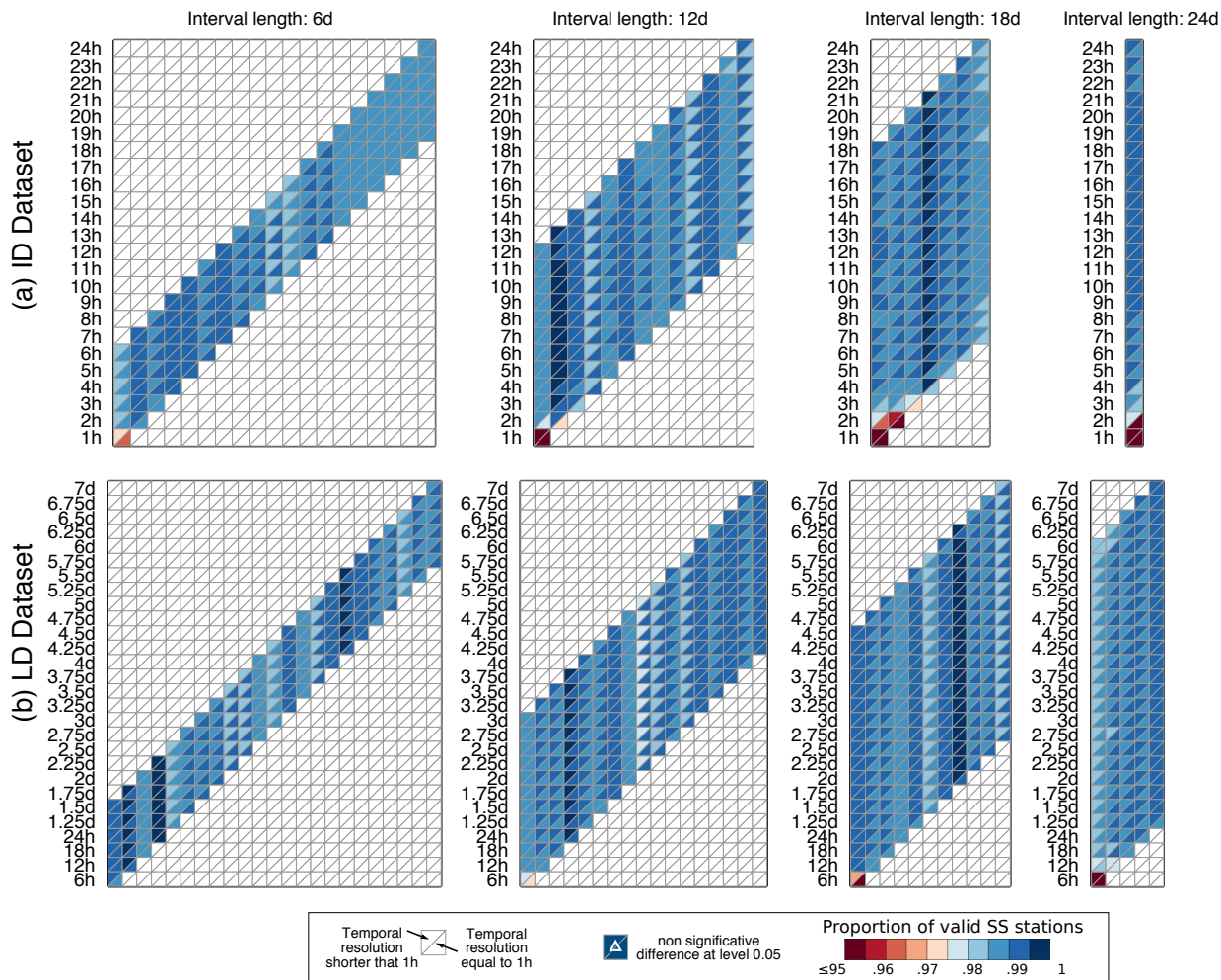


Figure S3: Proportion of valid SS stations for each duration and scaling interval for (a) ID and (b) LD datasets when accounting for series temporal resolutions. Upper triangles in Figures S3 correspond to the fraction of AMS with temporal resolution ≤ 1 h. Lower triangles correspond to the fraction of AMS estimated from hourly series only. White triangles indicate non-significant differences between upper and lower triangle proportions. See Sect. S1 for details.

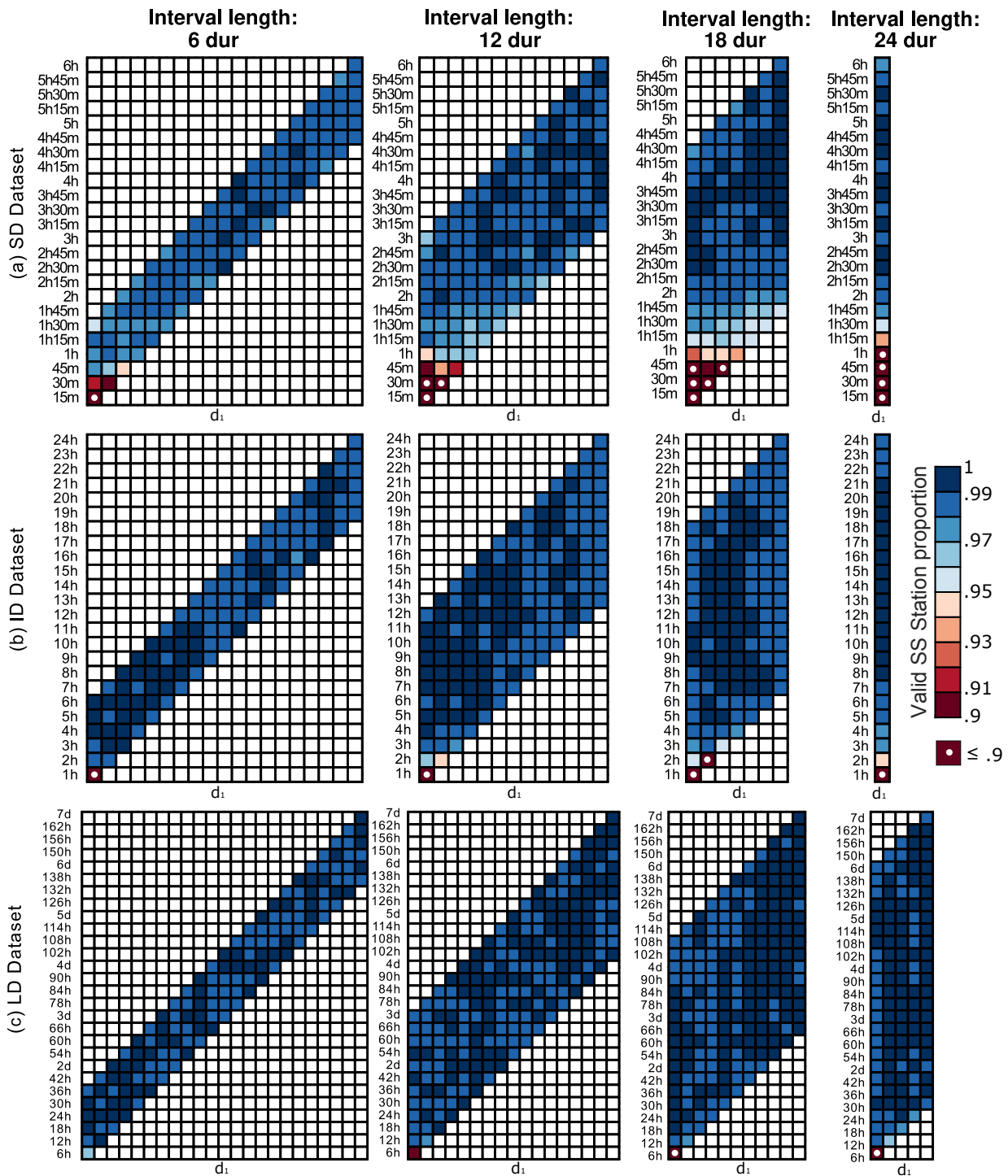


Figure S4: Proportion of stations satisfying both the Slope and GOF tests applied at the 0.95 confidence level in cross-validation. Each grid-box represents the proportion for a duration (vertical axis) and scaling interval (horizontal axis) for the SD, ID, and LD datasets [row a), b), and c) respectively] computed when that duration is excluded from the scaling interval. White circles indicate proportions lower than 0.90.

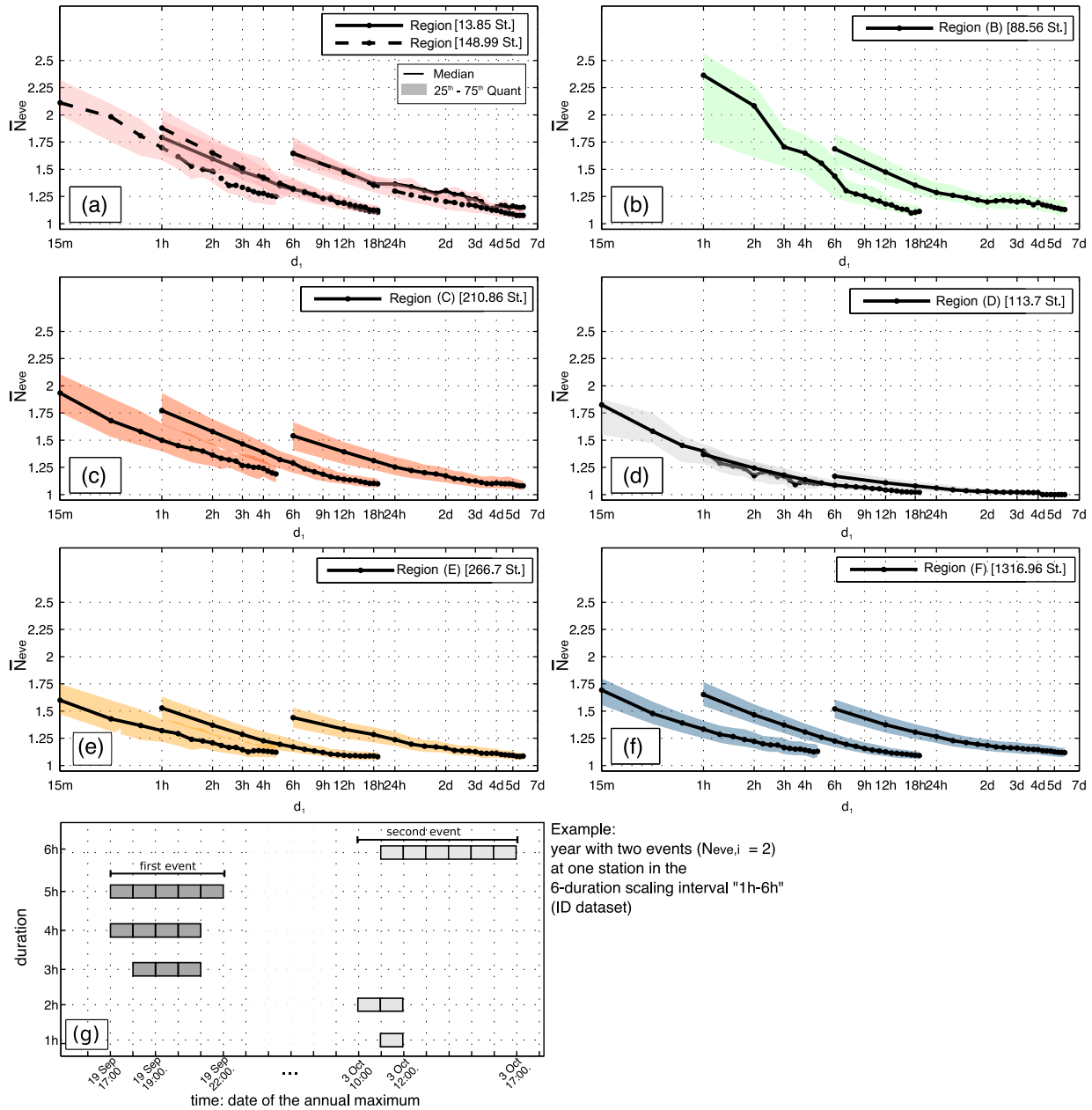


Figure S5: Median and Interquartile Range (IR) of the distribution over valid SS stations of the mean number of events per year, N_{vee} , within each region of Fig. 7 for each 6-duration scaling interval for the SD (left curve), ID (central curve), and LD (right curve) datasets. For each region, the mean number of valid SS stations over the scaling intervals is indicated in the legend in brackets. Panel (g) displays an example of how $N_{vee,i}$ is estimated for year i .

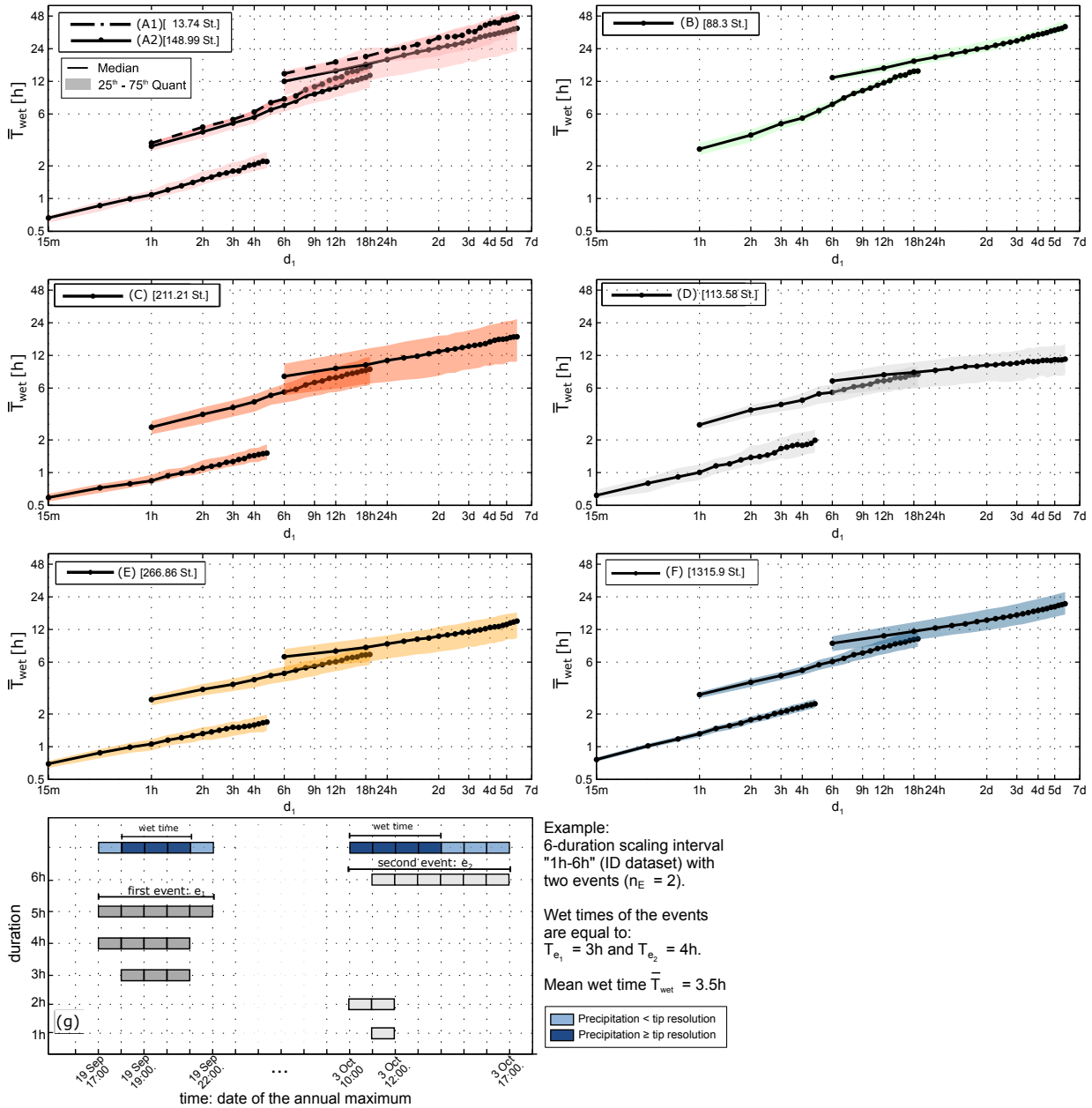


Figure S6: Median and Interquartile Range (IR) of the distribution over valid SS stations of the mean wet time, \bar{T}_{wet} , within each region for each 6-duration scaling interval in the SD (left curve), ID (central curve), and LD (right curve) datasets. Graph (g) displays an example of how \bar{T}_{wet} is estimated for one theoretical scaling interval. For each region, the mean number of valid SS stations over the scaling intervals is indicated in brackets.

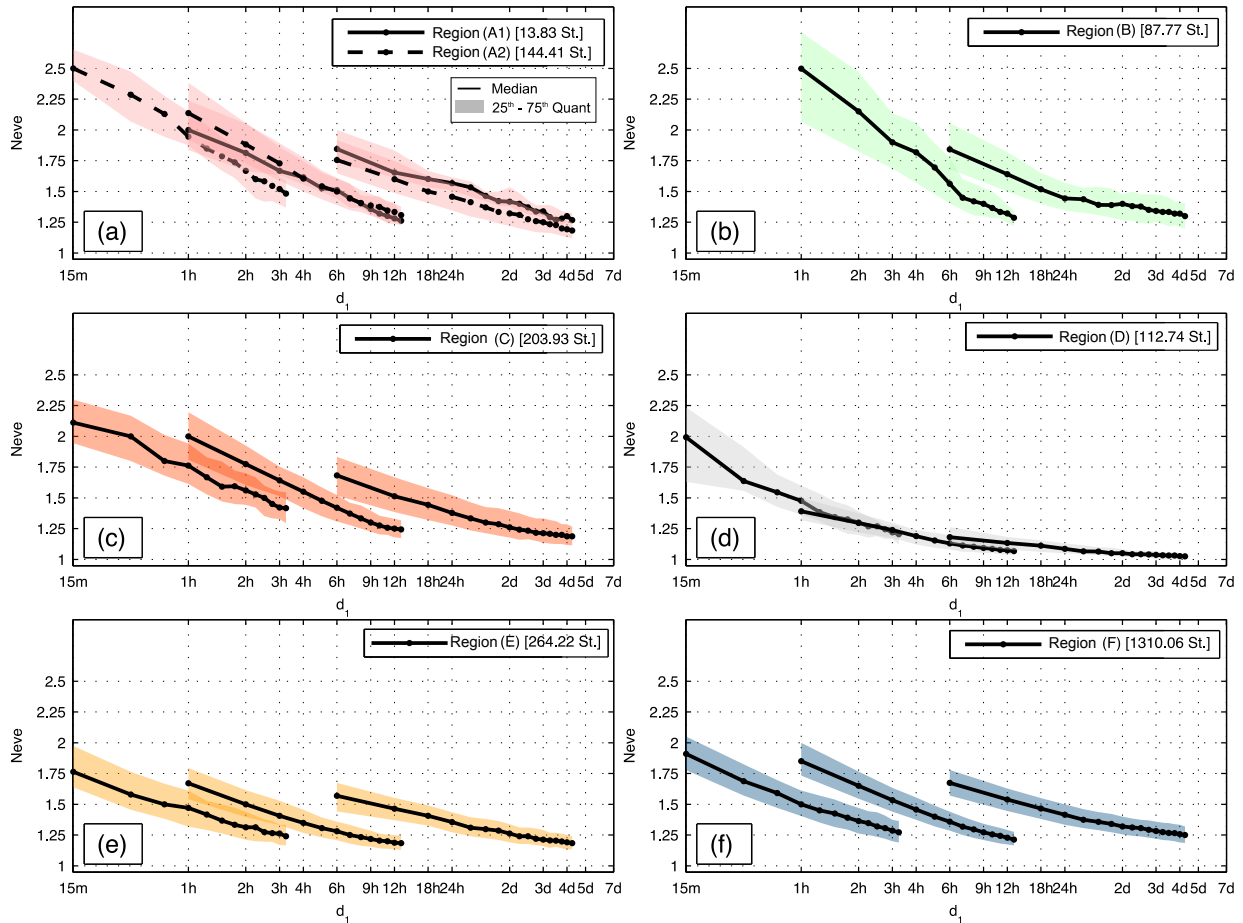


Figure S7: Median and Interquartile Range (IR) of the distribution over valid SS stations of the mean number of events per year, \bar{N}_{eve} , within each region for each 12-duration scaling interval for the SD (left curve), ID (central curve), and LD (right curve) datasets. For each region, the mean number of valid SS stations over the scaling intervals is indicated in brackets.

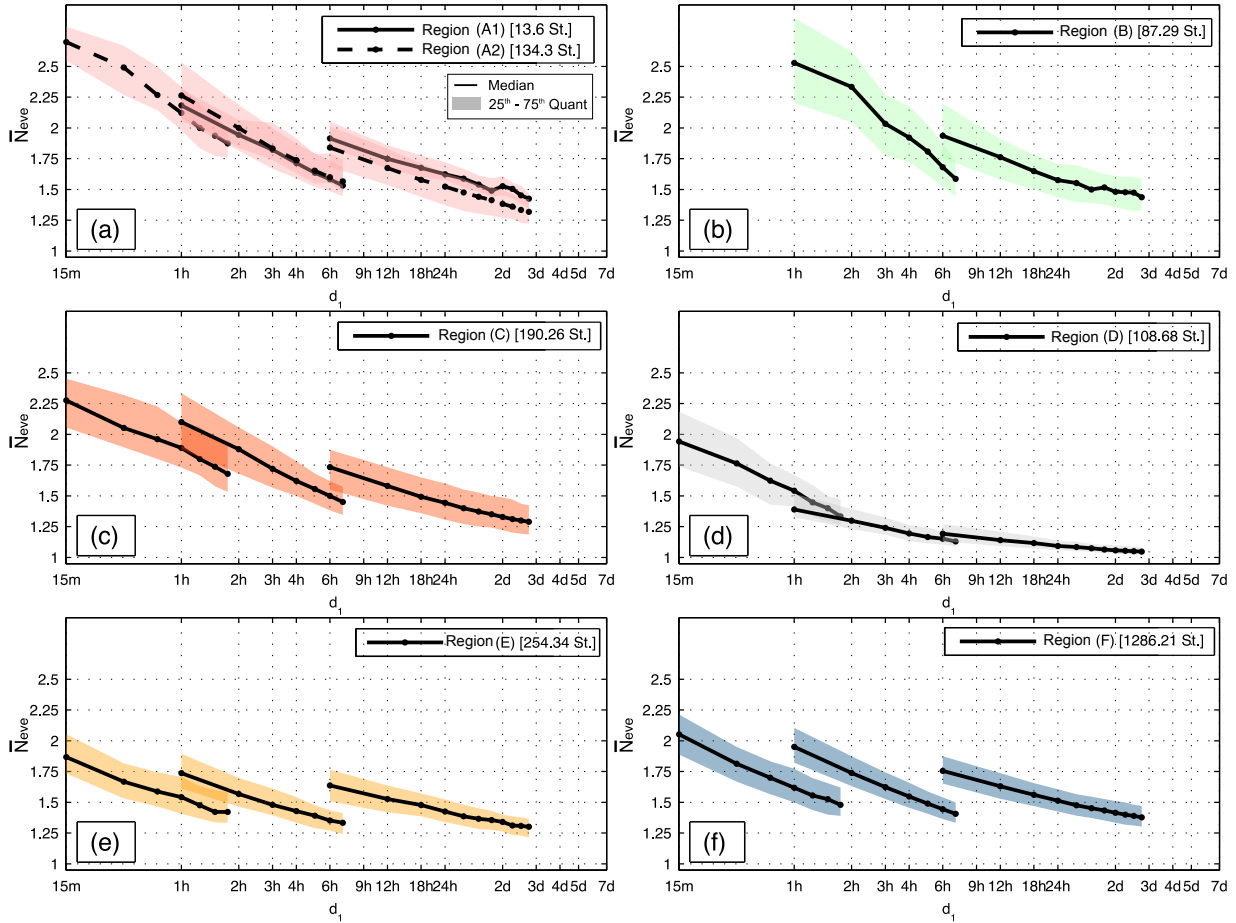


Figure S8: Median and Interquartile Range (IR) of the distribution over valid SS stations of the mean number of events per year, \bar{N}_{eve} , within each region for each 18-duration scaling interval for the SD (left curve), ID (central curve), and LD (right curve) datasets. For each region, the mean number of valid SS stations over the scaling intervals is indicated in brackets.

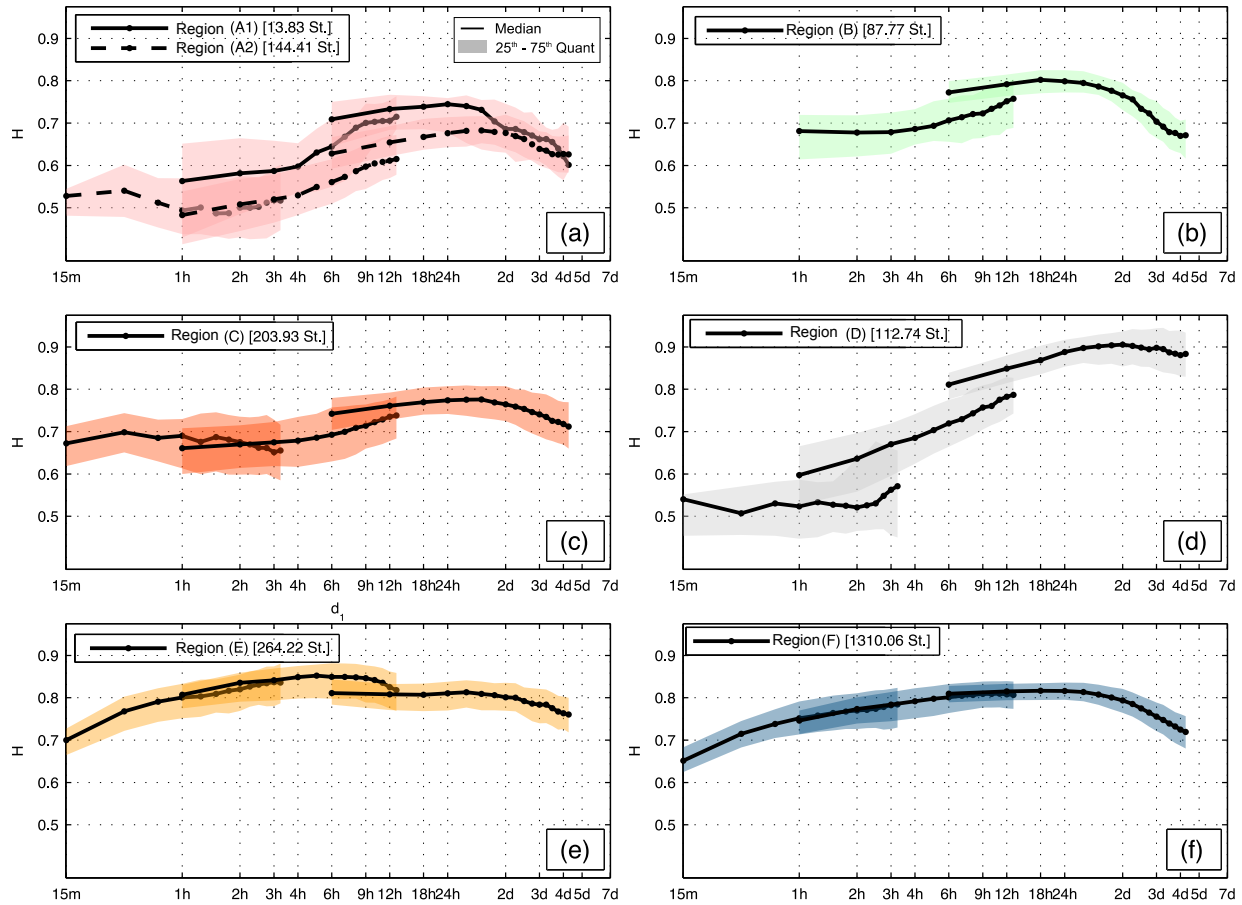


Figure S9: Median and Interquartile Range (IR) of the scaling exponent distribution over valid SS stations within each region for 12-duration scaling intervals in the SD (left curve), ID (central curve), and LD (right curve) datasets. For each region, the mean number of valid SS stations over the scaling intervals is indicated in brackets.

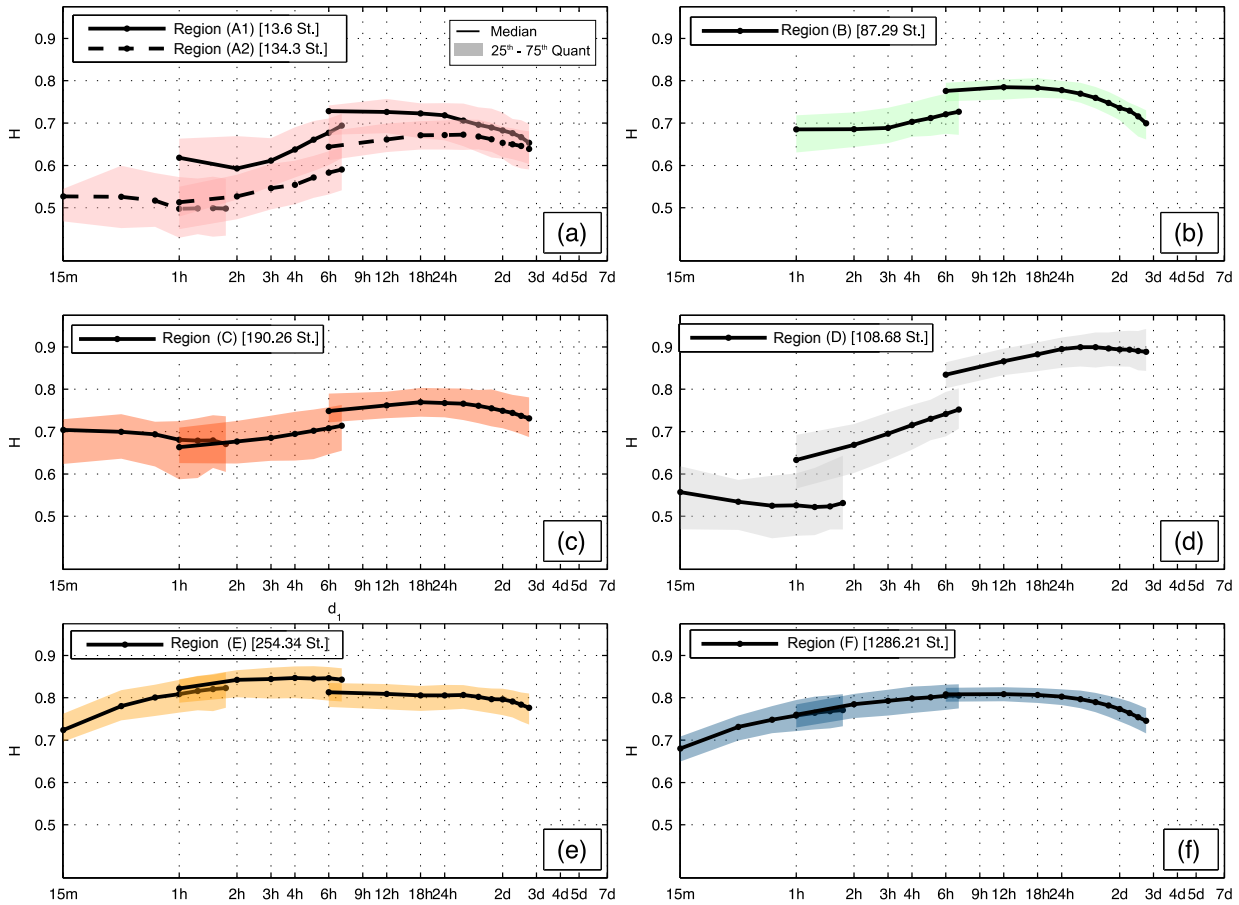


Figure S10: Median and Interquartile Range (IR) of the scaling exponent distribution over valid SS stations within each region for 18-duration scaling intervals for the SD (left curve), ID (central curve), and LD (right curve) datasets. For each region, the mean number of valid SS stations over the scaling intervals is indicated in brackets.

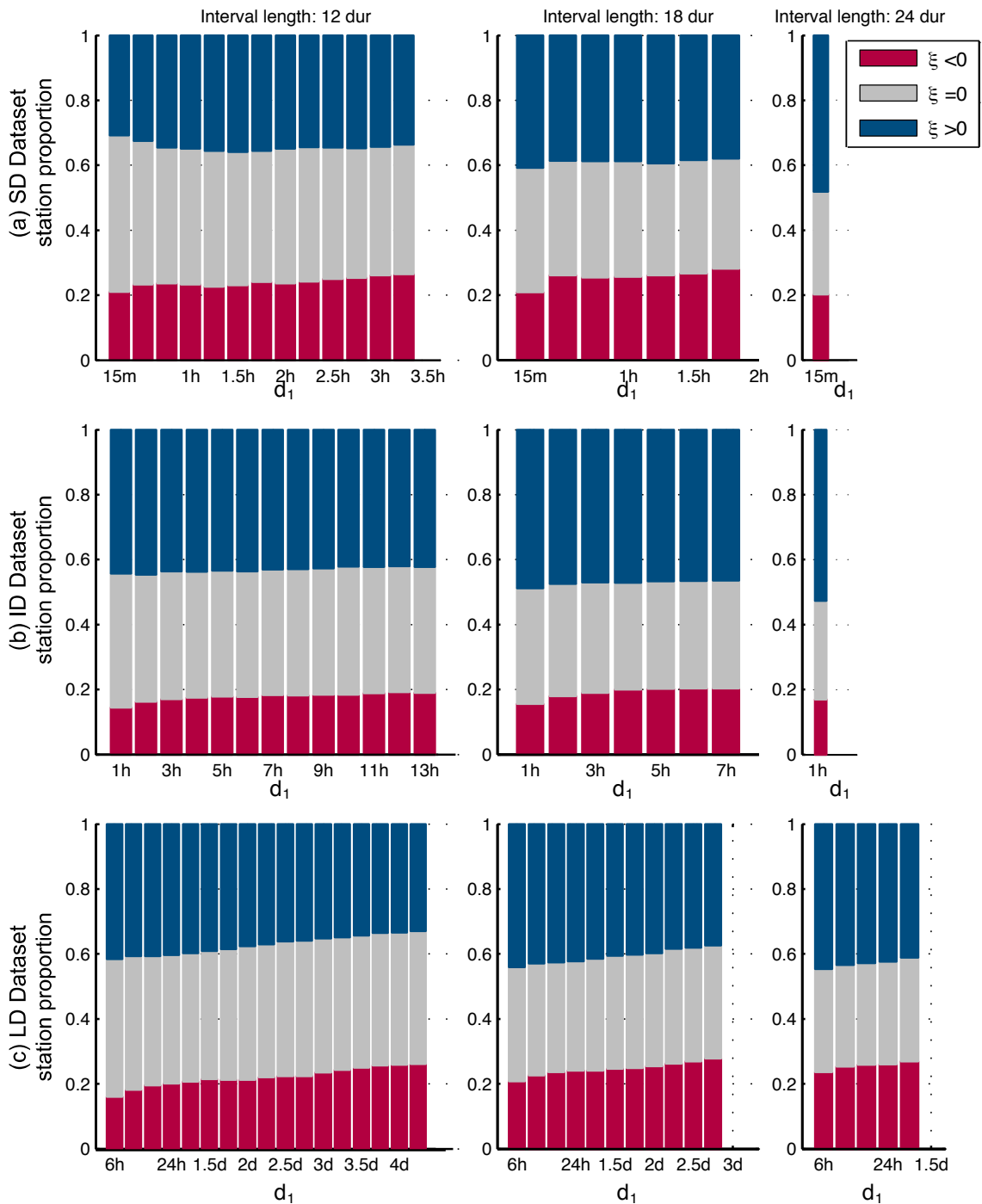


Figure S11: Stacked proportion of valid SS stations with $\xi < 0$ (in red), $\xi = 0$ (in grey), and $\xi > 0$ (in blue) for each 12-, 18-, and 24-duration scaling interval [1^{st} , 2^{nd} , and 3^{rd} col., respectively] in SD, ID, and LD datasets [(a), (b), and (c), respectively] .

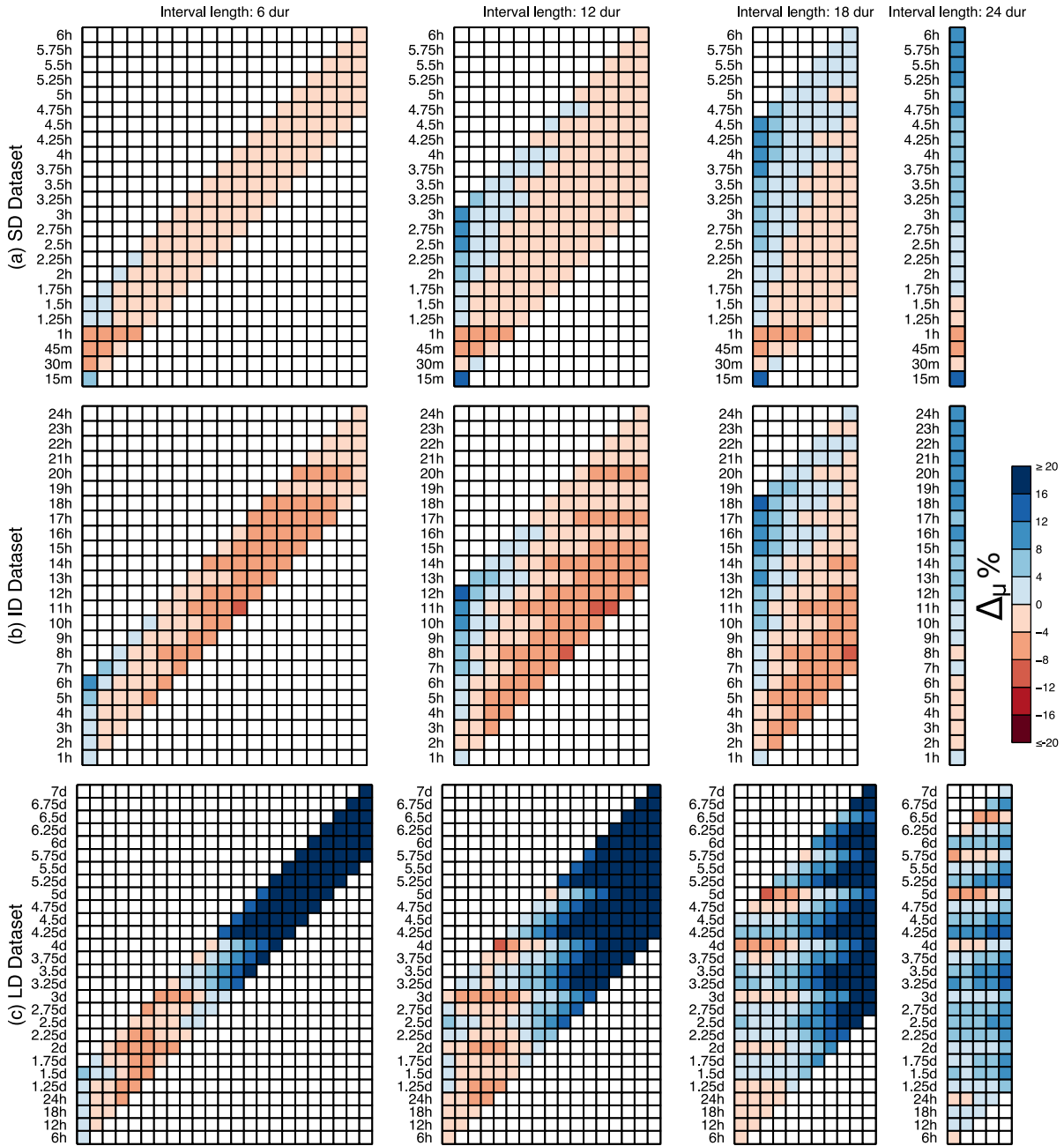


Figure S12: Median relative difference $\Delta\mu$ for each for each scaling interval (horizontal axis) and duration (vertical axis) in SD, ID, and LD datasets [(a), (b), and (c), respectively] .

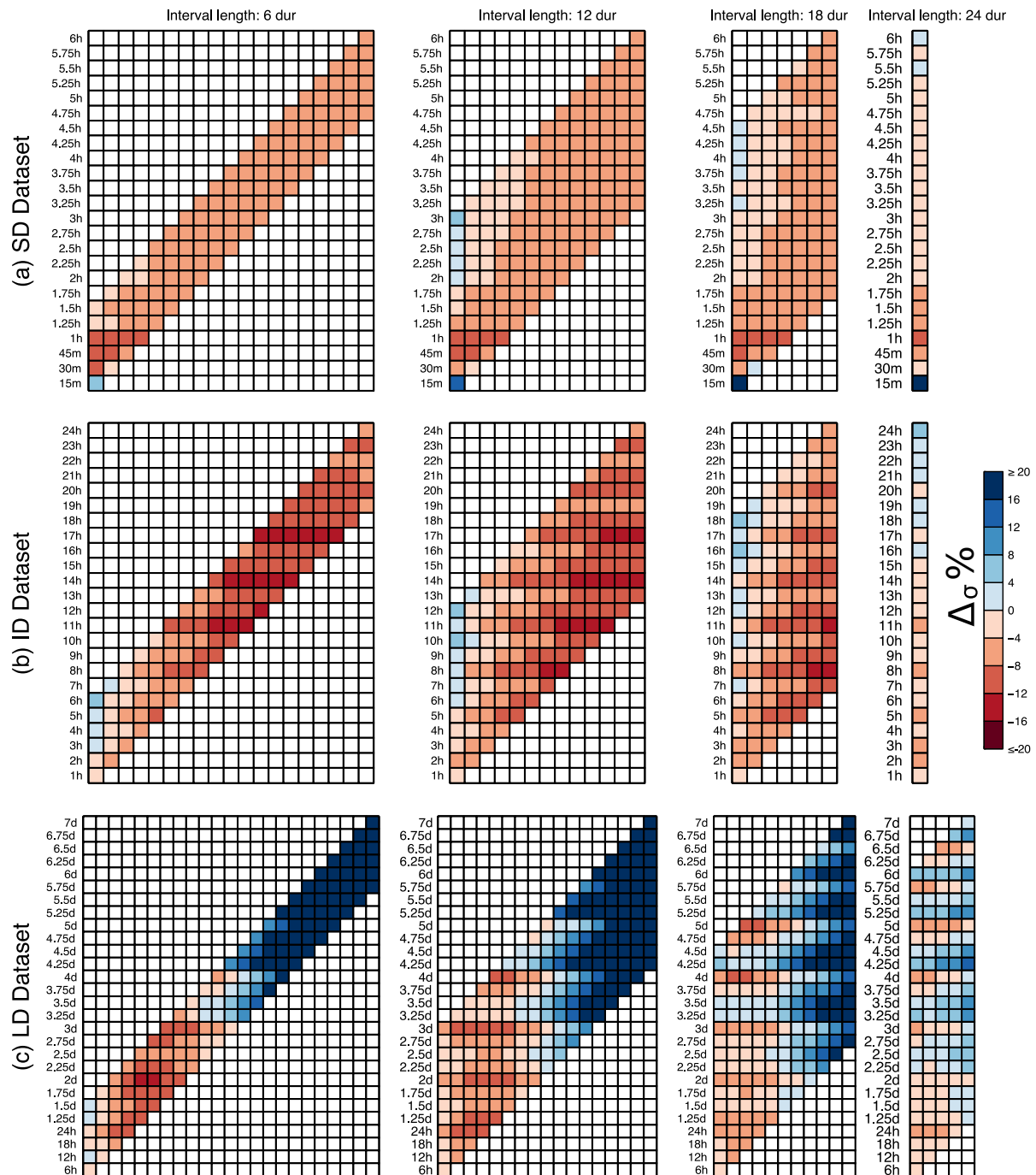


Figure S13: Median relative difference Δ_σ for each scaling interval (horizontal axis) and duration (vertical axis) in SD, ID, and LD datasets [(a), (b), and (c), respectively] .

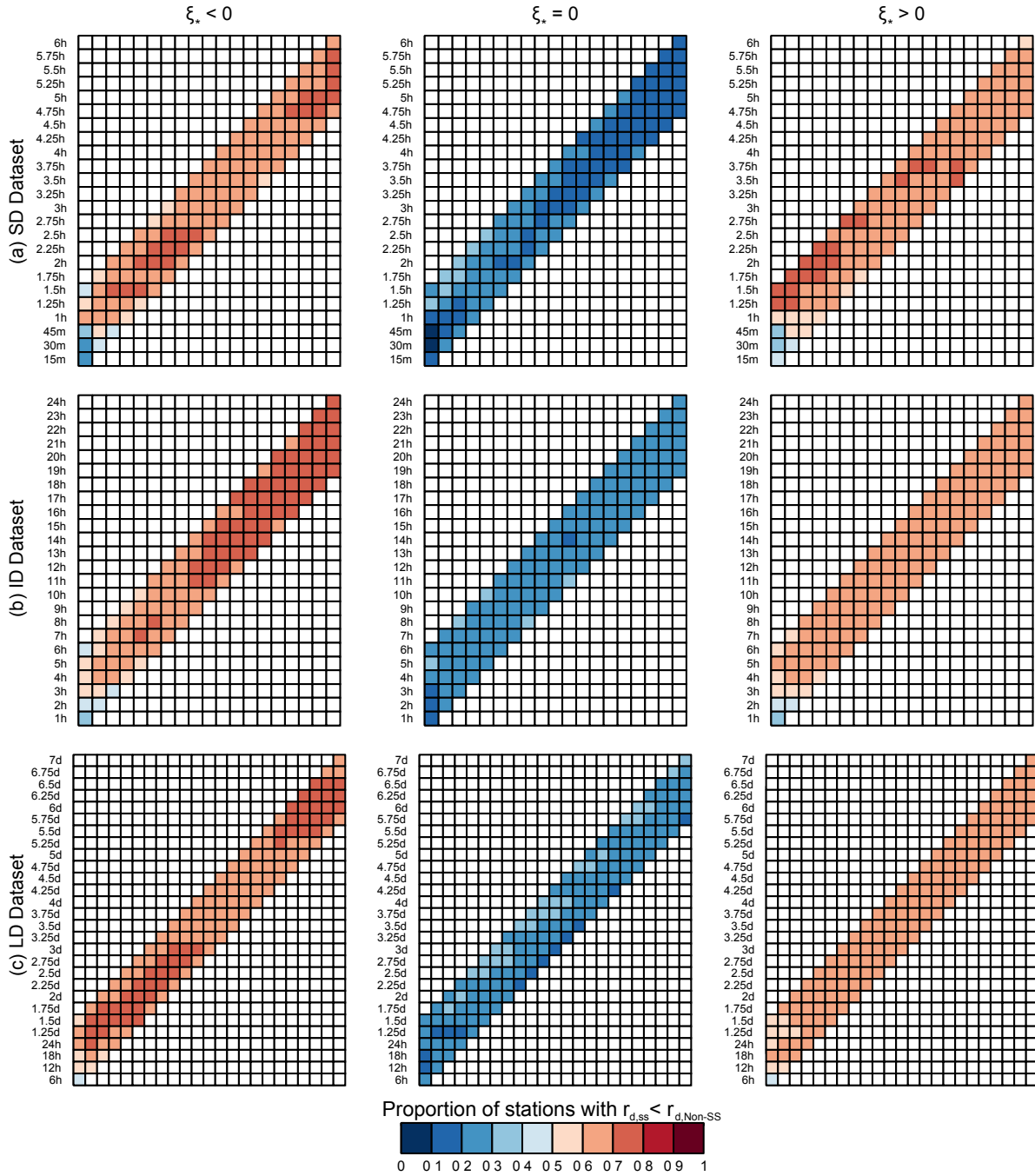


Figure S14: Proportion of valid SS stations having $r_{d,ss} < r_{d,non-SS}$ for $\xi_* < 0$ (1^{st} col.), $\xi_* = 0$ (2^{nd} col.), and $\xi_* > 0$ (3^{rd} col.) for each 6-duration scaling interval (horizontal axis) and duration (vertical axis) in SD, ID, and LD datasets [(a), (b), and (c), respectively].

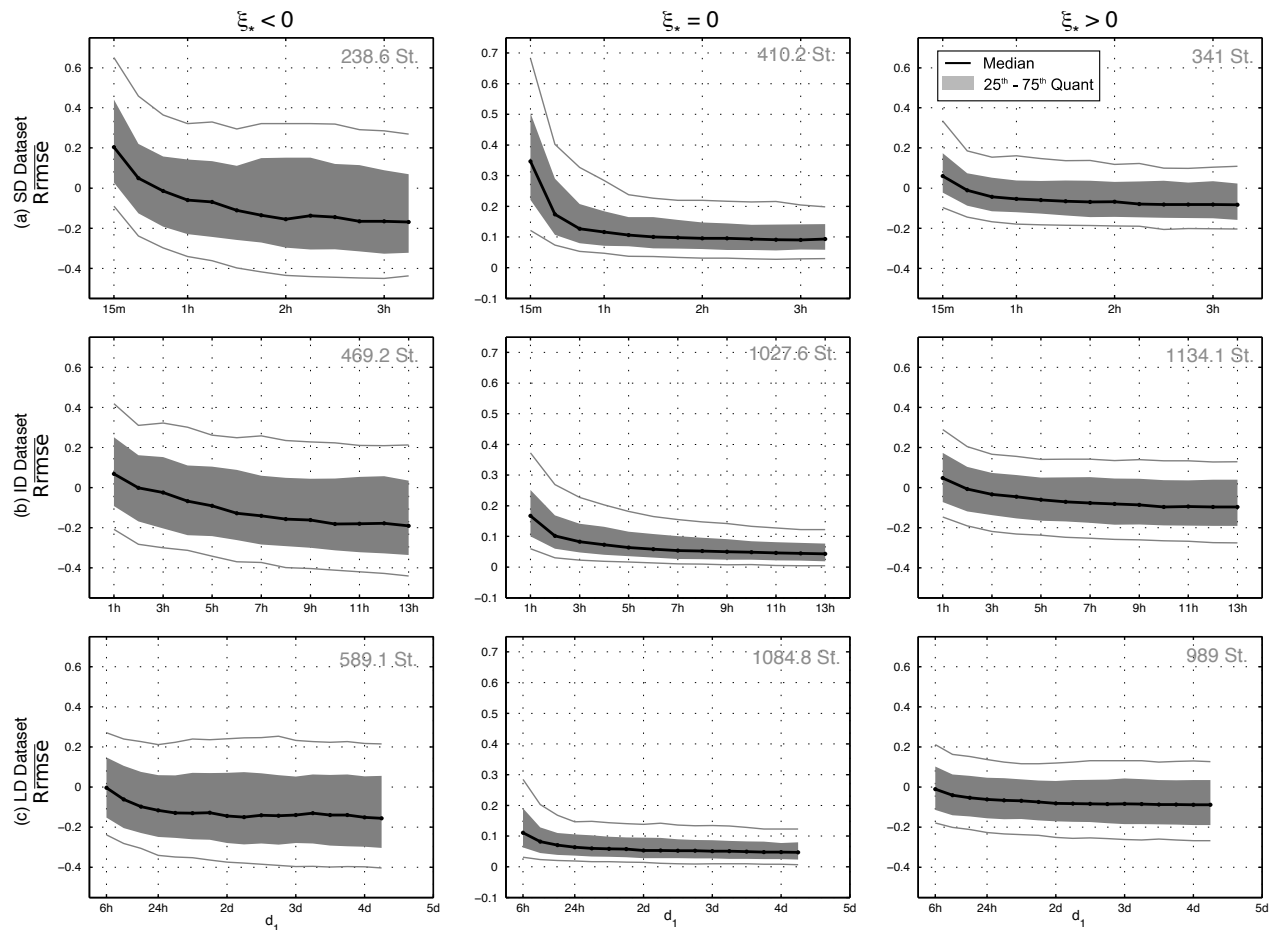


Figure S15: Distribution of the relative total RMSE ratio, $R_{\overline{rmse}}$, for $\xi_* < 0$ (1st col.), $\xi_* = 0$ (2nd col.), and $\xi_* > 0$ (3rd col.) for 12-duration scaling intervals in SD, ID, and LD datasets [(a), (b), and (c), respectively].

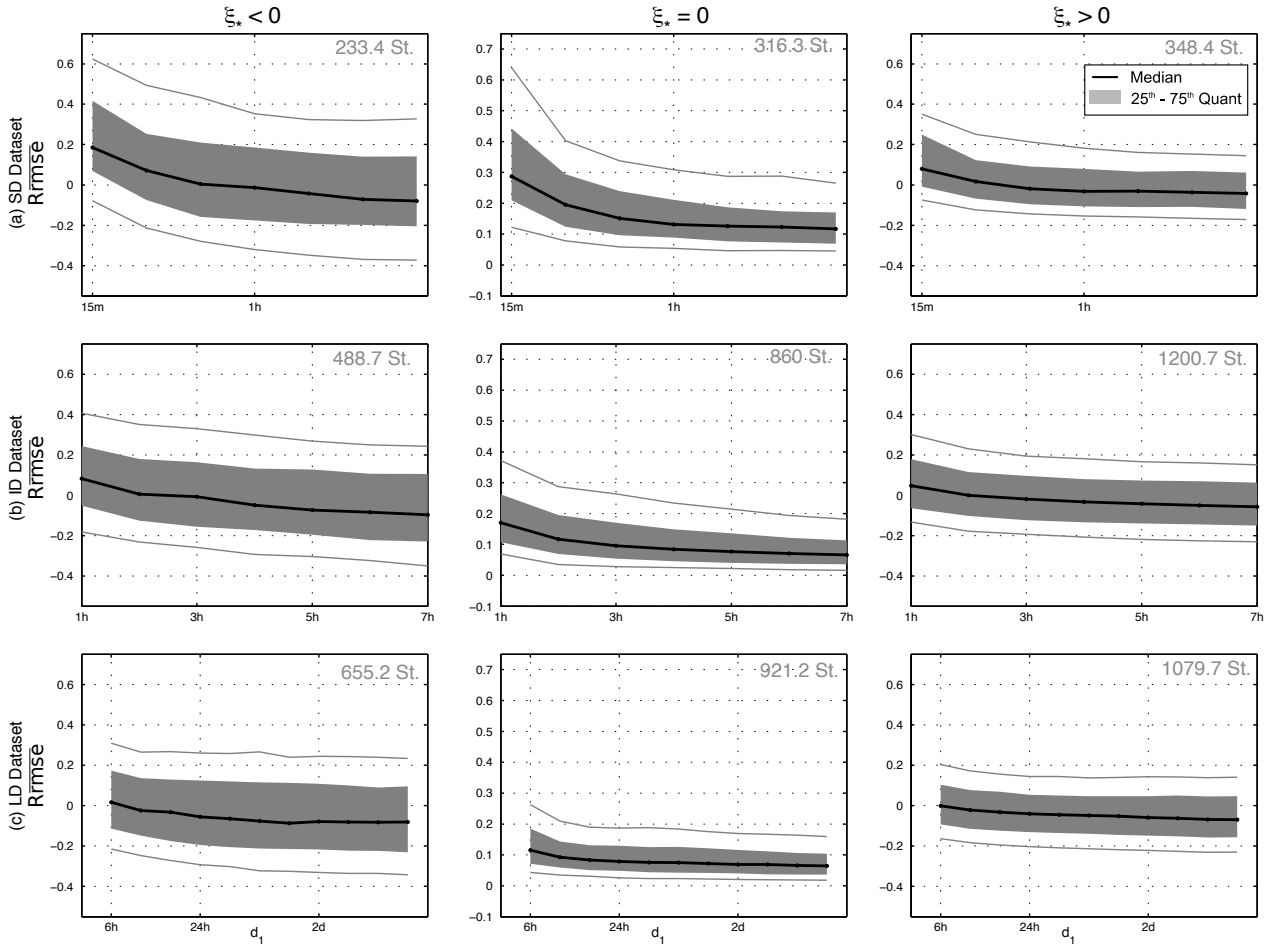


Figure S16: Distribution of the relative total RMSE ratio, R_{rmse} , for $\xi_* < 0$ (1st col.), $\xi_* = 0$ (2nd col.), and $\xi_* > 0$ (3rd col.) for 18-duration scaling intervals in SD, ID, and LD datasets [(a), (b), and (c), respectively].

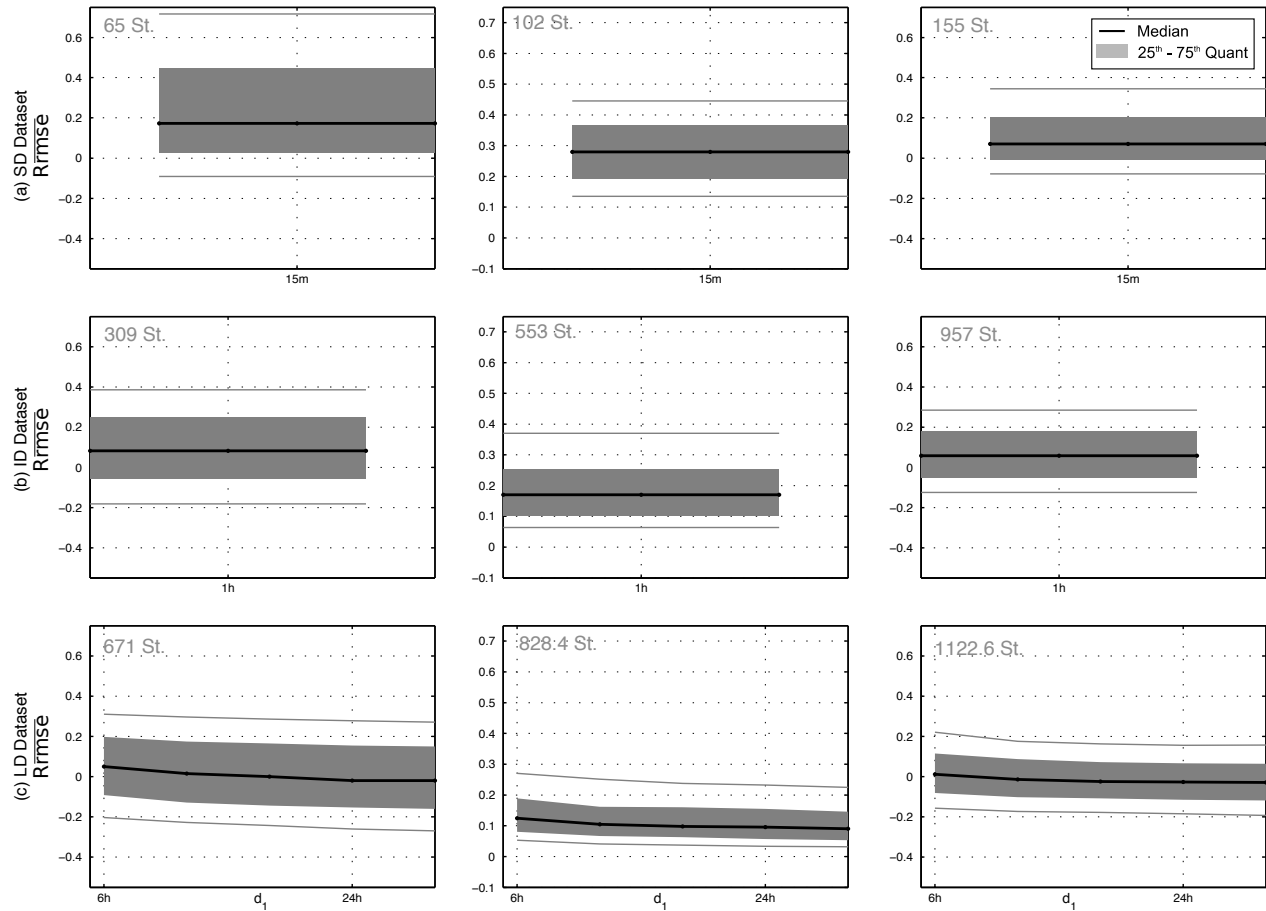


Figure S17: Distribution of the relative total RMSE ratio, $R_{\overline{rmse}}$, for $\xi_* < 0$ (1st col.), $\xi_* = 0$ (2nd col.), and $\xi_* > 0$ (3rd col.) for 24-duration scaling intervals in SD, ID, and LD datasets [(a), (b), and (c), respectively].

Supplementary Material of

"Observed and simulated precipitation over

North East North-America:

how do sub-daily extremes scale in space and

time?"

Silvia Innocenti,^{1,*} Alain Mailhot¹, Anne Frigon²,
Alex J. Cannon³, Martin Leduc²

1. Centre Eau-Terre-Environnement, INRS, Québec, Canada;

2. Consortium Ouranos, Montréal, Canada;

3. Climate Research Division, ECCC, Victoria, Canada.

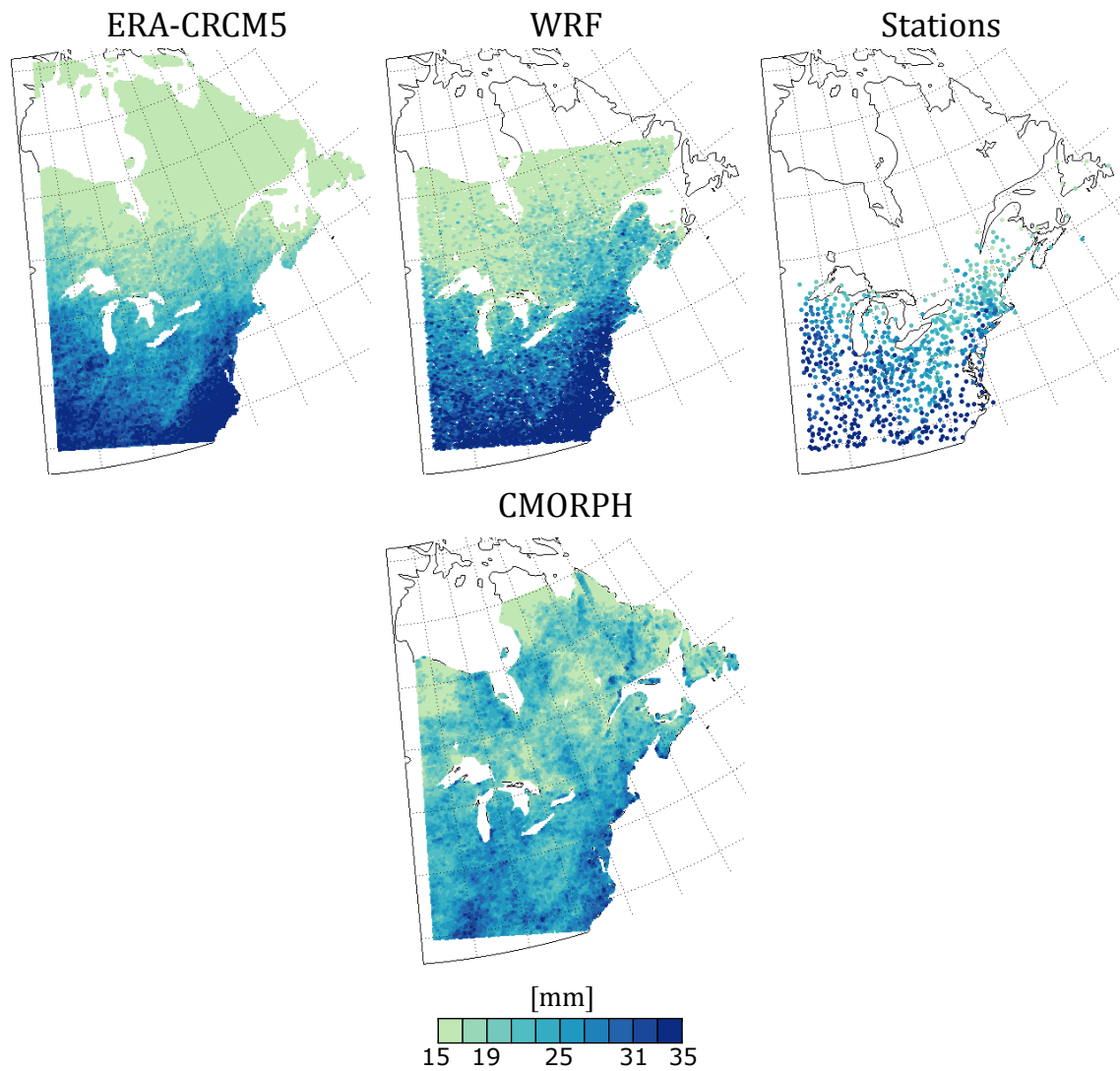


Figure S1: Two-yr AM precipitation for duration $d = 1h$ at the native spatial resolution of each dataset.

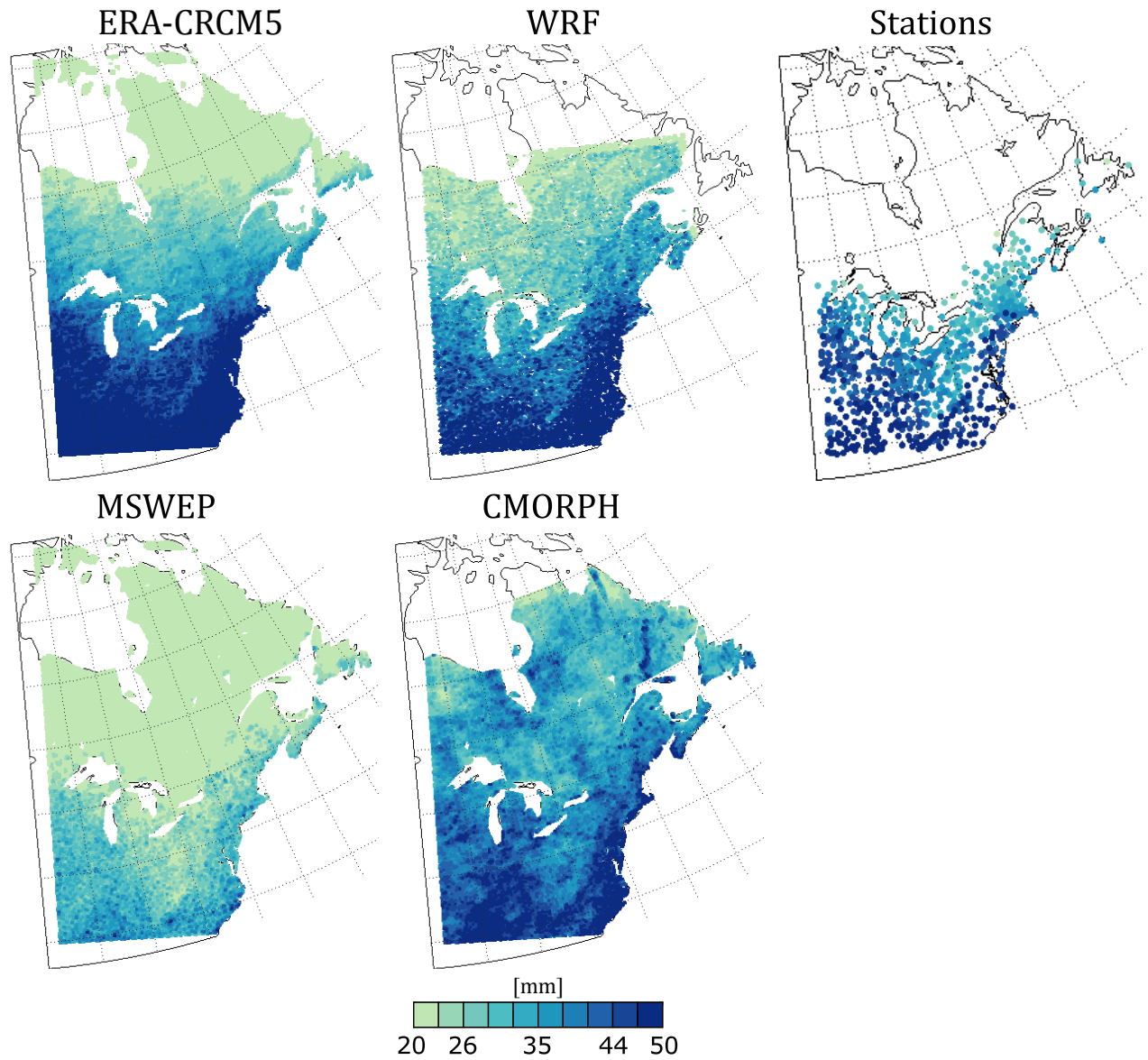


Figure S2: Two-yr AM precipitation for duration $d = 3h$ at the native spatial resolution of each dataset.

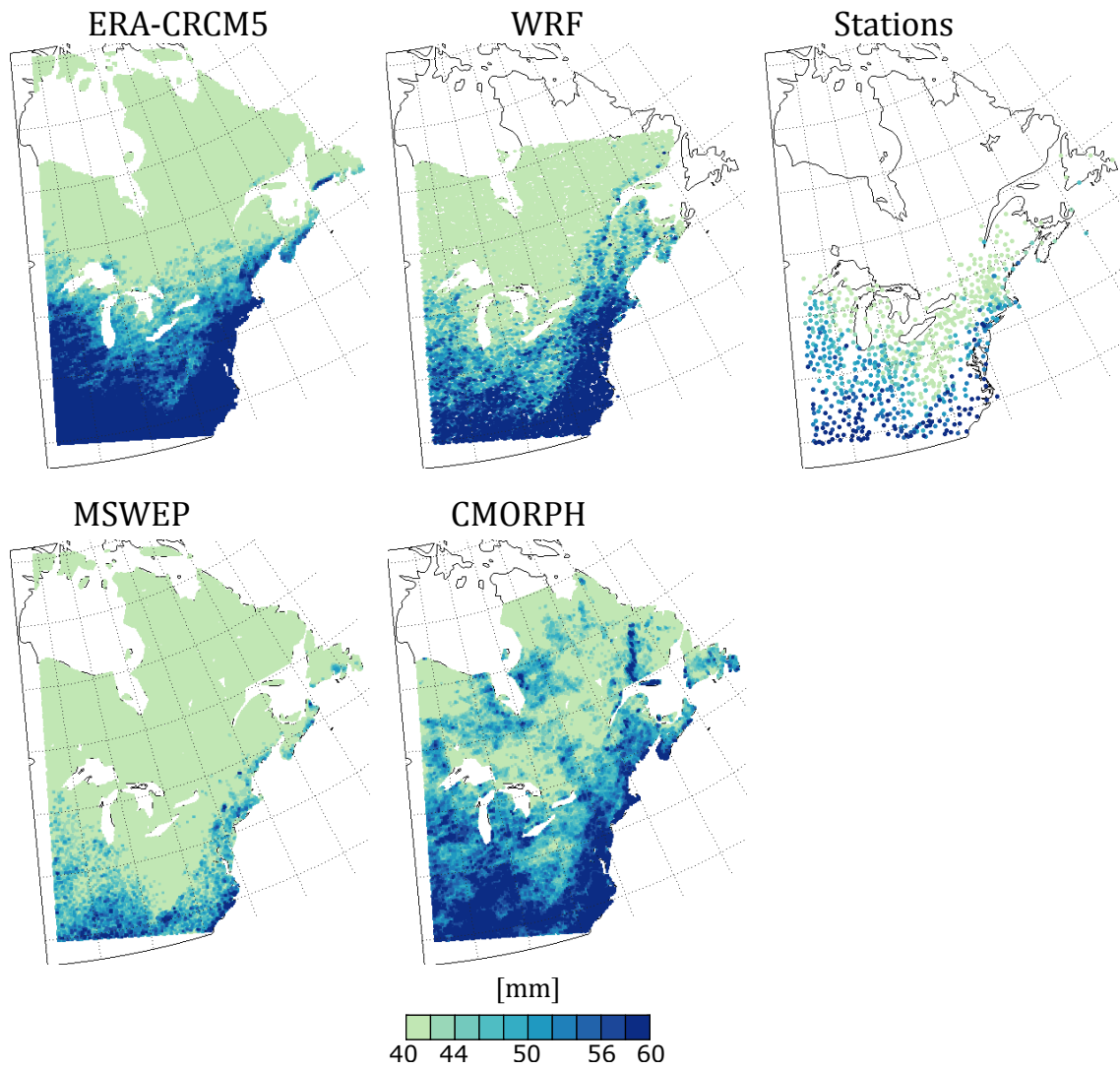


Figure S3: Two-yr AM precipitation for duration $d = 6h$ at the native spatial resolution of each dataset.

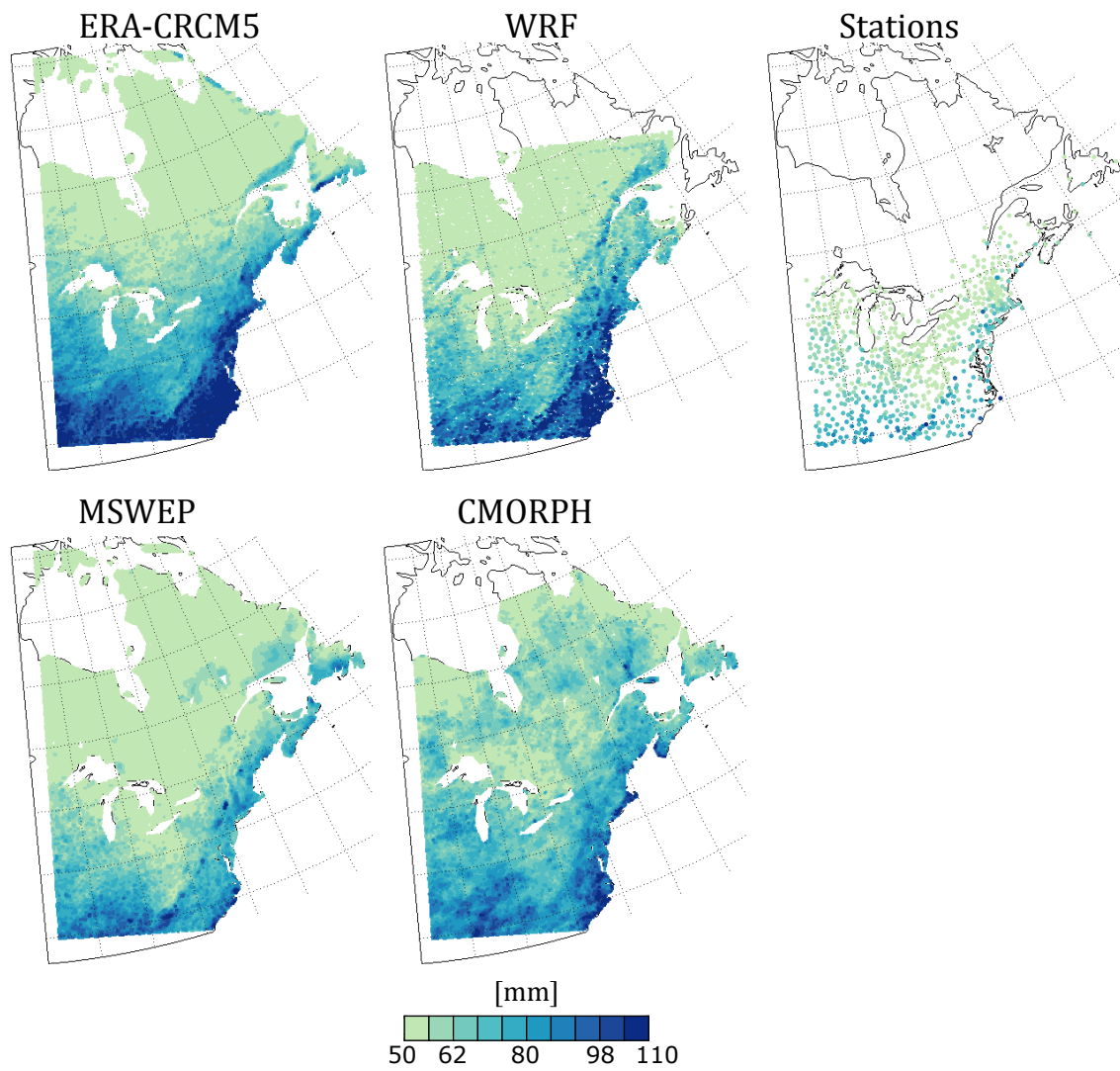


Figure S4: Two-yr AM precipitation for duration $d = 24h$ at the native spatial resolution of each dataset.

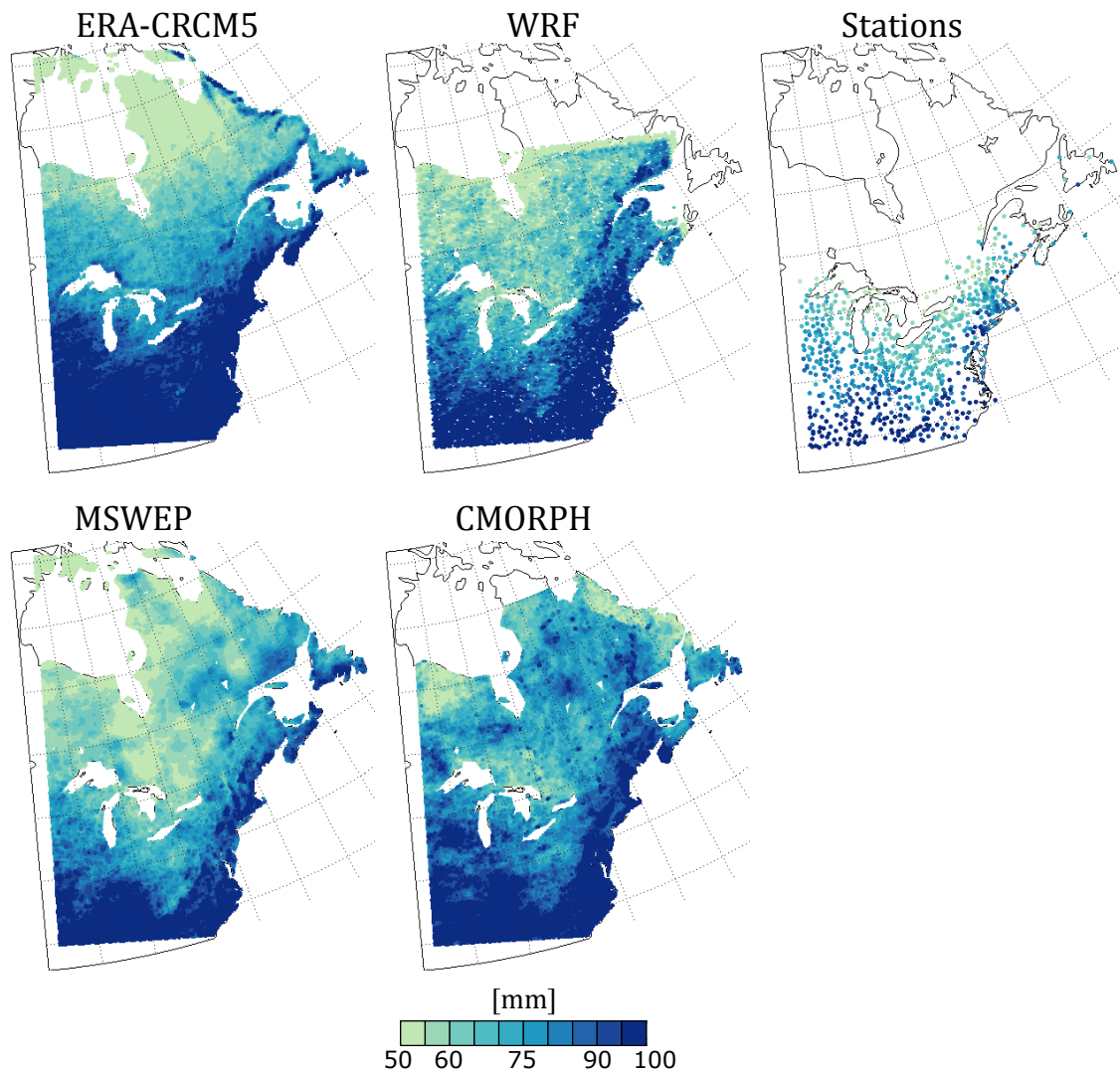


Figure S5: Two-yr AM precipitation for duration $d = 72h$ at the native spatial resolution of each dataset.

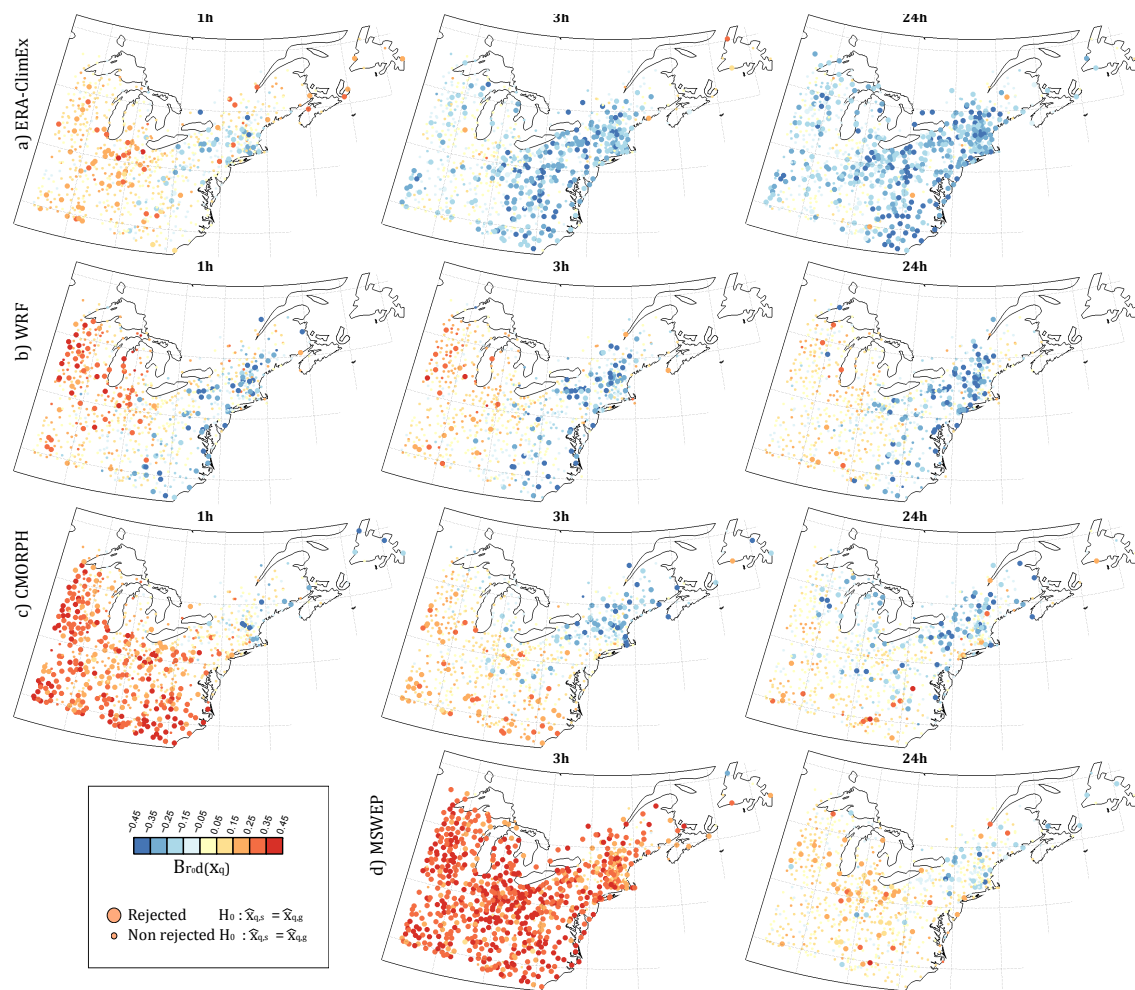


Figure S6: Spatial distribution over $L1$ locations of the relative difference, $B_{r_0,d}(\hat{x})$, for the 2-yr AM quantile at the native dataset resolution: a) ERA-CRCM5; b) WRF; c) CMORPH; and d) MSWEP. Smaller points represent locations with no statically significant bias (i.e. station-grid box pairs that did not reject the null hypothesis $H_0 : B_{r_0,d}(\hat{x}) = 0$ at the 0.05 significance level).

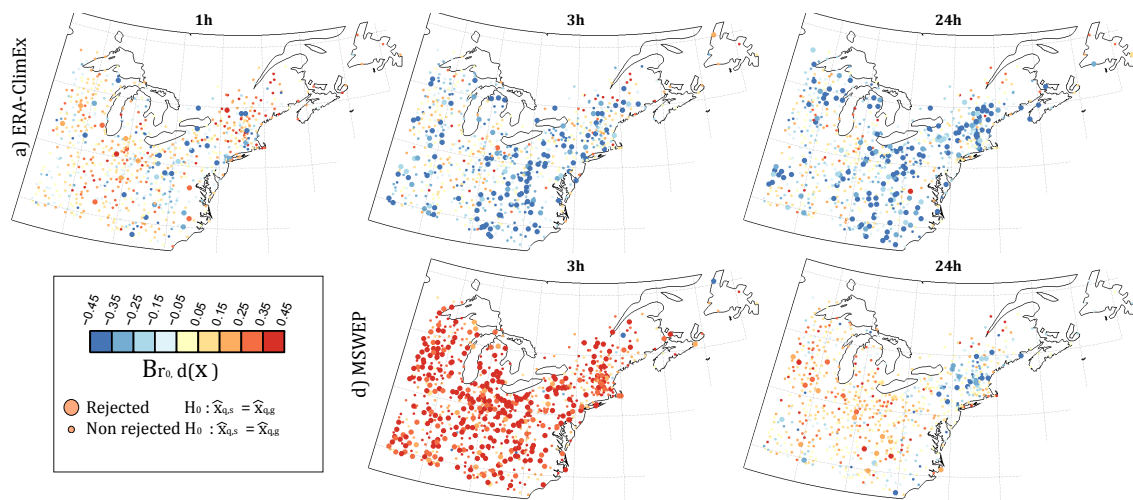


Figure S7: Spatial distribution over $L1$ locations of the relative difference, $B_{r_0,d}(\hat{x})$, for the 25-yr AM quantile at the native dataset resolution: a) ERA-CRCM5 and b) MSWEP. Smaller points represent locations with no statically significant bias (i.e. station-grid box pairs that did not reject the null hypothesis $H_0 : B_{r_0,d}(\hat{x}) = 0$ at the 0.05 significance level).

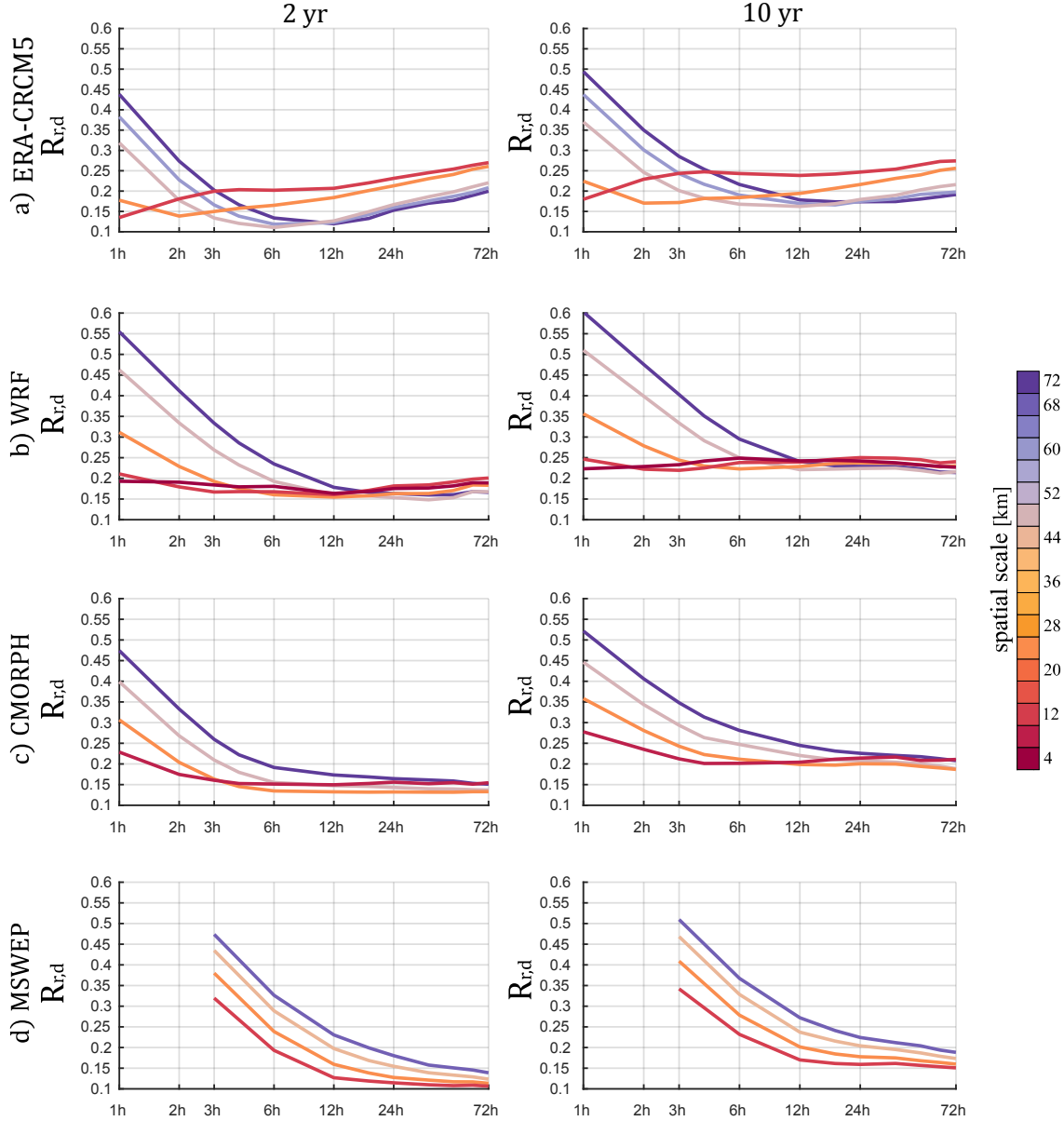


Figure S8: *Root Mean Squared Relative Error (RMSRE), $R_{r,d}$, defined for each spatio-temporal scale (r, d) as $R_{r,d} = (n^{-1} \sum_{i=1}^n B_{r,d}^2(\hat{x}))^{1/2}$, where the sum is over the n relevant $L1$ locations i , $i = 1, 2, \dots, n$. RMSRE for 2-yr (1^{st} col.) and 10-yr AM (2^{nd} col) quantiles are presented for: a) ERA-CRCM5; b) WRF; c) CMORPH; and d) MSWEP.*

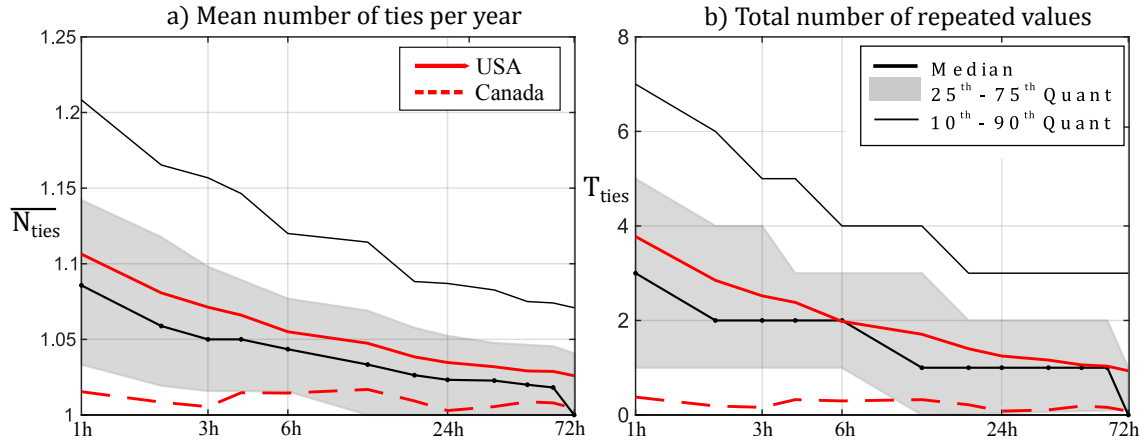


Figure S9: Distribution over L1 locations of AM tie statistics: a) Mean number of ties per year (i.e., mean number of equal AM sampled each year); b) Total number of ties exceeding the number n of years included in precipitation AMS (i.e. number of $N_{tie} \geq 1$ over the entire observation period).

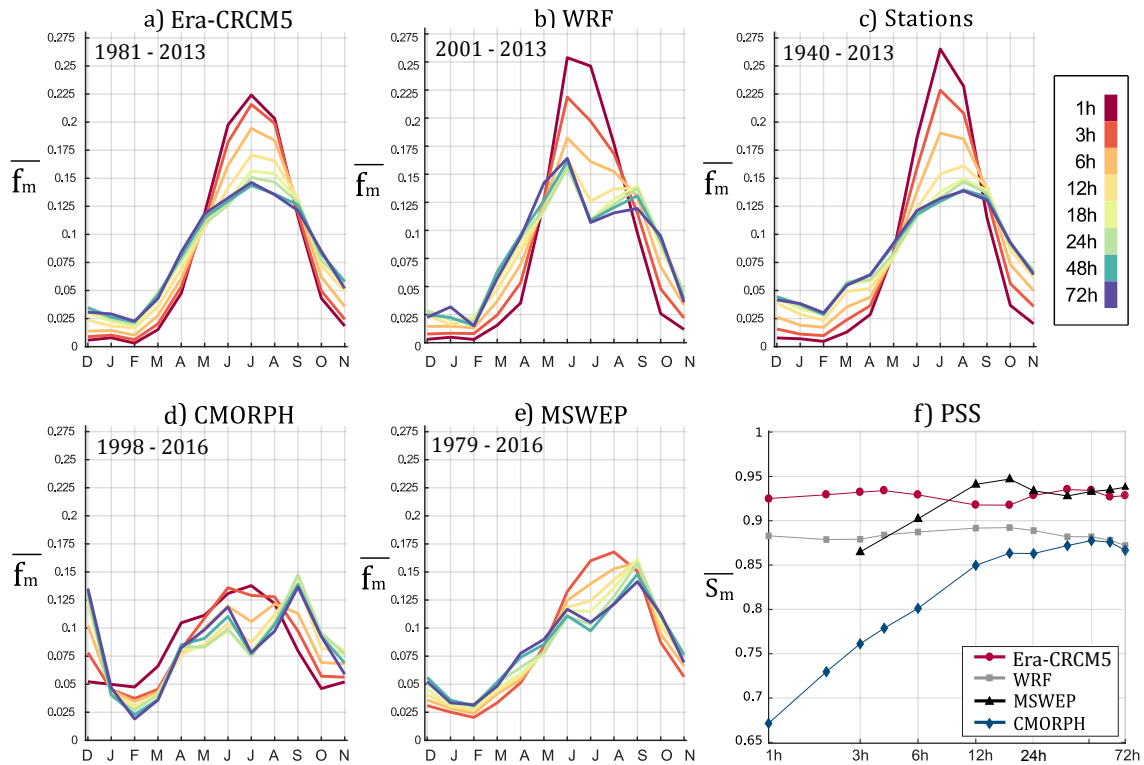


Figure S10: Annual cycles of AM occurrences at the native dataset resolution, r_0 , for: a) ERA-CRCM5; b) WRF; c) stations; d) CMORPH; and e) MSWEP. The period over which the annual cycles are estimated for each dataset is indicated at the top right corner of panels a to e. Panel f) displays the PSS between station and gridded dataset annual cycles averaged over L1-locations, \overline{S}_m as a function of duration.

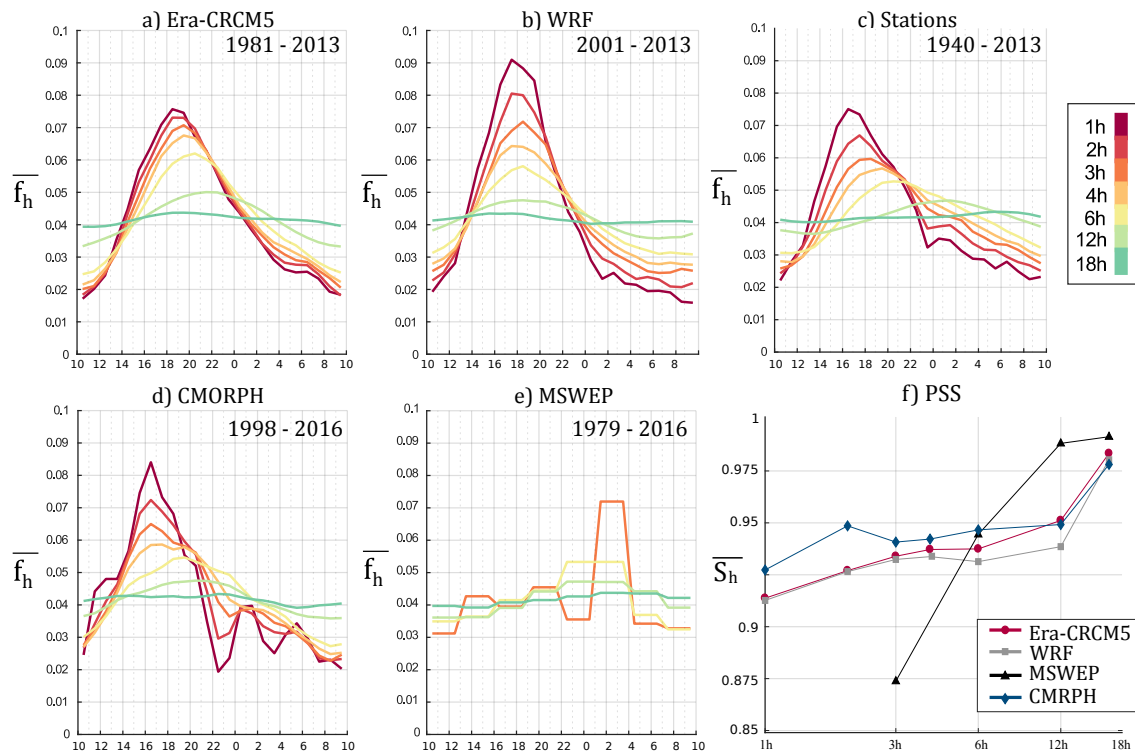


Figure S11: Daily cycles of sub-daily AM occurrence at the native dataset resolution, r_0 , for: a) ERA-CRCM5; b) WRF; c) stations; d) CMORPH; and e) MSWEP. The period over which the diurnal cycles are estimated for each dataset is indicated at the top right corner of panel a to e. Panel f) displays the PSS between station and gridded dataset diurnal cycles averaged over L1-locations, \overline{S}_h , as a function of duration.

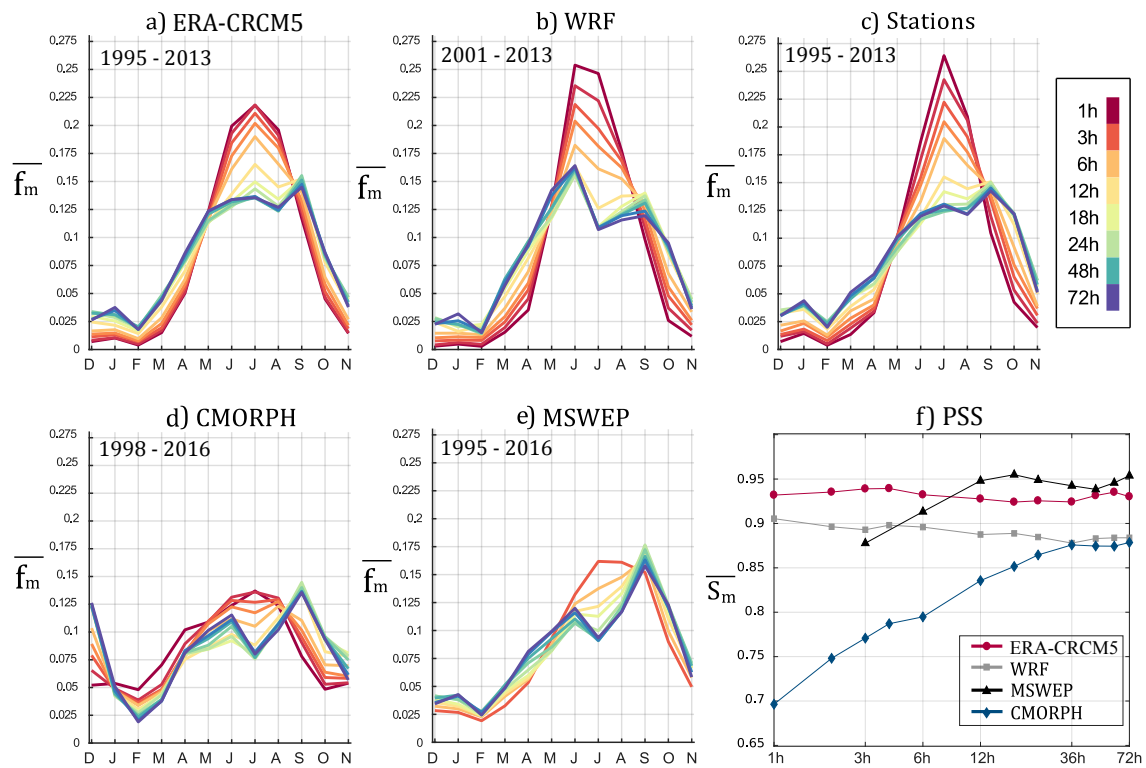


Figure S12: Annual cycles of AM occurrences at the native dataset resolution computed starting from 1995 for: a) ERA-CRCM5; b) WRF; c) stations; d) CMORPH; and e) MSWEP. Panel f) displays the PSS between station and gridded dataset annual cycles averaged over L1-locations, $\overline{S_m}$ as a function of duration.

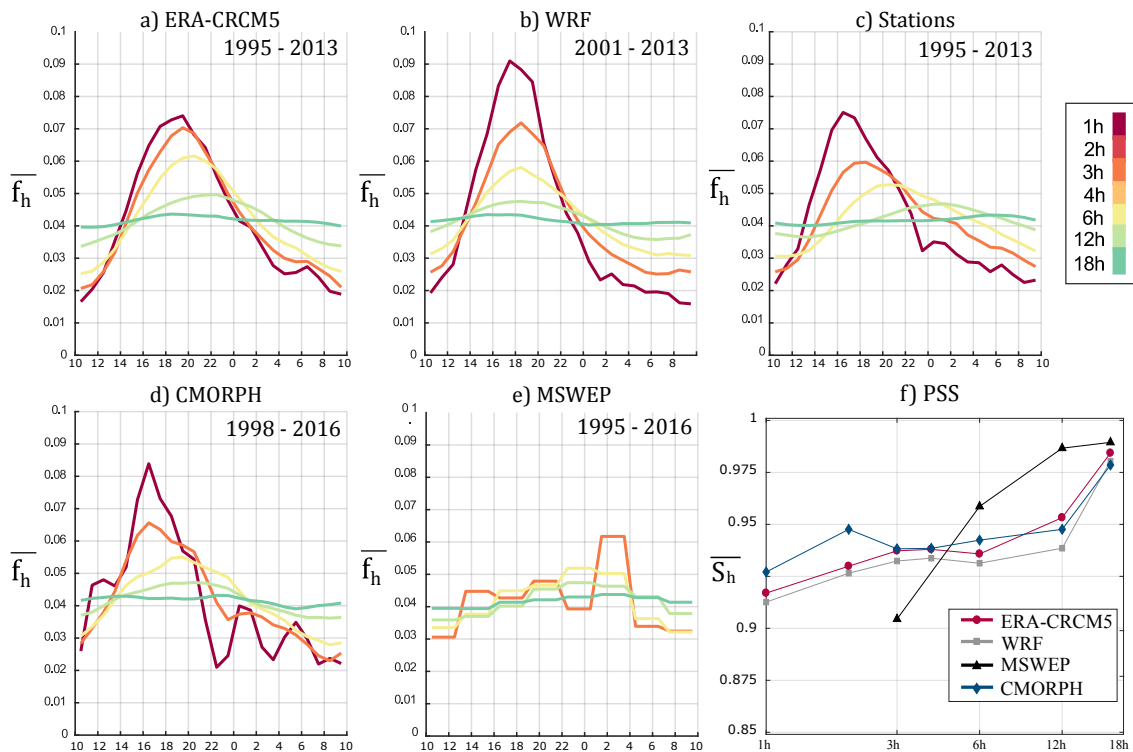


Figure S13: Daily cycles of sub-daily AM occurrence at the native dataset resolution computed starting from 1995 for: a) ERA-CRCM5; b) WRF; c) stations; d) CMORPH; and e) MSWEP. Panel f) displays the PSS between station and gridded dataset diurnal cycles averaged over L1-locations, \overline{S}_h as a function of duration.

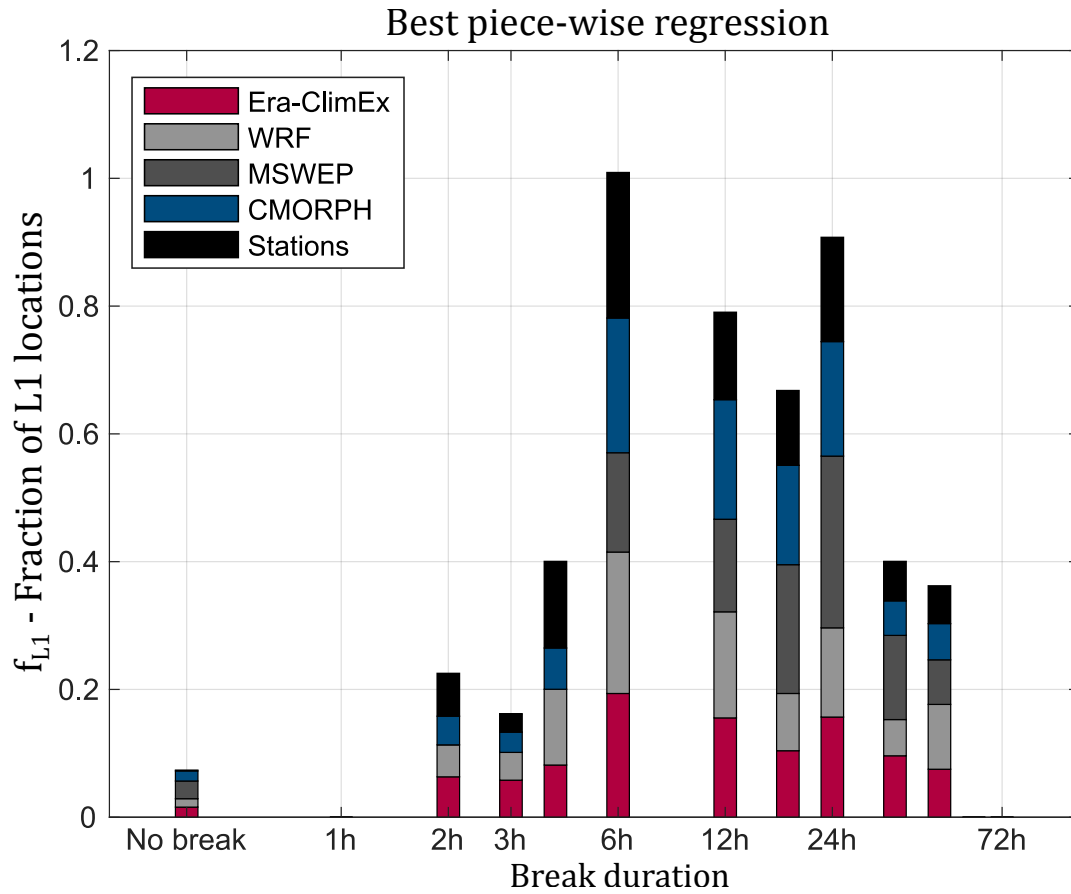


Figure S14: Break duration for AM temporal scaling for 10-yr return period quantiles: proportion of *L1 locations* achieving the best fit for a particular break duration (knot) in piece-wise models for the temporal scaling linear regression [Eq.(4)] in terms of the adjusted coefficient of determination, R_{adj}^2 . "No break" category corresponds to cases in which all possible 1-knot piece-wise regressions had lower R_{adj}^2 than the linear model that uses all available durations.

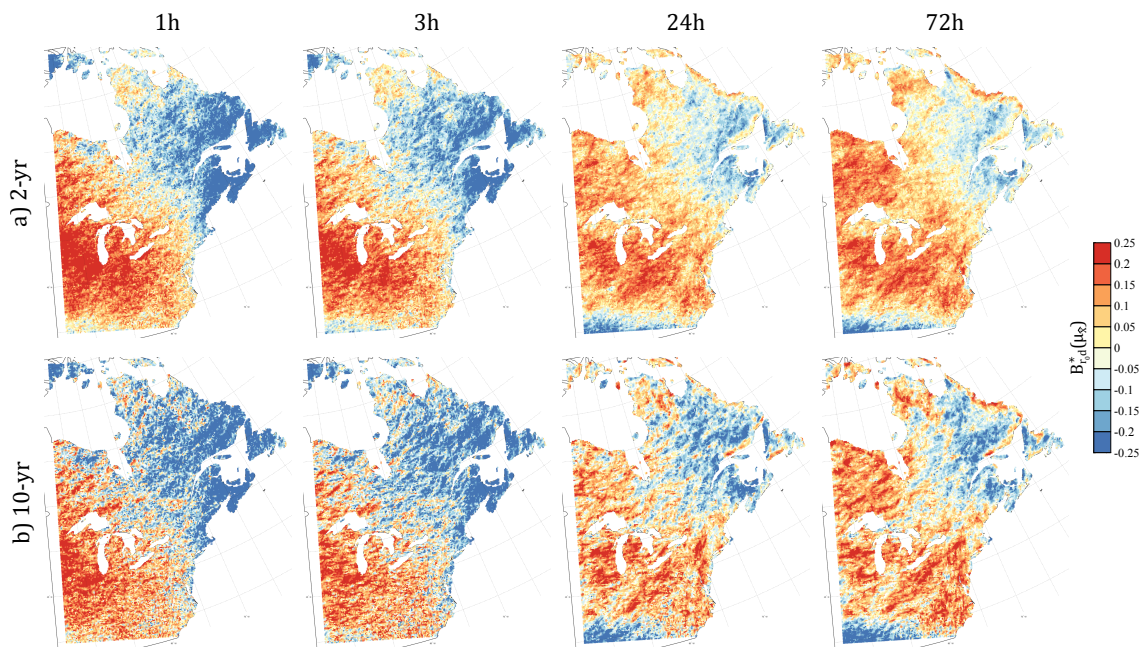


Figure S15: Spatial distribution of the relative difference, $B_{*r_0,d}(\hat{x}) = (x_{ERA-CRCM5} - x_{CRCM5-LE}) / (x_{ERA-CRCM5})$ between ERA-CRCM5 quantiles and the CRCM5-LE estimations for a) 2-yr and b) 10-yr AM quantile at the native dataset resolution.

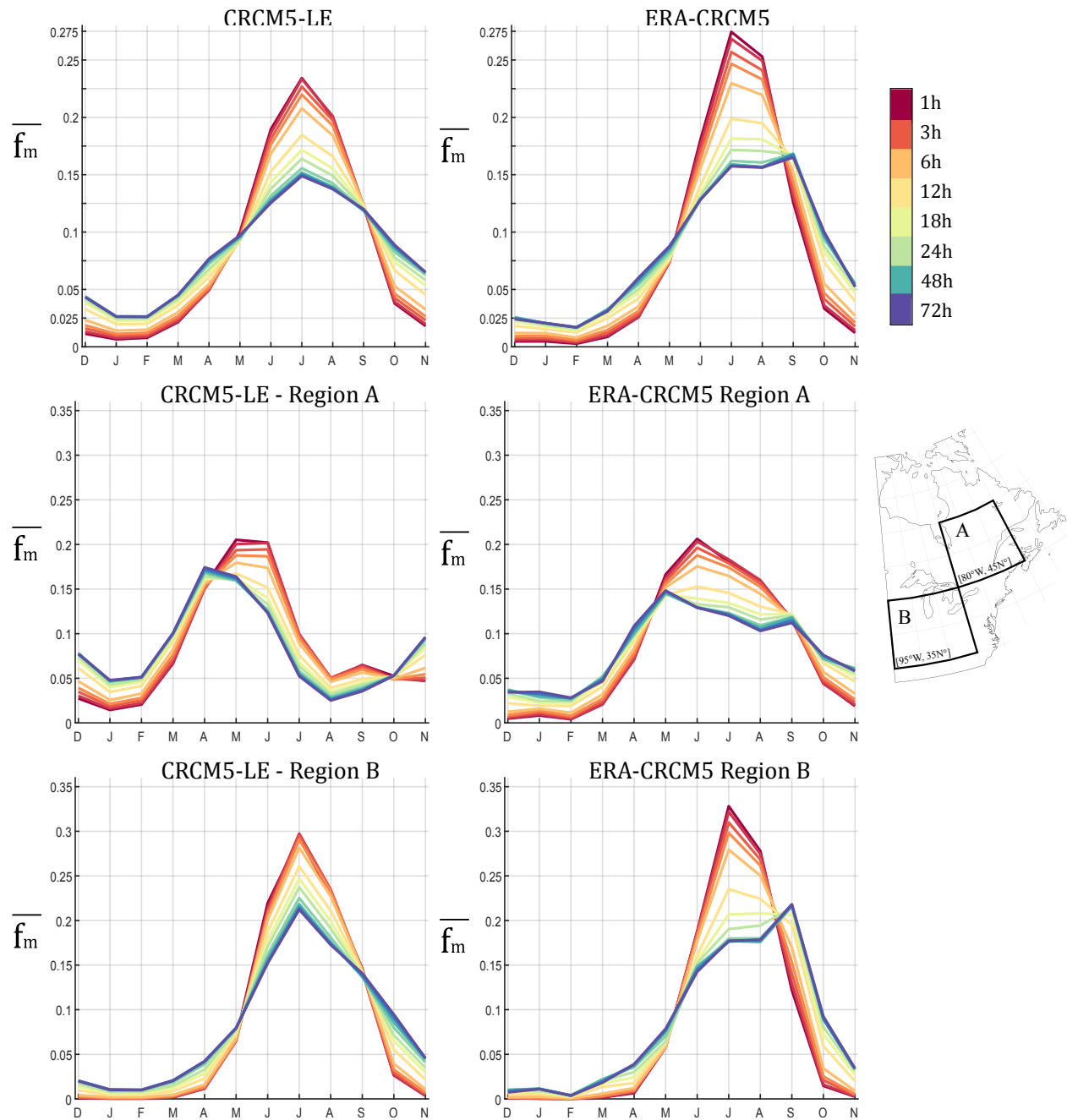


Figure S16: Annual cycles of AM occurrences at the native dataset resolution for ERA-CRCM5 (1st col.) and CRCM5-LE (2nd col.) computed for all grid boxes (1st row), grid boxes in region A (2nd row), and grid boxes in region B (3rd row).

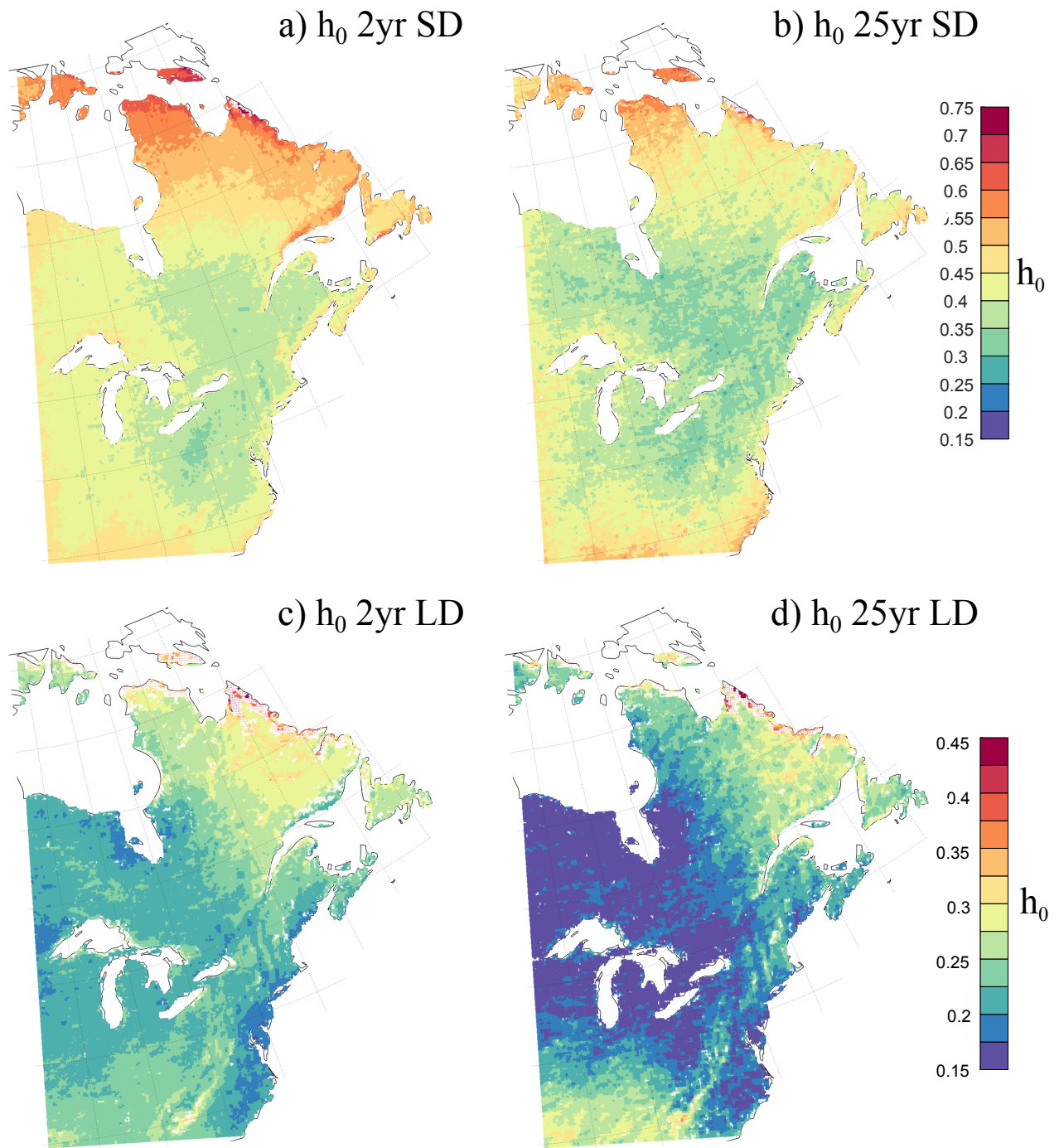


Figure S17: Spatial distribution of the extrapolated scaling slopes, h_0 , computed at each box for SD (1st row) and LD (2nd row) using the 50 member ensemble mean of the CRCM5-LE for a) 2-yr SD, b) 25-yr SD, c) 2-yr LD, and d) 25-yr LD AM quantiles.

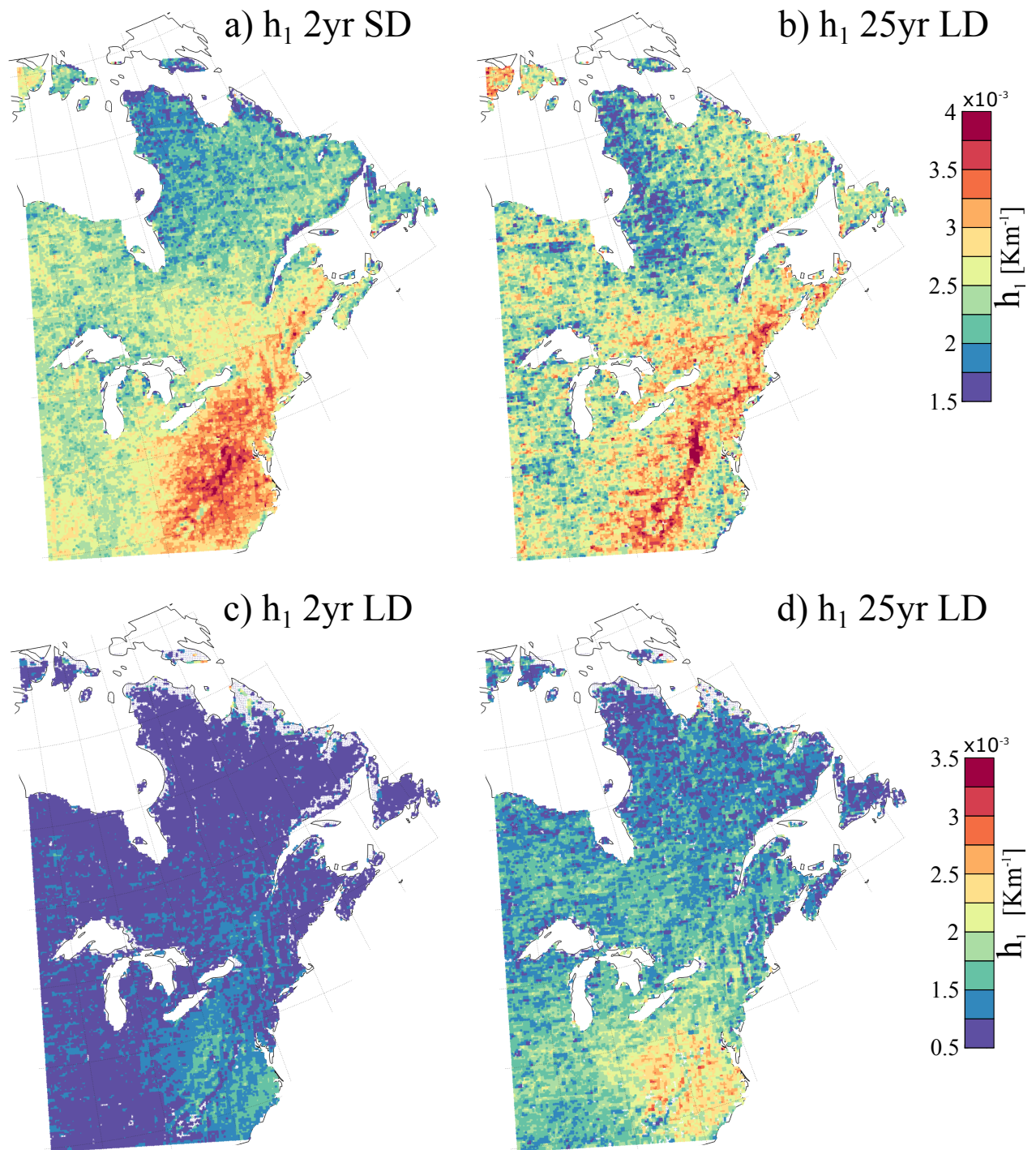


Figure S18: Spatial distribution of the extrapolated scaling slopes, h_1 , computed at each box for SD (1st row) and LD (2nd row) using the 50 member ensemble mean of the CRCM5-LE for a) 2-yr SD, b) 25-yr SD, c) 2-yr LD, and d) 25-yr LD AM quantiles.

Supplementary Material of

**"Extreme precipitation under climate change:
probability distributions, seasonality, and
spatio-temporal scaling of sub-daily annual
maxima"**

**Silvia Innocenti,^{1,*} Alain Mailhot¹, Anne Frigon²,
Alex J. Cannon³, Martin Leduc²**

1. Centre Eau-Terre-Environnement, INRS, Québec, Canada;
2. Consortium Ouranos, Montréal, Canada;
3. Climate Research Division, ECCC, Victoria, Canada.

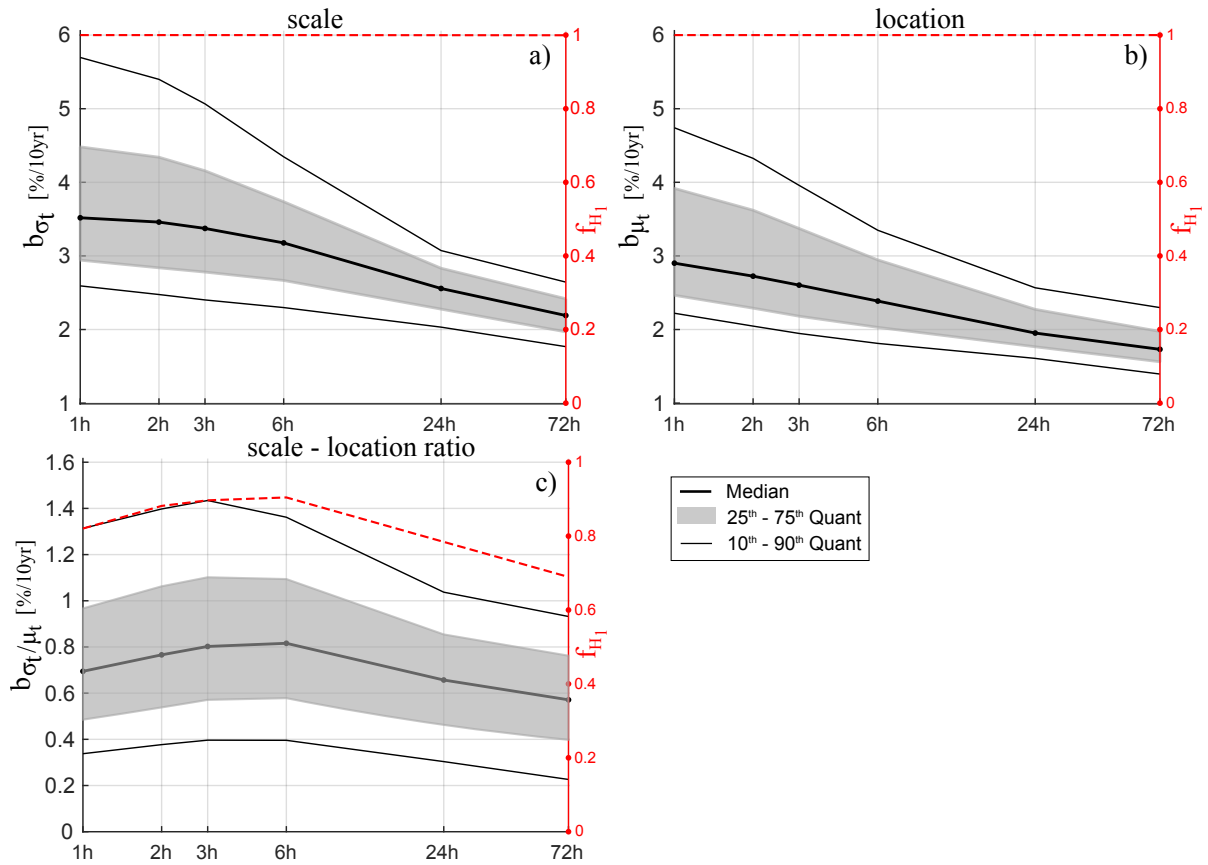


Figure S1: Expected decadal percent increase for 3SP GEV distribution parameters for durations $d=1,2,3,6,24$ and $72h$ (x-axis): a) scale, σ_t ; b) location, μ_t ; c) scale-location ratio, σ_t/μ_t . The red dashed curves (y-axis on the right) corresponds to the fractions, f_{H_1} , of grid boxes with statistically significant trend (MK at the at the $\alpha_{glo} = 0.1$ FDR level).

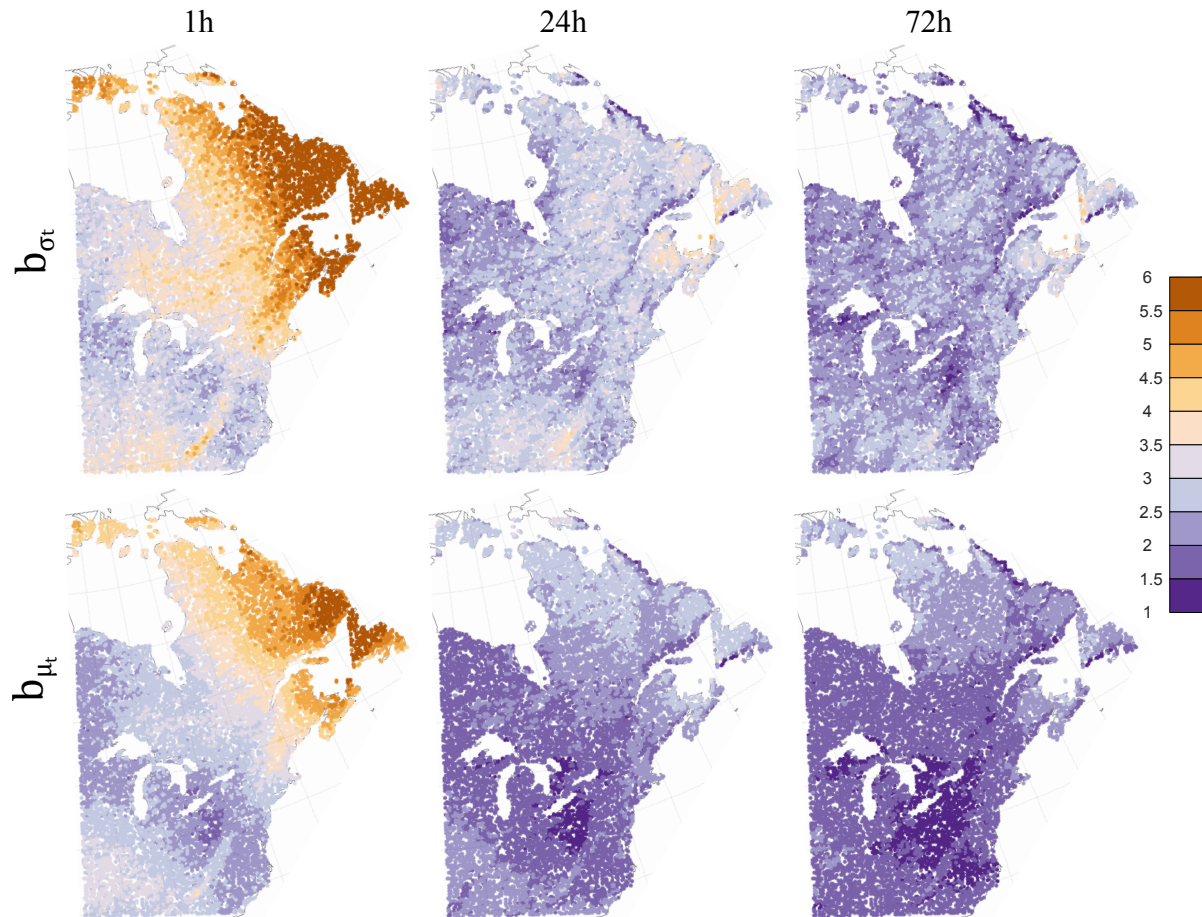


Figure S2: Spatial distribution of the decadal percent variation computed over 3SP for the GEV scale (σ_t , 1st row) and location (μ_t , 2nd row) for 1h (1st col.), 24h (2nd col.), and 72h (3rd col.).

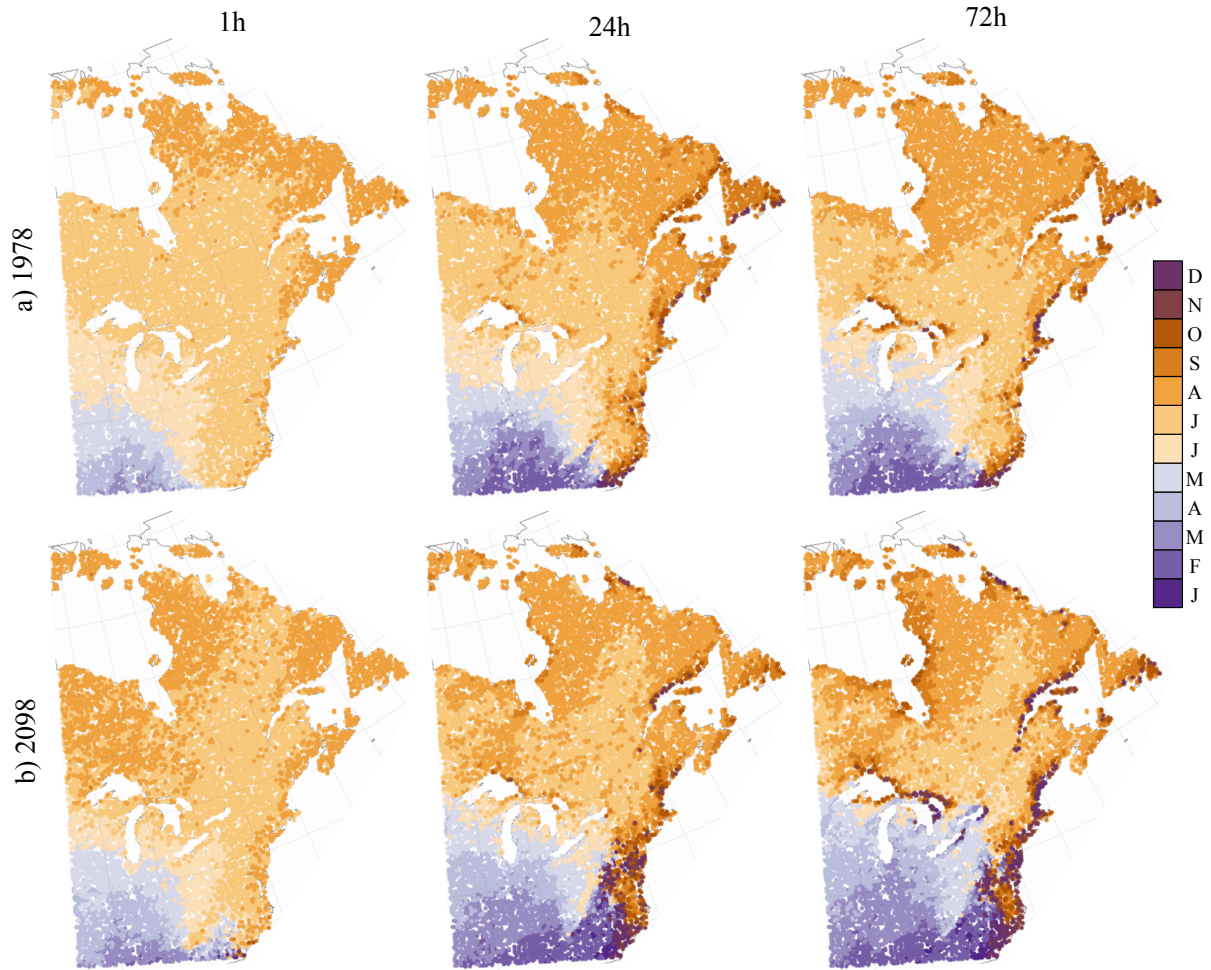


Figure S3: Spatial distribution of mean date of occurrence for a) $t = 1978$, and b) $t = 2098$ and for $d = 1h$ (1st col.), $d = 24h$ (2nd col.), and $d = 72h$ (3rd col.).

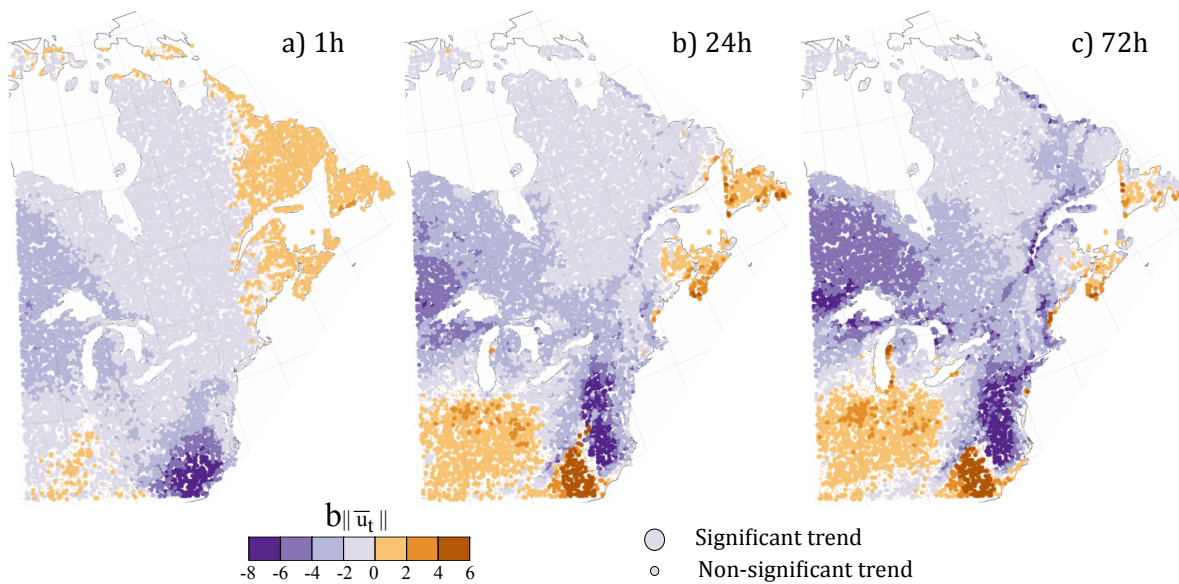


Figure S4: Spatial distribution of the decadal percent variation computed over 3SP for the mean vector length for the date of occurrence of a) hourly and b) daily AM.

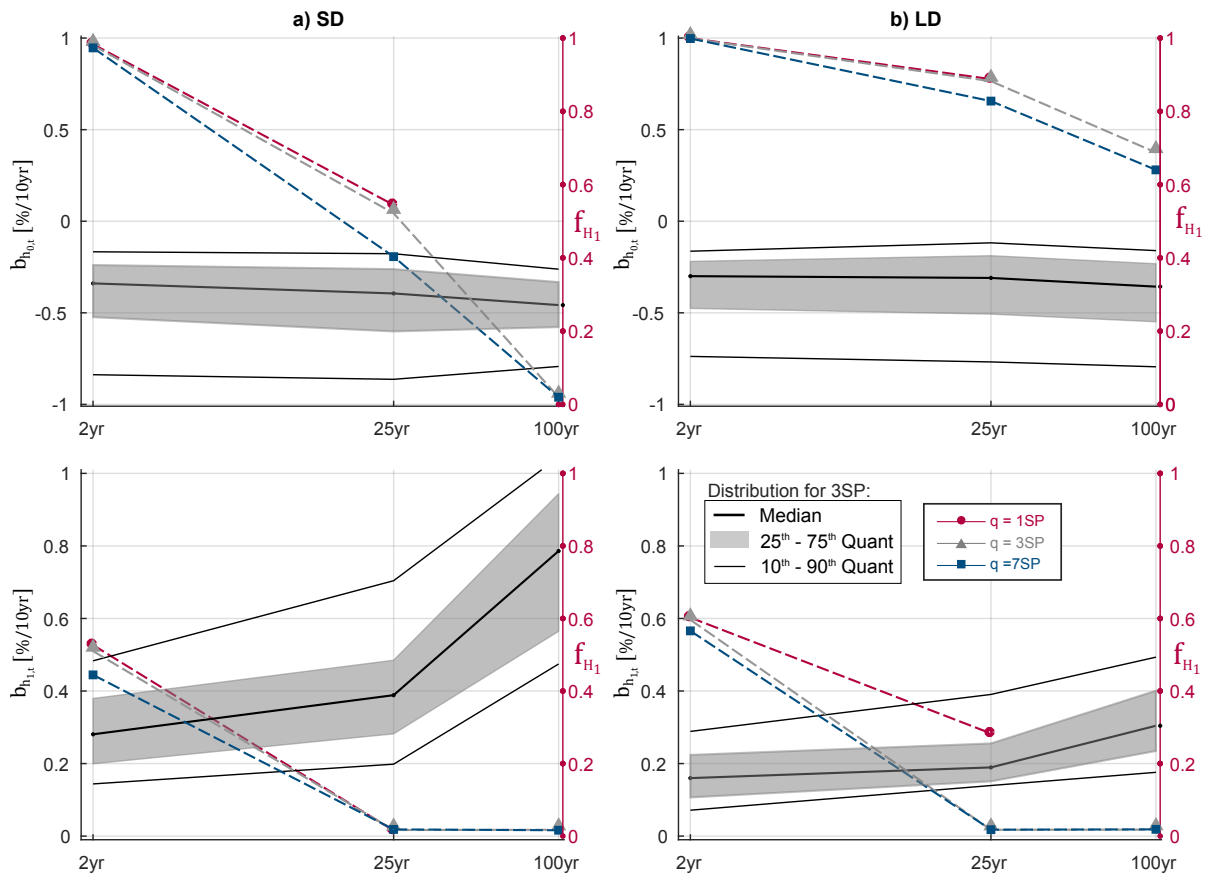


Figure S5: Distribution over CRCM5 grid boxes of the decadal percent variations for the scaling parameters $h_{0,t}$ (1st row) and $h_{1,t}$ (2nd row) for a) SD and b) LD. The dashed curves (y-axis on the right) corresponds to the fractions, f_{H1} , of grid boxes with statistically significant trend (MK at the $\alpha_{glo} = 0.1$ FDR level).

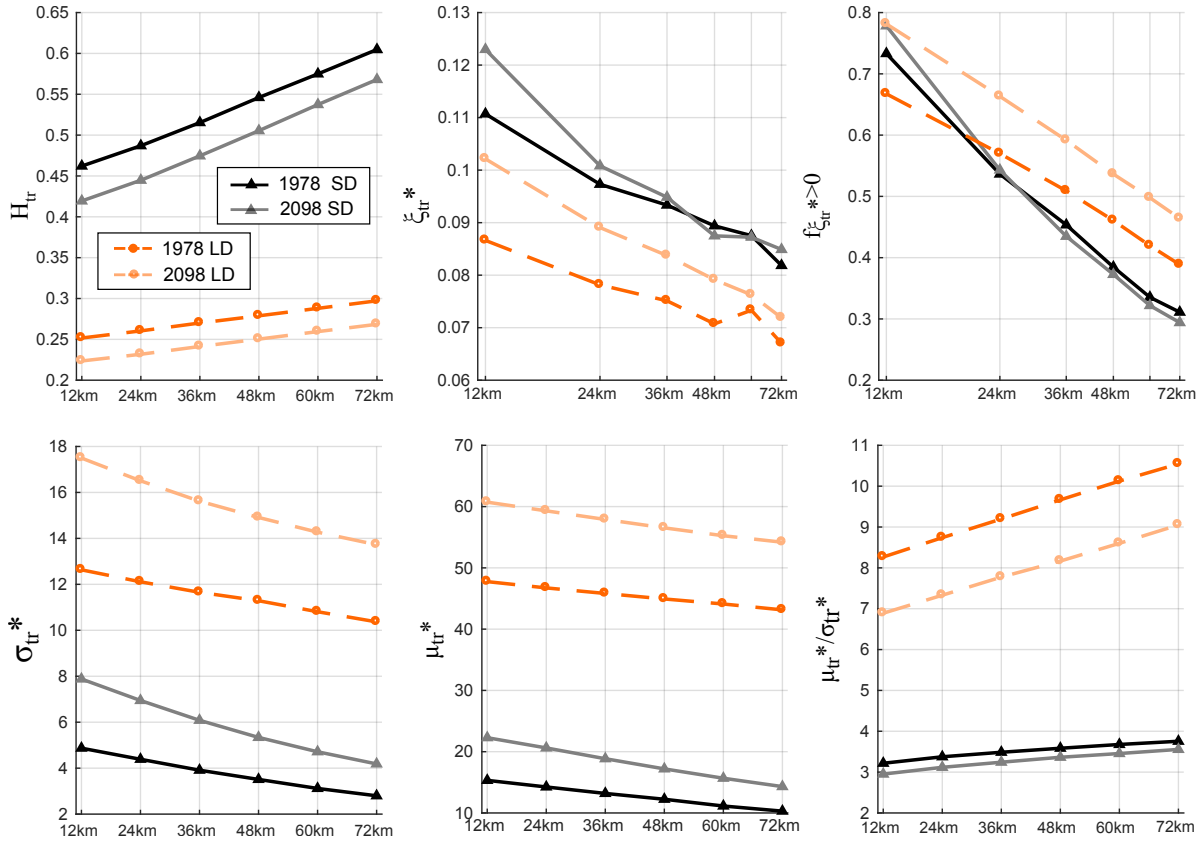


Figure S6: Median over CRCM5 grid boxes of 3SP S-GEV estimates for $t = 1978$ and $t = 2098$. The reference duration $d^* = 1h$ has been considered for SD and $d^* = 24h$ for LD.

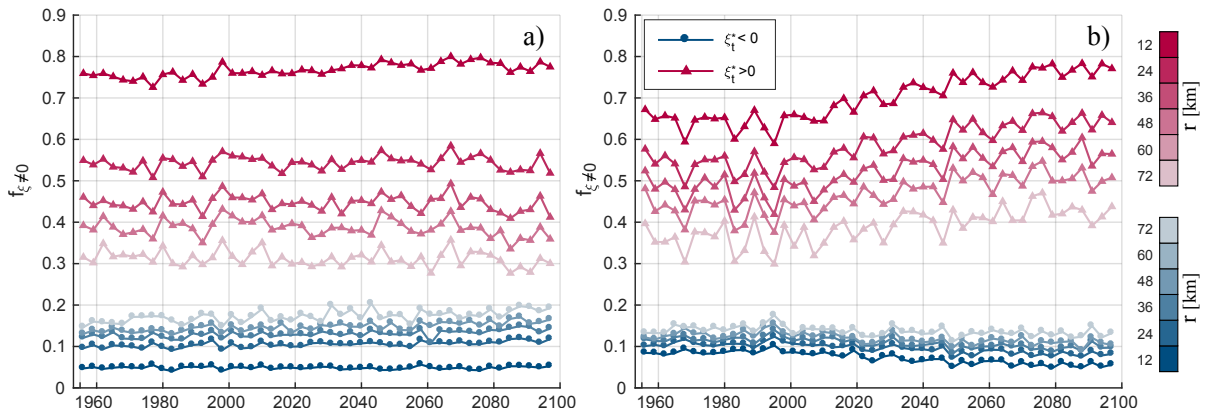


Figure S7: Proportion of grid boxes with S-GEV shape parameter, ξ_t^* , significantly different from 0 according to the LR test at the $\alpha_{glo} = 0.01$ FDR level for a) SD and b) LD.

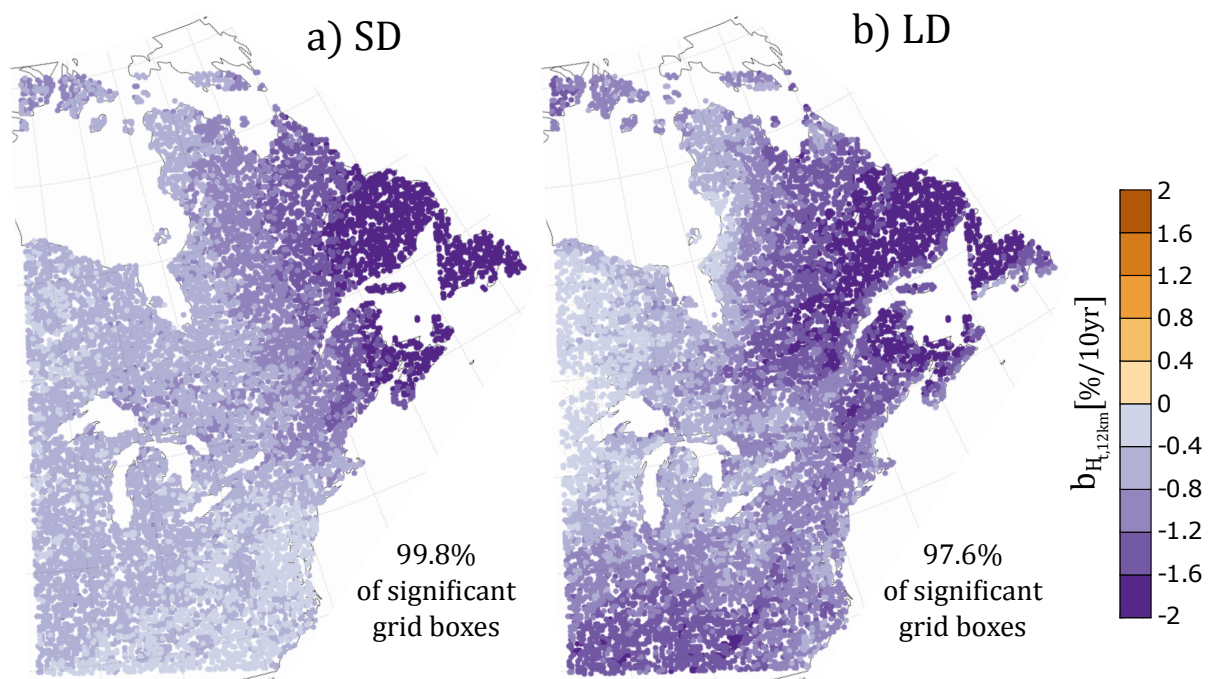


Figure S8: Spatial distribution of the decadal percent variation of temporal scaling 3SP S-GEV parameters for a) SD and b) LD at the native spatial resolution (i.e. $r = 12km$).

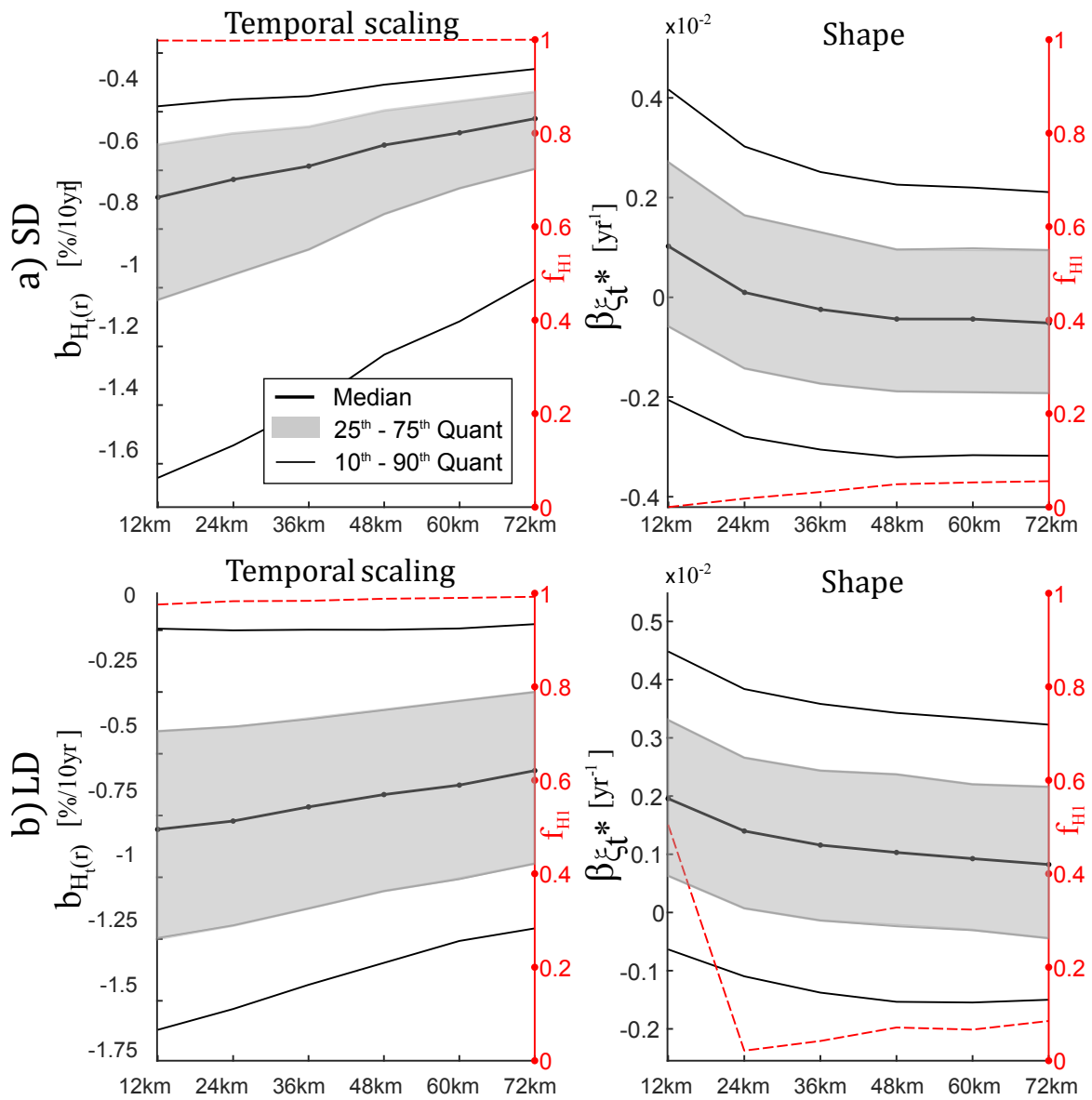


Figure S9: Distribution over CRCM5 grid boxes of the decadal percent (absolute) variation for 3SP S-GEV scaling (shape) parameters for a) SD and b) LD. The dashed curves (y-axis on the right) corresponds to the fractions, f_{H_1} , of grid boxes with statistically significant trend (MK at the at the $\alpha_{glo} = 0.1$ FDR level).

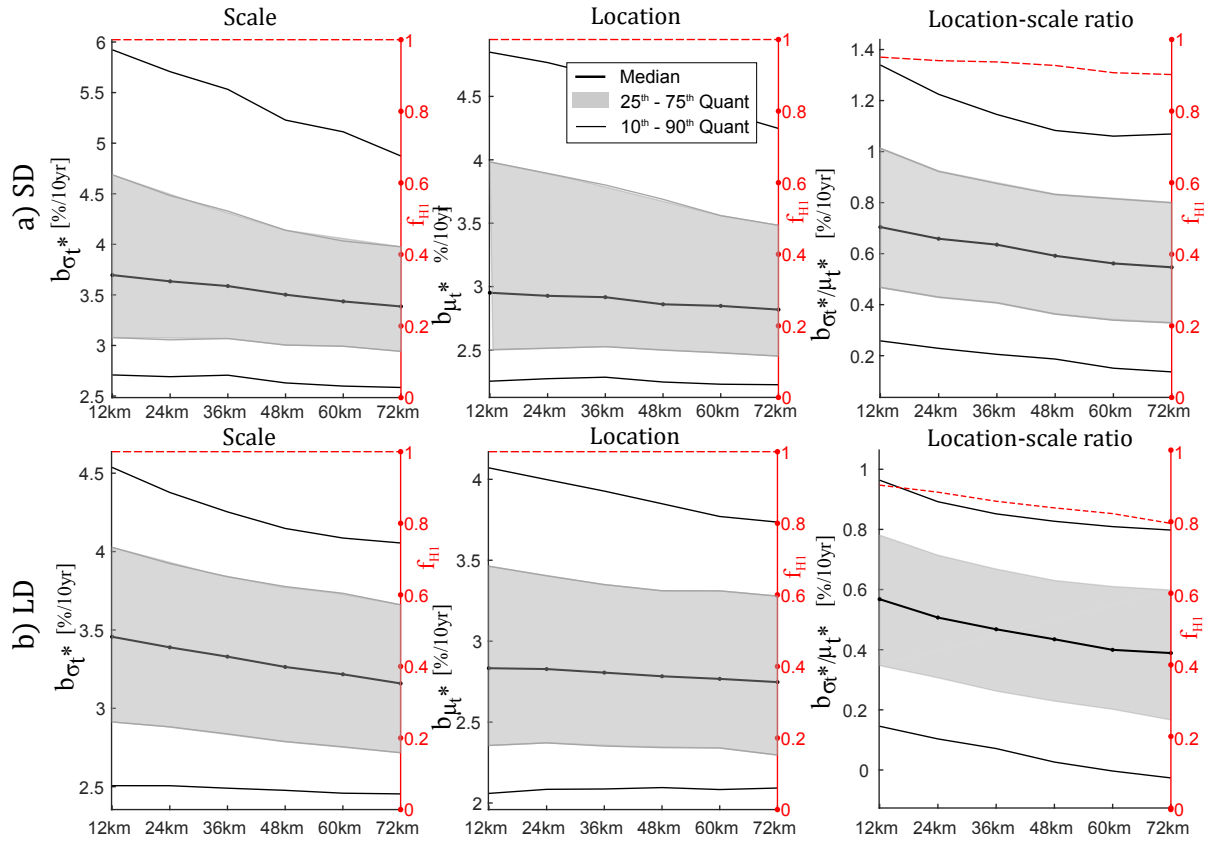


Figure S10: Distribution over CRCM5 grid boxes of the decadal percent variation for 3SP S-GEV scale (σ_t^* , 1st col.) and location (μ_t^* , 2nd col.) parameters, and for the normalized dispersion coefficient (σ_t^*/μ_t^* , 3rd col. The dashed curves (y-axis on the right) corresponds to the fractions, f_{H1} , of grid boxes with statistically significant trend (MK at the at the $\alpha_{glo} = 0.1$ FDR level).) for a) SD and b) LD.